A TEMPORARY CONNECTION FOR AN ALUMINIUM SPACE FRAME.

Humayun Idrees Hanif

Doctor of Philosophy

THE UNIVERSITY OF ASTON IN BIRMINGHAM

JULY 1988

The University of Aston in Birmingham.

A TEMPORARY CONNECTION FOR AN ALUMINIUM SPACE FRAME.

By

Humayun Idrees Hanif

Thesis submitted for the degree of Doctor of Philosophy
July 1988

SUMMARY

This thesis examines theoretically and experimentally the behaviour of a temporary end plate connection for an aluminium space frame structure, subjected to static loading conditions.

Theoretical weld failure criterions are derived from basic fundementals for both tensile and shear fillet welds. Direct account of weld penetration is taken by incorporating it into a more exact proposed weld model. Theoretical relationships between weld penetration and weld failure loads, failure planes and failure lengths are derived. Also, the variation in strength between tensile and shear fillet welds is shown to be dependant upon the extent of weld penetration achieved.

The proposed tensile weld failure theory is extended to predict the theoretical failure of the welds in the end plate space frame connection. A finite element analysis is conducted to verify the assumptions made for this theory.

Experimental hardness and tensile tests are conducted to substantiate the extent and severity of the heat affected zone in aluminium alloy 6082-T6. Simple transverse and longitudinal fillet welded specimens of the same alloy, are tested to failure. These results together with those of other authors are compared to the theoretical predictions made by the proposed weld failure theories and by those made using Kamtekar's and Kato and Morita's failure equations, the β-formula and BS 8118.

Experimental tests are also conducted on the temporary space frame connection. The maximum stresses and displacements recorded are checked against results obtained from a finite element analysis of the connection. Failure predictions made by the proposed extended weld failure theory, are compared against the experimental results.

Key Words:

Space frame, temporary connection, weld failure theories, heat affected zones.

In the name of Allah the Almighty, Most Merciful and Compassionate,

I dedicate this thesis to my beloved parents, brothers and sister.

DECLARATION

The author wishes to declare that, except for commonly understood and accepted ideas, or where specific reference is made, the work reported in this dissertation is his own. The work has not previously been submitted in part or in whole to any University for any degree, diploma or other qualification.

H. I. HANIF

This dissertation is the result of my own work and includes nothing which is the outcome of work done in collaboration.

ACKNOWLEDGEMENTS

The research described in this dissertation was carried out in the Department of Civil Engineering at the University of Aston in Birmingham.

I am grateful to my supervisor Dr.C.S.Bahia who introduced me to the research and encouraged me by his continued enthusiastic support. My gratitude also extends to Dr.J.Just for his advice given and interest shown in the research conducted.

My sincere thanks go to Mr.Kevin Cotter of British Oxygen Welding for his unselfish co-operation, help and advice given throughout the course of this research. I would also like to thank the structures workshop in the Civil Engineering Department for their assistance and co-operation with the experiments. In particular I should mention Mr. P.Green, Mr. B.Curtis and Mr. C.Geens.

I am indebted to Dr. J.Jones and Miss I.Whittier of the Engineering Computer Faculty, for their co-operation, help and advice given to me throughout this research. I should also like to extend my thanks to Mr. M.Linskill, Mr. D.Stops, Mr. R.Parsons and Mr. A.D. Bray, of the Computer Science Faculty for their interest, help and generosity shown.

Finally I thank everybody else who has contributed to the work either with practical help or interesting ideas.

CONTENTS

	PageNumber.
THESIS TITLE	1
SUMMARY	2
DEDICATION	3
DECLARATION	4
ACKNOWLEDGEMENTS	5
CONTENTS	6
LIST OF TABLES	11
LIST OF FIGURES	14
LIST OF PLATES	20
NOTATION	21
CHAPTER 1 INTRODUCTION	24
1.1 Space frame structures.	24
1.1.1 Temporary space frame structures.	26
1.2 Structural connections in aluminium.	27
1.3 Weld failure criterions.	30
1.4 Aluminium alloy designation.	31
1.4.1 Temper designations.	32
1.5 Aluminium alloys for structural applications.	33
1.5.1 The 5XXX series - Aluminium Magnesium Alloys.	34
1.5.2 The 6XXX series - Aluminium Magnesium Silicon Alloys.	35

PageNumber.

1.5.3 The 7XXX series - Aluminium Zinc Magnesium Alloys. 35

1.6 Aluminium alloy selection. 36

1.7 Filler metal selection. 37

1.8 The Metal Inert Gas (MIG) welding process. 37

1.8.1 Advantages the MIG welding. 38

1.8.2 Disadvantages of MIG welding. 40

1.9 The Tungsten Inert Gas (TIG) welding process. 40

1.9.1 Advantages of TIG welding. 41

1.9.2 Disadvantages of TIG welding. 42

CHAPTER 2 LITERATURE REVIEW 43

2.1 Heat affected zones in aluminium alloys. 43

2.1.1 Background. 43

2.1.2 The extent of HAZ r for thin plates. 49

2.1.2.1 The extent of HAZ r for thick plates. 51

2.1.3 Multi - pass welds. 53

2.1.4 Extent of the HAZ when no thermal control is exercised. 53

2.1.5 Severity of softening in the HAZ. 54

2.2.0 The weld metal profile. 54

2.3.0 Weld failure criterions. 59

CHAPTER 3 A PROPOSED WELD FAILURE THEORY 83

3.1 Introduction. 83

PageNumber.

3.2 The proposed weld model. 84

3.3 Assumptions for the derivation of a failure criterion for tensile and shear fillet welds. 86

3.4 Notation used for stresses. 87

3.5 The proposed failure theory for tensile fillet welds. 88

3.5.1 Conclusions from the proposed tensile failure weld theory. 109

3.6 A proposed failure theory for shear fillet welds. 110

3.6.1 Conclusions from proposed shear fillet weld theory. 122

CHAPTER 4 FAILURE ANALYSIS OF END PLATE CONNECTION **123**

4.1 Introduction. 123

4.2 Failure analysis of end welds. 126

4.3 Application of Kamtekar's weld model to predict failure of the welds of the end plate connection. 135

4.4 Application of the derived weld failure theory for the end plate connection. 136

CHAPTER 5 EXPERIMENTATION METHODS AND RESULTS **137**

5.1 Introduction. 137

5.2 Specimens. 138

5.2.1 Material. 138

5.2.2 Specimen preperation. 139

PageNumber.

5.2.3 Butt - welded specimen. 141

5.2.3.1 Strength coupons. 141

5.2.4 Hardness traverse. 150

5.2.5 Fillet welded specimen. 154

5.2.5.1 The transverse fillet welded specimen. 154

5.2.5.2 The longitudinal fillet welded specimen. 162

5.2.5.2 The cruciform shaped specimen. 169

5.2.5.4 The temporary space frame end plate connection. 172

5.2.5.4.1 Preperation of the test specimen type F. 175

5.2.5.4.2 Testing procedure for the end plate test connection. 183

5.3 Measurement of weld failure planes. 189

CHAPTER 6 FINITE ELEMENT ANALYSIS OF END PLATE 190

6.1 Introduction. 190

6.2 The finite element method. 191

6.3 Finite elements. 192

6.4 Finite element computer software. 194

6.4.1 Program for automatic finite element calculations - PAFEC. 194

6.4.2 Pafec Interactive Graphics System - PIGS. 195

6.5 Finite element analysis of the trapezium shaped end plate. 197

6.6 Results from finite element analysis. 211

6.7 Replacement of point load by an equivalent line load. 216

PageNumber.

CHAPTER 7 DISCUSSION OF RESULTS 220

7.1 Tensile coupons. 220

7.2 Hardness traverse. 222

7.2.1 Extent of the HAZ. 223

7.2.2 Severity of the HAZ. 223

7.3 Tensile fillet welds. 226

7.3.1 Comparison of tensile weld failure theories. 227

7.4 Shear fillet welds. 249

7.4.1 Comparison of shear weld failure theories. 254

7.5 Cruciform shaped test specimens. 266

7.6 Comparison of the variation in strength between tensile and shear fillet welds. 269

7.7.1 Failure predictions of the temporary end plate connection. 268

7.7.2 Experimental and FE results of point loaded end plate connection. 272

CHAPTER 8 CONCLUSIONS 279

CHAPTER 9 RECOMMENDATIONS FOR FURTHER WORK 282

REFERENCES 283

APPENDICIES

APPENDIX A 293

APPENDIX B 300

APPENDIX C 306

APPENDIX D 323

LIST OF TABLES

Table Number	Title	Page Number
1.1	Aluminium alloy designation system.	32
3.1	Calculated values of tensile weld failure loads and failure planes as weld penetration (p) changes.	107
3.2	Calculated values of shear weld failure loads and failure planes as weld penetration (p) changes.	121
5.1	Composition of aluminium alloy 6082	138
5.2	Tensile properties of parent aluminium alloy 6082-T6 taken from delivered plate.	146
5.3	Tensile properties of parent metal alloy 6082-T6 coupons.	147
5.4	Tensile properties of heat affected zone coupons in aluminium 6082-T6.	148
5.5	Tensile properties of weld metal 4043A longitudinal coupons.	149
5.6	Tensile properties of weld metal 4043A loaded in transverse direction.	150
5.7	Welding data for butt welded specimen.	154
5.8	Experimental results for transverse fillet welded specimens.	158
5.9	Extension of transverse fillet welds along the applied load.	160
5.10	Extension of longitudinal fillet welds in direction of applied load.	166
5.11	Experimental results for longitudinal fillet welded specimens.	168
5.12	Experimental results for cruciform shaped biaxial, (equal) loaded specimens.	170
5.13	Dimension measurements for test specimens F1 to F10.	181
5.14	Dimension measurements for test specimens F11 to F15.	182

Table Number	Title	Page Number
5.15	Dial gauge readings for test specimen F1.	186
5.16	Measured readings of location of dial gauges and strain gauges for specimens type F.	188
6.1	PAFEC results for maximum deflection of end plate as load increases.	213
7.1	Comparison of author's experimental results on tensile fillet welded aluminium specimen.	233
7.2	Comparison between predicted results and author's experimental tensile fillet weld results.	234
7.3	Higg's experimental transverse fillet welded specimen results.	235
7.4	Predicted failure loads and planes for Higg's transverse welded specimens.	236
7.5	Comparison between predicted results and Higg's experimental results.	237
7.6	Kato and Morita's experimental transverse fillet welded specimen results.	240
7.7	Comparison of Kato and Morita's transverse welded specimen results.	241
7.8	Comparison between predicted weld failure loads for Kato and Morita's transverse weld specimens.	242
7.9	Soeten's average experimental results for aluminium transverse fillet welded specimens.	244
7.10	An indicative prediction for Soeten's transverse fillet welded aluminium specimens.	245
7.11	Comparison of predicted failure results using Soeten's experimental data.	246
7.12	Prediction of shear failure loads and angles using the author's longitudinal test specimen results.	255

Table Number	Title	Page Number
7.13	Comparison of predicted results for author's experimental longitudinal fillet weld specimens.	256
7.14	Kato and Morita's experimental longitudinal fillet welded specimen results.	258
7.15	Prediction of failure loads and angles for Kato and Morita's longitudinal test specimens.	259
7.16	Comparison between predicted failure results for Kato and Morita's longitudinal fillet welded specimen.	260
7.17	Soeten's average experimental results for longitudinal fillet welded test specimens.	262
7.18	Prediction of failure loads and planes for Soeten's longitudinal test specimens.	263
7.19	Comparison between predicted results for Soeten's longitudinal welded specimens.	264
7.20	Prediction of failure loads and angles for the author's cruciform shaped test specimens.	267
7.21	Comparison between predicted results for the author's cruciform shaped specimens.	268
7.22	Variation in strength between tensile and shear fillet welds as penetration values increase.	269
7.23	Prediction of weld failure loads and angles for the temporary end plate connections.	274
7.24	Comparison between experimental and predicted failure loads and angles for temporary end plate connections type F.	275

LIST OF FIGURES

Figure Number	Title	Page Number
1.1	Schematic drawing of a typical MIG welding unit.	39
1.2	Basics of the MIG welding process.	39
1.3	Basics of the TIG welding process.	41
2.1	Typical heating and cooling curves for points in the HAZ of a weld.	44
2.2	Extent of HAZ pattern assumed in design.	45
2.3	A typical hardness traverse for 6082 and 7019 aluminium alloys.	46
2.4a	Rosenthal's thin 2D heat flow model.	47
2.4b	Rosenthal's thick 3D heat flow model.	48
2.5	A simplified three zone pattern of HAZ strength variation for aluminium.	49
2.6	Extent of HAZ for fillet welded joints. (a) Single fillet corner weld, (b) 'T' fillet weld, (c) Cruciform joint.	51
2.7	(a) Fillet weld profile, (b) Butt weld profile.	55
2.8	(a) to (f) Effect of basic welding variables on weld penetration.	58
2.9	Bibber's transverse lap joint.	59
2.10	Force equilibrium diagrams for welds types A and B.	62
2.11	(a) Transverse fillet weld specimen tested by Norris, (b) Stress distribution on weld leg lengths as reported by Norris.	65
2.12	Kato and Morita's suggested weld model.	69
2.13	Soeten's suggested weld model.	73

Figure Number	Title	Page Number
2.14	Kamtekar's equivalent force weld models (a) tensile fillet welds, (b) shear fillet welds.	74
2.15	Cross - sectional view of unequal leg length weld.	77
3.1	The proposed weld model for analysing tensile and shear fillet welds.	85
3.2	The actual fillet weld profile in a welded connection.	85
3.3	Notation used for stresses acting on three perpendicular planes.	87
3.4	A simple tensile fillet welded connection.	88
3.5	Geometry of tensile fillet weld abcd.	88
3.6	Equilibrium of forces on a single tensile weld.	89
3.7	The equivalent force system.	90
3.8	The normal and shear stresses on weld abcd.	90
3.9	Mohr's Circle of stresses for weld model.	91
3.10	Principal plane when $p_1 = R$.	96
3.11	Principal plane when $p_2 = 0$.	97
3.12	Principal plane when $p_3 = 2\sigma / (1 + p)$.	98
3.13	Predicted failure plane for weld taking account of any penetration value.	99
3.14	The tensile weld abdc idealised to an equivalent area weld model abde.	100
3.15	The idealised unequal weld leg length weld abde.	100
3.16	Equivalent balanced force system acting on weld ade.	101
3.17	Stresses acting on weld ade.	101
3.18	Principal plane when $p_1 = R$.	104
3.19	Predicted failure plane for weld with any amount of penetration p.	106

Figure Number	Title	Page Number
3.20	Predicted failure planes as weld penetration increases for tensile fillet welds.	108
3.21	A simple shear fillet welded connection.	110
3.22	Geometry of shear weld abcdef.	110
3.23	Shear forces acting on weld abcdef.	111
3.24	Moment $F/2(\omega - h)$ acting parallel to weld y - axis.	112
3.25	Moment $F\omega/2$ acting in the z - axis.	112
3.26	Moment $Fh/2$ acting parallel to weld y - axis.	113
3.27	The total force system acting on the longitudinal shear fillet weld abcdef.	113
3.28	The balanced force system for moment $F\omega/2$ acting parallel to the weld y - axis.	114
3.29	The replaced force system for moment $F\omega/2$ acting in the z - axis.	115
3.30	The total forces only acting on the longitudinal shear weld abcdef.	115
3.31	Stresses acting on longitudinal shear fillet weld abcdef.	116
3.32	Principle plane for when principle stress $p = 0$.	119
3.33	Predicted failure plane for longitudinal shear fillet weld.	120
4.1	Actual loading of temporary end plate connection.	124
4.2	Trapezium plate sub - divided into x number of beam elements.	124
4.3	Summation of beam elements to give actual trapezium plate shape.	125
4.4	Assumed equivalent loading of temporary end plate connection.	125
4.5	Forces on fillet welds in the temporary end plate welded connection.	126
4.6	Actual forces acting on weld abcd.	127
4.7	Vertically balanced weld abcd.	127
4.8	Vertically and horizontally balanced weld abcd.	128
4.9	Balanced forces on weld abcd, due to application of forces	

Figure Number	Title	Page Number
	($F_x + 2F.r_a$) in y-direction.	130
4.10	A second balanced force distribution diagram for weld abcd, due to the application of eccentric forces ($F_x + 2F.r_a$) in the z-axis direction.	131
5.1	Extrapolation of weld, HAZ and parent metal coupons.	142
5.2	A typical parent metal coupon taken from main parent metal sheet.	142
5.3	Typical longitudinal tensile parent, weld and HAZ coupons taken from 'V' butt welded specimen.	143
5.4	Transverse weld coupon specimen.	144
5.5	Preperation of transverse weld coupon test specimen.	145
5.6	Location of hardness traverses for butt welded specimen.	152
5.7	Typical hardness traverse along line 1 of butt welded specimen.	153
5.8	Transverse fillet welded test specimen.	156
5.9	Test welds of the transverse fillet welded specimen.	157
5.10	Demec gauge measurements and calculations for transverse fillet specimen.	159
5.11	Load vs shear distortion graphs for transverse fillet welds.	161
5.12	Longitudinal fillet welded test specimen.	164
5.13	Test welds of the longitudinal fillet welded specimen.	165
5.14	Load vs shear distortion for longitudinal fillet welds.	167
5.15	Equal, biaxially loaded cruciform test specimen.	170
5.16	General arrangement of a space frame with end plate connections.	172
5.17	A symmetrical shaped experimental end plate connection simulating the actual temporary end plate in a space frame.	173

Figure Number	Title	Page Number
5.18	Effect of tube size on weld leg length.	174
5.19	View of end plate connections and gusset plates welded onto tubular arms.	177
5.20	Rossette strain gauge layout for specimen type F.	179
5.21	Experimental test specimen type F.	180
5.22	Location of dial gauges on test specimens type F.	187
6.1	Typical finite element idealisations of continua. (a) Dam wall, (b) Folded plate.	192
6.2	Typical finite element idealisations (a) triangular elements, (b) rectangular elements.	193
6.3	Typical example of a graded mesh.	194
6.4	Typical types of finite elements available in PAFEC library.	196
6.5	Typical PAFEC data input file.	198
6.6	Ratios of plate thickness, h to length of plate L.	200
6.7	A 20 x 20 dense finite element mesh of end plate connection.	201
6.8	A 35 x 35 dense finite element mesh of end plate connection.	202
6.9	A 40 x 40 dense finite element mesh of end plate connection.	203
6.10	Maximum stresses of the end plate connection using a 20 x 20 dense FE mesh.	205
6.11	Maximum stresses of the end plate connection using a 35 x 35 dense FE mesh.	206

Figure Number	Title	Page Number
6.12	Maximum stresses of the end plate connection using a 40 x 40 dense FE mesh.	207
6.13	Maximum deflection of the end plate connection using a 20 x 20 dense FE mesh.	208
6.14	Maximum deflection of the end plate connection using a 35 x 35 dense FE mesh.	209
6.15	Maximum deflection of the end plate connection using a 40 x 40 dense FE mesh.	210
6.16	Element type 44210 used for finite element analysis.	211
6.17	PAFEC results of load vs deflection.	214
6.18	PAFEC output of stresses at points A, B and C on fixed edges of end plate, with mesh densities increasing.	215
6.19	Maximum stresses of the end plate connection for a uniform line load, using a 20 x 20 dense FE mesh .	217
6.20	Maximum stresses of the end plate connection for a uniform line load,using a 35 x 35 dense FE mesh.	218
6.21	Maximum stresses of the end plate connection for a uniform line load,using a 40 x 40 dense FE mesh.	219
7.1	Typical stress - strain curves for coupons from 6082-T6 aluminium alloy.	221
7.2	Relationship between ultimate strength and hardness for 6082-T6.	225
7.3	Graph of penetration vs tensile fillet weld failure load F.	228
7.4	Graph of penetration vs weld failure angle θ, for tensile fillet welds.	229

7.5 Graph of penetration vs length of failure plane for tensile fillet welds. 230

7.6 Graph of length of failure plane vs tensile failure load F. 231

7.7 Graph of penetration vs shear weld failure load. 250

7.8 Graph of penetration vs $Tan^{-1}\theta$, for shear fillet welds. 251

7.9 Graph of penetration vs length of shear failure plane. 252

7.10 Graph of length of shear failure plane vs failure load. 253

7.11 Effect of change in weld penetration on the strength between tensile and shear fillet welds. 270

7.12 A typical load vs deflection graph for the end plate connection. 277

7.13 A typical comparison graph of stresses along the fixed edge of the end plate connection. 278

LIST OF PLATES.

Plate Number	Title	Page Number
1.1	A typical complex, temporary space frame structure.	25
1.2	The temporary end plate space frame connection.	29
5.1	Testing arrangement of end plate test specimen type F.	184
5.2	Failure of end plate test specimen type F.	185

NOTATION.

a'	Effective weld throat.
a	Weld throat.
A	Cross - sectional area.
A'	Effective cross - sectional area.
A_2	Welding current.
A_w	Area of deposited weld metal.
e	Eccentricity of force.
F	Force.
F_u	Experimental failure load.
F_{u1}	Author's predicted weld failure load.
F_{u2}	Kamtekar's predicted weld failure load.
F_{u3}	Kato and Morita's predicted weld failure load.
F_{u4}	β-formula predicted weld failure load.
F_{u5}	BS 8118 predicted weld failure load.
h	Loading plate thickness.
H	Hardness value.
k	Horizontal leg length for unequal leg length welds.
K_A	Coefficient defining extent of zone A.
K_B	Coefficient defining extent of zone B.
K'_A	Coefficient for fixed end moment.
L_p	Length of plate.
L_ω	Length of weld.
M	Moment.

p Projected weld penetration to horizontal weld leg length.

P Weld penetration.

β_1 Principal stress 1.

β_2 Principal stress 2.

β_3 Principal stress 3.

Q/v Measured heat input.

r Extent of heat affected zone.

r_A Force coefficient in terms of r_B.

r_B Force coefficient for fixed end condition.

R Residual stress.

s Softening factor.

T Load transfer plate thickness.

T_p Peak temperature.

T_0 Initial or ambient temperature.

UTL Ultimate Tensile Load.

v Vertical leg length for unequal leg length welds.

V Arc voltage.

W Weld width.

X_A Distance from centre line of weld to outer edge of Zone A.

X_B Distance from centre line of weld to outer edge of Zone B.

α Ratio of vertical to horizontal leg length for unequal weld leg lengths.

β Experimentally derived constant.

ϕ Experimental measured weld failure angle.

ϕ_1 Author's predicted weld failure angle.

ϕ_2 Kamtekar's predicted weld failure angle.

ϕ_3 Kato and Morita's predicted weld failure angle.

ϕ_4 β-formula assumed weld failure angle.

ϕ_5 BS 8118 assumed weld failure angle.

γ_m Partial material factor for parent metal.

η Welding process efficiency.

θ Angle between horizontal weld leg length and weld sloping face.

σ Normal stress.

σ_c Comparable or critical stress.

σ_u Ultimate normal stress.

τ Shearing stress.

υ Welding speed.

ω Weld leg length.

ξ Theoretically derived constant.

CHAPTER 1 INTRODUCTION

1.1 Space frame structures.

A space frame structure may be defined as the repetative connection of a number of pre-fabricated, three dimensional frames - usually of a standard shape and size - to overcome any applied loads. The completed structure may be a simple two framed connection or a more complex one involving several thousand frames shown in plate 1.1.

Such structures offer a greater degree of freedom at the design, fabrication and construction stages, than the conventional beam and column type construction. More intricate, larger and greater spanning structures can be attempted which would otherwise not be possible. Further, the completed structures are aesthetically appealing and much more readily accepted by environmentalists and planners.

The whole space frame concept of constructing structures is a highly economical one with respect to material, labour and time savings. Individual units can be mass produced in the workshop, easily transported and readily constructed on site, even by an unskilled labour force.

Further advantages can be exploited by the use of aluminium alloys for the space frame material. These alloys are more suited for space frame structures than their counterpart steels. Aluminium alloy structures offer added economy in terms of lightness in weight

Plate 1.1 A typical complex, temporary space frame structure.

but high in strength properties, require smaller and, or simpler foundations, easier to machine, fabricate, transport, construct and most importantly are cheaper to maintain[1].

Recent years have witnessed the proliferation in the construction of space frame structures - especially those using aluminium alloys. This can be attributed to the following factors;

i) The ever increasing demand for more economic and efficient structures,

ii) The ease of accessibility of the designer to computers and associated software packages,

iii) The advancement of welding technology, especially in the field of aluminium,

iv) A greater number of todays designers are better informed on aluminium for structural uses and in welding technology.

1.1.1 Temporary space frame structures.

The confidence and knowledge acquired in the design and construction of space framed structures, has lured the more astute designers to exploit the field in temporary structures. Today, gigantic temporary aluminium space frame structures are constructed, dismantled and re-constructed, repetatively by specialist firms to perform various structural tasks. The added advantage of such a system is that only a nominal financial outlay is required.

An example of such temporary structures was the construction of a 20 metre high

'scorpion' shaped structure for a pop concert by Light and Sound International[2], which was later dismantled and re-used for another different construction project.

Another typical example is the construction of a 27 metre span semi-circular arch in Aberdeen [1]. It provides a temporary weather tight working area for the construction of accommodation units. The arch can be rolled away to enable a crane to lift the units away.

Such complex space frame structures are built up from a number of smaller pre-fabricated tubular (aluminium alloy) frames - usually of a standard shape and size. Any configuration can be achieved by the repetative connection of these frames.
Depending upon the size and shape of the overall space structure, there can be several joints connecting one frame to another. These connections have to be simple, quick and easy to connect and dismantle, and yet be able to transfer forces from one frame to another.

1.2 Structural connections in aluminium.

There are basically two main types of connections (excluding riveting) available to the designer of metal structures - either welded or bolted connections.

Welded connections achieve a more efficient and cost effective joint. They are extremely strong relative to their size. The type of joint obtained is one which is rigid, but more importantly it is permenant. With regards to aluminium connections, welding

softens zones immediately adjacent to the weld metal, which exhibit a significant loss of strength. The extent and severity of this loss has to be accounted for in design (3,4,5,6,7,8).

Bolted connections offer the advantage that they can be easily and rapidly fastened to achieve the required assembly on site - even by unskilled labour. Unlike welding, no meticulous cleaning and preperation procedures are required, and the only tool required is a hand wrench tool. This allows the fixer to reach greater heights more easily and conveniently. However, the main advantage of bolted connections is that they need not be permenant.

Structural connections used in space frames have been directed towards individual members. These have been restricted to two main group types - either the permenant welded K, L, M or N type joints for tubular frames, or the patented Triodetic tubular type systems which are based upon a bolted only type of connector system.
The temporary space frame connection put forward by this thesis is directed towards the repetative connection of aluminium space frames, plate 1.2. The connection uses both the methods - welding and bolting. Trapezoidal shaped end plates, with a circular hole for the insertion of a bolt are welded to the tubular arms of the space frame.

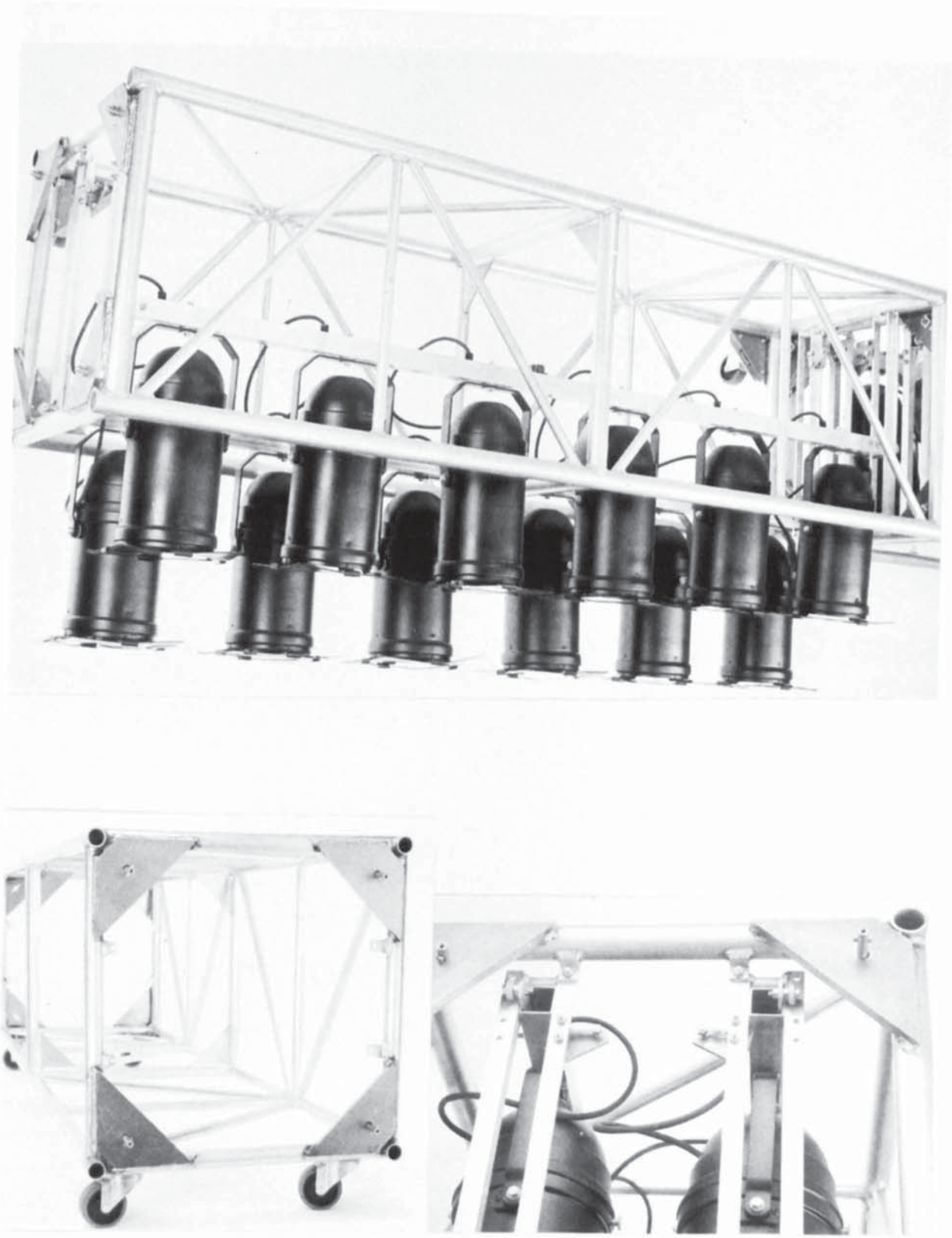

Plate 1.2 The temporary end plate space frame connection.

1.3 Weld failure criteria.

The design of welded connections is dependant upon the assumptions made during the theoretical analysis. The fewer these assumptions, the more real the theoretical analysis.

The assumptions made in the current British Codes of Practice CP 118[8], BS 5950[9] (replacing BS 449) and also by almost all other weld failure theories proposed by numerous authors, remains the same as those first proposed by Bibber[10] in 1930. The main assumption then was that welds always failed at the throat section. Experimental results conducted by independent authors, have since shown this to be incorrect and over cautious. Tensile fillet welds have been found to fail close to the weld leg length lying in the direction of the applied load. Whereas shear fillet welds have been found to fail at or near the weld throat.

Almost all theoretical weld failure criteria take the weld throat as the critical section. The reason generally given is that it leads to a simple design rule which can predict loads fairly accurately.

A recent theory published by Kamtekar[11] shows that tensile weld failure loads are very sensitive to the slightest variation in their cross-sectional area. Also experimental research by Kato and Morita[12] in 1974 showed that weld failure loads are governed by the extent of weld penetration achieved. Thus, by reference to these two authors works it would indicate that tensile weld failure loads too should be very sensitive to any changes in the extent of penetration achieved. However, many failure theories and

codes of practice fail to emphasize the importance of the extent of penetration upon weld failures. It is usually relegated to being a secondary issue. However when it is accounted for, it is normally suggested that the assumed throat failure plane be extended proportionately to indirectly account for the penetration achieved. No attempt is made to directly incorporate it into their weld model or failure analysis.

Further, all weld failure theories have been developed based on or for steel fillet welds. Little or no attention is given to aluminium alloy fillet welds. It is generally expected that aluminium fillet welds would fail similarly to steel fillet welds. However, due to the more pronounced regions of HAZ present in aluminium welded connections, and the various series of aluminium alloys and filler metals, care is required in applying any weld failure theory. Weld failure theories based upon experimental constants like the β-formula would require new experimental constants to be derived.

The design of aluminium welded connections requires the designer to be familiar with the various series of aluminium alloys, and their possible combinations with the different filler metals. An understanding of the HAZ due to welding is a necessity, if failure is required in the weld metal only.

1.4 Aluminium alloy designation.

Recent international agreement adopted a four figure alloy designation system, based upon the American system. This standardisation identifies the aluminium alloys by groups, depending upon the major alloying element. An example of the four digit designation system being 1100 or 6082. The first digit identifies the alloy series as

shown in Table 1[13].

For the series 1XXX, the last two digits specify the purity of the aluminium. For example, 1050 indicates 99.5% pure aluminium. For the series 2XXX through to 8XXX, the last two digits identify the specific alloy. The second digit indicates any modifications made to the original alloy. Examples are given in Table 1.

Aluminium alloys grouped by major alloying elements.

	Group designation	Example
Aluminium - 99.00% minimum and greater	1XXX	1100
Major alloying elements		
Copper	2XXX	2219
Manganese	3XXX	3003
Silicon	4XXX	4043
Magnesium	5XXX	5086
Magnesium and silicon	6XXX	6082
Zinc	7XXX	7005
Other elements	8XXX	
Unused series	9XXX	

Table 1.1 Aluminium alloy designation system[13].

1.4.1 Temper designations.

Four basic tempers exist for aluminium alloys. These are indicated by one of the letters 'F', 'O', 'H', and 'T'. The letter may be followed by a digit to identify the type of treatment and hardness of the alloy - examples being 5082-H32 or 6082-T6.

'F' - indicates the as fabricated condition.

'O' - designates the annealed state or softest temper.

'H' - is applicable to strain hardened alloys.

'T' - is designated to an alloy product, thermally treated to enhance hardness and other properties.

A full list of the various types of temper designations available for aluminium can be found in most aluminium data text books.

1.5 Aluminium alloys for structural applications.

Aluminium alloys can be categorised into two groups; either non-heat treatable or heat treatable.

The strength of non-heat treatable alloys is derived from cold working. The strength of the Heat Affected Zone (HAZ) in these alloys is reduced to that of the annealed strength of the alloy, irrespective of the alloys original condition. Alloys of the 1XXX, 3XXX, 4XXX, and 5XXX series fall into this category.

Heat treatable alloys derive their strength from a controlled, two stage heat treatment process. Firstly the alloy is solution heat treated. This stage involves heating the alloy uniformly, to below its eutectic melting temperature (in the 900F to 1000F range). Secondly, controlled quenching from the solution treating temperature is carried out - rapidly enough to avoid overageing. Alloys of the 2XXX. 6XXX and 7XXX series are classified into this category.

The aluminium alloys suitable to be used for structural applications are those of the series 5XXX, 6XXX and 7XXX.

1.5.1 The 5XXX series - Aluminium Magnesium Alloys.

Alloys of the 5XXX series are non-heat treatable and their strength is acquired by cold working. As with other non-heat treatable alloys, their strength in the HAZ is taken to be equal to the annealed strength of the parent metal - irrespective of the original temper condition. The chief alloying element is magnesium. A relatively high strength is achieved with good weldability.

These alloys are widely used for heavy industrial applications, examples being cranes, ship super-structures, pressure and cyrogenic vessels, and transport applications [13]. The most commonly used form is as plate and sheet metal. Because of the significant amount of magnesium content in these alloys, it makes it relatively difficult to produce complex structural sections. Thus, in practise it is not uncommon to employ these alloys for the plate work requirements of a structure, together with extruded structural sections from the 6XXX or 7XXX series alloys.

The 6XXX and 7XXX series alloys are heat treatable. Their strength is acquired by a controlled heat treatment process.

1.5.2 The 6XXX series - Aluminium Magnesium Silicon Alloys.

The alloys in this series contain magnesium and silicon, which results in the formation of magnesium silicide. It is this which makes these alloys heat treatable and is responsible for the strength exhibited by these alloys.

Their good workability accounts for the wide range of complex and thin section shapes available on the market. Also, their good weldability and high strength favours their use for a wide range of structural applications.

1.5.3 The 7XXX series - Aluminium Zinc Magnesium Alloys.

The major alloying element is zinc, up to 8% followed by a smaller percentage of magnesium.

These alloys exhibit high strength and extra hardness. They too suffer from HAZ strength reduction, when welded. But unlike other alloys from the other series, this loss of strength is recovered by a natural ageing process to full parent metal strength. Thus, the loss of strength is not permenant, but the time taken to reach full parent metal strength is about four to eight weeks. For design purposes, this loss in strength is taken to be permenant.

Like the 6XXX series alloys, these alloys also possess good workability which accounts for the wide selection of structural sections available.

Recent research within this group of alloys has seen the development of a new range of alloys - principally the 7019 alloy. These new alloys are of higher strength which can be easily welded and still maintain high mechanical properties. Robertson and Dwight [3,4] indicate that for a given weld the HAZ extends further in 7019 (plate) than it does in 6082 (plate), but the degree of softening is less severe.

Their suitability for trade and trailer components, cryogenic applications, military vehicles and structural applications are being investigated at present. Insufficient service experience is restricting their use for a wider range of applications. Nevertheless, as stated in a paper [13], given at the Aluminium Welding Seminars in America, these newer alloys may gradually take their place as highly weldable alloys in the near future.

1.6 Aluminium alloy selection.

Although a variety of aluminium alloys exist, the choice of an alloy is usually restricted to a few, when considering the engineering requirements. There are four main factors to be considered [13] ;

i) Strength,

ii) Workability,

iii) Corrosion resistance,

iv) Weldability.

No alloy exists which can offer the highest degree of all the four mentioned factors. Thus, the designer must base his choice upon the final required properties.

1.7 Filler metal selection.

For a given alloy the ultimate strength of a weld is governed by the choice of filler metal (11,12,13,14,15). The aim of the filler metal chosen should be to provide adequate weld strength and minimise crack susceptibility. More importantly, the selection of the correct filler alloy greatly influences the service life of an aluminium weldment.

The weld deposit formed is an alloy of the filler and parent metal mixture. The properties of the welded joint are dependant upon those of the alloy, which themselves are governed by the degree of dilution achieved between parent and filler metals. The degree of dilution itself being influenced by the edge preperation, edge spacing and welding techniques used. Thus a straight edge butt preperation achieves a greater dilution effect than a single-vee butt preperation.

1.8 The metal inert gas (MIG) welding process.

The Metal Inert Gas (MIG) welding process operates on a direct current, electrode positive (DCEP) polarity. It is based upon the Tungsten Inert Gas (TIG) welding process, maintaining the inert gas shielding concept. The MIG electrical equipment consists of a direct current power supply, a filler wire feeder, an electrical circuit for starting and stopping the flow of inert gas, coolant, welding current and the filler wire electrode, figures 1.1 and 1.2 (16,17,18).

The greatest advantages of this process stem from the use of extremely high welding

current densities. This is only possible because the filler wire, which acts as the current carrying electrode is consumable. The current not being limited to the melting temperature of the electrode, as in the TIG process.

1.8.1 Advantage of MIG welding.

The use of high current densities coupled with a very efficient heat transfer, results in achieving the following advantages;

i) Higher welding speeds (approximately twice those of TIG [19]) achieve faster chilling of the weld area, minimising weld distortions and the extent of HAZ [3,4]. Furthermore, faster welding speeds give MIG a lower cost per metre of finished weld, making it possible for aluminium to compete favourably against steel and other metals in many applications.

ii) Lower welding costs.

iii) Deeper penetrated welds are achieved, making this process good for fillet welds and minimising edge preperation.

iv) No flux required. This eliminates the costly process of flux removal and the possibility of postweld corrosion due to flux residue.

vi) Easily portable and readily adaptable to machine welding.

vii) It is ideally suited for welding in any position. This is important where assemblies or sub-assemblies cannot be positioned for welding.

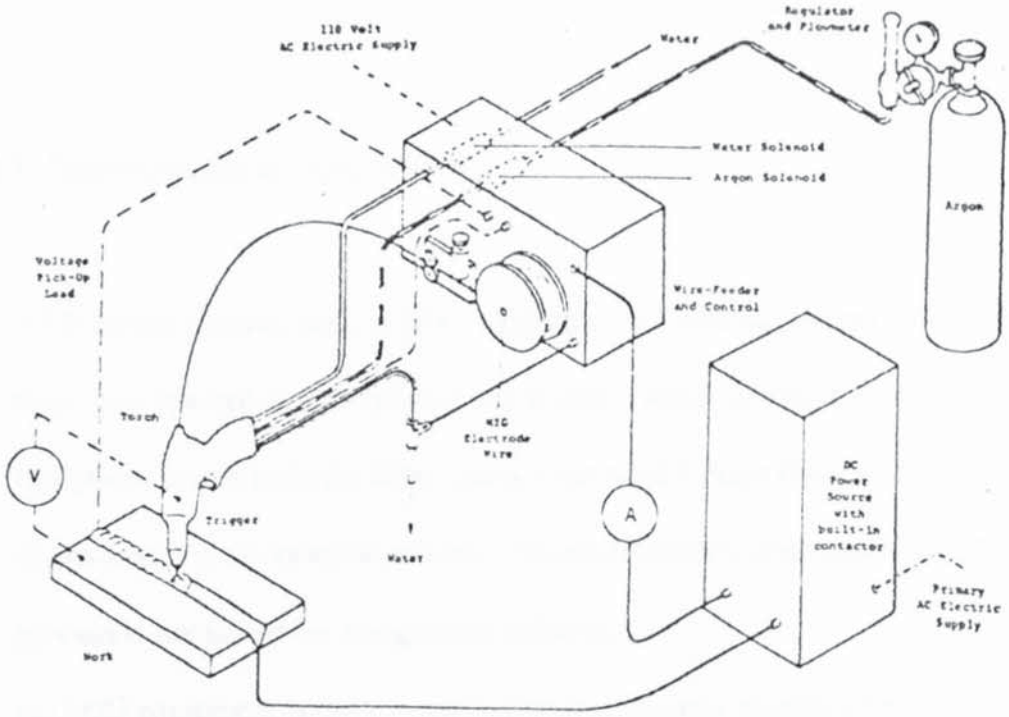

Figure 1.1 Schematic drawing of a typical MIG welding unit.

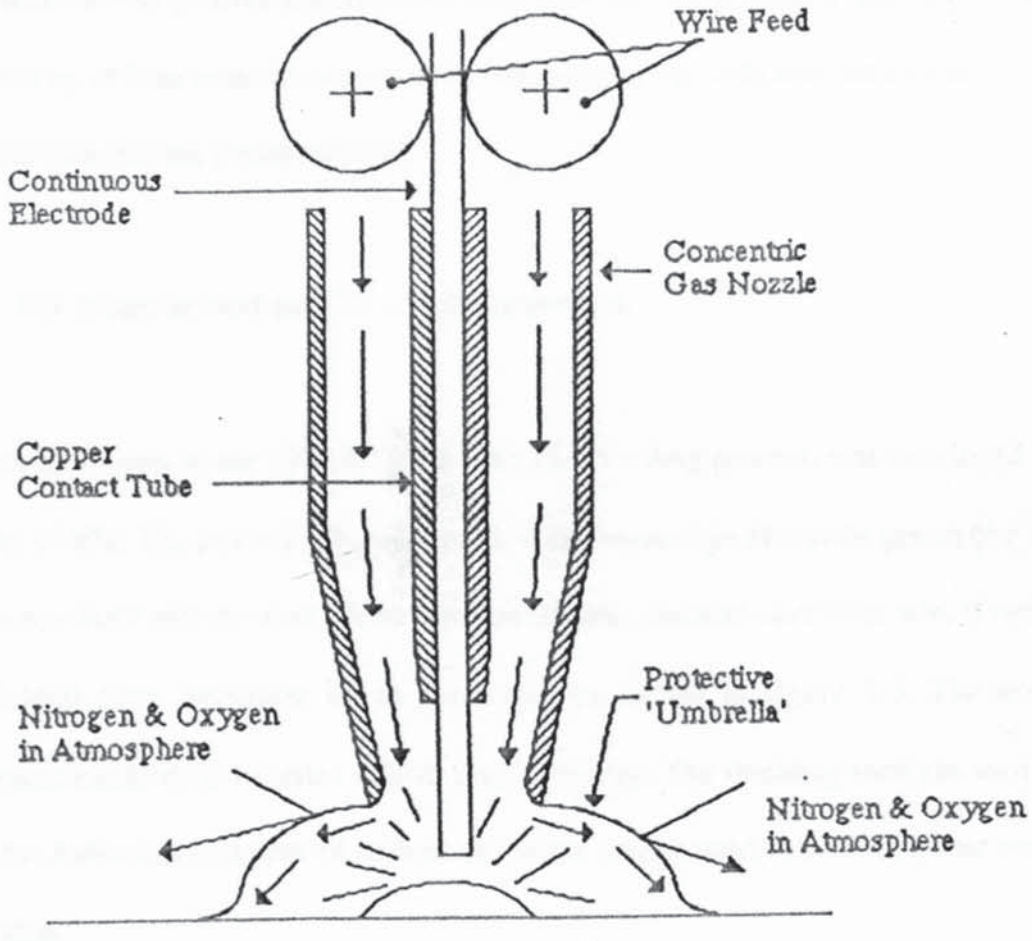

Figure 1.2 Basics of the MIG welding process

1.8.2 Disadvantages of MIG welding.

i) The major disadvantage of MIG welding is that with equipment which pushes the filler wire through, 2.4mm sheet is the thinnest which can be manually welded. equipment which pulls the filler through can weld 1.3mm sheet as the thinnest.

ii) Because it is not possible to weld without depositing filler metal, the MIG process is not suited for autogenous welding.

iii) MIG equipment is more complicated and requires greater attention to maintain than TIG equipment.

iv) When welding heavy material cold weld starts may be produced. This is because a build up of filler material occurs at the beginning of the weld with little or no penetration into the parent material.

1.9 The tungsten inert gas (TIG) welding process.

This process known as the TIG (tungsten inert gas) welding process, was developed in the early 1940's. The process is based upon a non-consumable electrode generating an arc between itself and the work piece. The weld metal, electrode and filler wire if used, are shielded from oxidation by an inert gas, as shown in figure 1.3. The non-consumable electrode is tungsten - either pure or treated. The shielding inert gas used is argon, but helium or mixtures of helium and argon can be used to achieve better weld penetration.

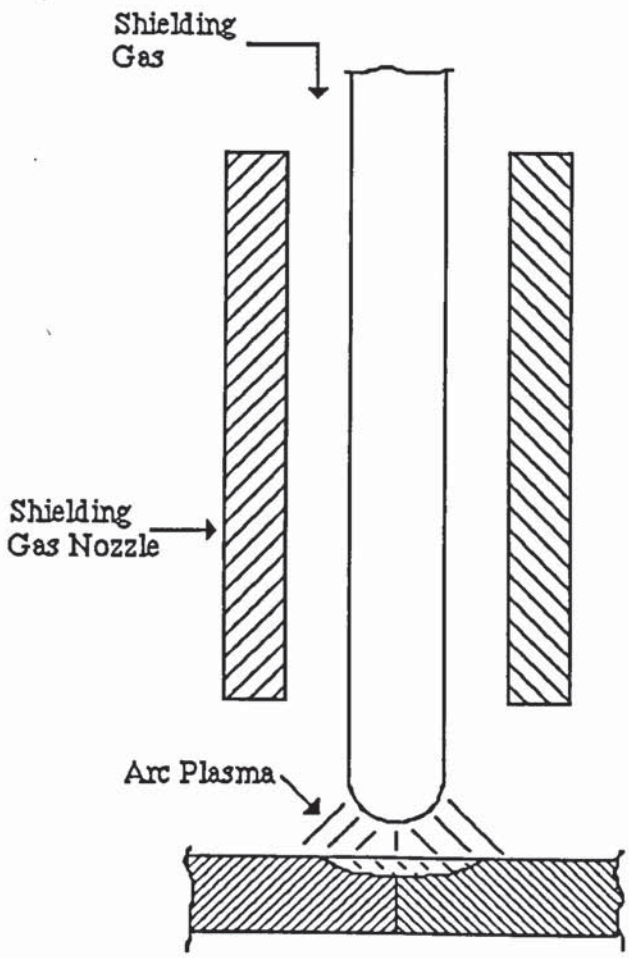

Figure 1.3 Basics of the TIG welding process.

1.9.1 Advantages of TIG welding.

In short, TIG welding is highly suited for welding thin sections of metal. The thinnest being 0.5mm and the thickest being up to 25mm, but from practical aspects the thickest recommended is 10mm [19]. This advantage stems from the fact that the heat input in TIG welding can be controlled with great ease.

Also, this process is autogenous, that is filler metal does not have to be added to

complete a weld. This is important in joints where an upturned flange is to be melted or where fusing of tightly butted edges is required. Welded joints achieved of this type are very smooth and require no cleaning or grinding.

1.9.2 Disadvantages of TIG welding.

The main disadvantage of the TIG process is that welding speeds are low and the total heat input to the joint is high. Welding speeds are half those possible with MIG and even less for materials thicker than 10mm [19]. Consequently greater heat affected zones are present. Other disadvantages are;

i) The efficiency of the weld arc is low and thus takes longer to bring the weld area up to welding temperature. This causes the surrounding metal to expand and distort when heated [19].

ii) Some transfer of molten tungsten from the electrode to the weld can occur, causing weld contamination [18].

iii) Execution of improper welding techniques can lead to exposure of the filler rod to air, which would also lead to weld contamination.

CHAPTER 2 LITERATURE REVIEW

The literature review conducted by the author is sub-divided into three main categories;

i) Heat affected zones in aluminium alloys,

ii) The weld metal profile and,

iii) Weld failure criteria.

2.1 Heat affected zones in aluminium alloys.

2.1.1 Background.

The very nature of the process of welding subjects the part of the structure being joined to extremely severe temperatures. This results in metallurgical changes to take place in regions immediately adjacent to the weld metal, and are referred to as the Heat Affected Zones (HAZ).

The severity of the temperature varies from the molten metal temperature at the weld pool to room temperature at the outer edge of the HAZ (the parent metal originally being at room temperature) as shown in figure 2.1, by Pascoe [20]

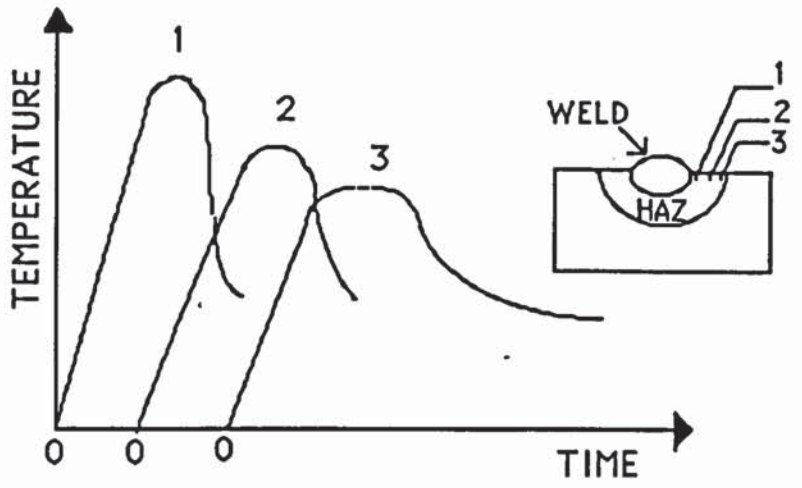

Figure 2.1 Typical heating and cooling curves for points in the HAZ of a weld[20].

The heat affected zone in aluminium alloys exhibits a significant loss in strength compared to that of the parent metal. The extent and severity of this HAZ has to be accounted for in design. However, a very little and scarce amount of research has been available to the designer. It has thus normally been approximated by the basic model shown in figure 2.2, based upon a well known 'one inch rule' which originated from the USA, as reported by Robertson and Dwight [3]. It is assumed that immediately adjacent to the weld metal, there is a uniform softened zone, followed by a sudden jump to full parent metal strength. In practice the true variation of the softened zone from the weld metal is shown by the hardness traverses highlighted in figure 2.3

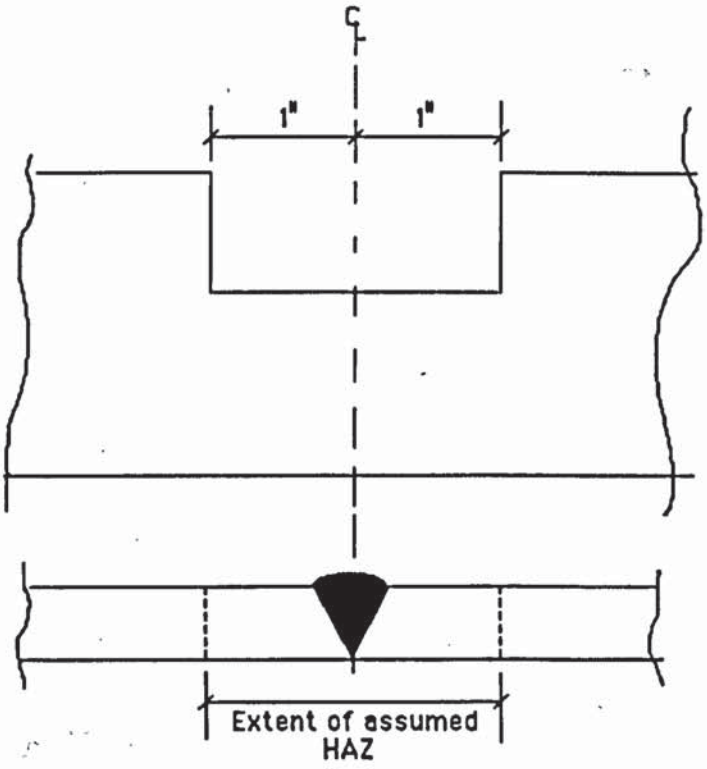

Figure 2.2 Extent of HAZ pattern assumed in design.

The loss of strength can be regained in non-heat treatable alloys by work hardening and in heat treatable alloys by solution heat treating and ageing. Although this would be a most desirable measure to take for a welded assembly, it is found to be uneconomical and impractical, as underlined at an Aluminium Welding Seminar [21], because of the following factors;

--the costs involved in heat treating,

--the size of the furnace required and,

--the resultant distortion which occurs primarily due to the rapid cold water quench in solution heat treating.

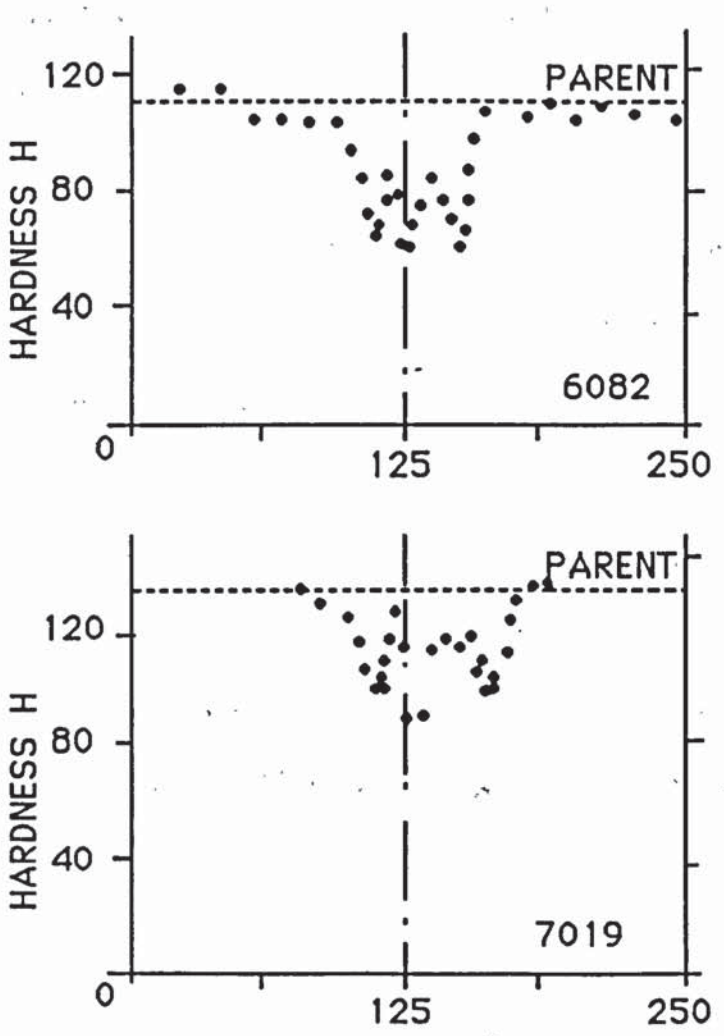

Figure 2.3 **A typical hardness traverse for 6082 and 7019 aluminium alloys[3,4].**

Recent research conducted by Robertson and Dwight [3,4] on the severity and extent of HAZ softening at welds, made by the mechanised Metal Inert Gas (MIG) process in 6082 and 7019 alloys, has drawn attention to the following two important points;

i) For multi-pass welds and successive welds laid in close proximity, the extent and severity of the loss of strength in the heat affected zone (HAZ) is dependant upon

the thermal control exercised. They recommend that the metal should be allowed to cool fully between the laying of successive weld passes.

ii) A weld laid in close proximity to a free edge leads to a greater amount of softening compared to one laid on a wider plate. This also applies to welds laid on members whose total cross- sectional area is small.

From experimental results Robertson and Dwight have developed equations to calculate the extent and severity of the HAZ in aluminium alloys 6082 and 7019 plates - for both thick and thin plate types. The plates are classified as thick or thin depending upon whether the 2D or 3D Rosenthal[22] heat flow model is applicable figures 2.4a and 2.4b.

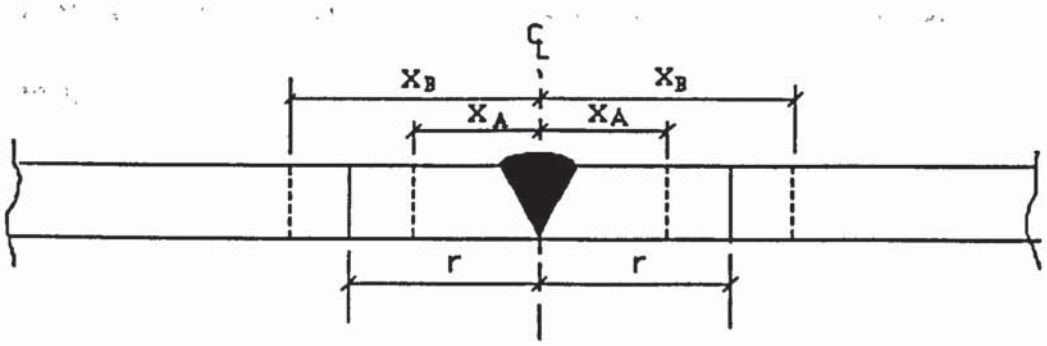

Figure 2.4a Rosenthal's Thin 2D heat flow model.

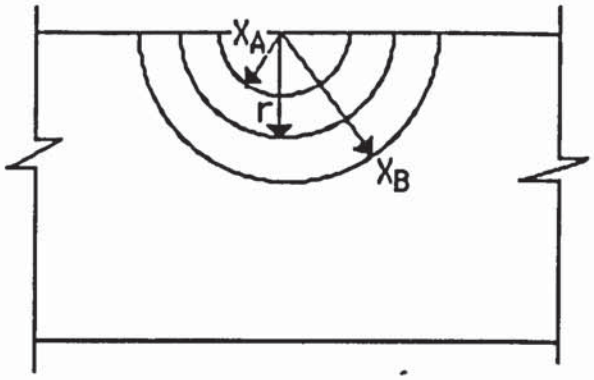

Figure 2.4b Rosenthal's Thick 3D heat flow model.

The severity of the HAZ is investigated employing Rosenthal's heat conduction equations, which enable temperature - time variations to be calculated for a moving point heat source.

Two possible cases are considered;

a) 2D or 'thin' case - where the point source moves along a thin sheet of infinite area,

b) 3D or 'thick' case - where the point source moves along the surface of a semi-infinite continuum.

The extent of the HAZ investigated by Robertson and Dwight is based on a model originally defined by Kelsey[23] and shown in figure 2.5.

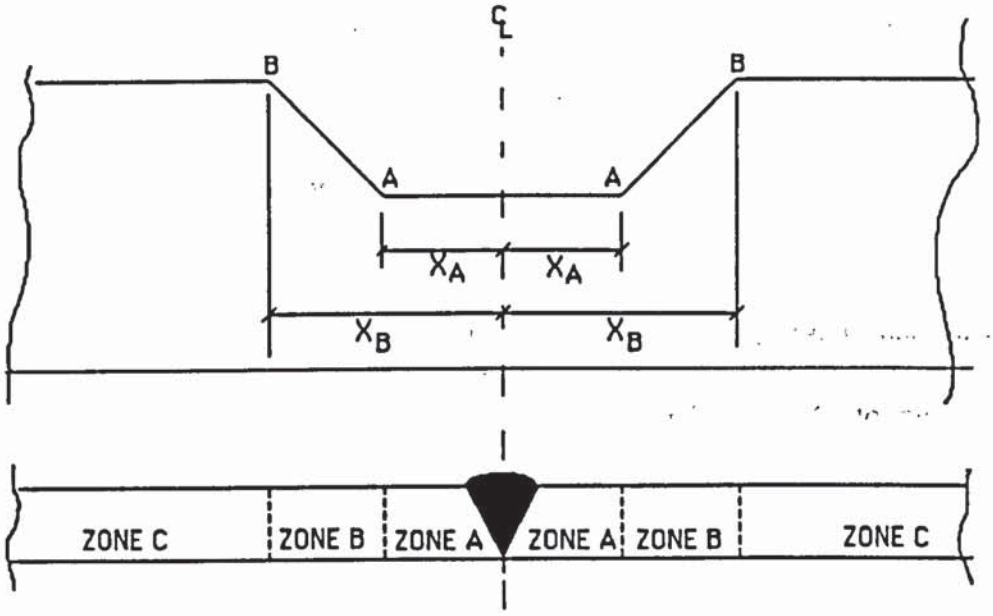

Figure 2.5 A simplified three zone pattern of HAZ strength variation for aluminium.

The three distinct zones defined by this model are;

Zone A - where the metal is assumed to be uniformly weakened.

Zone B - where there is a linear variation in properties from the HAZ to full parent metal value.

Zone C - full parent metal strength.

2.1.2 The extent of the HAZ for thin plates.

With reference to the model shown in figure 2.4a, Robertson and Dwight[3,4] propose that for design purposes, the extent of the HAZ, r, can be calculated by;

$$r = \frac{X_A + X_B}{2} \qquad \text{Equation 2.1}$$

where X_A and X_B are defined on the model , X_A being the distance from the centre line of the weld to the outer edge of Zone A. and X_B being the distance from the centre line of weld to the outer edge of Zone B.

From hardness surveys on single pass bead on plate and butt welded specimen, Robertson and Dwight found a linear relationship to exist for X_A and X_B to the weld deposit area A_w and plate thickness d, by equations 2.2 and 2.3;

$$X_A = K_A (A_w/d) \qquad \text{Equation 2.2}$$

$$X_B = K_B (A_w/d) \qquad \text{Equation 2.3}$$

where for 6082 alloy $K_A = 3.0$, $K_B = 6.6$,

and for 7019 alloy $K_A = 5.8$, $K_B = 8.0$.

Thus defining the extent of the HAZ from equation 2.1 as;

for alloy 6082 $r = 4.8 (A_w/d)$ Equation 2.4

for alloy 7019 $r = 6.9 (A_w/d)$ Equation 2.5

Robertson and Dwight state that these equations 2.4 and 2.5 can also be used to estimate the extent of the HAZ for fillet welds, provided account is taken of the number of heat paths available at the time of laying any weld.

For a single fillet corner weld, the value of r is as given by equations 2.4 and 2.5.

For a 'T' fillet joint, figure 2.6, assuming thermal control is exercised, the value of r is taken to be two-thirds that given by equations 2.4 and 2.5, depending upon whether three or four heat paths are available at the time of laying any weld.

For these estimations no account is taken of the member thicknesses. Also, the extent of the HAZ in two different thickness members is assumed to be equal to that of equal thickness members.

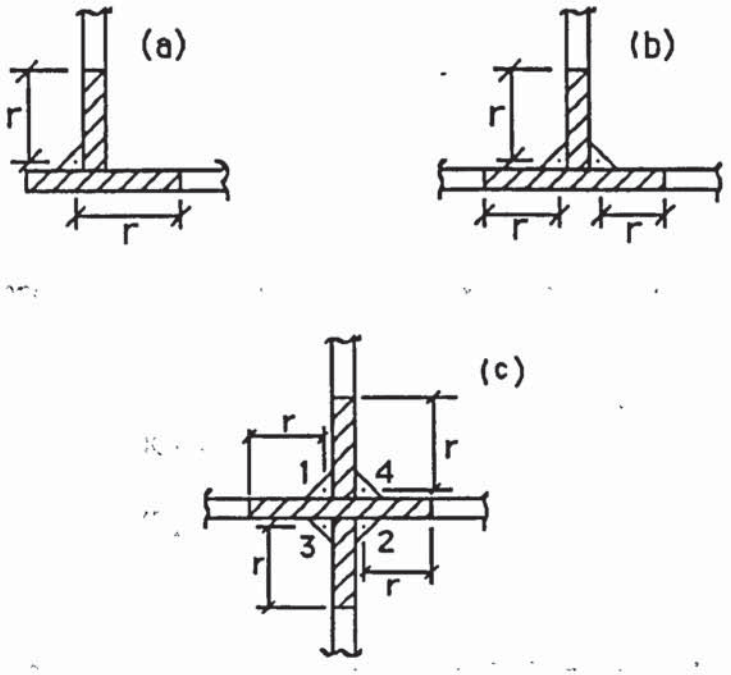

Figure 2.6 Extent of HAZ for fillet welded joints[3,4]. (a) Single fillet corner weld, (b) 'T' fillet weld, (c) Cruciform joint.

2.1.2.1 Extent of the HAZ r for thick plates.

Thick plates are those where Rosenthal's 3D heat flow model is applicable. According to Robertson and Dwight, this 'thick' treatment may be applied to multi-pass welded plates in thicknesses exceeding about 25mm.

The extent of the HAZ, r, is calculated from Rosenthal's 3D heat flow model which

relates the peak temperature attained during welding T_p, at a now radial distance from the centre line of the weld, given by equation 2.6;

$$T_p - T_0 = \frac{96\,Q/v}{x^2} \qquad \text{Equation 2.6}$$

Robertson and Dwight assume an initial temperature $T_0 = 20^0C$ and then propose constants K_A and K_B for equations 2.2 and 2.3 be taken as follows;

for alloy 6082 $K_A = 1.7$, $K_B = 2.6$

and for alloy 7019 $K_A = 2.4$, $K_B = 2.6$

Then by taking $A_w = 40mm^2$, which according to Robertson and Dwight is a practical area for the largest weld deposit, values of X_A and X_B are calculated. The extent, r ,is then selected to make the assumed HAZ area equal to the area of Zone A plus half that of Zone B, given by equation 2.7.

$$r = \{\, 0.5(X_A^2 + X_B^2) \,\}^{1/2} \qquad \text{Equation 2.7}$$

where r is now a radial distance.

2.1.3 Multi-pass welds.

The extent and severity of the HAZ for multi-pass welds, have normally been calculated as for single pass welds. However, Robertson and Dwight recommend that where thermal control is excercised, the extent of the HAZ should be approximated by drawing a tangent at a perpendicular distance, r, from the prepared surface. Each weld pass having its own "zone of influence" of radius r.

2.1.4 Extent of the HAZ when no thermal control is exercised.

If no thermal control is exercised on laying a weld, then Robertson and Dwight, recommend the values of X_A, X_B, and r, should be modified. They suggest multiplying them by an appropriate factor F, depending upon whether a thick or thin plate is being considered. The increase of the parent metal temperature (due to no thermal control), would increase the size of the HAZ. The factor F is recommended so as a more 'real' value of the HAZ may be obtained.

For thin plates; $$\text{Factor } F = \frac{T_p - 20}{T_p - T_0}$$ Equation 2.8

For thick plates; $$\text{Factor } F = \left[(T_p - 20) / (T_p - T_0) \right]^{1/2}$$ Equation 2.9

2.1.5 Severity of softening in the HAZ.

Robertson and Dwight also investigated into the severity of softening of the HAZ in 6082 and 7019 alloys. They suggest severity be expressed as a softening factor S, which is defined by the ratio;

$$S = \frac{\text{HAZ strength}}{\text{Parent metal strength}} \qquad \text{Equation 2.10}$$

They also recommend this ratio S, be related to the tensile properties rather than be based upon a hardness ratio between the HAZ and parent metal. Typical values of S are found to be

S = 0.50 for 6082 alloy and,

S = 0.75 for 7019 alloy.

2.2.0 The weld metal profile.

The weld metal profile is defined by the weld penetration and weld width, as seen in figure 2.7.

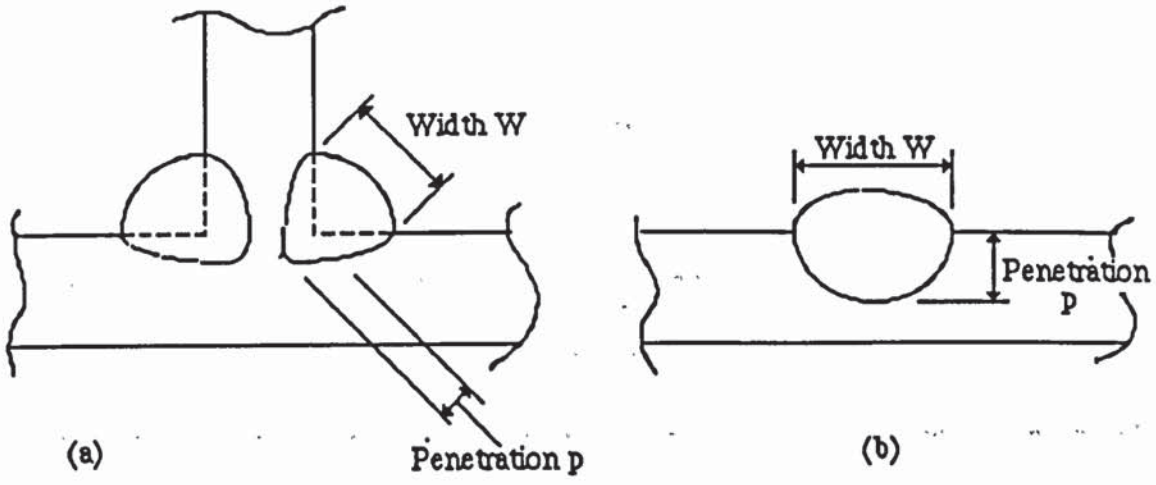

Figure 2.7 (a) Fillet weld profile, (b) Butt weld profile.

Weld penetration (p) can be defined as the extent of weld metal present below the joined parent metal surface, measured on the torch angle plane. The weld width (w) is the geometrical plan distance of the weld metal. Both weld penetration and width are primarily a function of the rate of energy input to the workpiece.

From the literature survey conducted, the author found a very scarce amount of literature available on extent of weld penetration or weld widths. The only relevant literature cited was that of Smith[24], who refers to data produced by himself and Newman[25] which substantiates the value of penetration 'p' beyond the root. Although this work is based upon steel welds layed using CO_2 welding techniques, the author suggests these results would be equally relevant to any other welding technique and material used. Smith and Newman found that for a fillet joint (for 12.5mm plate) welded by the CO_2 welding process at standard conditions of;

Curent = 350Amps,

Arc voltage = 33Volts,

Welding speed = 625mm/min.,

Electrode extension = 22mm and,

Diameter of wire = 1.56mm,

The weld leg lengths are primarily dependant upon the chosen welding speed and arc voltage. The arc voltage is reported to be easily fixed and controlled. The most important parameter to affect weld leg length values was found to be the welding speed. Smith and Newman noted that decreases in welding speeds gave an increase in leg length and penetration values. They established a relationship between penetration (p) and leg length (ω) to be;

$p = 0.3\omega$, for speeds of 250 to 750mm/min. It is recommended by Smith that for design purposes fillet weld leg length values, should be taken as ;

1.3 times the nominal leg length value (ω) and the throat dimension as ; $0.7(1.3\omega) = 0.91\omega$. It is also suggested that a 25 percent reduction be made for fully automatic spray type welding conditions and a 15 percent reduction for semi-automatic welding.

The variables which dictate weld penetration and width are;

a) arc voltage V,

b) current A_2 ,

c) welding speed v,

d) torch angle,

e) electrode extension,

f) initial workpiece temperature T_0,

g) thermal diffusivity of the workpiece metal and,

h) the workpiece's end profile.

The relationship of these important variables to penetration are shown by Smith[25] in figures 2.8a to 2.8f for bead on 25mm thick mild steel plate.

The most important relationship is that shown by figure 2.8b, where penetration is seen to be more sharply affected by welding current values than the arc voltage values figure 2.8a.

Increased welding speeds reduce penetration as seen in figure 2.8c. This largely due to the reduction of the rate of energy input, resulting in the failure to achieve a greater depth of melting of the workpiece, otherwise known as penetration.

Further, parameters effecting welding current are also capable of effecting penetration. This is highlighted by figure 2.8f, where a loss of penetration is observed as the electrode extension increases - which itself is related to current. A point made by Smith is that if an over-size contact tube is used, it would permit the current pick up point to move up inside the bore of the tube, which would be an 'effective' extension of the electrode. Also any wire feed fluctuations while depositing long lengths of weld would also affect penetration values.

The welding torch angle is recommended to be held at 10 to 20 degrees to the vertical, by Smith. The importance of this is illustrated by him in figure 2.8d. Any torch angle

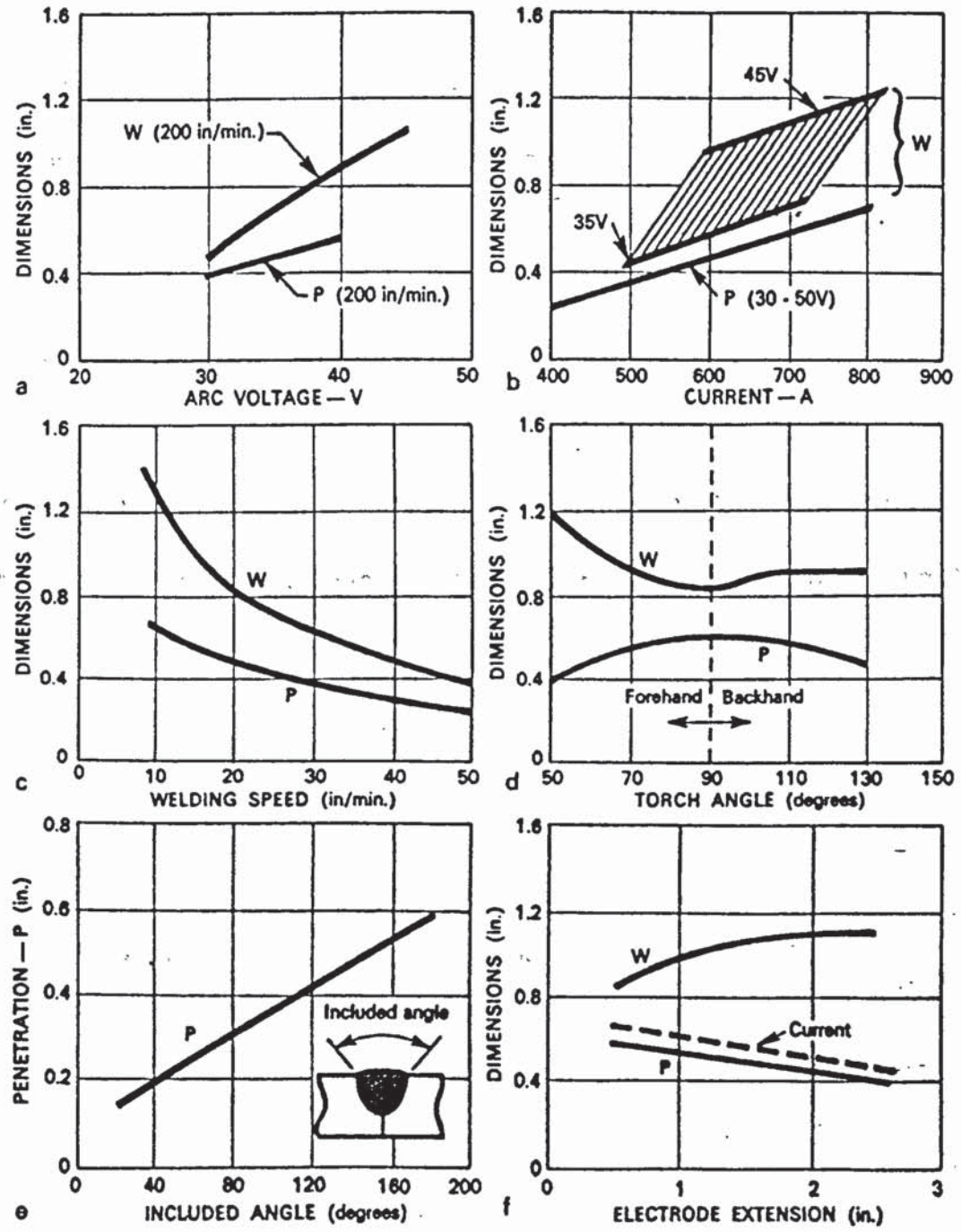

Figures 2.8 (a) to (f) **Effect of basic welding variables on weld penetration [25].**

variation to the extremes of 40 degrees from the vertical has little effect on penetration, with maximum obtained in the vertical position.

BS4870, Parts 1 and 2[26,27] stipulates a limit on the maximum extent of penetration - known as excess penetration - to be $h \leq 3mm$, where h is the height of the excess penetration.

2.3.0 Weld failure criteria.

The first theoretical weld analysis was carried out by Bibber[10] in 1930. This was based on a simple lap, steel transverse fillet welded connection, shown in figure 2.9.

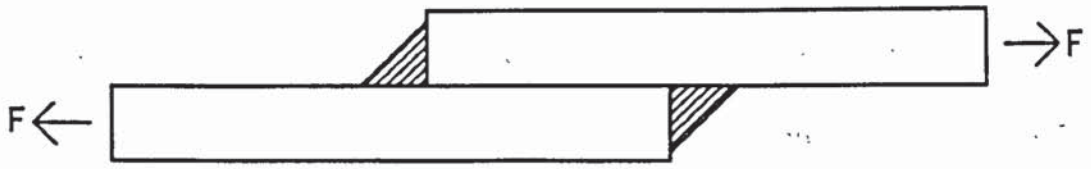

Figure 2.9 Bibber's transverse lap joint.

Bibber was interested in determining where the critical section of the connection lay. He assumed a uniform stress distribution acts on the weld, and took no account of the load eccentricity inherent to his connection and the fillet welds. Further, welds in tension were assumed to have the same strength as welds in compression.

Bibber reported the weld throat as being the critical section for welds of equal leg lengths. Further, failure would occur due to only tensile stresses on the throat. The

failure plane for such welds has since been shown to vary[15,28,29,30]. Bibber's further analysis on fillet welds with unequal weld leg lengths, showed that the critical plane could change from the throat to either the parallel or transverse weld leg length of the fillet, depending upon the ratio of the leg lengths.

An analysis of the weld profile was also conducted by Bibber. This revealed that a concave shaped weld profile reduced the strength of the weld and ensured the weld throat, as the critical section. A convex weld profile showed an increase in weld strength, to a point at which the weld leg length became the critical section.

Later in the same year, Schuster[31] conducted a similar weld analysis to Bibber's. Although in his analysis, Schuster highlighted the signifance of the fillet weld root in relation to weld penetration and stress concentrations, he could not offer an alternative method of solution to Bibbers. However, his suggested approach is a more refined solution than Bibbers.

Schuster assumed that a uniform load acted along the critical plane, which he stipulated need not be the throat. The uniformity assumption was justified with the suggestion that the stress distribution would become more or less uniform when the weld became plastic just prior to failure.

The load eccentricity inherent to the connection and fillet weld was neglected. However, the fillet weld was assumed to be subjected to both tensile and shear stresses. The finding based on these assumptions was that failure occured at an angle of

41.5 degrees from the horizontal leg length along the direction of the applied load. Schuster suggested that because this was close to the throat, the critical plane could be taken to be the throat.

In 1932, Freeman[32] conducted tests on full size welded specimen. Longitudinal, side and transverse fillet welds were tested under both tensile and compressive loads. These tests involved varying the weld lengths, thicknesses and plate widths, to establish a relationship to the weld strength. However, due to insufficient results no firm conclusions were made. Only a confusing relationship was indicated by Freeman. This was that a reduction in strength of the weld occured as the fillet length increased.

Later in 1934, Jensen[33] proposed improved experimental techniques in preparing fillet welded connections. This important contribution - which was later adopted by most authors - involved having run-on and run-off plates, for all test specimen. This ensured good consistency in the welds tested and the results obtained. Jensen also developed a new type of test specimen, which made it possible to vary the forces applied to the legs of the weld. Up till now only lap welds had been investigated.

Jensen also investigated into the location of the failure plane, and compared his findings with Bibber's[9] and Schuster's[31]. Jensen criticised the assumption that the throat of the weld should be taken as the critical section, as suggested by the aforesaid authors. Jensen proposed that consideration should be given to the angle of the resultant load on the throat or any other plane. He also found that because these methods were simplistic, they underestimated the weld strength by approximately 37 percent, when using the

ultimate shear strength of the weld instead of safe working stresses.

Jensen went on to further Schuster's[31] work, by combining both the tensile and shear stresses acting on the critical plane, using the principal stress theory. However, for this he assumed that the weld in a type A specimen, figure 2.10, would be predominantly in shear and that of type B, figure 2.10, would be predominantly in tension. The couples from eccentricity of forces, were assumed to either cancel each other in type B connection or be insignificant in type A connection.

Jensen predicted the ultimate strength of the welds with varying ratios of the forces applied to the weld leg lengths, using the maximum shear stress criterion. The value of the ultimate shear strength was obtained from control tests. Even though Jensen suggested that weld type B was predominantly in tension, he applied the maximum shear stress criterion to predict failure.

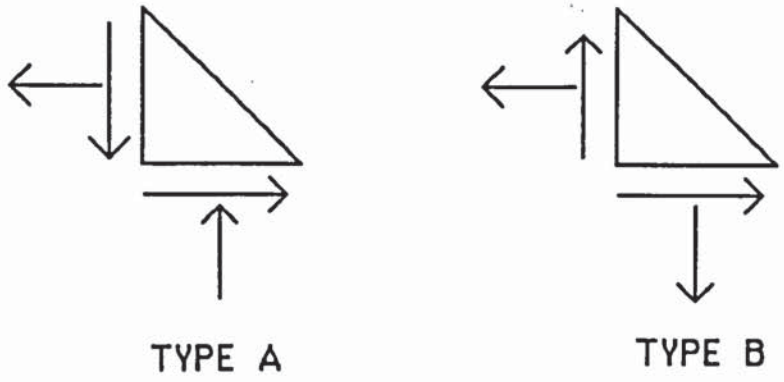

Figure 2.10 Force equilibrium diagrams for welds types A and B.

Jensen conducted a comparison of the actual failure planes with the planes of maximum shear stress and maximum principal stress. This comparison was presented pictorially and actual failure plane angles were not quoted.

For the type A welds, Jensen found a good correlation existed between the actual and predicted weld strength. Also, a resonably close result was seen to exist between the actual failure plane and the maximum shear stress plane. Further, these planes were shown to be approximately at the throat.

For type B welds, Jensen found a poor comparison between the actual and predicted weld strength for low values of F_x/F_y. Also the maximum principal stress plane bore little relationship to the actual failure planes, which were well away from the throat.

Jensen has clearly shown that the failure plane is not at the throat of the weld and fails to use this finding for his results. Further, he has also shown that welds of type A and B do not behave in the same way. Type B were found to be approximately 40 percent stronger than type A welds.

Schreiner[34] in 1935, conducted experimental tests on longitudinal fillet welds of lapped specimen, under pure bending and under bending and shear. These showed that when there was no plate bearing, the neutral axis passed through the centroid of the weld. Also, the failure stress distribution was rectangular and not triangular.

In 1936, Jennings[35] was the first to show an interest in residual stresses. He recommended rigid joints be eliminated as much as possible in order to prevent the development of excessive residual stresses. Jennings also assumes the failure plane for fillet welds to lie at the throat of the weld. An important acknowledgement was made by Jennings with regards to load eccentricities. He felt that the moment due to load eccentricities contributed significantly to weld failure and that account should be taken

in any strength predictions. Jennings suggested the bending moment is of magnitude Fh/4, giving a rectangular distribution at failure.

In 1938, Jensen and Crispen[36] investigated the stress distribution along the weld of a simple longitudinal welded connection with plate bearing, under combined bending and shear. Jensen and Crispen also investigated the contemporary theories of Shedd[37] and Schreiner[34]. Shedd's theory was directed towards repetitive loadings producing elastic rather than plastic stresses.

In 1945, Norris[38] established the stress distribution in fillet welds by photoelastic methods. However his attempts to solve the problem of the theory of elasticity were unsuccessful. Norris reported the stress distribution along the weld leg lengths AB and BC of the welded connection, in figure 2.11(a). The approximate graph of his results is shown in figure 2.11(b).

It was not until 1951 that Koenigsberger[39] presented his idea for a limit state design for welded connections. He proposed determining working loads for welded connections by first establishing the weld stresses in the plastic state, just prior to failure and then applying a load factor. Koenigsberger assumed the weld as being in a fully plastic state immediately prior to failure. This was a similar suggestion to Schreiner's[30].

Koenigsberger's was directed towards the analysis of brackets subjected to torsion and shear.

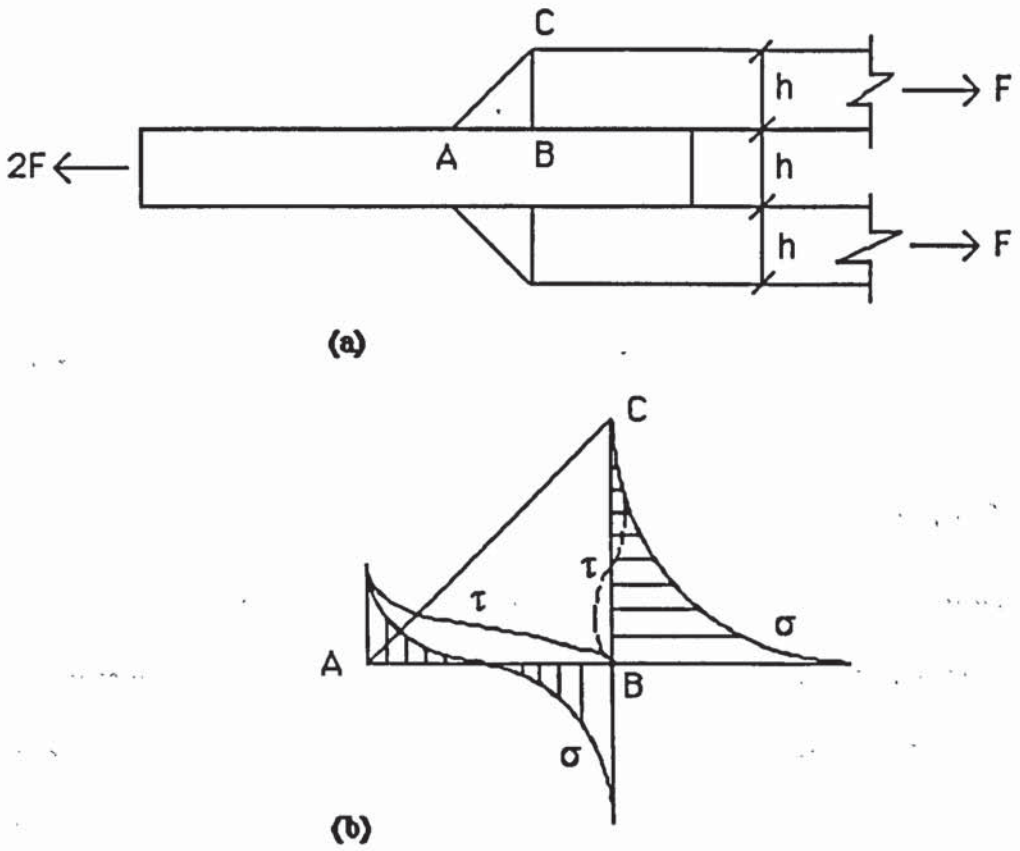

Figure 2.11 (a) Transverse fillet weld specimen tested by Norris.

(b) Stress distribution on weld leg lengths as reported by Norris [38].

Vreedenburgh[40] analysed all contemporary limiting stress theories in 1954. He compared them with his own results and others and found none of them compatible. He went on to propose an empirical solution based upon his experimental limit shape curve.

In 1959, Archer et al[41] investigated experimentally, the combined effects of shear force and bending moment on fillet welds. These tests were conducted on column bracket type specimen. They found the failure angle of the welds was always below 45 degrees and that this angle decreased with an increase in eccentricity. An empirical

maximum shear stress criterion was proposed;

$$\text{Maximum shear stress} = 0.5.\left[(0.7\sigma_b^2 + 4\,\tau^2)\right]^{1/2} \qquad \text{Equation 2.11}$$

where σ_b = normal stress due to bending at extreme fibre,

and τ = shear stress due to vertical shear load.

Comission XV of the International Institution of Welding (IIW) [42] in 1964, published their member countries views on welded connections. An approved formula was presented, to analyse welded connections subjected to static loads. This was based upon Van der Eb's approved criterion at the ISO/TC44 meeting in Helsinki in 1961. The criterion proposed was;

$$\sigma_c = \sigma_1^2 + 1.8\,(\tau_1^2 + \tau_{II}^2) \qquad \text{Equation 2.12}$$

where σ_c is the critical stress and σ_1,τ_1 and τ_{II} are the normal and shear stresses acting on the throat section. Stresses were assumed to be uniformly distributed. Failure was assumed to occur at the weld throat.

Higgins and Preece[28] published their findings in 1968, for one hundred and sixty-eight lapped fillet specimen. These included both longitudinal and transverse fillet welds, with various weld size, base metal and electrodes used. All welds were machined in length to account for run on and run off welding effects. No machining of the weld profile was made.

Higgins and Preece detected no change in the weld metal strength when combined with incompatible base metals. Further, they observed that for longitudinal fillet welds the failure plane was generally at an angle less than 45 degrees to the plane of the weld leg length. For transverse fillet welds the failure plane was even closer to the plane of the weld leg length. The weld leg length from which the failure angles were observed, was the one lying parallel to the applied load. Higgins and Preece went on to establish safe working stresses for the throat of the weld. No differentiation is made between transverse and longitudinal fillet welds.

In 1971 Clark[43] reviewed the various criteria - used at home and abroad - estimating the strength of fillet welded connections. He commented that generally, relatively high load factors were being used against failure. All rules led to safe designs for welds, although the proposed factors of safety varied. Clark went on to propose his own design method for brackets subjected to a torsional moment and shear force. This method of analysis was similar to that of Koenisberger's[39].

Douwen and Wittenven[44] in 1966, presented a criterion based upon the results of six hundred and twenty tests. These were conducted at the Steven Laboratories of the Delft Technological University. The criterion incorporated a factor, β , into the Von Mises equation, shown in equation 2.13;

$$\sigma_c = \beta \sqrt{\sigma_I^2 + 3(\tau_I^2 + \tau_{II}^2)} \leq \sigma_d \quad \text{Equation 2.13}$$

σ_c is the equivalent or comparative stress.

$\sigma_{\perp}$, $\tau_{\perp}$ and $\tau_{\parallel}$ are the normal and shear stresses on the throat section.

β is an experimentally derived constant. It is calculated by comparing the ultimate strength of fillet welds to the ultimate strength of the corresponding weld metal.

σ_d is the design stress.

This criterion was recommended for guideline use by the Comission XV of the International Institute of Welding, in 1975. It was later adopted by the International Standards Organisation (ISO).

In 1973 Kato and Morita[29] conducted experimental tests to investigate the strength of fillet welded joints. These results were later published by the International Institute of Welding.

From their tests, Kato and Morita concluded that the factors which influenced the ultimate strength of fillet welded joints were;

a) the tensile strength of the weld metal,

b) the extent of weld penetration achieved,

c) the dimensions of the fillet weld and,

d) the deformation capacity of the fillet weld.

They went on to suggest that weld penetration could be indirectly accounted into weld failure theories. They proposed that 'effective' throat lengths could and should be used, rather than the actual throat lengths. These 'effective' lengths are proposed to be calculated using equation 2.14;

$$a' = a + p/\sqrt{2} \qquad \text{Equation 2.14}$$

where a' = effective throat length,

a = actual throat length,

p = extent of horizontal weld penetration as seen in figure 2.12.

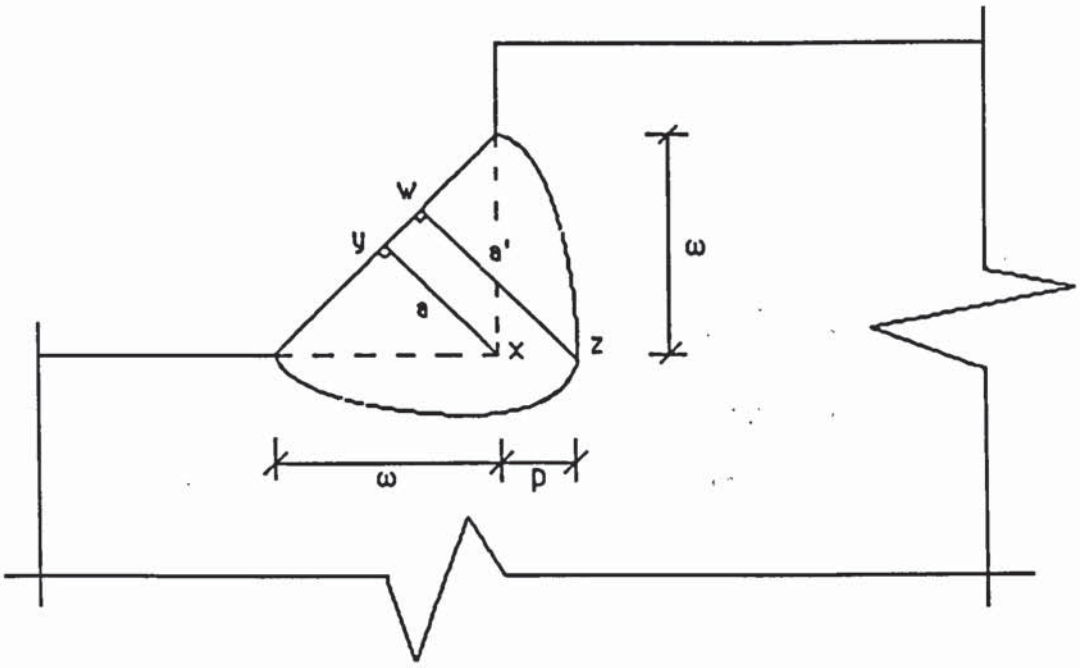

$$a' = \frac{p}{\sqrt{2}} + a$$

$$A' = \Sigma a' l_{\omega}$$

Figure 2.12 Kato and Morita's suggested weld model.

By this suggested approach the effective throat is 'pushed' up from the horizontal leg length and is always at a distance of $p/\sqrt{2}$ from the throat length xy, shown in figure 2.12.

In 1974, Kato and Morita [12] published their approximate theory, to predict the failure

of transverse and longitudinal fillet welds. It was based upon the theory of elasticity, assuming that;

a) stresses on the face of a weld are uniformly distributed,

b) the pattern of elastic stress distribution remains the same until failure of the weld occurs and,

c) failure occurs when the maximum shear stress $\tau_{max} = \sigma_T/\sqrt{3}$, where σ_T is the ultimate tensile strength of the weld metal.

Kato and Morita's theory predicts the maximum strength of equal leg length transverse fillet welds to occur when $\theta = 22.5^0$, where θ is the angle of failure measured from the horizontal leg length, parallel to the direction of the applied load. The maximum strength of transverse fillet welds is given by equation 2.15;

$$T_{T\,max} = \frac{(1 - \pi/4)\,.\,\sigma_u\,.\,\omega\,.\,L_\omega}{\sin^2\pi/8\,.\,\sqrt{6}}$$

giving

$$T_{T\,max} = \frac{1.46\,.\,\sigma_u\,.\,\omega\,.\,L_\omega}{\sqrt{6}} \qquad \text{Equation 2.15}$$

For longitudinal fillet welds, Kato and Morita's theory predicts the weld throat as the failure plane. The maximum strength of the longitudinal fillet welds is given by equation 2.16;

$$T_{L\,max} = \frac{\sigma_u\,.\,\omega\,.\,L_\omega}{\sqrt{6}} \qquad \text{Equation 2.16}$$

Kato and Morita's theory represented a landmark for all previous weld failure theories. For the first time a theory analytically predicted not only the failure load, but also where the actual failure plane occurred. Different failure planes were predicted for transverse and longitudinal fillet welds. The weld throat was shown not to be the failure plane for transverse fillet welds and that it actually lay at 22.5^0 from the horizontal leg length. For longitudinal fillet welds, the throat was predicted as the failure plane. Such distinction had never previously been theoretically substantiated, although it had been observed and acknowledged by numerous authors[10,28,43,44] in the past.

Kato and Morita were also the first to indirectly account for weld penetration in their failure theory. This was achieved by their suggestion that effective throat values be used instead of actual throat lengths. These lengths were calculated from equation 2.14, and shown in figure 2.12.

Kato and Morita compared their proposed theory with experimental data obtained from simple fillet welded connections in 1973[29], by themselves. Their theory showed good agreement with the experimental failure loads. However, Kato and Morita neither recorded nor compared their experimental failure planes to their theoretical predictions.

In May 1982, Soetens[5,6,14,30] conducted experimental tests on simple tensile and shear fillet welded aluminium connections. The principal objective of Soetens experimental tests was to determine the suitability of the β-formula for aluminium welded connections. Thus, although Soeten's work was quite intense in its own right it was directed towards determining the β-values for fillet welds of varying combinations

of aluminium alloys and filler metals.

For the welded connections, it appears Soetens did not plane down the weld profiles to achieve a given, exact weld leg length value. Further, no thermal control was exercised when laying the welds.

Soetens measured the failure planes and their angles of inclination to the weld leg length lying in the direction to the applied load. However only average readings for five specimens are given, and no result given for individual specimens. From these average readings it is seen by Soetens that for the tensile fillet welds the failure plane lay between the horizontal leg length and the weld throat, but never at the weld throat. For the longitudinal fillet weld he found the failure planes to be close to the welds throat.

Because the β-formula is based upon the over simplified assumption that weld failure occurs at the weld throat, Soetens has attempted to use approximate, weld failure plane lengths. He found that an effective throat length ($a_{eff.}$) plus the weld penetration value (p), gave well estimated lengths of the actual experimental failure plane. This relationship was proposed by equation 2.17, and accompanied by figure 2.13.

$$\text{Failure plane} = p + a_{eff.} \qquad \text{Equation 2.17}$$

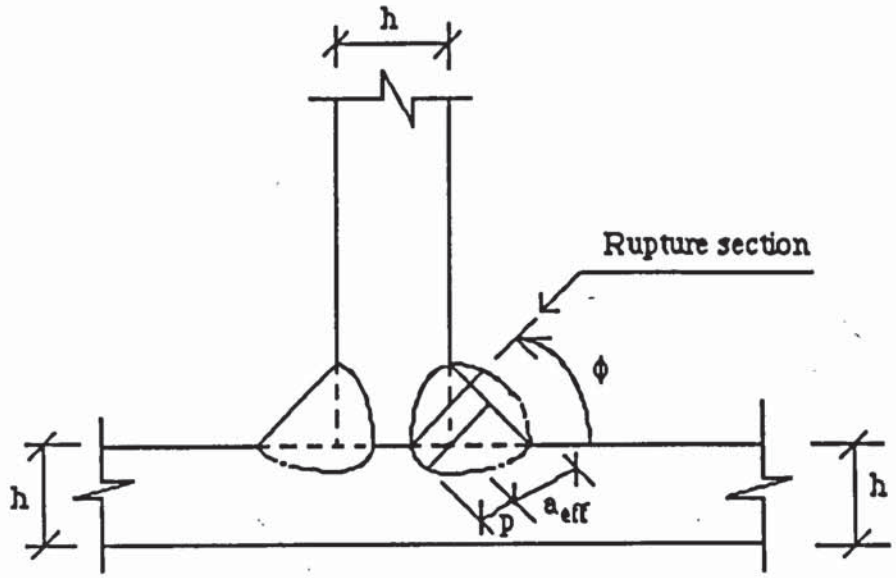

Figure 2.13 Soetens suggested weld model.

It is assumed by Soetens that penetration is always measured at 45^0 to the horizontal leg lengths.By this suggested estimation Soetens is indicating that weld failure initiates from the tip of the horizontal weld penetration, which lies on the seperation plane.

Soetens went on to establish the β-factor values based on these approximated failure planes, for different aluminium alloys and weld metal combinations.

A new method for the analysis of fillet welds was suggested by Kamtekar(11) in June 1982. It predicts strength formulae for fillet welds subjected to all different loading conditions. The method - specifically developed for steel welded connections - ensures that the force systems on the weld are in equilibrium. A force system of direct and shear forces, and moments acting on the faces of a weld is replaced by another 'equivalent'

force system, figure 2.14.

In this equivalent system the moments are considered to be a result of direct and,or shear forces, applied in such a way so as to ensure equilibrium of the weld.

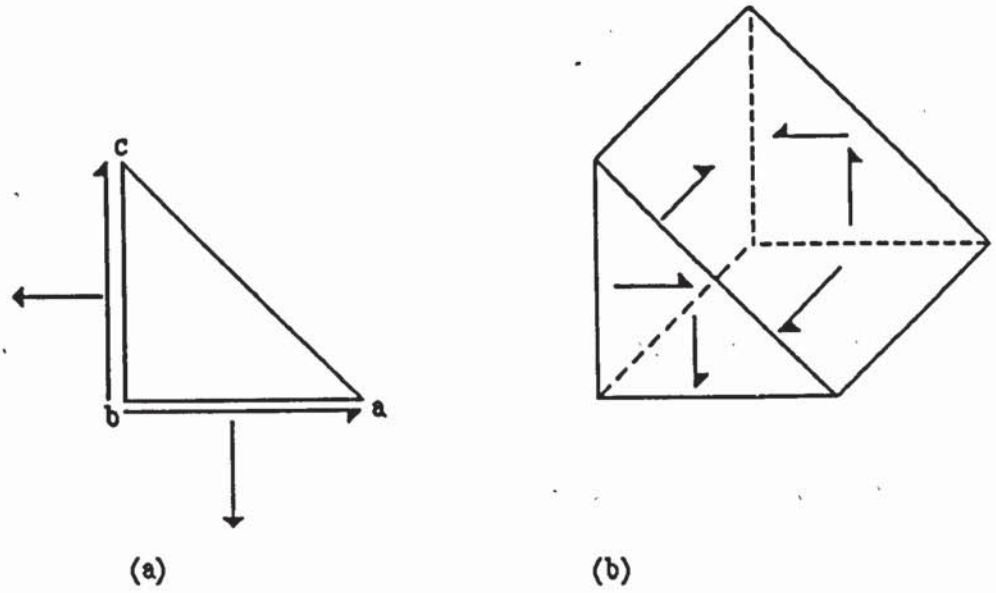

Figure 2.14 Kamtekar's equivalent force weld models (a) tensile fillet welds, (b) shear fillet welds.

It is assumed by Kamtekar that ;

a) the strength of the weld subjected to this equivalent force system is equal to the strength under the actual force system,

b) because no moments are acting in the equivalent force system, the stresses on the faces of the weld are taken to be uniform,

c) the weld metal will obey the Von Mises yield criterion,

d) the failure of the welds would be expected along the plane of maximum shear stress.

This proposed method of analysis can be commended in preference to those put forward by Kato and Morita (12), Soetens (14), and Higgs (15) on the following grounds;

i) Any load couples inherent due to the eccentricity of applied loads on welded connections, are taken account of by replacing them with an equivalent force system, figure 2.14.

ii) Unlike the other proposed failure criterions, no specific plane is assumed to be the critical plane. Failure of the welds is taken to be along the plane of maximum shear stress. The location of this plane is found from the calculated direction of the principal plane,

iii) Accountability of 'locked in' longitudinal residual stresses in the weld, can also be taken into the analysis. Kamtekar shows that ;

(a) for transversely loaded fillet welds, the presence of residual stress increases the strength by about 15 percent and,

(b)for longitudinally loaded fillet welds the strength is not affected by any residual stress present.

iv) The method of approach is applicable to any type of weld.

For steel welds, the residual stress is taken to be equal in magnitude to the yield stress of the weld metal. However, it must be pointed out that for welded aluminium alloys,

the values of residual stresses are lower than those in corresponding steel sections and that the maximum values do not exceed 0.6 times the 0.2 percent proof stress of the parent metal value - unaffected by welding heat (45,46,47)

Kamtekar acknowledges and states that the validity of such a fundemental method, for the analysis of fillet welds can only be verified by comparing theoretical failure loads with those obtained experimentally. He has not carried out any experimental tests himself, but has used experimental test results from work carried out by Kato and Morita (12) and by Freeman(32) to verify this theory.

Generally Kamtekar finds his theoretical predictions are lower than the experimental results, in most cases within 15 percent. He finds there is better agreement between theory and experimental results for tension fillet welds than for shear fillet welds, but no explanations are given for this.

The author draws the reader's attention to the fact that when Kamtekar compares his theoretical predictions to experimental results form Kato and Morita's test programme, he uses the effective throat values which incoroporate weld penetration. This is incorrect, since his weld failure theory is based upon normal and not 'effective' leg length values. Further Kamtekars proposed method of weld failure analysis takes no account of weld penetration in any way. By using the 'effective' leg length values, the predicted failure loads suggest a closer prediction to the experimental values.

The theoretical equations developed for simple tensile and shear welded connections by Kamtekar, show that tension fillet welds are 42 percent stronger than shear fillet welds,

of the same leg length and length. This is in close agreement with findings of Kato and Morita[12] of a figure of 46 percent for steel fillet welds and also with those of Soetens [6] findings of 50 percent for aluminium welds.

The most interesting conclusion arrived at by Kamtekar, is when he applies his theory to investigate the strength of fillet welds with unequal leg lengths. It is found that the failure load of tension fillet welds is very markedly governed by the weld cross-section shape, whereas for shear fillets such sensitivity does not exist.

The maximum load a tension fillet weld can carry is found - from optimisation of the failure load equations developed - to be when $\theta = 30^0$, where θ is as shown in figure 2.15. Further when $\alpha > 1/\sqrt{3}$, the failure load F decreases as α increases. Kamtekar underlines this very important finding by quoting a numerical example, which shall be used here to re-iterate how important small variations in the leg lengths are with respect to the failure of tension fillet welds.

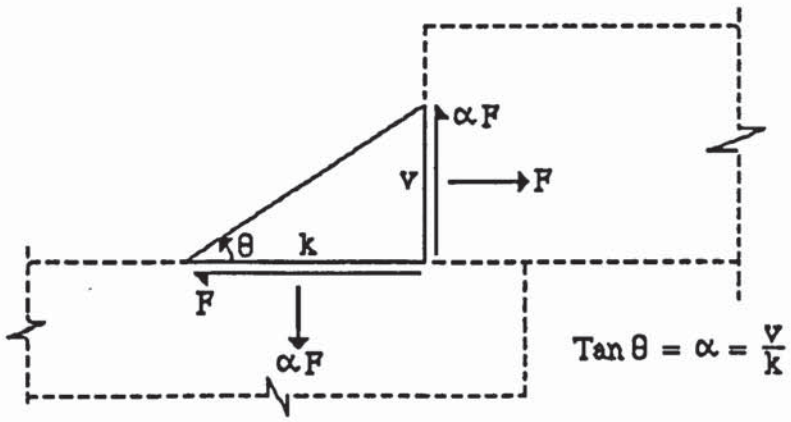

Figure 2.15 Cross - sectional view of unequal leg length weld.

The failure load F for a tension fillet weld with unequal leg lengths figure 2.15, is found by Kamtekar to be;

$$F = \frac{2\sigma_u L_\omega \sqrt{2A\alpha}}{\sqrt{3}\,(1+\alpha)^2} \qquad \text{Equation 2.18}$$

where σ_u = ultimate weld strength,

L_ω = length of weld,

A = weld cross-sectional area, and $\alpha = v/k$

Now to illustrate the point numerically, take $L\omega = 80mm$, $v = k = 6mm$, $\alpha = 1$, $2A = 36mm^2$, and take $\sigma_u = 600\ N/mm^2$.

Substitute these values into equation 2.18 and the failure load arrived at is F = 166.20 KN.

Now, also known is that the maximum load of the weld is when $\alpha = 1/\sqrt{3}$. Substituting this for the same value of $2A = 36mm^2$, we find $F_{max.} = 189.50$ KN.

However, now if the vertical leg is reduced by 10 percent, i.e.to 5.40mm, then the horizontal leg must be 6.67mm in order to maintain the same weld cross-sectional area. This gives $\alpha = 0.81$ and from equation 2.18, the failure load is found to be $F_{10\%} = 180.70$ KN, which is closer to the maximum load the weld can carry.

The point of concern is when the dimensions of the weld leg lengths are reversed. Then

α = 1.235 resulting in a failure load $F_{10\%}$ = 146.40 KN, which is significantly less than the specified load capacity for the weld.

It must be emphasised that a 10 percent variation in reality can on average represent anything from 0.4mm to 1.0mm. Thus, depending upon the size of weld laid, the percentage of variation in either the vertical or horizontal leg length would lead to a significantly over or under designed weldment.

The author's only criticism of Kamtekar's theory is that the actual weld profile 'model' used to predict the failure loads and planes for transverse and longitudinal welds, figures 2.14a and 2.14b, falls short of actual experimental findings. No account of weld penetration is taken in any way whatsoever. Consequently the results achieved by Kamtekar when using his method are only resonable when compared with the experimental findings of Kato and Morita and Freeman.

For tension fillet welds, according to Kamtekar's weld model (where no penetration is considered), the planes of maximum shear stress always coincide with the leg length faces ab and bc of the weld model, figure 2.4a. Failure is expected on any one of these planes. This contradicts experimental findings by numerous authors (6,12,15,31,33, 41,28).

However, Kamtekar acknowledges this and refers to the observations published by Higgs and Preece(28), which were;

a) the failure plane for transverse fillet welds lies close to the plane of the weld leg length parallel to the applied load.

b) the failure of longitudinal fillet welds is at or less than 45 degrees to the plane of the weld leg length parallel to the applied load.

Kamtekar recommends that for his tensile failure theory only the horizontal weld leg length should be considered as the location of the failure plane.This leg length being parallel to the direction of the applied load.

For shear fillet welds Kamtekar predicts only one plane of maximum shear stress, namely the throat of the weld. This is in close agreement with experimental observations and of the same as the prediction made by Kato and Morita[12,29] for shear fillet welds.

Kamtekar also acknowledges that the failure load predictions made for shear fillet weld using his proposed theory, are not as close as those made for tensile fillet welds. He tries to explain this anomaly on the fact that his equivalent force system is an approximate analysis of the actual force system. The author feels this is not where the anomaly arises from. It lies in the basic shape assumed for the weld profile model. No account of any weld penetration is taken by the model. It is widely acknowledged by Kato and Morita[12,29], Smith[24,25], and Soetens[5,6,14] that the extent of penetration greatly influences the ultimate strength of fillet welds. Therefore any weld model used to predict failure loads and planes, must incorporate or account for the extent of penetration present.

The method of approach to analyse fillet welds presented by Kamtekar is applicable to any type of weld. Kamtekar has theoretically demonstrated this in a later paper [48], where he has applied his theoretical approach to welds in beam to column connections,

where shearing forces are applied outside the weld planes.

The British Code of Practice for Aluminum Structures CP118[8] assumes failure occurs at the weld throat. The design of fillet welds is based upon the permissable stresses design concept. The permissable load on a fillet welded joint has to be the lower of the value obtained from either equation 2.19 or 2.20 given below;

$$\text{Permissable load} = \rho_{\omega} \cdot l_e \cdot t_e \qquad \text{Equation 2.19}$$

$$\text{or Permissable load} = \rho_{HAZ} \cdot l_e \cdot 1.1 \cdot \omega \qquad \text{Equation 2.20}$$

A draft Code of Practice BS8118[7] for the Design of Aluminium Structures is at present out for comment. This code is based upon the limit state design concept . However, the design of all fillet welds is still based upon the assumption that failure will occur at the weld throat. The permissable stresses recommended in CP118 are replaced by design stresses based upon the minimum expected shear strength for the combined parent and filler metal combination. A partial material factor γ_m for the weld metal is taken to be 1.3 and different coefficients, K, are proposed for side, end and all other types of fillet welds. The factored resistance of fillet welds, for both tensile and shear, is given by equation 2.21;

$$P_{FR} = f_{df} \cdot l_e \cdot g_t \cdot K / \gamma_m \qquad \text{Equation 2.21}$$

where K = 0.9 for side fillets,

= 1.4 for end fillets,

= 1.0 for all other fillet welds.

Because failure of the welded connection is required to occur in the weld only, it is expected that P_{FR} be checked to ensure it is not greater than the factored resistance P_{HR}, for the HAZ in the parent metal. The value of P_{HR} is found from equation 2.22;

$$P_{HR} = \{f_d \cdot W \cdot l_e \cdot 1.1g_t/0.7\} \gamma_m \qquad \text{Equation 2.22}$$

where f_d = design stress for parent metal,

W = reduction factor for HAZ properties. For 6000 series W = 0.5 and for 7000 series W = 0.75.

γ_m = partial material factor for parent metal (= 1.3)

CHAPTER 3 A PROPOSED WELD FAILURE THEORY.

3.1 Introduction.

Although weld penetration is a compulsory requirement for all structural weldments, no failure theory or weld model takes direct account of it. Kato and Morita [29] and Soetens[6,14] established that weld penetration has a direct effect upon weld failure loads. They suggested that the failure plane, assumed to be the weld throat by both these authors, should be modified to indirectly account for weld penetration.

A conclusion arrived by Kamtekar [11], from his weld failure analysis shows that great sensitivity is exhibited by tension fillet welds for small variations in their cross sectional areas. This has convinced the author that weld penetrations too, should show a similar marked difference upon weld failure loads.

In this chapter the author proposes a modified weld model which incorporates the extent of penetration inherent to all structural welds. The author develops a theoretical approach to analyse this model based on a simple and fundemental approach. A similar approach was considered by Kamtekar [11] on a simple weld model, with no account of penetration.

Theoretical relationships between penetration and weld failure loads and failure planes are derived for tensile and shear fillet welds.

3.2 The proposed weld model.

The proposed weld model shown in figure 3.1, is based upon the actual weld profile present in a fillet welded connection, figure 3.2.

The following assumptions are made;

i) Failure initiates from point a, shown in figure 3.2. This point is the tip of the horizontal penetration and always lies on the seperation plane of connected plates.

ii) Although face ab on the weld profile is curved figure 3.2, it can be well approximated by a straight line shown as ab in figure 3.1.

iii) The value of the horizontal penetration p, shown by length da in figures 3.1 and 3.2, can be well approximated by resolving the root penetration about an angle of 45^0.

iv) The weld face ac on the model figure 3.1 is taken to be a straight line along the seperation plane and not curved as in the actual weld profile figure 3.2.

v) Failure will not occur in any part of the weld deposit below ac, seen in figure 3.2.

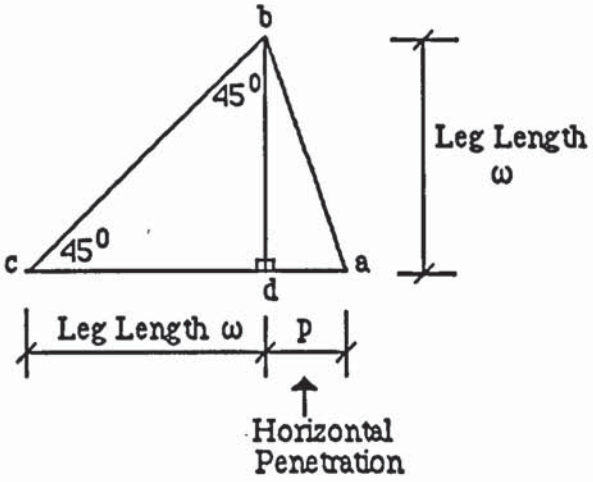

Figure 3.1 The proposed weld model for analysing tensile and shear fillet welds.

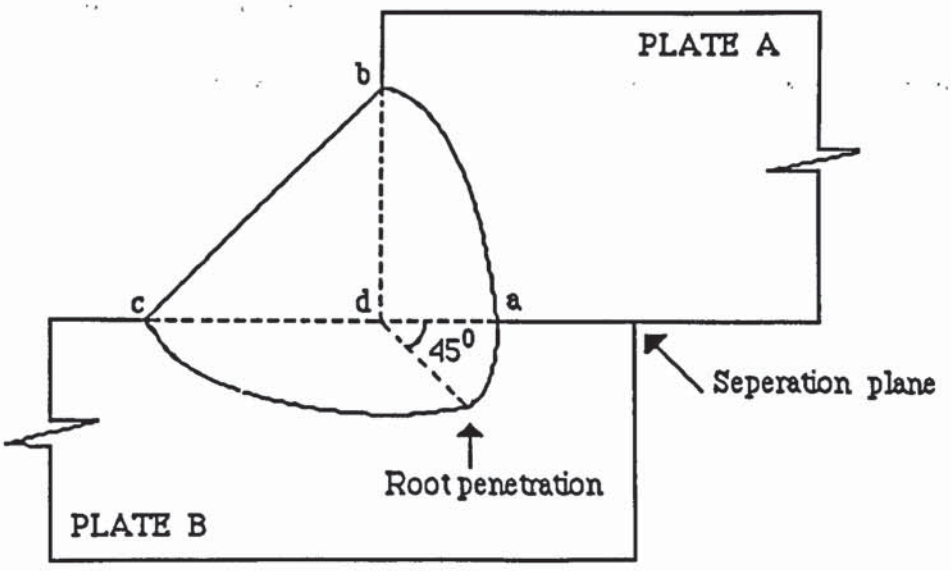

Figure 3.2 The actual fillet weld profile in a welded connection.

3.3 Assumptions for the derivation of a failure criterion for tensile and shear fillet welds.

The assumptions made for the proposed weld failure criterions are;

i) Any moments acting on the weld can be replaced by a pair of eccentric forces acting on the weld leg lengths.

ii) Stresses acting on the weld are uniformly distributed.

iii) Only the longitudinal residual stress R, inherent in the weld metal, is significant. Residual stresses in all other directions are taken to be negligible.

iv) Failure occurs in the weld metal, described by the weld model in figure 3.1.

v) The Von Mises failure criterion applies to the weld. The yield stress of the weld metal in this criterion can be replaced by the ultimate weld tensile stress as shown by Kamtekar (11) and indicated by Mendelson (49).

vi) Failure in the weld metal always occurs along the plane of maximum shear stress.

3.4 Notation used for stresses.

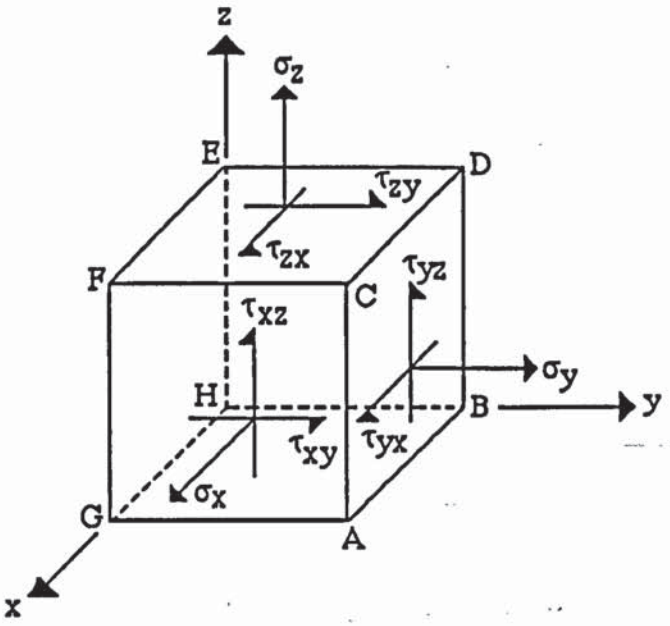

Figure 3.3 Notation used for stresses acting on three perpendicular planes.

The notation used to describe stresses is as that indicated in figure 3.3. The stresses shown are acting on the faces of the cube and taken to be acting positively. On face ABCD the normal positive stress is σ_y, and the positive shearing stresses are τ_{yx} and τ_{yz}. On face ACFG the normal positive stress is σ_x and the positive shearing stresses are τ_{xz} and τ_{xy}. Finally on face CDEF the positive normal and shearing stresses are $\sigma_z, \tau_{zx}, \tau_{zy}$. The stresses on all the other opposite faces are positive when applied in an opposite direction.

3.5 The proposed failure theory for tensile fillet welds.

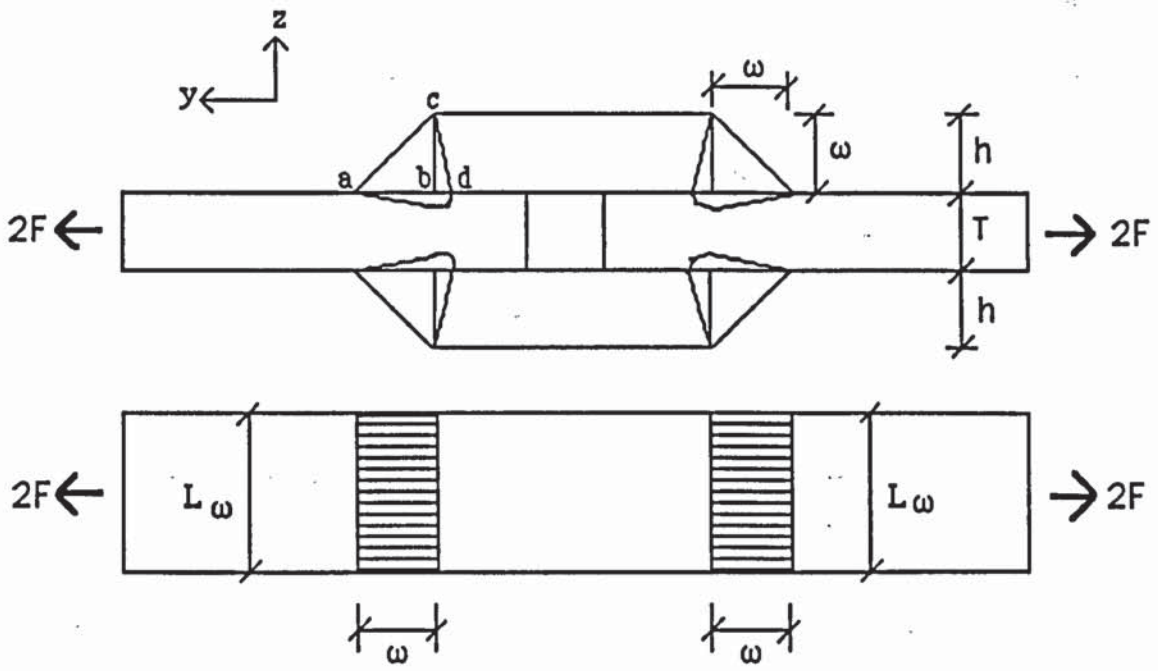

Figure 3.4 A simple tensile fillet welded connection.

Consider geometry of the weld abdc in the above tensile connection and shown below in figure 3.5, for projected horizontal weld penetration value of pω. The value of p is suggested by Smith[24,25] to be equal to 0.3 times the weld leg length, giving a designed leg length value of 1.3ω.

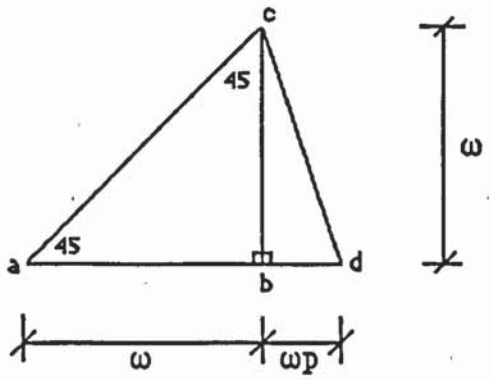

Figure 3.5 Geometry of tensile fillet weld abcd.

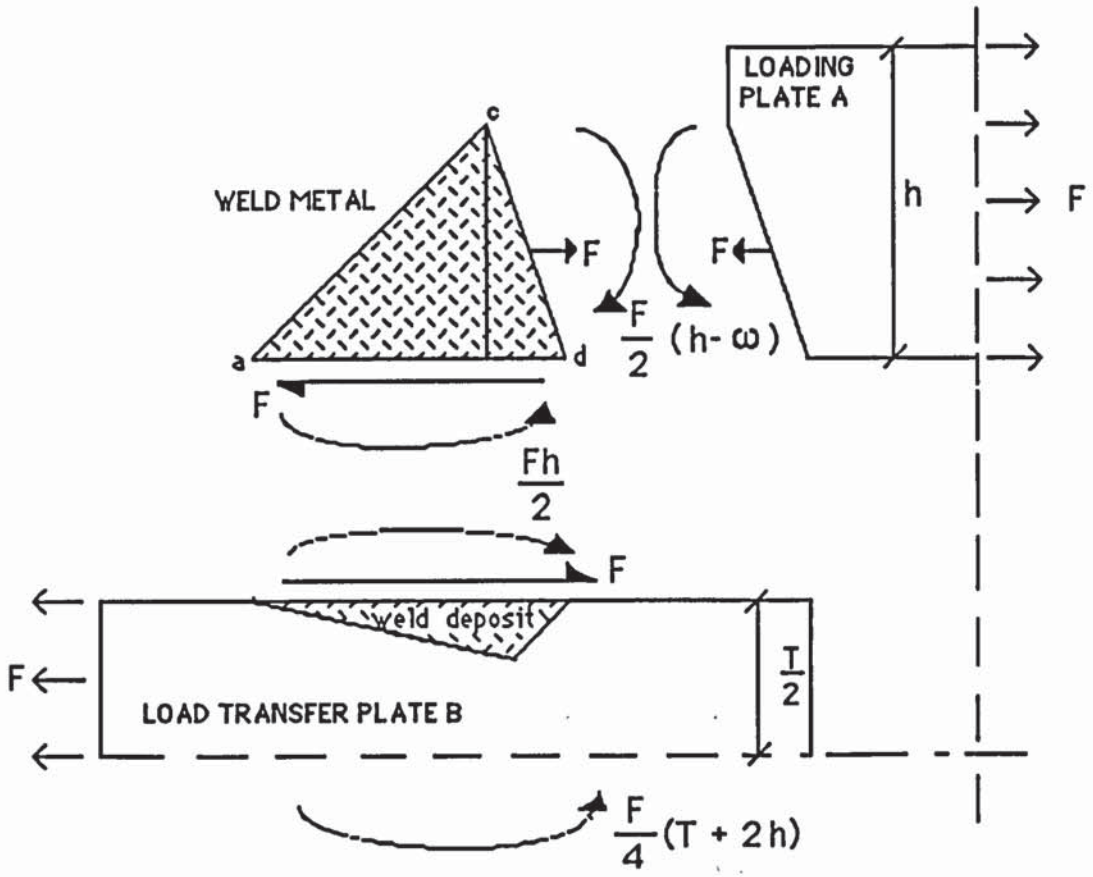

Figure 3.6 Equilibrium of forces on a single tensile weld.

The dotted line in the load transfer plate B, is the penetration of weld existing below the surface of the plate B. This zone of penetration is ignored as stated in section 3.2.

From figure 3.6 it is clear that the applied force system on the weld needs a balancing moment $F\omega/2$, applied in an anticlockwise manner to maintain equilibrium. Further, this balancing moment $F\omega/2$, can be replaced by a force system, without affecting the equilibrium of the weld. This can be achieved by applying a tensile force F at the centre of the sloping leg length and a shearing force F on the horizontal design leg length, as shown in figure 3.7.

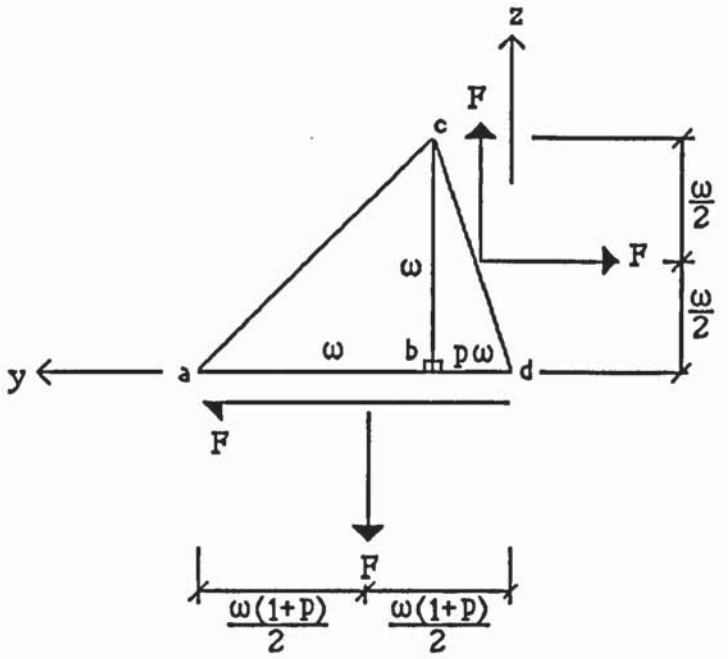

Figure 3.7 The equivalent force system.

The normal and shear stresses due to the above forces, acting on the weld would be as shown in figure 3.8 below.

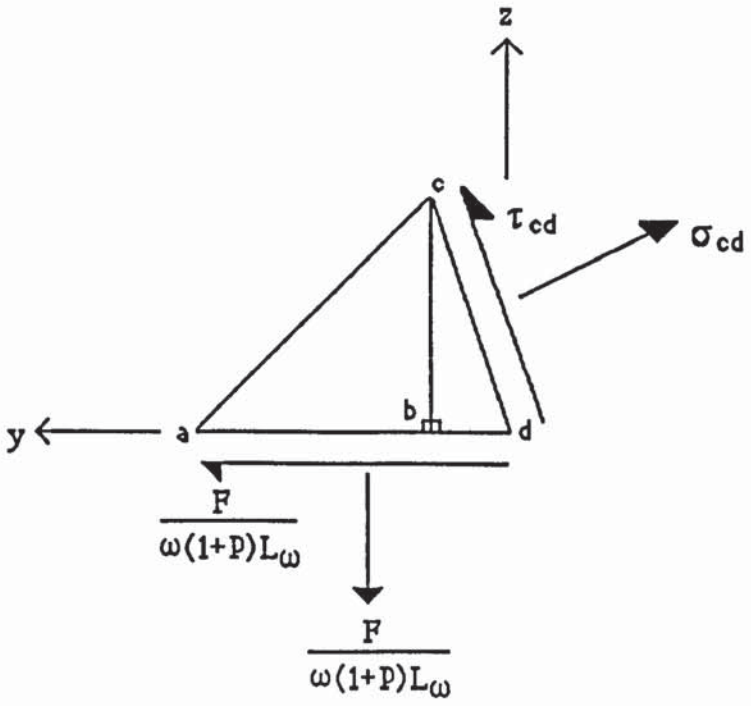

Figure 3.8 The normal and shear stresses on weld abcd.

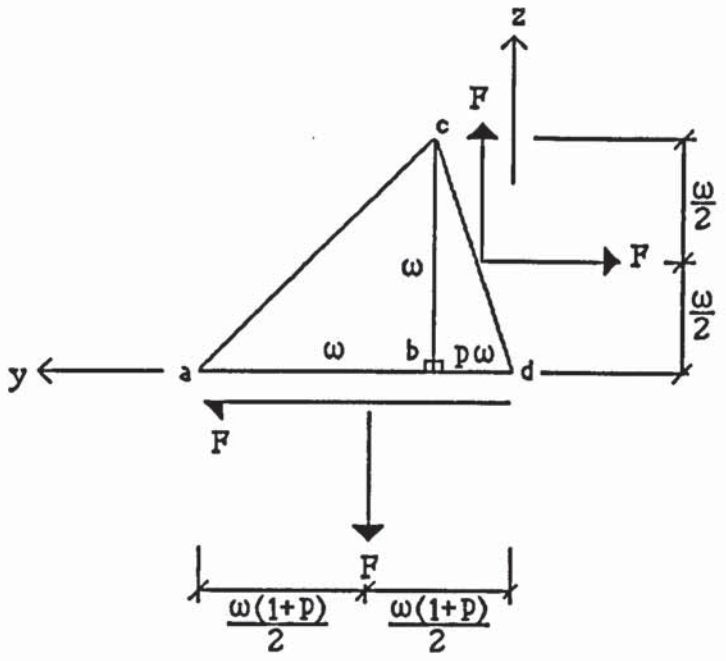

Figure 3.7 The equivalent force system.

The normal and shear stresses due to the above forces, acting on the weld would be as shown in figure 3.8 below.

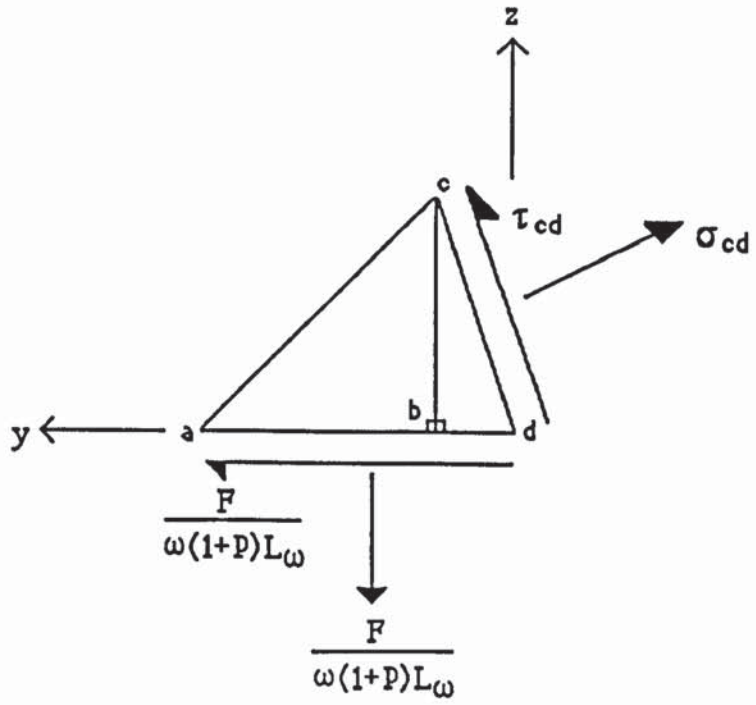

Figure 3.8 The normal and shear stresses on weld abcd.

For a unit length of weld, the stresses acting on theweld abcd are;

$\sigma_x = R$ where R is equal to the longitudinal residual stress in the weld metal.

$\sigma_z = F/\omega(1+p).L_\omega$

$= \sigma/(1+p)$ where $\sigma = F/\omega L_\omega$

$\tau_{yz} = F/\omega(1+p).L_\omega = \sigma/(1+p)$

$\tau_{zy} = F/\omega(1+p).L_\omega = \sigma/(1+p)$

$\tau_{zx} = \tau_{xz} = \tau_{yx} = \tau_{xy} = 0$

$$\sigma_{cd} = \frac{F(\sin\theta + \cos\theta)}{\omega L_\omega \sqrt{1+p^2}}$$

$$= \frac{\sigma(1+p)}{(1+p^2)}$$

since $\sin\theta = \frac{1}{\sqrt{1+p^2}}$ and $\cos\theta = \frac{p}{\sqrt{1+p^2}}$

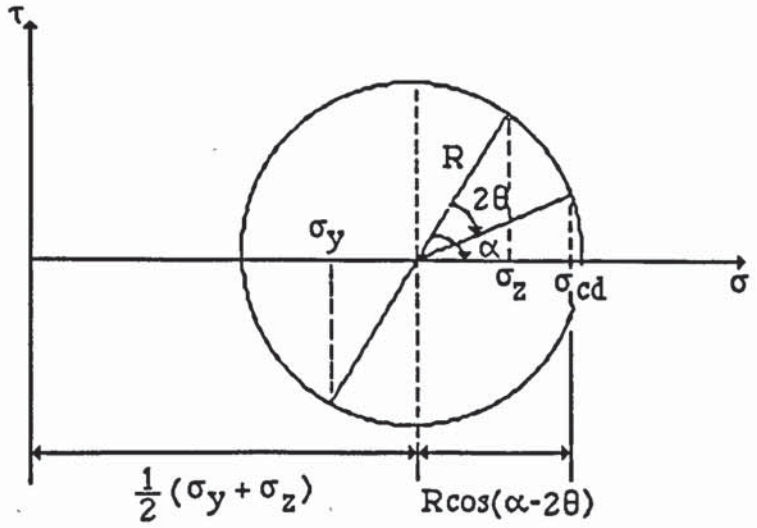

Figure 3.9 Mohr's Circle of stresses for weld model.

From Mohr's Circle in figure 3.9

$$\sigma_{cd} = 0.5 (\sigma_y + \sigma_z) + R \cos (\alpha - \theta)$$

$$\sigma_{cd} = 0.5 (\sigma_y + \sigma_z) + R \cos\alpha \cos 2\theta + R \sin\alpha \sin 2\theta$$

$$= 0.5 (\sigma_y + \sigma_z) + 0.5 (\sigma_z - \sigma_y) \cos 2\theta + 0.5 (\sigma_z - \sigma_y) \tan\alpha \sin 2\theta$$

$$= 0.5 (\sigma_y + \sigma_z) + 0.5 (\sigma_z - \sigma_y) \cos 2\theta + \tau_{yz} \sin 2\theta$$

$$= \sigma_y \cos^2\theta + \sigma_z \sin^2\theta + 2\tau_{yz} \sin\theta \cos\theta$$

$$= \sigma_y \frac{p^2}{(1+p^2)} + \sigma_z \frac{1}{(1+p^2)} + 2\tau_{yz} \frac{p}{(1+p^2)}$$

therefore;

$$\frac{\sigma(1+p)}{(1+p^2)} = \sigma_y \frac{p^2}{(1+p^2)} + \sigma_z \frac{1}{(1+p^2)} + 2\tau_{yz} \frac{p}{(1+p^2)}$$

$$\sigma_y p^2 = \sigma(1+p) - \sigma_z - 2\tau_{yz} p$$

$$\sigma_y p^2 = \sigma(1+p) - \frac{\sigma}{(1+p)} - \frac{2p\sigma}{(1+p)}$$

$$\sigma_y p^2 = \frac{\sigma}{(1+p)} [(1+p)^2 - 1 - 2p]$$

$$\sigma_y = \frac{\sigma}{(1+p)}$$

Substitute these values of stresses into the general stress equation 3.1(50)

$$\ell (\sigma_x - p) + m \tau_{yx} + n \tau_{zx} = 0$$

$$\ell \tau_{xy} + m (\sigma_x - p) + n \tau_{zy} = 0 \qquad \text{Equation 3.1}$$

$$\ell \tau_{xz} + m \tau_{yz} + n(\sigma_z - p) = 0$$

and also ; $\ell^2 + m^2 + n^2 = 1$ Equation 3.2

to give;

$$\begin{bmatrix} (R-p) & 0 & 0 \\ 0 & (\sigma_1 - p) & -\sigma_1 \\ 0 & -\sigma_1 & (\sigma_1 - p) \end{bmatrix} \begin{bmatrix} \ell \\ m \\ n \end{bmatrix} = 0 \quad \text{Equation 3.3}$$

Hence from the determinant of the matrix we can obtain the values of the three principal stresses.

$$[\Delta] = \{(R-p)(\sigma_1 - p)(\sigma_1 - p)\} - \{-\sigma_1 . -\sigma_1 . (R-p)\} = 0$$

$$(R-p)[(\sigma_1 - p)^2 - \sigma_1^2] = 0$$

solving for p gives; $p_1 = R$, $p_2 = 0$, $p_3 = 2\sigma_1 = 2\sigma/(1+p)$.

Substituting these values of p_1, p_2, and p_3 into the Von Mises failure criterion;

$$(p_1 - p_2)^2 + (p_2 - p_3)^2 + (p_3 - p_1)^2 = 2\sigma_u^2 \quad \text{Equation 3.4}$$

$$(R-0)^2 + (0 - 2\sigma_1)^2 + (2\sigma_1 - R)^2 = 2\sigma_u^2$$

$$R^2 + 4\sigma_1^2 + 4\sigma_1^2 - 4\sigma_1 R + R^2 = 2\sigma_u^2$$

$$2R^2 - 4\sigma_1 R + 8\sigma_1^2 - 2\sigma_u^2 = 0$$

$$4\sigma_1^2 - 2\sigma_1 R + (R^2 - \sigma_u^2) = 0$$

Solve for σ_1

$$\sigma_1 = \{2R \pm \sqrt{[4R^2 - 16(R^2 - \sigma_u^2)]}\}/8$$

$$\sigma_1 = \{ 2R \pm \sqrt{[16\sigma_u^2 - 12R^2]} \} / 8 \qquad \text{Equation 3.5}$$

Differentiating equation 3.5 with respect to R, to find the maximum value of σ_y

$$\frac{\delta\sigma_1}{dR} = \frac{2}{8} \pm \frac{0.5\,[(16\sigma_u^2 - 12R^2)^{-1/2}(-24R)]}{8}$$

$$\therefore \quad 16\,\sigma_u^2 - 12\,R^2 = 36\,R^2$$

$$\frac{\sigma_u^2}{\sqrt{3}} = R$$

Substitute back into equation 3.5, to give;

$$\sigma_1 = \frac{2(\sigma_u/\sqrt{3}) \pm \sqrt{16\sigma_u^2 - 12(\sigma_u^2/3)}}{8}$$

Taking +ve value of σ_1 to give;

$$\sigma_1 = \sigma_u / \sqrt{3}$$

but also

$$\sigma_1 = \frac{\sigma}{(1+p)} = \frac{\sigma_u}{\sqrt{3}}$$

$$\frac{\sigma_u(1+p)}{\sqrt{3}} = \frac{F}{\omega.L_\omega}$$

$$\therefore \quad F = \frac{\omega L_\omega \sigma_u (1 + p)}{\sqrt{3}}$$

The load applied to the transverse weld specimen is 2F.

$$\therefore \quad 2F = \frac{2\omega L_\omega \sigma_u (1 + p)}{\sqrt{3}}$$

In order to establish the location of the failure planes, values of the directional cosines of the normals to the principal planes can be derived from equation 3.3, to give;

$$\ell (R - p) = 0 \qquad \text{Equation 3.6}$$

$$m (\sigma_1 - p) - n \sigma_1 = 0 \qquad \text{Equation 3.7}$$

$$- \sigma_1 m + n (\sigma_1 - p) = 0 \qquad \text{Equation 3.8}$$

Substituting values of $p_1 = R$, $p_2 = 0$, $p_3 = 2\sigma_1 = \sigma/(1 + p)$ in turn into equations 3.6, 3.7 and 3.8.

Therefore for $p_1 = R$;

From equation 3.6 : $\ell (R - R) = 0$ ----(i)

From equation 3.7: $m (\sigma_1 - R) - n \sigma_1 = 0$

$$m = n [(\sigma_1)/(\sigma_1 - R)] \qquad \text{----(ii)}$$

From equation 3.8: $- \sigma_1 m + n (\sigma_1 - R) = 0$ ----(iii)

substitute (iii) into (ii) to give; $n (- \sigma_1 . R - R^2) = 0$

$$\therefore \quad n = 0$$

back substitute $n = 0$ into equation (g) to give $m = 0$

Also from equation 3.2 $\ell^2 + m^2 + n^2 = 1 \qquad \ell = 0$

Therefore the directional cosines of the normal to the plane on which $p_1 = R$ is the principal stress are;

$$\begin{bmatrix} \ell \\ m \\ n \end{bmatrix} = \begin{bmatrix} 1 \\ 0 \\ 0 \end{bmatrix} = \begin{bmatrix} 0^0 \\ 90^0 \\ 90^0 \end{bmatrix}$$

This gives the weld cross - section abdc as the principal plane shown in figure 3.10;

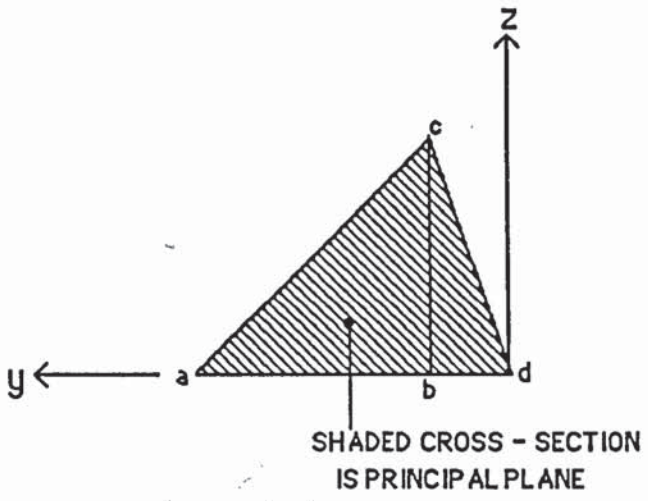

Figure 3.10 Principal plane when $p_1 = R$.

For $p_2 = 0$

From equation 3.6 : $\ell (R - 0) = 0$

$\therefore \quad \ell = 0$

From equation 3.7: $m (\sigma_1 - 0) - n \sigma_1 = 0$

$\therefore \quad m = n$

From equation 3.8: $- \sigma_1 m + n \sigma_1 = 0$

$\therefore$ again $m = n$

and from equation 3.2: $2m^2 = 1$

$\therefore \quad m = 1/\sqrt{2}$ and also $n = 1/\sqrt{2}$

Thus, the direction cosines of the normal to the plane on which $p_2 = 0$ is the principal

stress are;

$$\begin{bmatrix} \ell \\ m \\ n \end{bmatrix} = \begin{bmatrix} 0 \\ \frac{1}{\sqrt{2}} \\ \frac{1}{\sqrt{2}} \end{bmatrix} = \begin{bmatrix} 90^0 \\ 45^0 \\ 45^0 \end{bmatrix}$$

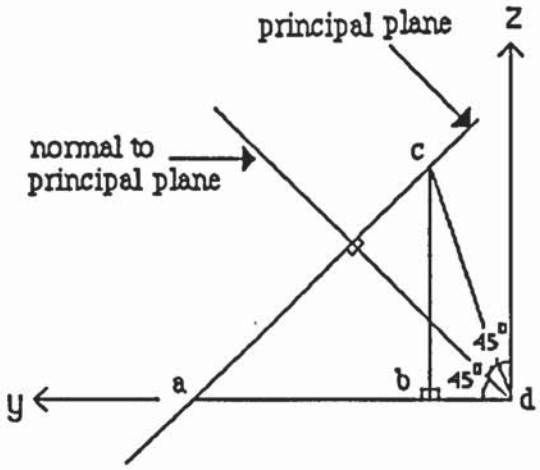

Figure 3.11 Principal plane when $p_2 = 0$

This gives the sloping face of the weld ac, as the principal plane. This is as would be expected from a visual inspection.

For $p_3 = 2\sigma/(1 + p)$

From equation 3.6 : $\ell\,(R - 2\sigma/(1 + p)) = 0$

$\therefore \quad \ell = 0$

From equation 3.7: $m\,(\sigma/(1 + p) - 2\sigma/(1 + p)) - n\,\sigma/(1 + p) = 0$

$\therefore \quad m = -n$

From equation 3.8: $-\sigma/(1 + p)\,m + n\,(\sigma/(1 + p) - 2\sigma/(1 + p)) = 0$

$\therefore$ again $m = -n$

and from equation 3.2 $m^2 + n^2 = 1$

$$\therefore \quad m = 1/\sqrt{2}$$

and also, $n = -1/\sqrt{2}$

Therefore, the direction cosines of the normal to the plane on which $p_3 = 2\sigma/(1 + p)$ is the principal stress are;

$$\begin{bmatrix} \ell \\ m \\ n \end{bmatrix} = \begin{bmatrix} 0 \\ \frac{1}{\sqrt{2}} \\ -\frac{1}{\sqrt{2}} \end{bmatrix} = \begin{bmatrix} 90^0 \\ 45^0 \\ 135^0 \end{bmatrix}$$

The location of the principal plane is shown in figure 3.12.

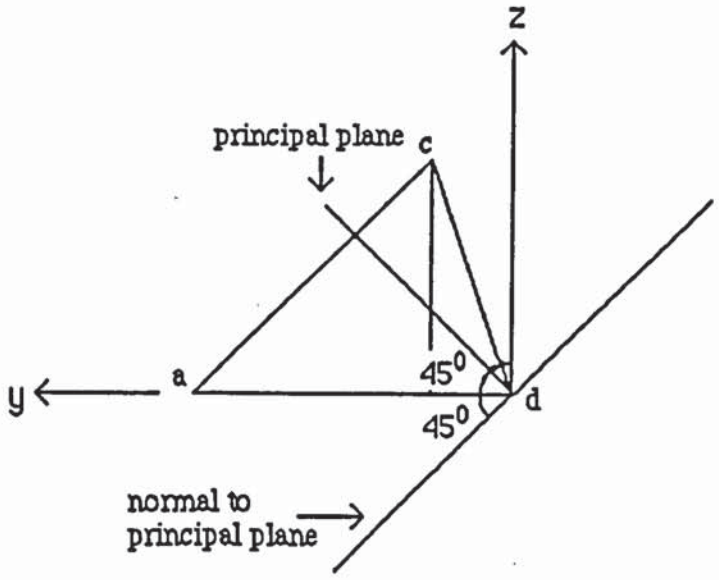

Figure 3.12 Principal plane when $p_3 = 2\sigma/(1 + p)$

The rupture of the weld abdc will occur along the plane of maximum shear stress, as discussed in the assumptions made in section 3.2. Further the plane of maximum shear stress is always inclined at 45^0 to the planes of principal stresses (Mohr's Circle).

Therefore when $p_1 = R$, the plane of maximum shear stress is inclined at 45^0 to the weld cross section, which is the principal plane shown in figure 3.10.

When $p_2 = 0$, the plane of maximum shear stress is the horizontal leg length ad, shown in figure 3.11.

When $p_3 = 1.539\sigma_y$, the plane of maximum shear stress, inclined at an angle of 45^0 to the principal plane is the horizontal weld leg length. This is shown as length ad in figure 3.13. Failure of the weld metal would be expected along this most critical plane of maximum shear stress.

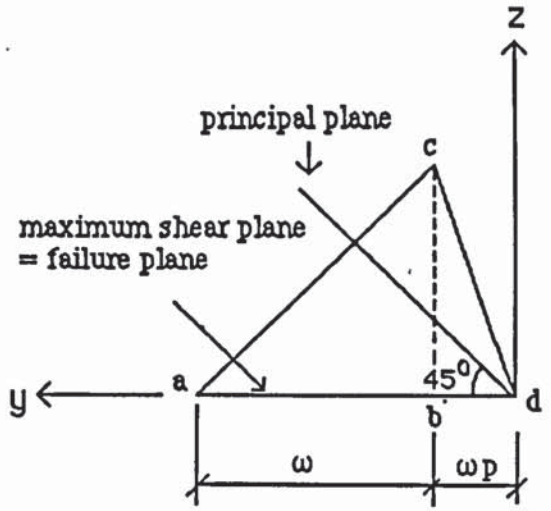

Figure 3.13 Predicted failure plane for a weld taking account of any penetration value.

Although the weld model proposed in figure 3.1 gives increasing weld failure loads as penetration values increase, it always predicts the horizontal weld leg length as the failure plane. This is contrary to experimental results obtained by the author and to those of numerous other authors (12, 15, 28, 32).

However, by inspecting the proposed weld mobel abdc in figure 3.1, it is evident that the vertical weld leg length ω, is not equal to the horizontal weld leg length ($\omega + \omega p$). It

is therefore proposed that this weld model abdc in figure 3.1 be idealised as an unequal leg length weld abde - figure 3.14, whose cross-sectional area is equal to that of the weld model abdc.

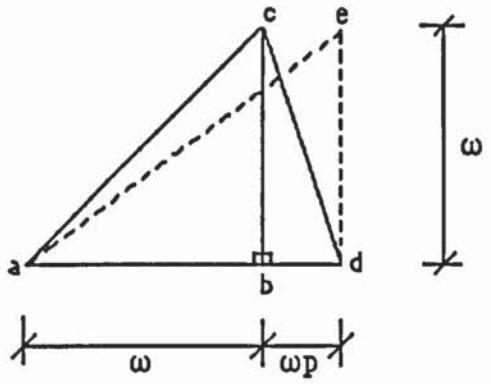

Figure 3.14 The tensile weld abdc idealised to an equivalent area weld model abde.

Analysis of the weld model abde.

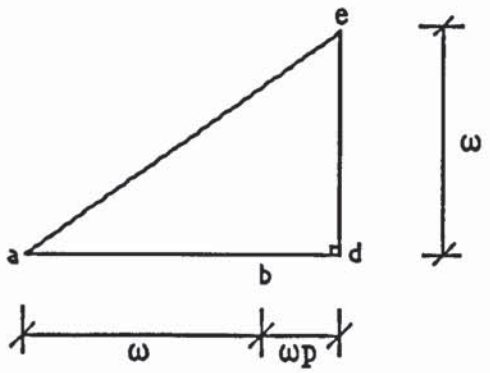

Figure 3.15 The idealised unequal weld leg length weld abde.

The forces acting on weld abde for a unit weld length are as those shown in figure 3.6. The equivalent balanced force system acting on the weld are is shown below in figure 3.16 ;

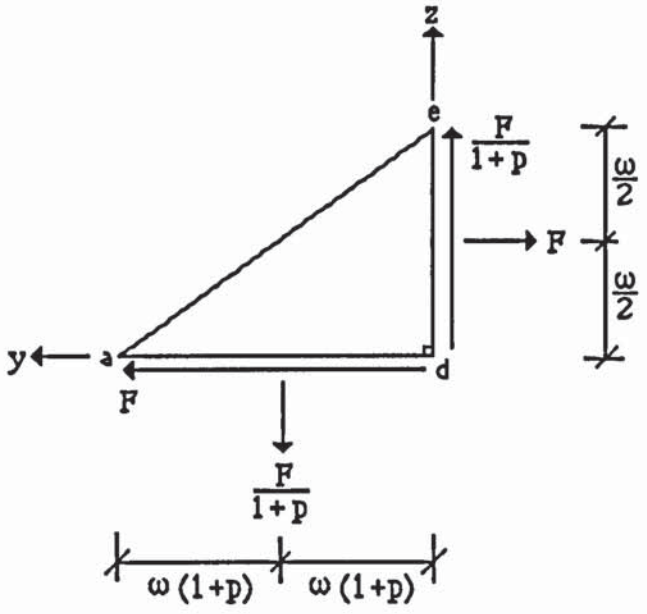

Figure 3.16 Equivalent balanced force system acting on weld ade.

The normal and shear stresses due to the above forces is shown in figure 3.17 below;

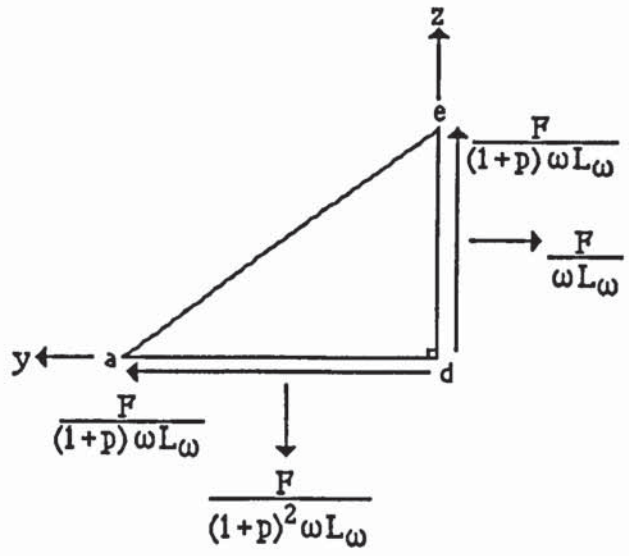

Figure 3.17 Stresses acting on weld ade.

For a unit length of weld, the stresses acting on the weld ade are;

$\sigma_x = R$ where R is equal to the longitudinal residual stress in the weld metal.

$\sigma_y = F/\omega.L_\omega$

$\sigma_z = F/\omega(1+p)^2.L_\omega$

$= \sigma_y/(1+p)^2$

$\tau_{yz} = -F/\omega(1+p).L_\omega = -\sigma_y/(1+p)$

$\tau_{zy} = -F/\omega(1+p).L_\omega = -\sigma_y/(1+p)$

$\tau_{zx} = \tau_{xz} = \tau_{yx} = \tau_{xy} = 0$

Substitute these values of stresses into the general stress equation 3.1 to give;

$$\begin{bmatrix} (R-p) & 0 & 0 \\ 0 & (\sigma_y - p) & \frac{-\sigma_y}{(1+p)} \\ 0 & \frac{-\sigma_y}{(1+p)} & (\frac{\sigma_y}{(1+p)^2} - p) \end{bmatrix} \begin{bmatrix} l \\ m \\ n \end{bmatrix} = 0 \qquad \text{Equation 3.9}$$

From the determinant of the above matrix, we can obtain the three principle stresses;

$$[\Delta] = \{ (R-p)(\sigma_y - p)([\sigma_y/(1+p)^2] - p) \} - \{ -\sigma_y(1+p) - \sigma_y(1+p)(R-p) \} = 0$$

$$(R-p)\{ (p^2 - \sigma_y p - [\sigma_y/(1+p)^2]p) \} = 0$$

solving for p gives; $p_1 = R$, $p_2 = 0$, $p_3 = \sigma_y[1 + 1/(1+p)^2]$

Substituting these values of p_1, p_2, and p_3 into the Von Mises failure criterion;

$$(p_1 - p_2)^2 + (p_2 - p_3)^2 + (p_3 - p_1)^2 = 2\sigma_u^2 \qquad \text{Equation 3.4}$$

$$(R - 0)^2 + (0 - \sigma_y [1 + 1/(1+p)^2])^2 + (\sigma_y [1 + 1/(1+p)^2] - R)^2 = 2\sigma_u^2$$

expanding to give;

$$\sigma_y^2[1 + 1/(1+p)^2]^2 - \sigma_y [1 + 1/(1+p)^2] R + (R^2 - \sigma_u^2) = 0$$

Solve for σ_y

$$\sigma_y = \{ [1 + 1/(1+p)^2].R \pm \sqrt{[[1 + 1/(1+p)^2]^2 R^2 - 4[1 + 1/(1+p)^2]^2 (R^2 - \sigma_u^2)]} \} / 2[1 + 1/(1+p)^2]^2$$

Differentiating with respect to R, to find the maximum value of σ_y gives $R = \sigma_u/\sqrt{3}$.

Substituting this back to find σ_y in terms of σ_u gives;

$$\sigma_y = 2\sigma_u / \sqrt{3}[1 + 1/(1+p)^2]^2$$

also $\sigma_y = F/\omega.L_\omega$

Equating to find F;

$$F = \frac{2\sigma_u \omega L_\omega}{\sqrt{3}\left(1 + \frac{1}{(1+p^2)}\right)}$$

$$2F = \frac{4\sigma_u \omega L_\omega}{\sqrt{3}\left(1 + \frac{1}{(1+p^2)}\right)}$$

The values of the directional cosines of the normals to the principal planes can be found as before to give;

When $p_1 = R$;

The directional cosines of the normal to the plane on which $p_1 = R$ is the principal stress are;

$$\begin{bmatrix} \ell \\ m \\ n \end{bmatrix} = \begin{bmatrix} 1 \\ 0 \\ 0 \end{bmatrix} = \begin{bmatrix} 0^0 \\ 90^0 \\ 90^0 \end{bmatrix}$$

This gives the weld cross - section abdc as the principal plane shown in figure 3.18;

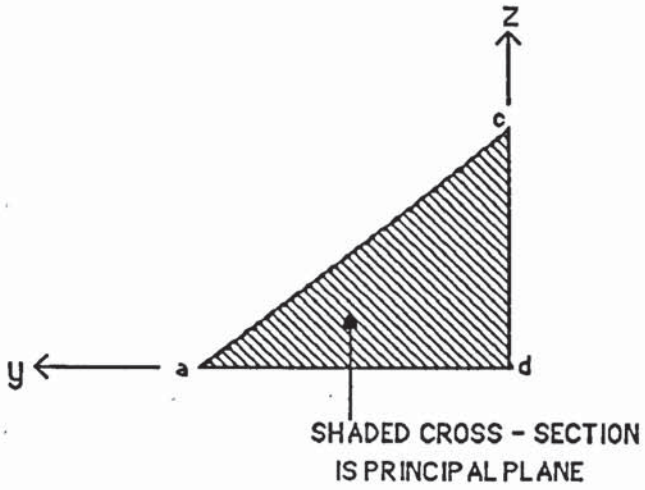

Figure 3.18 Principal plane when $p_1 = R$.

For $p_2 = 0$

The direction cosines of the normal to the plane on which $p_2 = 0$ is the principal stress are;

$$\begin{bmatrix} \ell \\ m \\ n \end{bmatrix} = \begin{bmatrix} 0 \\ \frac{\psi}{\sqrt{1+\psi^2}} \\ \frac{1}{\sqrt{1+\psi^2}} \end{bmatrix} = \begin{bmatrix} 90^0 \\ 45^0 \\ 45^0 \end{bmatrix} \quad \text{where } \psi = \frac{1}{(1+p)}$$

This can be shown to give the sloping face of the weld ac, as the principal plane for all values of penetration p. This is as would be expected from a visual inspection.

For $p_3 = \sigma_y (1 + [1 / (1+p)])$

Therefore, the direction cosines of the normal to the plane on which $p_3 = \sigma_y [1+ 1/(1+p)^2]$ is the principal stress are;

$$\begin{bmatrix} \ell \\ m \\ n \end{bmatrix} = \begin{bmatrix} 0 \\ \frac{1}{\sqrt{1+\psi^2}} \\ -\frac{\psi}{\sqrt{1+\psi^2}} \end{bmatrix} = \begin{bmatrix} 90^0 \\ 45^0 \\ 135^0 \end{bmatrix} \quad \text{where } \psi = \frac{1}{(1+p)}$$

The location of the principal plane is shown in figure 3.19, as the normal to the weld sloping face ae.

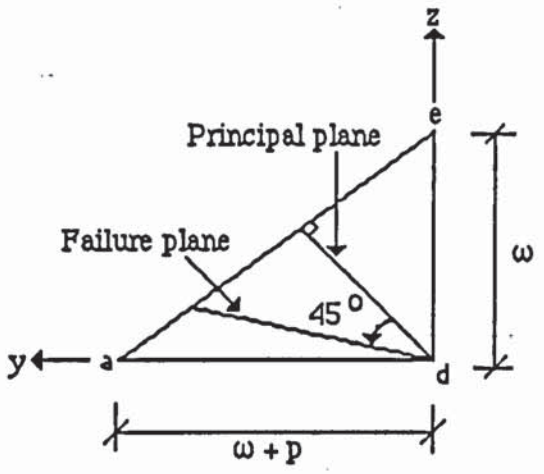

Figure 3.19 Predicted failure plane for weld with any amount of penetration p.

The rupture of the weld ade will occur along the plane of maximum shear stress, as discussed in the assumptions made in section 3.2. Further the plane of maximum shear stress is always inclined at 45^0 to the planes of principal stresses (Mohr's Circle).

The critical plane of maximum shear stress occurs when $p_3 = 1.539\sigma_y$. This is shown in figure 3.19, as the plane inclined at an angle to the weld horizontal leg length. The location of this failure plane can be shown to be;

$$\text{Failure plane} = 45^0 - \text{Tan}^{-1}\,(\,1/1+p\,)$$

Leg Length ω (mm)	Horizontal penetration p (mm)	Tensile failure load F_t (KN)	Tensile failure load $2F_t$ (KN)	Failure plane ϕ^0	Length of failure plane (mm)
ω	0	0.5774 UTL	1.155 UTL	0	ω
ω	0.1ω	0.6322 UTL	1.264 UTL	2.726	$1.046\ \omega$
ω	0.2ω	0.6815 UTL	1.363 UTL	5.194	$1.087\ \omega$
ω	0.3ω	0.7254 UTL	1.451 UTL	7.431	$1.121\ \omega$
ω	0.4ω	0.7646 UTL	1.529 UTL	9.462	$1.151\ \omega$
ω	0.5ω	0.7994 UTL	1.599 UTL	11.31	$1.177\ \omega$
ω	0.6ω	0.8304 UTL	1.661 UTL	13.00	$1.199\ \omega$

UTL = Ultimate Tensile Load $\sigma_u.\omega.L_\omega$

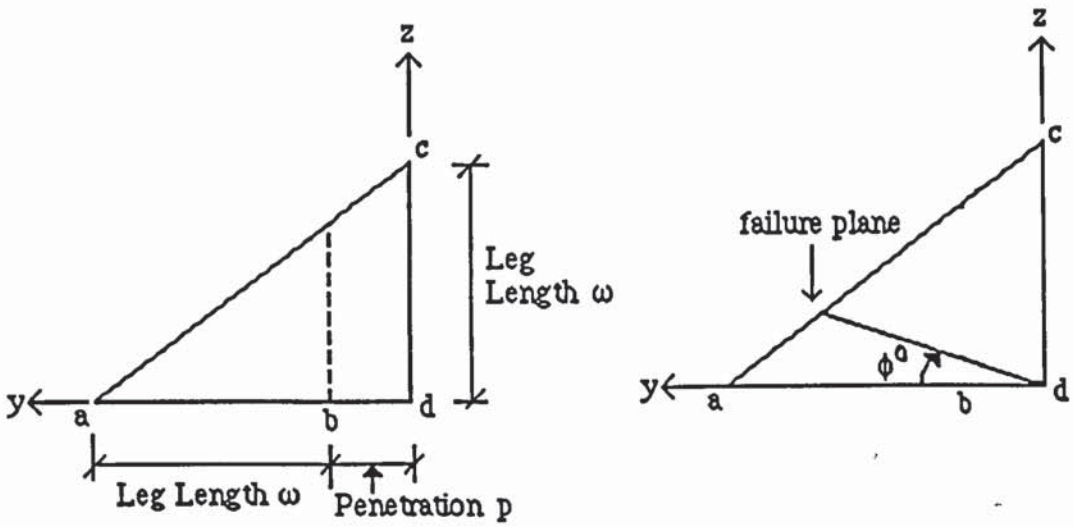

Table 3.1 Calculated values of tensile weld failure loads and failure planes as weld penetration (p) changes.

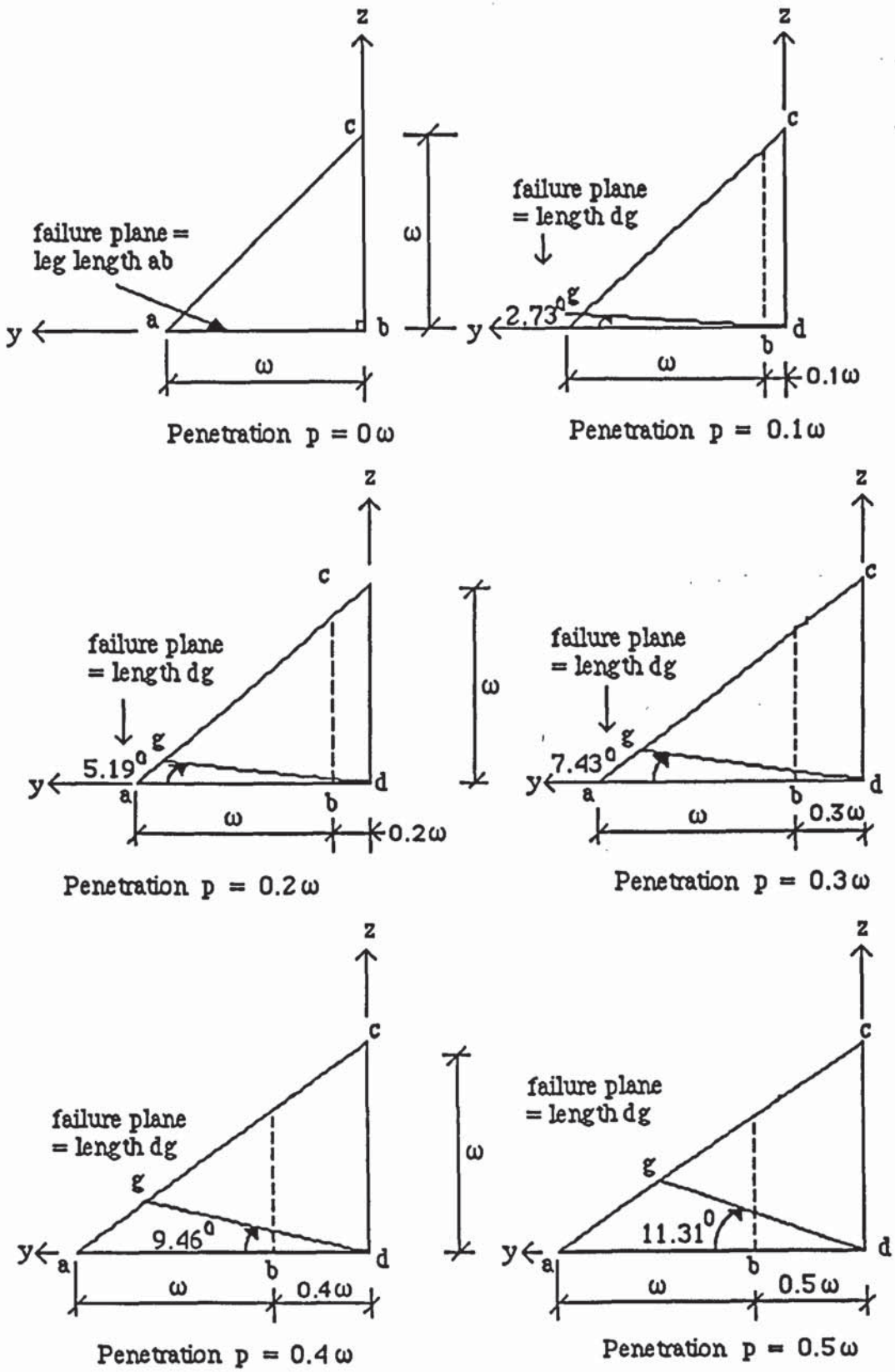

Figure 3.20 Predicted failure planes as weld penetration increases for tensile fillet welds.

It is worth highlighting the approximate nature of the present weld model and weld failure theories. Of all the existing weld failure theories, only two authors attempted to predict the location of the weld failure plane. These are the weld failure theories proposed by Kato and Morita[11], and that by Kamtekar[10]. Many of the other authors [10,35,42,44] theories and the present codes of practice BS 5950 and CP 118, have merely assumed the weld throat as the failure plane for convenience.

3.5.1 Conclusions from the proposed tensile failure weld theory.

1) Weld failure loads and failure planes can be predicted using the proposed weld model, incroporating weld penetration.

2) Weld failure loads increase as weld penetration values increase.

3) Location of the weld failure plane changes as weld penetration changes.

4) The length of the weld failure plane increases as weld penetration increases.

5) There is a unique failure plane for a given weld penetration value.

3.6 Proposed failure theory for shear fillet welds.

Considering the simple longitudinal fillet welded specimen shown in figure 3.21 below;

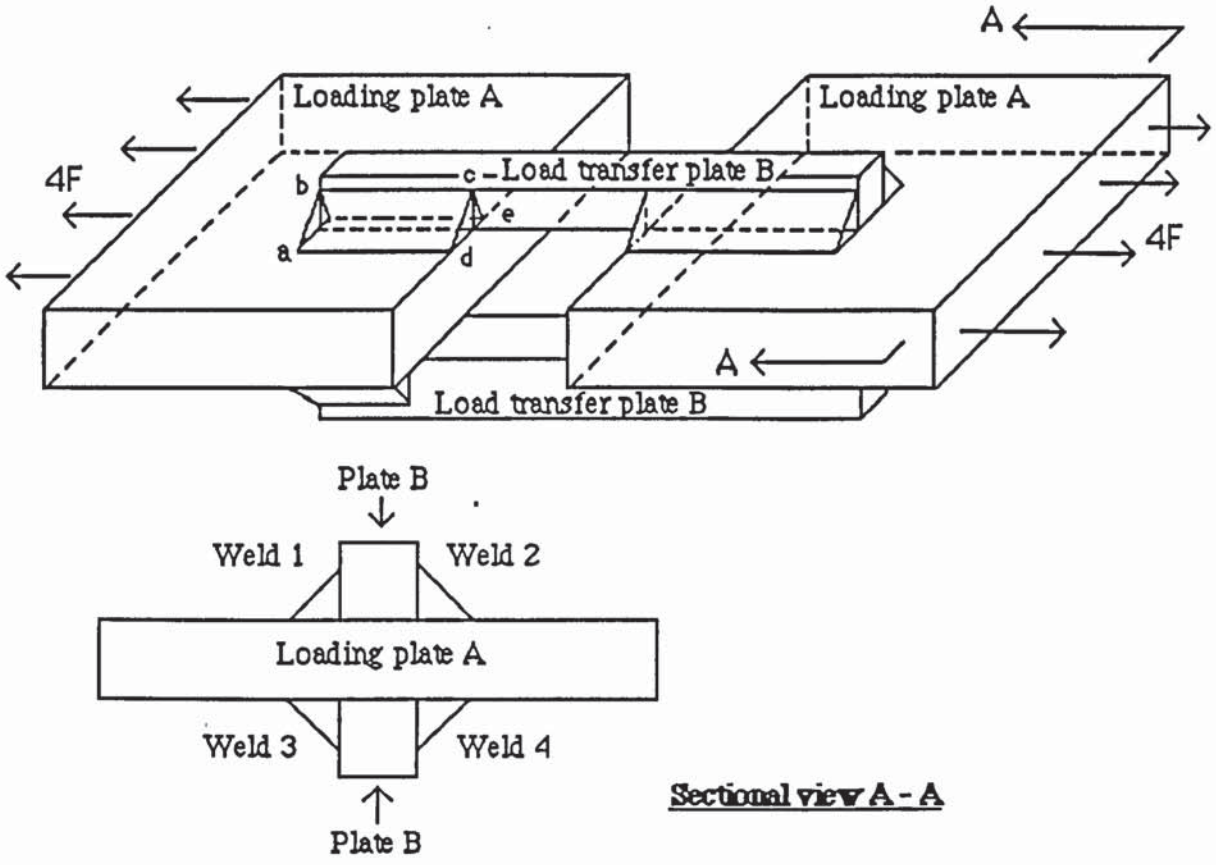

Figure 3.21 A simple shear fillet welded connection.

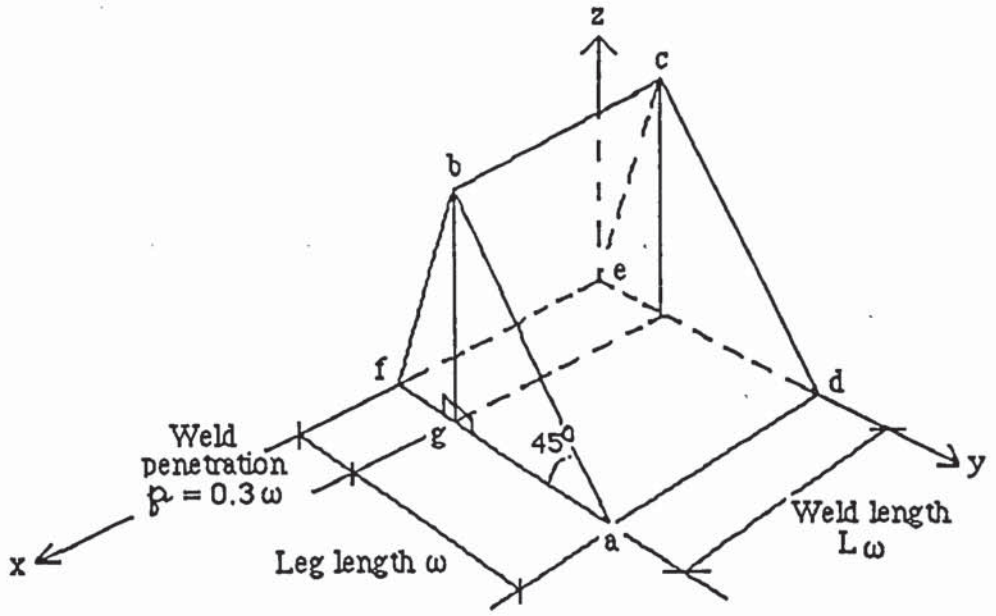

Figure 3.22 Geometry of shear weld abcdef.

The geometry of weld abcd, for a projected weld penetration value of 0.3ω is;

Length bf = 1.044ω

Angle bfg = 73.30^0

Angle fbg = 16.70^0

The forces acting on one weld abcdef, shown in figure 3.21 and below in figure 3.23;

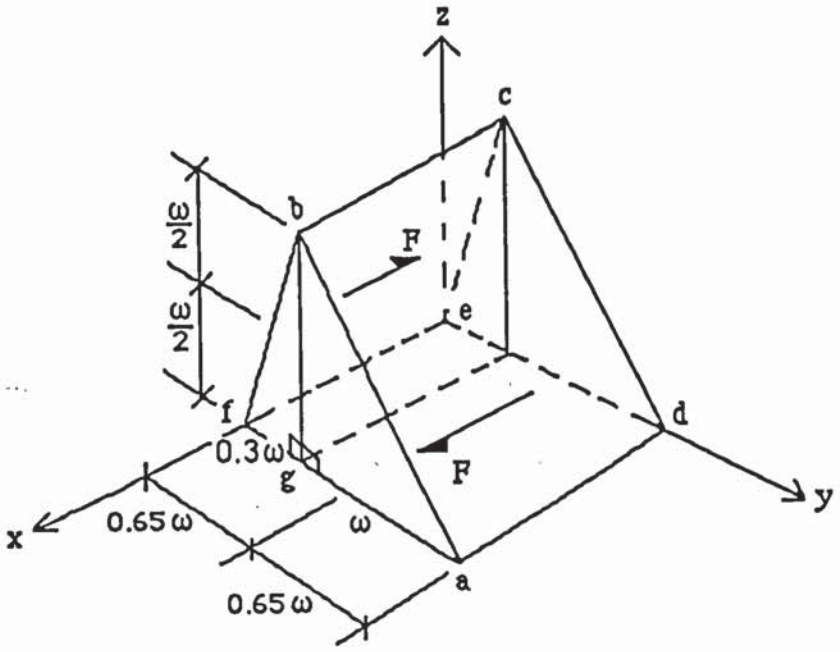

Figure 3.23 Shear forces acting on weld abcdef.

From statics, equal and opposite shearing forces F, act on faces bcef and efad, as shown in figure 3.23.

The sloping weld leg length bcef is also subjected to a moment $F/2(\omega - h)$, due to the eccentricity of the applied force F on the loading plate A and the force F on the sloping weld leg length bcef. This moment $F/2(\omega - h)$ acts parallel to the y axis and is shown below in figure 3.24.

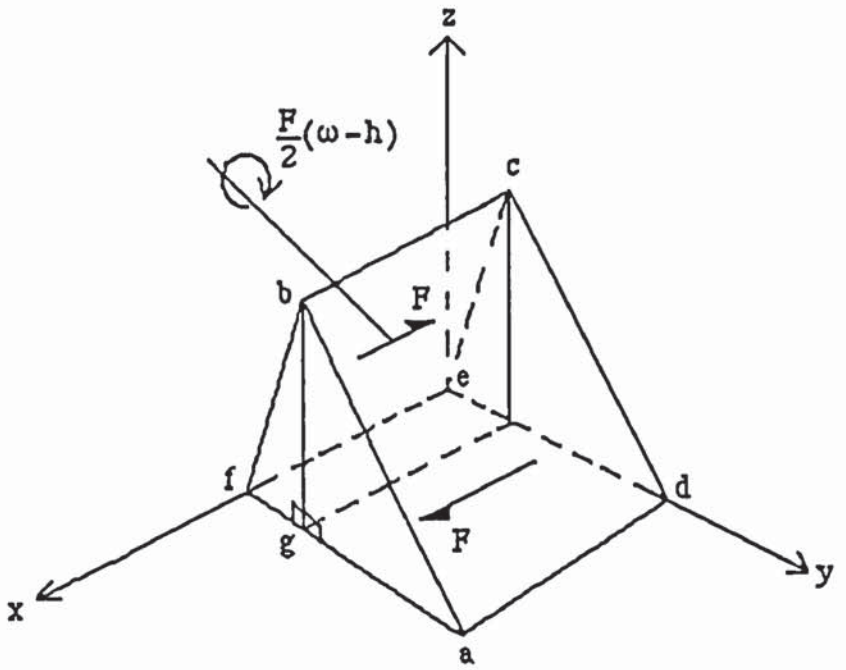

Figure 3.24 Moment F/2(ω - h) acting parallel to weld y - axis.

The sloping leg length bcef is also subjected to a moment Fω/2, due to the eccentricity of the two shearing forces F, acting on the sloping leg length bcef and the horizontal leg length adfe. This moment is applied in the z axis direction, as shown below in figure 3.25.

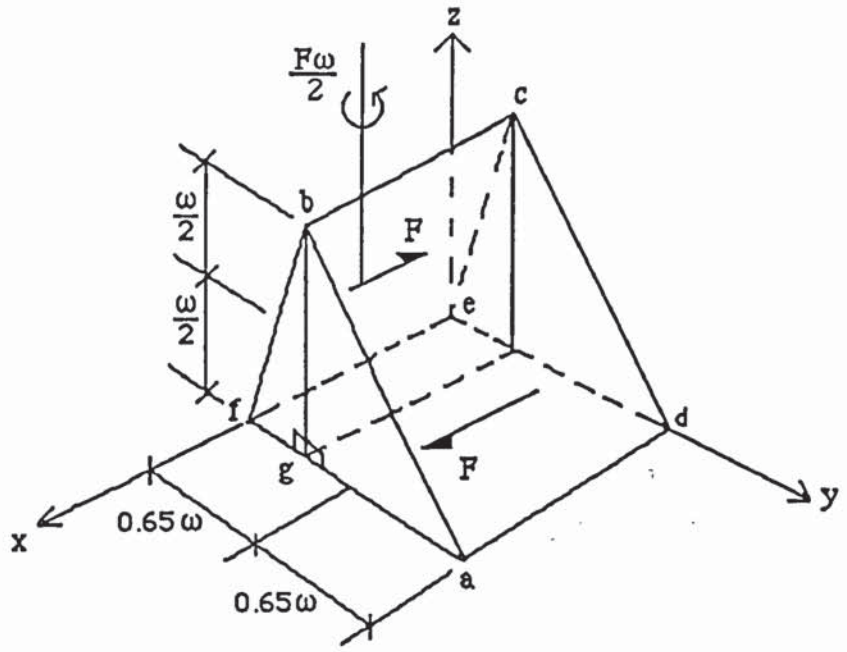

Figure 3.25 Moment Fω/2 acting in the Z axis

Finally, a moment Fh/2 also exists on the horizontal weld leg length adfe. This moment is due to the force F and moment F/2(ω - h) acting on the sloped leg length bcef. This moment Fh/2 acts parallel to the y axis direction as shown in the figure 3.26, below.

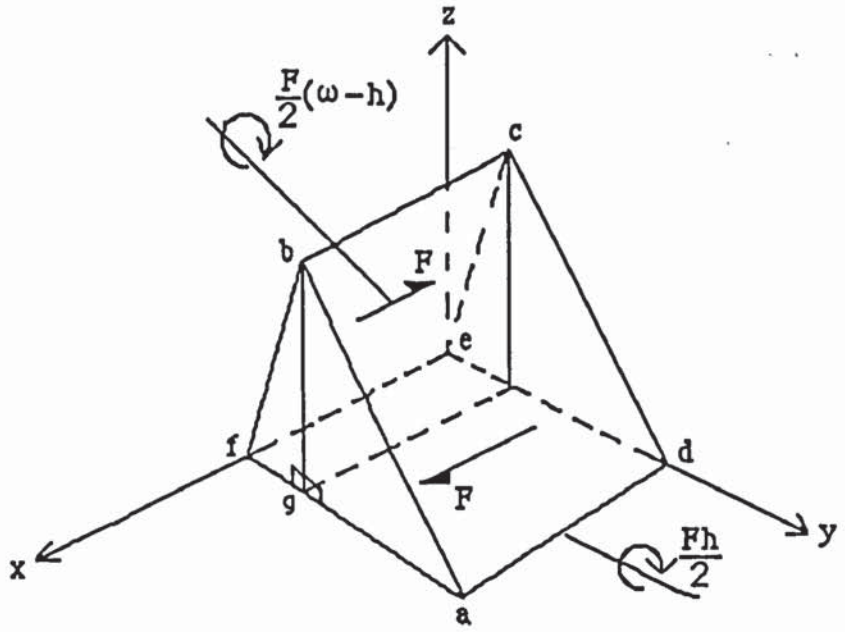

Figure 3.26 Moment Fh/2 acting parallel to weld y - axis.

Thus the total force system acting on the longitudinal fillet weld abcdef is as shown below in figure 3.27.

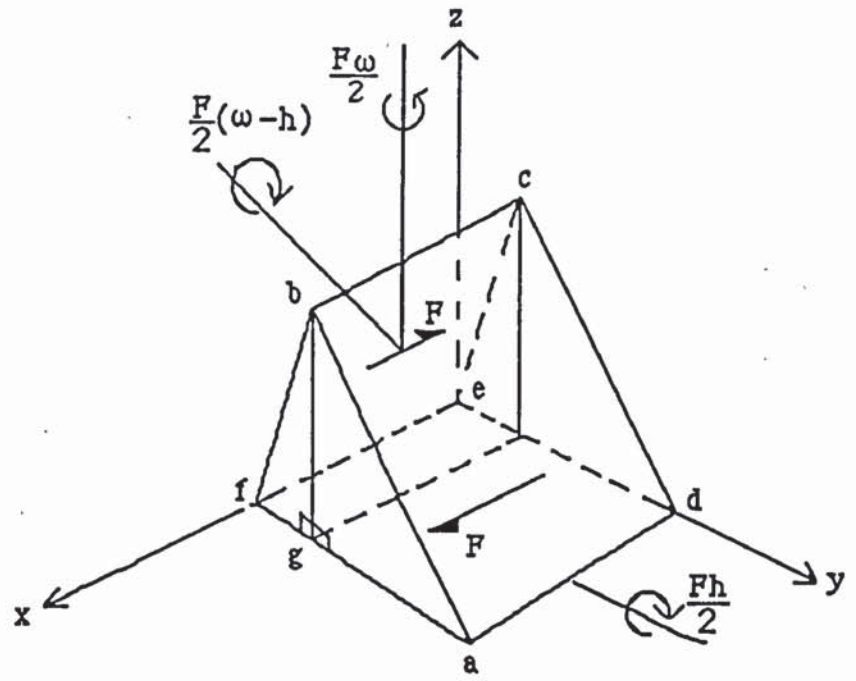

Figure 3.27 The total force system acting on the longitudinal shear fillet weld abcdef.

From figure 3.27, it is clear that the balancing moment needed in the y-axis,can be reduced to only $F\omega/2$. Further this balancing moment can be replaced by a force system such that the equilibrium of the weld force system is not affected. This can be achieved by applying a shearing force $F\omega/(2L_\omega)$, vertically downwards on the weld end face abf, which is balanced by a complementary shearing force $F\omega/(2L_\omega)$ applied on face dec, as shown in figure 3.28, below.

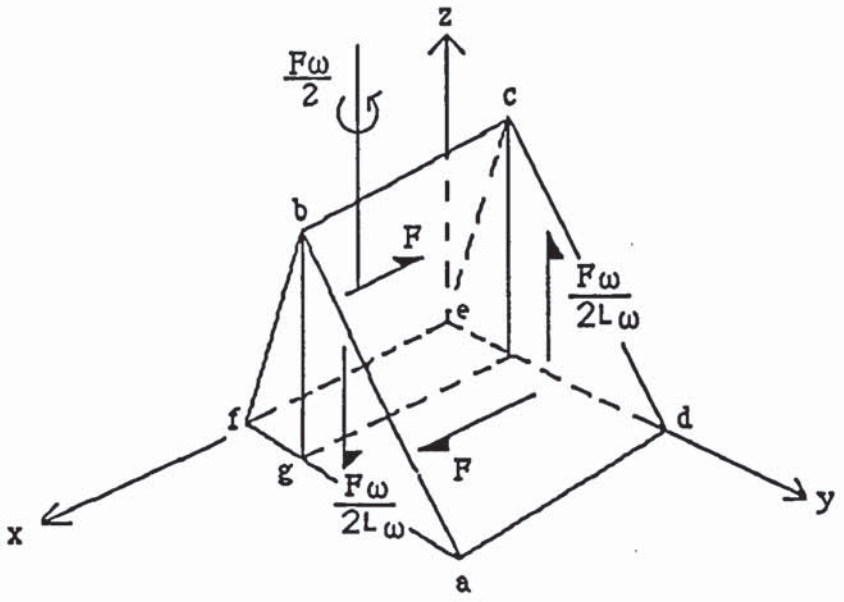

Figure 3.28 The balanced force system for moment $F\omega/2$ acting parallel to the weld y - axis.

Finally, also the moment $F\omega/2$ acting in the z-axis direction can be replaced by a force system such that the overall equilibrium of the weld is not altered. This is achieved by applying a horizontal shearing force $F\omega/(2L_\omega)$ on the weld end face abf which is balanced by a complementary shear force $F\omega/(2L_\omega)$ on weld face dec, as shown in figure 3.29 below.

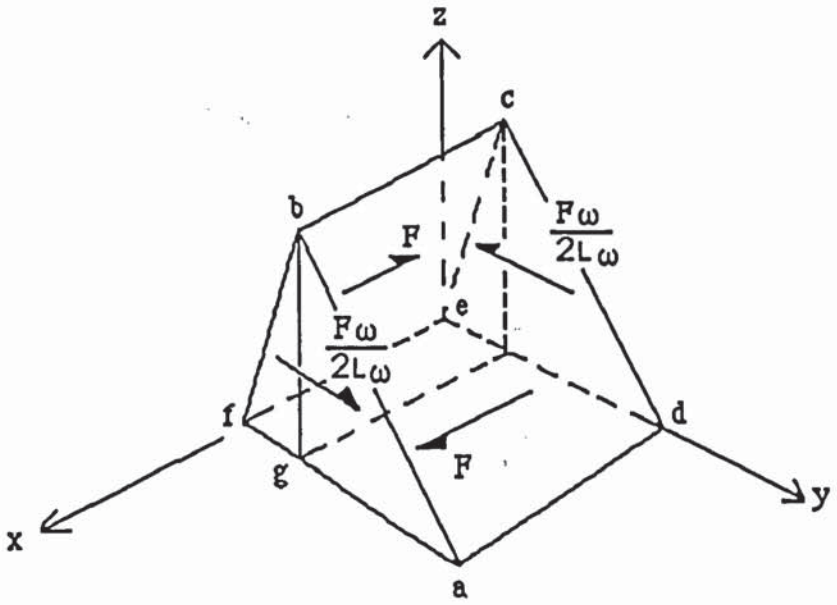

Figure 3.29 The replaced force system for moment Fω/2 acting in the z-axis.

Thus the total final force system is as shown below in figure 3.30, where the moments have been replaced by force systems, while retaining the weld in equilibrium.

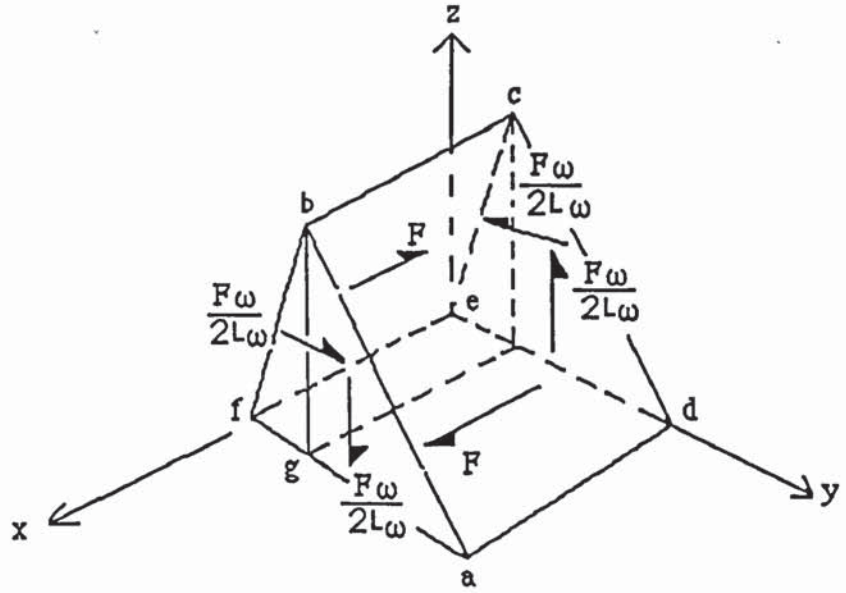

Figure 3.30 The total forces only acting on the longitudinal shear weld abcdef.

Strength of the longitudinal shear fillet weld.

The stresses acting on the weld faces shown below in figure 3.31 are obtained from the force diagram shown in figure 3.30.

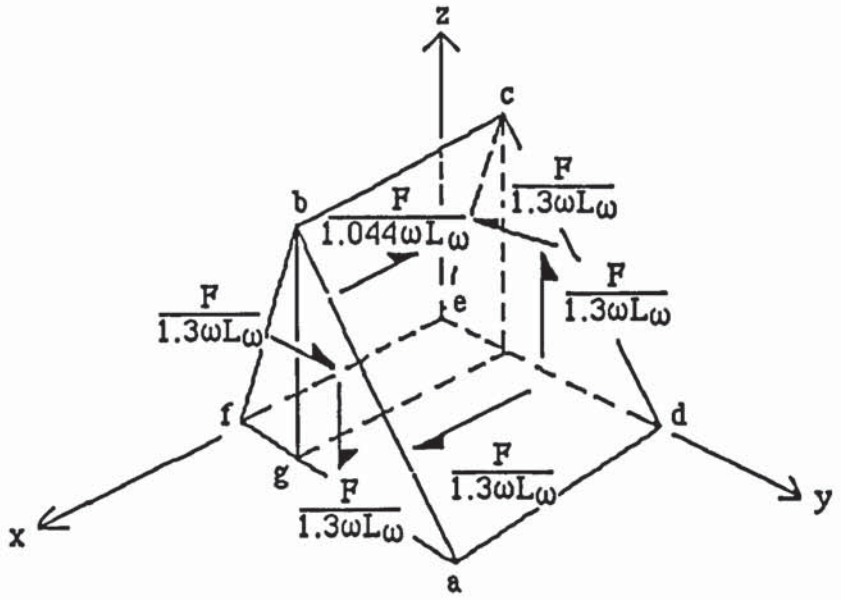

Figure 3.31 Stresses acting on longitudinal shear fillet weld abcdef.

Using the sign convention shown in section 3.4, the stresses σ_x, σ_y, σ_z, τ_{xy}, τ_{yx}, τ_{zx}, τ_{xz}, τ_{zy}, τ_{yz} can be listed as follows;

$\sigma_x = R$,

$\sigma_y = 0$,

$\sigma_z = 0$,

$\tau_{yx} = F/1.3\omega L_\omega$,

$\tau_{zx} = -F/1.3\omega L_\omega$,

$\tau_{xy} = F/1.3\omega L_\omega$,

$\tau_{xz} = -F/1.3\omega L_\omega$,

$\tau_{yz} = 0$,

$\tau_{zy} = 0$.

Let $\tau_1 = F/1.3\omega L_\omega$, then;

$\sigma_x = R$, $\sigma_y = 0$, $\sigma_z = 0$,

$\tau_{yx} = \tau_1$,

$\tau_{zx} = -\tau_1$,

$\tau_{xy} = \tau_1$,

$\tau_{xz} = -\tau_1$,

$\tau_{yz} = 0$,

$\tau_{zy} = 0$.

The value of the principal stresses can now be obtained for the above stresses, by using Southwell's[50] described method of solution, given by the equations 3.1 and 3.2.

Substituting these stress values into equation 3.1;

$$\begin{bmatrix} (R-p) & \tau_1 & -\tau_1 \\ \tau_1 & -p & 0 \\ -\tau_1 & 0 & -p \end{bmatrix} \begin{bmatrix} l \\ m \\ n \end{bmatrix} = 0$$

The solution for the above equation is found from the determinant which is of the same form given on page 93.

Thus the three principal stresses are found to be;

$p_1 = 0$, $p_2 = 0.5(R - U)$, $p_3 = 0.5(R + U)$

where $U = \sqrt{(R^2 + 8\,\tau_1^2)}$.

Substituting these three principal stresses p_1, p_2, and p_3 into the Von Mises

equation, given by equation 3.4 to give;

$$R^2 + 3(R^2 + 8\tau_1^2) = 4\sigma_u^2$$

rearranging to give; $$\tau_1 = \sqrt{\frac{\sigma_u^2 - R^2}{6}}$$

However, τ_1 is maximum when $R = 0$

$$\therefore \quad \tau_{max} = \frac{\sigma_u}{\sqrt{6}}$$

but also $$\tau_1 = F/1.3\omega L_\omega,$$

$$\therefore \quad \tau = \frac{\sigma_u}{\sqrt{6}} = \frac{F}{1.3\omega L_\omega}$$

$$\therefore \quad F = \frac{1.3\sigma_u.\omega.L_\omega}{\sqrt{6}} = 0.5307\sigma_u.\omega.L_\omega$$

The failure load of the simple longitudinal fillet welded connection is 4F;

$$4F = 2.123\,\sigma_u.\omega.L_\omega$$

The directional cosines (dcs) ℓ, m, n of the normals to the principal planes are obtained from equations 3.1 and 3.2, to give the following results;

When $p_1 = 0$ $\quad (\ell, m, n) = (0, 1/\sqrt{2}, 1/\sqrt{2})$

$$= (90^0, 45^0, 45^0)$$

This gives the weld sloping face abdc as the principal plane, see figure 3.32 below.

This is as expected, since the exposed weld face is always a principal plane.

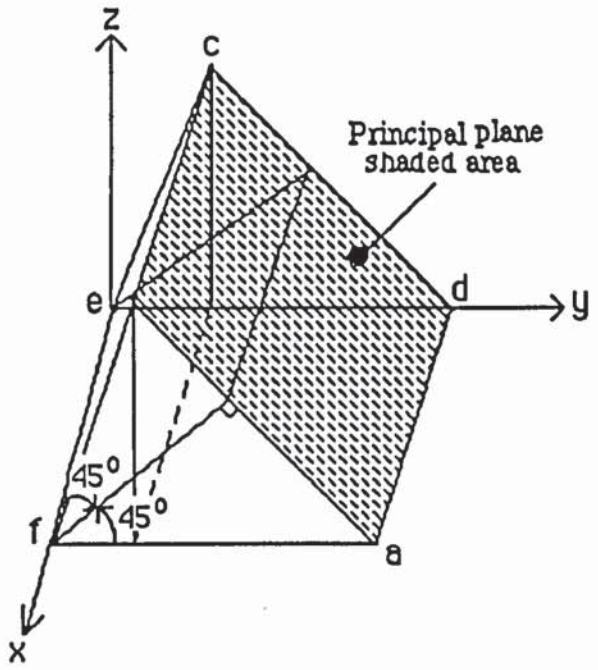

Figure 3.32 Principal plane for when principal stress $p = 0$.

Similarly when $p_2 = 0.5\,(R+U) = \sqrt{2}\,\tau$,

then $(l, m, n) = (1/\sqrt{2}, 1/2, -1/2)$

$$= (45^0, 120^0, 60^0)$$

Finally when $p_3 = 0.5\,(R - U) = -\sqrt{2}\,\tau$,

then $(l, m, n) = (1/\sqrt{2}, -1/2, 1/2)$

$$= (45^0, 60^0, 120^0)$$

and the position of the principal planes can be found.

From the results because $p_2 > p_1 > p_3$, the plane of maximum shear stress will be

inclined at 45^0 to the planes on which p_2 and p_3 are the principal stresses (Mohr's Circle). For this case, the plane of maximum shear stress is found to lie at 45^0 to the horizontal leg length adfe, as shown in figure 3.33. Failure would be expected along this plane.

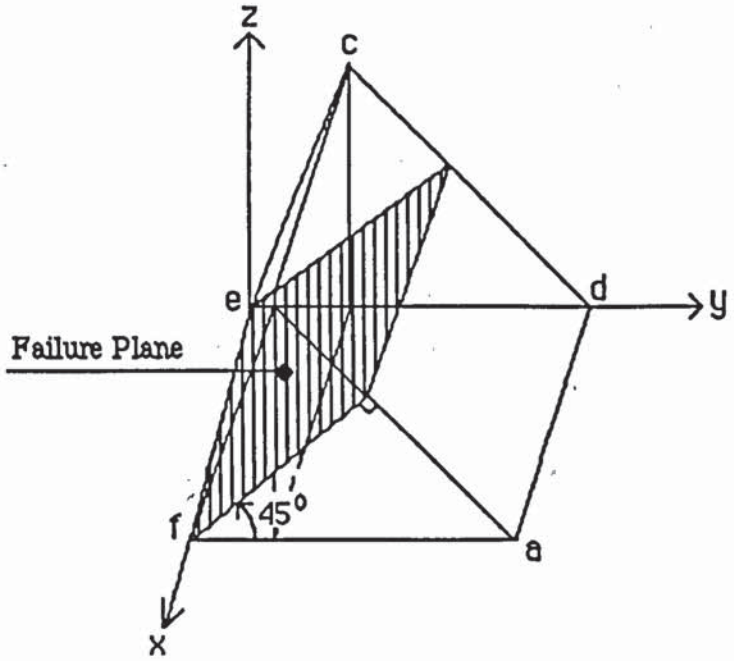

Figure 3.33 Predicted failure plane for longitudinal shear fillet weld.

If welds of equal leg lengths, but with varying projected penetration values are considered, Table 3.2, it is found that different failure load values and planes are obtained. As the projected penetration increases, the predicted failure loads also increase. However, the angle of the failure plane from the horizontal does not vary at all - always remaining at 45^0 -, but the length of the plane does increase Table 3.2. This finding is unlike that established earlier for tensile fillet welds, where it was shown that the slightest variation in penetration greatly effects the failure plane.

In comparison to Kato and Morita's[12] and Kamtekar's[11] theories, this result for the

failure angle is exactly the same. They too predict the failure angle for shear fillet welds to be at 45^0 from the horizontal leg length. This result of theirs corresponds to one where penetration is zero. The author has also shown this to be the case. Further the author has shown that the length of the failure plane increases as penetration increases, which in turn increases the failure load of the shear fillet weld, Table 3.2.

Leg Length ω (mm)	Horizontal penetration p (mm)	Shear failure load F_s (KN)	Shear failure load $4F_s$ (KN)	Failure plane ϕ^0	$\text{Tan}^{-1}\phi^0$	Length of failure plane (mm)
ω	0	0.4082 UTL	1.6328 UTL	45	1	$0.7071\,\omega$
ω	0.1ω	0.4490 UTL	1.7963 UTL	45	1	$0.7778\,\omega$
ω	0.2ω	0.4899 UTL	1.9596 UTL	45	1	$0.8485\,\omega$
ω	0.3ω	0.5307 UTL	2.1229 UTL	45	1	$0.9192\,\omega$
ω	0.4ω	0.5715 UTL	2.2860 UTL	45	1	$0.9899\,\omega$
ω	0.5ω	0.6124 UTL	2.4495 UTL	45	1	$1.0607\,\omega$
ω	0.6ω	0.6532 UTL	2.6128 UTL	45	1	$1.1314\,\omega$

UTS = Ultimate Tensile Load $\sigma_u.\omega.L_\omega$

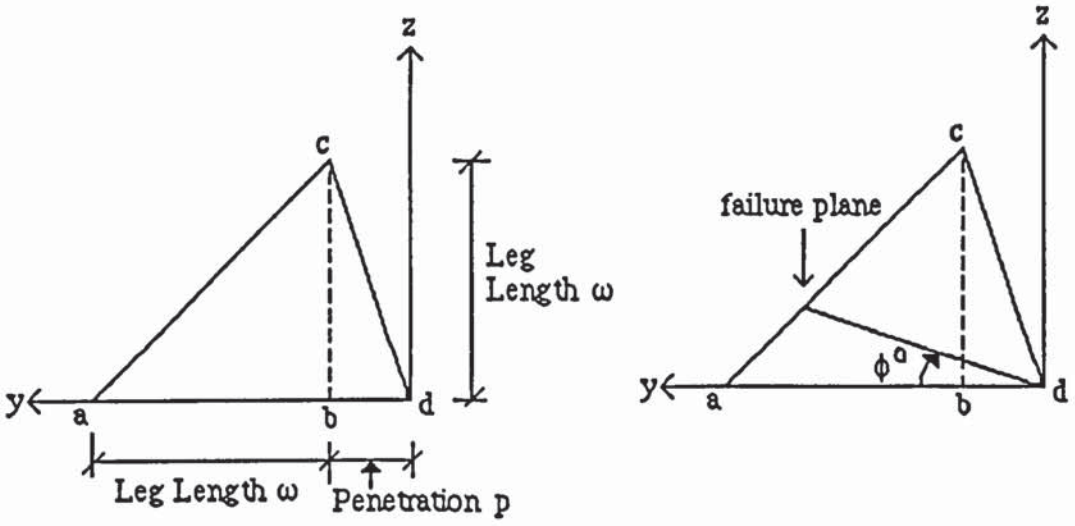

Table 3.2 Calculated values of shear weld failure loads and failure planes as weld penetration (p) changes.

3.6.1 Conclusions from proposed shear fillet weld theory .

1) Shear failure loads and failure planes can be predicted for a given amount of weld penetration.

2) Weld failure loads increase as penetration values increase.

3) The angle of the failure plane is always at 45^0 to the horizontal leg length, despite the increase in penetration.

4) The length of the weld failure plane increases as weld penetration increases.

CHAPTER 4 FAILURE ANALYSIS OF THE TEMPORARY END PLATE CONNECTION.

4.1 Introduction.

The temporary connection shown in figure 4.1, is to be analysed by the same approach applied to the tensile and shear fillet welded connections, i.e. to replace the acting forces by an 'equivalent' system of equilibrium forces. For this connection it is not simply a matter of replacing an eccentric force F, but also to replace an applied moment MF, (shown as M_x and M_y in figure 4.1) arising from the nature of the applied load, acting out of the plane.

The additional assumptions to those made in Chapter 3, section 3.3, for this analysis are;

i) The total failure load is equal to the summation of the load on a number of smaller width plates, acting as beams with a central point loading, figures 4.2 and 4.3.

ii) The applied end moments and forces on the welds from the plate strips are equal to those for a fully fixed end condition, and act uniformly along the length of the weld.

iii).The point loading can be replaced by an equivalent uniform line load acting along the length ab, figure 4.4.

iv) Failure is expected to occur in the welds only.

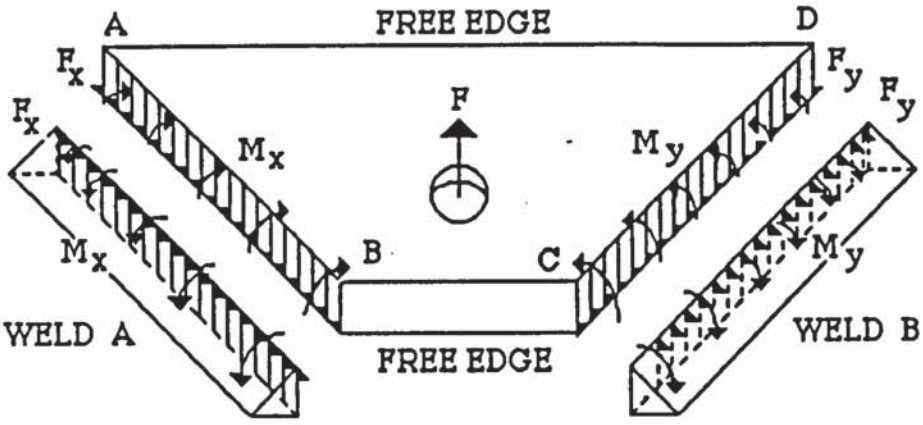

Figure 4.1 Actual loading of temporary end plate connection .

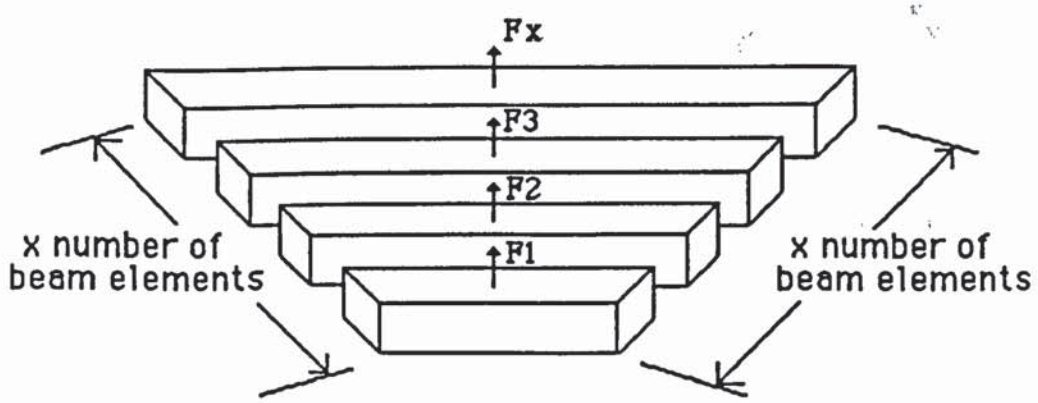

Figure 4.2 Trapezium plate sub-divided into x number of beam elements.

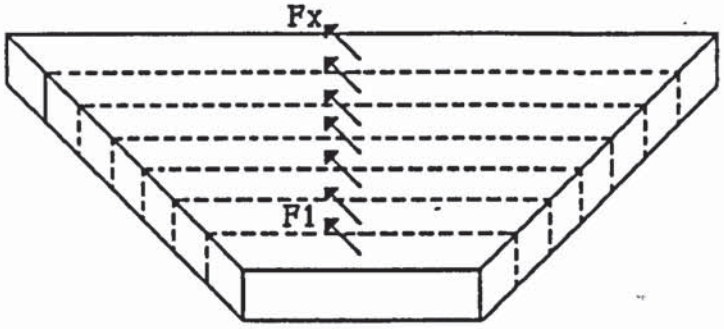

Figure 4.3 Summation of beam elements to give actual trapezium plate shape.

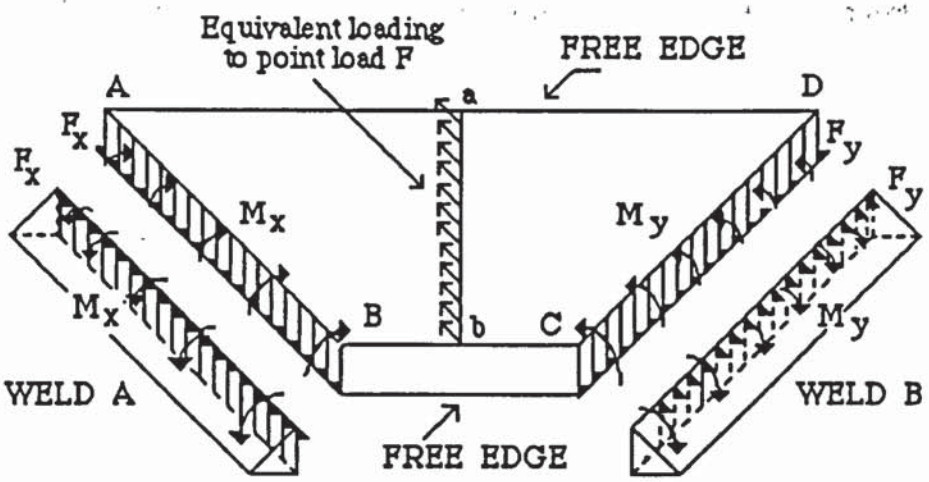

Figure 4.4 Assumed equivalent loading of temporary end plate connection.

4.2 Failure analysis of end welds.

For the general case of a point load 2F consider forces acting on the welds A and B at any typical cross section X-X through the end plate, as shown in figure 4.5.

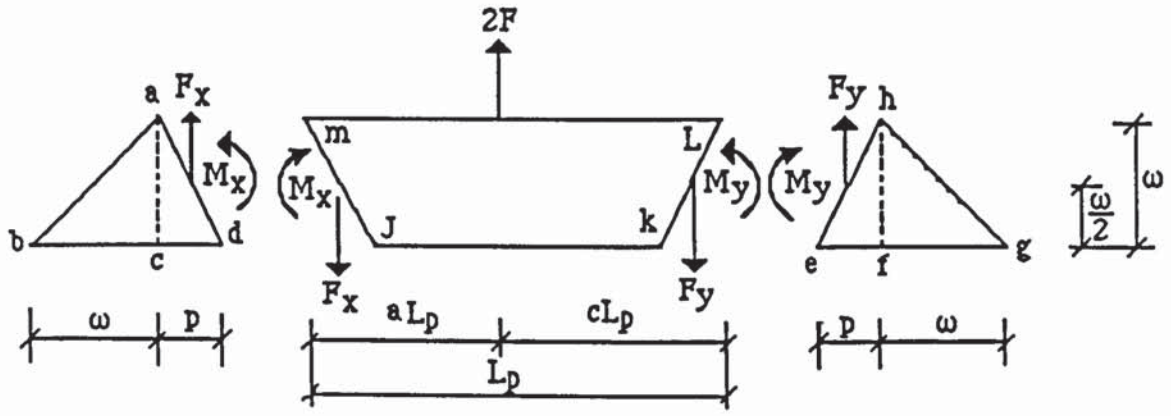

Figure 4.5 Forces on fillet welds in the temporary end plate welded connection.

For a fixed end condition we have;

$$M_x = K'_A.2F.L_p$$

$$M_y = K'_B.2F.L_p$$

$$F_x = 2F\,(1 - r_b)$$

$$F_y = 2F.\, r_b$$

where $K'_A = a\,(1 - a)^2$

$K'_B = a^2\,(1 - a)$

$r_b = a^2\,(3 - 2a)$

Forces on weld abcd;

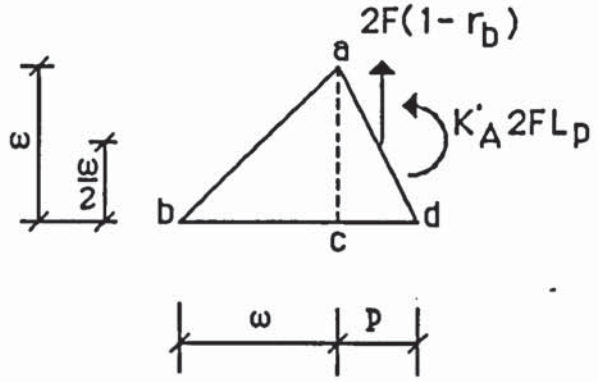

Figure 4.6 Actual forces acting on weld abcd.

satisfying vertical equilibrium;

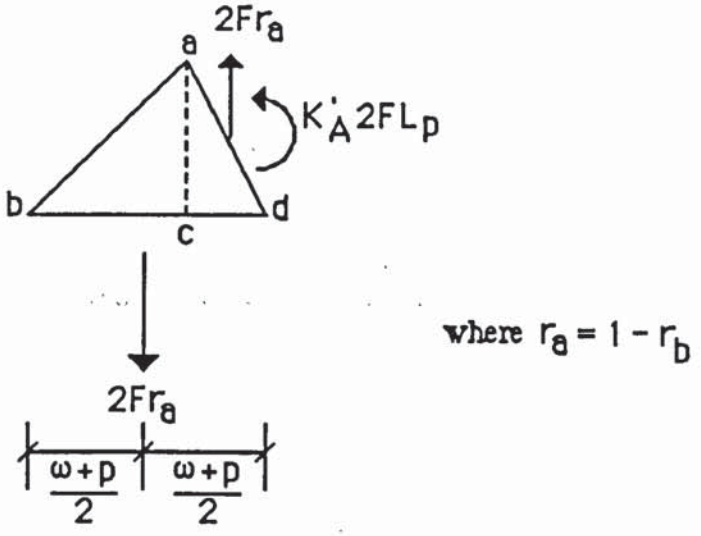

Figure 4.7 Vertically balanced weld abcd.

The applied moment $K'_A 2FL_p$ can be replaced by a pair of eccentric forces, to induce a moment of this magnitude on the weld. The eccentricity between these forces is taken to equal ω/2, such that;

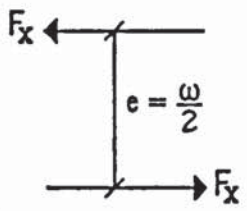

$$F_x \cdot \frac{\omega}{2} = K_A 2FLp \quad \text{---- Equation 4.1}$$

These forces are applied on the weld such that a force F_x shears along the horizontal leg length and the balancing force F_x acts as a compressive force on the sloping weld leg length ad, as shown in figure 4.8.

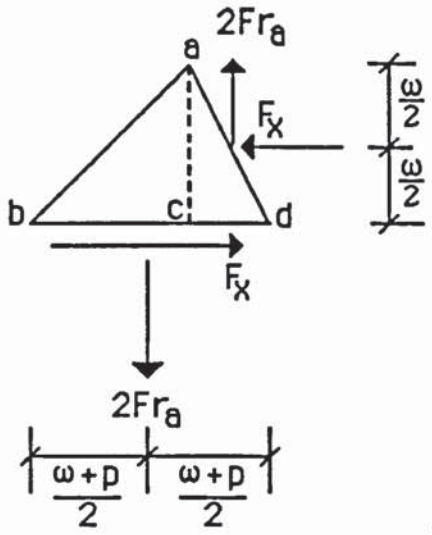

Figure 4.8 Vertically and horizontally balanced weld abcd.

Thus, so far the applied moment has been replaced by a horizontal shear force F_x, and satisfied equilibrium horizontally and vertically.

The final stage is to satisfy the net out of balance moment. Therefore, taking moments at d, figure 4.8.

$$M_d = F_x \frac{\omega}{2} + 2F \cdot r_a \left(\frac{\omega + p}{2} - \frac{p}{2}\right)$$

$$M_d = \frac{\omega}{2}\left(F_x + 2F \cdot r_a\right)$$

This moment M_d needs to be replaced by a pair of eccentric forces, such that the resulting couple is equal to this moment. From inspection of the forces present on the weld model in figure 4.8, it is clear that the desired moment M_d can be achieved in two different ways.

The first method requires eccentric forces equal to $(F_x + 2F.r_a)$ to act in the y - direction, at a distance of $\omega/2$ apart, as shown below;

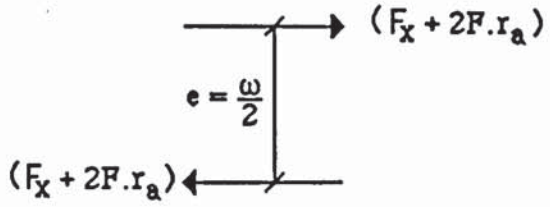

This pair of eccentric forces produces a couple equal to the moment M_d. It is applied to the weld metal profile, shown in figure 4.8, such that the force $(F_x + 2F.r_a)$ shears along the horizontal leg length bd on which an opposing shear force F_x already exists. The other balancing force acts as a tensile force on the sloping leg length ad on which a compressive force F_x already exists, figure 4.8. This results in the total force system being represented by figure 4.9, which shows the weld metal is now in tension under tensile forces $2F.r_a$ only.

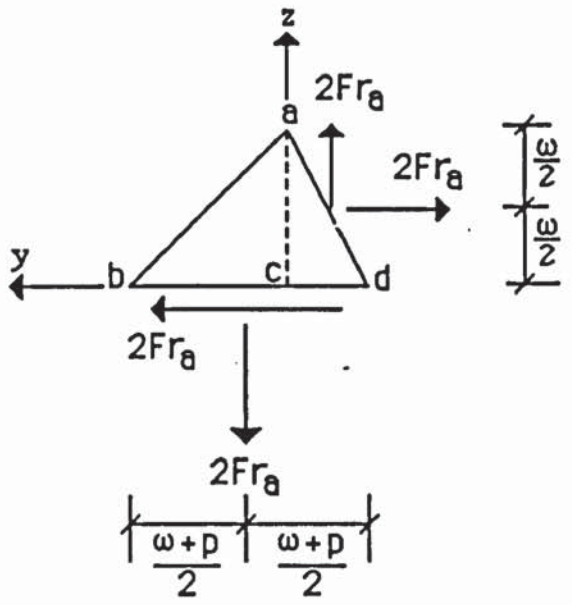

Figure 4.9 Balanced forces on weld abcd, due to application of forces ($F_x + 2F.r_a$) in y-direction.

The second method of achieving the moment M_d, requires the eccentric forces of magnitude ($F_x + 2F.r_a$), to act in the z - direction, on the weld metal profile figure 4.8. In this case a force ($F_x + 2F.r_a$) would act compressively on the horizontal weld leg length, where a tensile force $2F.r_a$ already exists. Similarly, a compressive force ($F_x + 2F.r_a$) acts on the sloping weld leg length, where a tensile force $2F.r_a$ also already exists.This results in the total replaced force system being represented by figure 4.10 The weld metal is now under compressive forces F_x only.

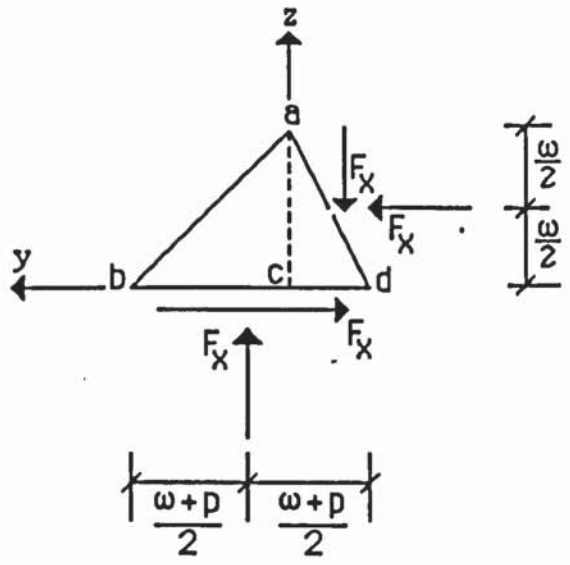

Figure 4.10 A second balanced force distribution diagram for weld abcd, due to the application of eccentric forces ($F_x + 2F.r_a$) in the z-axis direction.

Thus, two different force systems acting on the weld abcd have been produced, for a single loading case - a shear force $F_x = 2F\ (1 - r_b)$ and a moment $M_x = K'_A.2F.L_p$.

The first force system is one where the weld is totally in tension, due to only tensile forces $2F.r_a$ acting , as shown in figure 4.9.

The second force system is where the weld is under totally compressive forces only, of magnitude F_x. This is shown in figure 4.10.

The failure load for the first force system (tensile) acting on the weld figure 4.9, corresponds to the failure for a fillet weld in tension. The theory for tensile fillet welds with equal leg lengths and a given penetration, derived in Chapter 3 can be used to predict failure of the weld.

Therefore, from Chapter 3 section 3.5, the failure equation for a fillet weld in tension is given as;

$$F = \xi.\sigma_u.\omega.L_\omega$$

where ξ is the constant depending upon the extent of weld penetration achieved. ξ.can be obtained from either the theoretical derivation in chapter 3 or from a general graph obtained from table 3.1, which is given in the discussion chapter 7, figure 7.2.

For the weld case at hand, the applied tensile force $F = F_X$ and $F_X = 2F.r_a$

Therefore $$2F.r_a = \xi.\sigma_u.\omega.L_\omega$$

Rearranging to give $$F = \frac{\xi \,.\, \sigma_u .\, \omega \,.\, L_\omega}{2r_a}$$ Equation 4.2

Thus the failure of the weld in tension is predicted by equation 4.2, However, the total failure load for the temporary end plate connection is 4F;

$$F_{TOTAL} = \frac{2\xi \,.\, \sigma_u .\, \omega \,.\, L_\omega}{r_a}$$ Equation 4.3

The failure load for the second force system (compressive) acting on the weld, figure 4.10, corresponds to the failure of a fillet weld in compression. It can be shown that this failure load is the same as that for a fillet weld in tension, i.e.weld failure loads predicted by this method are the same for either tensile or compressive force conditions.Thus, for this compressive force system, the predicted failure equation is that given in chapter 3 by;

$$F = \xi.\sigma_u.\omega.L_\omega$$

However, for this case F relates to F_X ,

but $F_X.\omega = K'_A.4F.L_p$ from equation 4.1.

this gives $$F_x = \frac{K'_A . 4 . F . L_p}{\omega}$$

therefore; $$\frac{K'_A . 4 . F . L_p}{\omega} = \xi . \sigma_u . \omega . L_\omega$$

this gives; $$F = \frac{\xi . \sigma_u . \omega^2 . L_\omega}{4 . K'_A . L_p} \qquad \text{Equation 4.4}$$

Equation 4.4 is the failure of the weld corresponding to the force system shown in figure 4.10. The total failure load F_{Total} is equal to 4F ;

$$F_{TOTAL} = \frac{\xi . \sigma_u . \omega^2 . L_\omega}{K'_A . L_p} \qquad \text{Equation 4.5}$$

Thus, it is found that two different failure loads exist for the one loading case figure 4.5, for a weld with equal leg lengths and any given penetration value, p. This would suggest that there actually exists two different conditions for the weld to fail. The first equation 4.3, would correspond to when the weld is under predominantly tensile forces, i.e. when the tensile force $F_X = 2P(1 - r_b)$ is larger than the moment $M_X = K'_A.2P.L_p$. The second failure equation 4.5 corresponds to when the weld is under predominantly compressive forces, i.e. when the moment $M_X = K'_A.2P.L_p$ is larger than the tensile force $F_X = 2P(1 - r_b)$.

For the end plate connection with the loading situation as shown in figure 4.5, it would be expected that equation 4.5, would define the failure of the connection. This is

because the point of application of the load, at a distance of $0.5L_p$, would result in a much larger value of the moment M_x than of force F_x.

This can be verified by equating equations 4.3 and 4.5 as follows;

Equation 4.3 can be re-written for a value of $r_a = 0.5$, where the load is applied at $0.5L_p$, as;

$$F_{Total} = 4.\xi.\sigma_u.\omega.L_\omega \qquad \text{Equation 4.6}$$

Equation 4.5 can also be rewritten for the same value of $r_a = 0.5$ which results in $K'_A = 0.125$ to give;

$$F_{TOTAL} = \frac{8 . \xi . \sigma_u . \omega^2 . L_\omega}{L_p} \qquad \text{Equation 4.7}$$

Therefore, equating equations 4.6 and 4.7 gives;

$$4 . \xi . \sigma_u . \omega . L_\omega = \frac{8 . \xi . \sigma_u . \omega^2 . L_\omega}{L_p}$$

$$L_p = 2\omega$$

This result shows that for equation 4.3 to give a lower load of failure than that predicted by equation 4.5, $2\omega > L_p$ or $L_p < 2\omega$.Neither of these conditions are ever possible for the temporary, end plate connection.Thus at all times $L_p > 2\omega$ and failure is predicted by equation 4.5 only.

A check of the method of applying the forces to the weld can also be made by finding the failure load if a = 0. This gives a failure load value, equal to that for a tensile fillet weld. This is correct since M_x is also equal to zero, and thus only a tensile force acts on the welds.

If the location of the point of application of the load is varied, i.e. between a = 0 and a = 1, then it would be expected that failure would occur at the lower of the two loads predicted by equations 4.3 and 4.5.

For a symmetrically loaded connection, that is when a = 0.5, as in the case for the connection under investigation, forces induced on the weld efgh will be the same as those experienced by weld abcd. However, should the penetration value, p, of the weld efgh be different to that of abcd, then the overall failure load would also be affected.Throughout this failure theory, it is assumed that penetration values for welds abcd and efgh are the same. This may not be the case in practise, since the numerous parameters affecting penetration (discussed in chapter 2), may vary from weld to weld. In this case an average penetration value may be used for predicting the failure load from the equations derived above.

4.3 Application of Kamtekar's weld model to predict failure of the welds of the end plate connection.

Kamtekar's weld model is basically a case when penetration is equal to zero in the author's weld model, figures 4.5 and 4.6. For this case i.e. zero penetration, the end plate welded connection failure load can be shown to be;

$$F_{TOTAL} = \frac{\sigma_u . \omega^2 . L_\omega}{\sqrt{3}\, K_A . L_p} \qquad \text{Equation 4.8}$$

4.4 Application of the derived weld failure theory for the end plate connection.

The end plate weld failure theory has been developed on the assumption that the applied end moments and forces on the welds, are equal to those for a fully fixed end beam. It is thus expected that the final failure load for the welds would be calculated as the summation of the failure loads for an x number of beam elements, making up the trapezoidal shaped plate figures 4.2 and 4.3. The x number chosen would depend upon the degree of accuracy required. Without this procedure becoming tedious, it is found good convergence of results is achieved if the plate is sub-divided into six beam elements. A good approximation is achieved by a sub-division into three beam elements.

CHAPTER 5 EXPERIMENTATION METHODS AND RESULTS.

5.1 Introduction

In this chapter the procedures adopted to fabricate and test all specimen, in this research programme are set out. All experimental results are given, but the discussions and full analysis is deferred to chapter 7.

Tensile tests were carried out to BS18; part 1, to establish the parent metal, heat affected zone (HAZ) and weld metal material properties. Hardness surveys using the Vickers Hardness test to BS 427; part 1, are conducted to establish the pattern and extent of softening present, due to welding. The results of these tests are given in sections 5.2.2 and appendix A.

Twenty - six tensile and shear fillet welded connections were produced from the parent plate material (6082 - T6 aluminium) and tested to failure, under a uniaxial tensile load.

Fifteen cruciform shaped fillet welded connections shown in figure 5.10, were also fabricated from the parent plate. These specimen were tested to failure, under equal biaxial loads.

For all test fillet welds, meticulous care and attention was taken to record the extent of weld penetration achieved, using a universal measuring machine. The angle of the failure plane of the welds was measured on a shadow graph recorder. These results are given in the experimental failure load tables in section 5.2.4, for each type of specimen tested.

Thirty temporary end plate (welded) aluminium space frame connections were produced from extruded tubular section and rolled plate aluminium 6082 - T6 and tested to failure. Rossette strain gauge arrangements were used to find the stress distribution along the welded edges of the end plate connections. Load deflection readings were also taken. These results are given in section 5.2.5.4.2 and appendix B.

5.2 Specimens.

5.2.1 Material.

All specimens are of the aluminium alloy 6082 - T6, obtained in the rolled plate and extruded tubular form of 13mm thickness. The composition of the 6082 - T6 alloy is shown in table 5.1.

METAL	%
Silicon	0.7 - 1.3
Iron	< 0.5
Copper	< 0.1
Manganese	0.4 - 1.0
Magnesium	0.6 - 1.2
Chromium	< 0.25
Zinc	< 0.20
Titanium	< 0.10
Zirconium	< 0.05
Aluminium	Remainder

Table 5.1 Composition of 6082 alloy.

The filler metal wire used for all welding was 4043A (NG21). This choice of combination of the parent metal and filler wire is as recommended by CP118, BS 2901; Part 4 and extensively used in industry .

All materials and specimen were stored in a clean, dry standard laboratory, away from any heat or high temperature environment.

5.2.2 Specimen preperation.

As pointed out at an aluminium welding seminar [51], high quality welds must be achieved the first time, in structural applications. This is because not only is repair welding expensive, but it also reduces the load carrying capacity of the joint. Furthermore, weld integrity does not only depend upon the cleaning procedures and welding techniques adopted, but also to a very large extent upon the welder proficiency. CP118 and BS 8118 stipulate that all structural welding must be carried out by an approved welder, whose capability of consistency must be demonstrated at regular intervals.

Throughout this experimental work, set welding procedures to BS 3571; part 1, BS 4870; part 2, and approval tests to BS 3451, have been adhered to by the author.

All plate and tubular specimen were liquid cooled, saw cut in order to eliminate any residual temperature effects which could be induced on the specimen. All edge preperations were cold planed and based upon recommendations made by BS 5371; part 1, CP 118, BS 8118, and BS 5135.

To achieve the high quality and consistent welds, the following set procedures were adopted. These are based upon recommendations made by Robertson and Dwight [3,4], Soetens [5,6,14], BS 3571, BS 3451, BS 4870; part 2, CP118 , the Aluminium Foundation seminars [13,16,21,51], and on the personal correspondence with British Oxygen U.K. Limited and Light and Sound International [2].

i) Welder proficiency was examined to the satisfaction of the author. Dummy replicas of the specimen were prepared just before the experimental specimens preperarion.First a visual inspection for quality, apperance, size, consistency, contamination and cracks was made. Then cross sectional cuttings were made, generally restricted to three, to inspect the achieved weld profile for root penetration, contamination, voids and any weld inconsistency.

ii) Cleaning of all fusion faces, by the removal of the oxide layer was executed in a set sequence. Degreasing first, then scratch brushing and then degreasing again.Scratch brushing was by a power driven, corrosion resisting, stainless steel brush. Care was taken to keep it clean and dry. The interval between cleaning and welding was kept as short as possible and did not exceed six hours.

iii) All multi - pass specimen with more than one weld run were allowed to fully cool to room temperature between successive weld runs.

iv) Run on and run off plate strips were machined off the final specimen.

v) Backing plates of the same alloy 6082 - T6, were used throughout.

vi) Any tacking required was minimised by the use of clamps, but where needed, it was both widely spaced and small in size.

5.2.3 Butt - welded specimen.

These specimen were used to determine the patterns of hardness and material properties in the weld, HAZ, and the parent metal. The size of the butt specimen and the location of the coupons is shown in figure 5.1. Two passes of weld were laid, with full cooling being allowed after each pass.

5.2.3.1 Strength coupons.

Two sets of parent metal (aluminium alloy 6082 - T6) coupons were tested for their material properties. The first set of twelve, denoted by the MP prefix and shown in figure 5.2, were saw cut from a large, as delivered parent metal sheet. The second set of twenty five specimens, denoted by the P prefix, were saw cut from the single 'V' butt welded specimen in a parallel direction to the weld , figures 5.1 and 5.3.

Thirty heat affected zone metal coupons, denoted by the H prefix and eighteen weld metal (4043A) coupons, denoted by the W prefix, were also tested for their material properties. These too were saw cut out, in a parallel direction to the weld laid, from the single 'V' butt welded specimen shown in figure 5.3. A further fifteen transverse weld metal specimen were tested in the transverse direction, obtained from a special butt welded specimen described later on below..

All coupons were waisted and prepared to BS 18; part 1, by milling and saw cutting at low speeds to reduce any heating effects on the specimens.

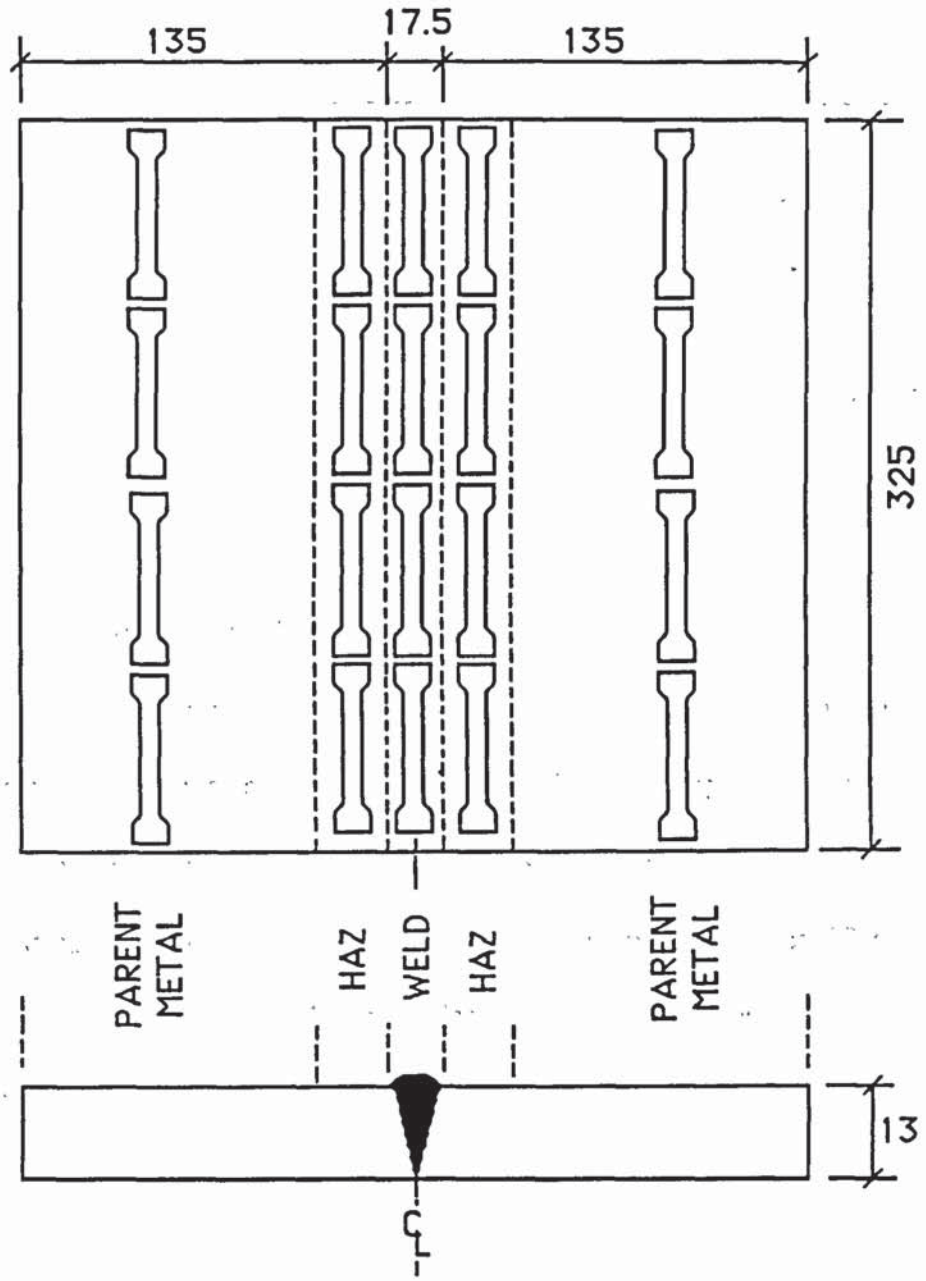

Figure 5.1 Extrapolation of weld, HAZ and parent metal coupons.

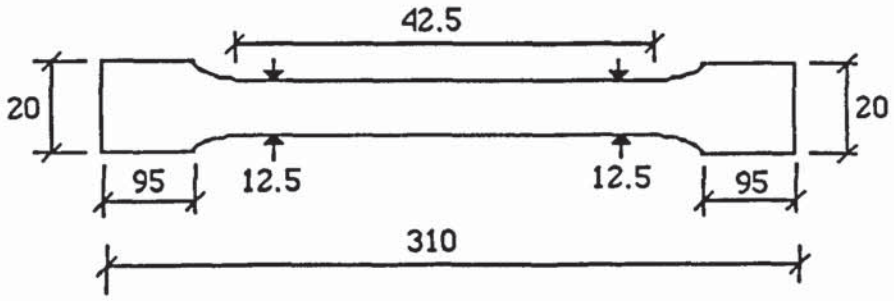

Figure 5.2 A typical parent metal coupon taken from main parent metal sheet.

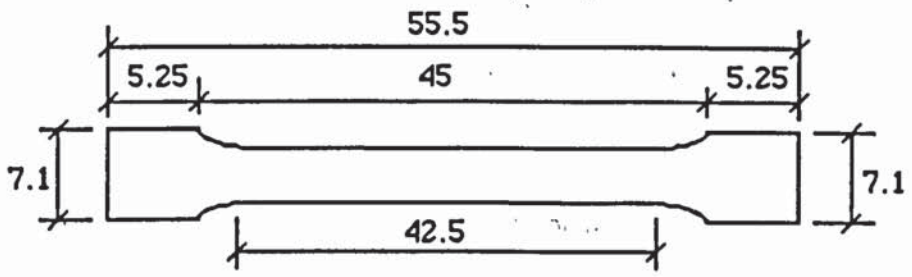

Figure 5.3 Typical longitudinal tensile parent,weld and HAZ coupons taken from 'V' butt welded specimen.

All tests were preformed on an Avery Dennison digital tensile testing machine. For the MP type coupons, a 50mm extensometer was attached to the gauge length to record extension. A loading rate of 0.5KN/min., was applied. For all other coupon specimen, strain was measured using electrical resistance strain gauges adhered on either side of their gauge lengths. Readings were recorded by a digital scanning strain recorder. The loading rate applied to these coupons was 0.1KN/min.The test results are given in Tables 5.2 to 5.6. The discussions are deferred to chapter 7.

Since the weld size for a 'V' shaped butt weld is narrow, a transverse coupon cannot be extracted from a welded specimen. A plain faced butt welded specimen was introduced to obtain a transverse weld specimen, figure 5.4. This specimen was obtained from two seperate plates. Each was welded on to a backing plate shown in figure 5.5a. The two halfves were then clamped and held together in a jig, and welded by a run on weld pass, seen in figure 5.5b. Eight consecutive weld passes were laid up to the plate surfaces.The eighth pass was the final capping pass. Full cooling of the specimen was allowed after each weld pass at every stage, to room temperature. Backing plates were machined off and transverse weld test specimens were taken, as shown in figure 5.5c. The test results of these specimens are given in table 5.6.

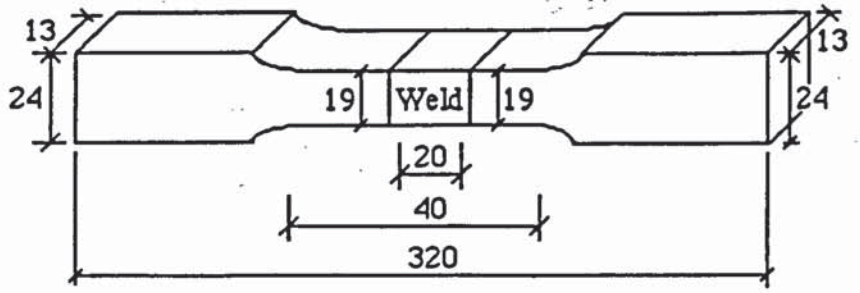

Figure 5.4 Transverse weld coupon specimen.

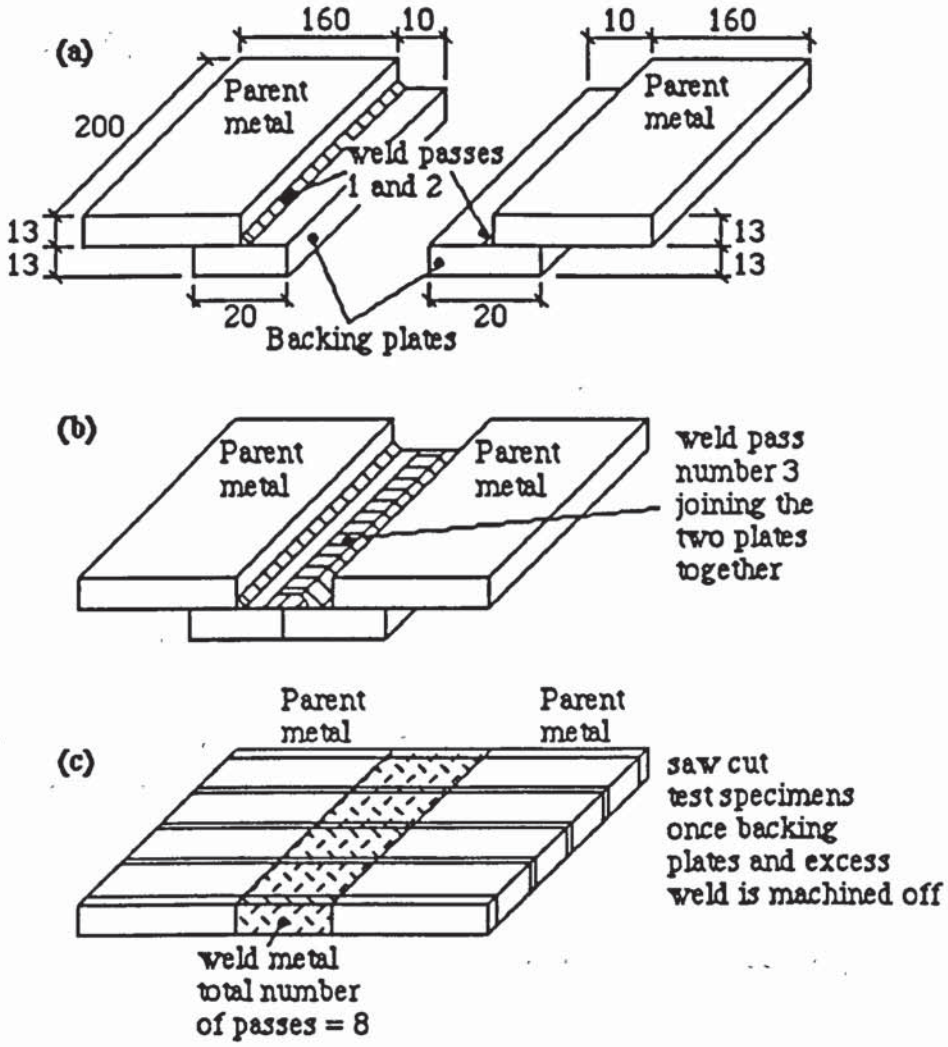

Figure 5.5 Preperation of transverse weld coupon test specimen.

Specimen number	0.2% Proof stress $\sigma_{0.2}$ N/mm^2	Young's Modulus E KN/mm^2	Ultimate Tensile Strength σ_u N/mm^2
MP1	312.04	72.000	354.37
MP2	296.50	86.522	340.58
MP3	304.11	63.821	343.57
MP4	296.56	63.371	343.43
MP5	300.68	66.316	344.38
MP6	303.80	73.333	347.88
MP7	302.17	80.000	346.28
MP8	300.08	80.930	346.68
MP9	286.50	70.986	323.92
MP10	294.47	80.125	347.45
MP11	300.95	72.320	340.25
MP12	298.55	70.560	344.40
MEAN	299.70±6.18	73.357±7.24	343.60±7.23

Table 5.2 Tensile properties of parent aluminium alloy 6082-T6 taken from delivered plate.

Specimen number	0.2% Proof stress $\sigma_{0.2}$ N/mm^2	Young's Modulus E KN/mm^2	Ultimate Tensile Strength σ_u N/mm^2
P1	299.93	69.278	349.93
P2	292.99	68.737	342.99
P3	297.61	61.021	347.61
P4	296.07	75.842	346.07
P5	296.00	69.342	330.60
P6	290.30	70.213	349.31
P7	304.29	75.477	351.32
P8	298.22	68.345	345.60
P9	288.35	69.399	346.60
P10	302.10	74.456	345.39
P11	296.31	63.220	347.30
P12	299.10	74.450	339.33
P13	299.20	70.103	328.31
P14	290.30	76.321	326.31
P15	300.00	69.311	354.30
P16	296.31	70.326	338.71
P17	295.10	73.333	345.07
P18	299.30	69.350	343.37
P19	296.27	74.216	349.89
P20	298.70	68.725	350.01
P21	299.31	68.931	341.10
P22	298.70	70.336	350.11
P23	301.01	69.736	348.38
P24	296.32	70.310	349.79
P25	298.30	70.010	345.60
MEAN	297.20 ± 3.7	70.431± 3.56	344.52±7.13

Table 5.3 Tensile properties of parent metal aluminium alloy 6082-T6 coupons.

Specimen number	0.2% Proof stress $\sigma_{0.2}$ N/mm^2	Young's Modulus E KN/mm^2	Ultimate Tensile Strength σ_u N/mm^2
H1	162.37	62.970	202.37
H2	154.20	70.052	194.20
H3	142.68	69.863	182.68
H4	153.89	66.865	193.89
H5	155.40	66.963	195.31
H6	160.31	69.376	200.31
H7	154.32	71.326	187.91
H8	159.80	66.533	189.35
H9	159.32	62.451	200.10
H10	145.31	66.371	195.31
H11	160.37	69.750	191.42
H12	155.31	69.377	196.33
H13	152.73	66.660	196.00
H14	149.95	63.101	187.37
H15	157.38	66.909	195.76
H16	155.90	68.125	190.38
H17	155.55	70.070	198.79
H18	153.21	62.970	191.50
H19	150.05	69.100	185.33
H20	159.35	66.961	192.33
H21	157.35	65.100	195.89
H22	151.71	66.709	201.77
H23	151.01	66.801	199.97
H24	155.70	69.777	191.30
H25	157.10	70.202	205.01
H26	149.30	66.783	199.50
H27	159.34	63.341	206.03
H28	147.71	69.950	221.30
H29	149.39	66.715	215.13
H30	155.77	65.615	190.23
MEAN	154.26±4.64	67.226±2.52	196.43±8.21

Table 5.4 Tensile properties of heat affected zone coupons in aluminium 6082-T6.

Specimen number	0.2% Proof stress $\sigma_{0.2}$ N/mm^2	Young's Modulus E KN/mm^2	Ultimate Tensile Strength σ_u N/mm^2
W1	97.21	66.832	198.92
W2	82.81	66.263	199.36
W3	106.40	66.992	186.21
W4	127.99	64.058	188.99
W5	152.31	66.832	193.07
W6	101.32	69.713	185.30
W7	88.30	64.321	195.47
W8	110.22	71.718	197.94
W9	90.13	58.118	195.75
W10	113.35	64.776	189.35
W11	122.80	69.517	201.75
W12	129.91	63.450	185.79
W13	88.31	64.313	194.22
W14	99.55	64.909	193.19
W15	107.71	66.732	190.79
W16	144.57	60.120	190.12
W17	103.35	67.223	187.01
W18	105.07	64.313	201.75
MEAN	109.52±19.38	65.567±3.24	193.05±5.44

Table 5.5 Tensile properties of weld metal 4043A, longitudinal coupons from aluminium alloy 6082-T6, two pass single 'V' butt welded specimen.

Specimen number	0.2% Proof stress $\sigma_{0.2}$ N/mm^2	Young's Modulus E KN/mm^2	Ultimate Tensile Strength σ_u N/mm^2
WT 1	119.87	68.507	189.58
WT 2	120.93	65.228	196.75
WT 3	126.19	61.858	188.97
WT 4	132.63	67.530	190.00
WT 5	126.19	60.740	201.37
WT 6	106.35	66.321	186.63
WT 7	115.32	63.941	199.32
WT 8	122.31	65.410	190.44
WT 9	119.39	64.340	188.03
WT 10	120.54	66.333	190.32
MEAN	120±7.01	65.021±2.40	192.14±5.08

Table 5.6 Tensile properties of weld metal 4043A loaded in transverse direction.

5.2.4 Hardness traverse.

Hardness traverses were carried out one month after welding across the top surface of the butt welded specimen as seen in figure 5.6. The Vickers Hardness testing machine was used with a 5Kg indentation load. Spacing of the readings were at 5mm centres from the weld centre line, and increased to 10mm centres in the parent metal zones.

The equations 5.1 and 5.2 proposed by Robertson and Dwight for the extent of the start of the HAZ, distance X_A and the end of the HAZ, distance X_B from the weld centre line were used to evaluate the theoretical distances X_A and X_B to be expected for the author's butt welded specimen.

$$X_A = K_A (A_w / d) \qquad \text{Equation 5.1}$$

$$X_B = K_B (A_w / d) \qquad \text{Equation 5.2}$$

where $K_A = 3$ and $K_B = 6.6$ for 6082 - T6 aluminium alloy.

A_w = deposited weld area and recommended by Robertson and Dwight to be related by equation 5.3;

$$A_w = 0.0437 (Q / v) \qquad \text{Equation 5.3}$$

d = plate thickness.

For the author's butt weld specimen shown in figure 5.6, X_A and X_B are calculated for both the weld passes 1 and 2 seperately.

For weld pass 1;

$$\frac{Q}{V} = \frac{\text{Volts x Amps x } \eta}{\text{Speed of torch}}$$

Taking $\eta = 0.65$ as from Robertson and Dwight's findings and also as recommended by Gray and Spencer [52]. From Table 5.7, the speed for pass 1 = (260/33.10) mm/sec. = 7.855mm/sec.

$$\frac{Q}{V} = \frac{28 \text{ x } 260 \text{ x } 0.65}{7.855}$$

$$= 602.42 \text{ J/mm}$$

$$A_w = 26.326 \text{ mm}^2$$

Thus $X_A = 6.075$mm and $X_B = 13.365$mm.

For weld pass 2;

weld torch speed = 4.286mm/sec.

$$\frac{Q}{V} = \frac{28 \times 260 \times 0.65}{4.286}$$

$$= 1104.01 \text{ J/mm}$$

$$A_w = 48.245\text{mm}^2$$

Therefore $X_A = 11.134$mm and $X_B = 24.494$mm.

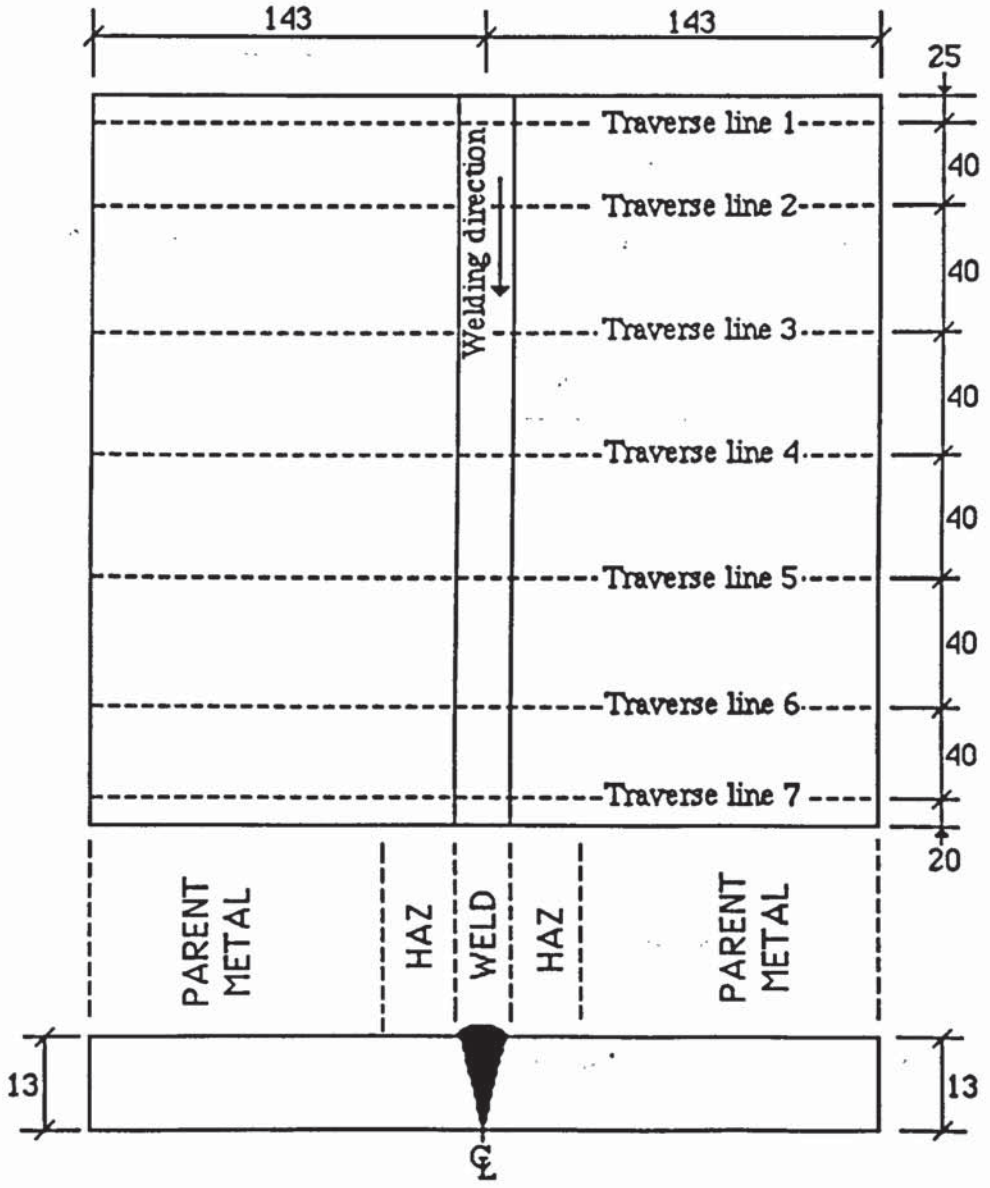

Figure 5.6 Location of hardness traverses for butt welded specimen.

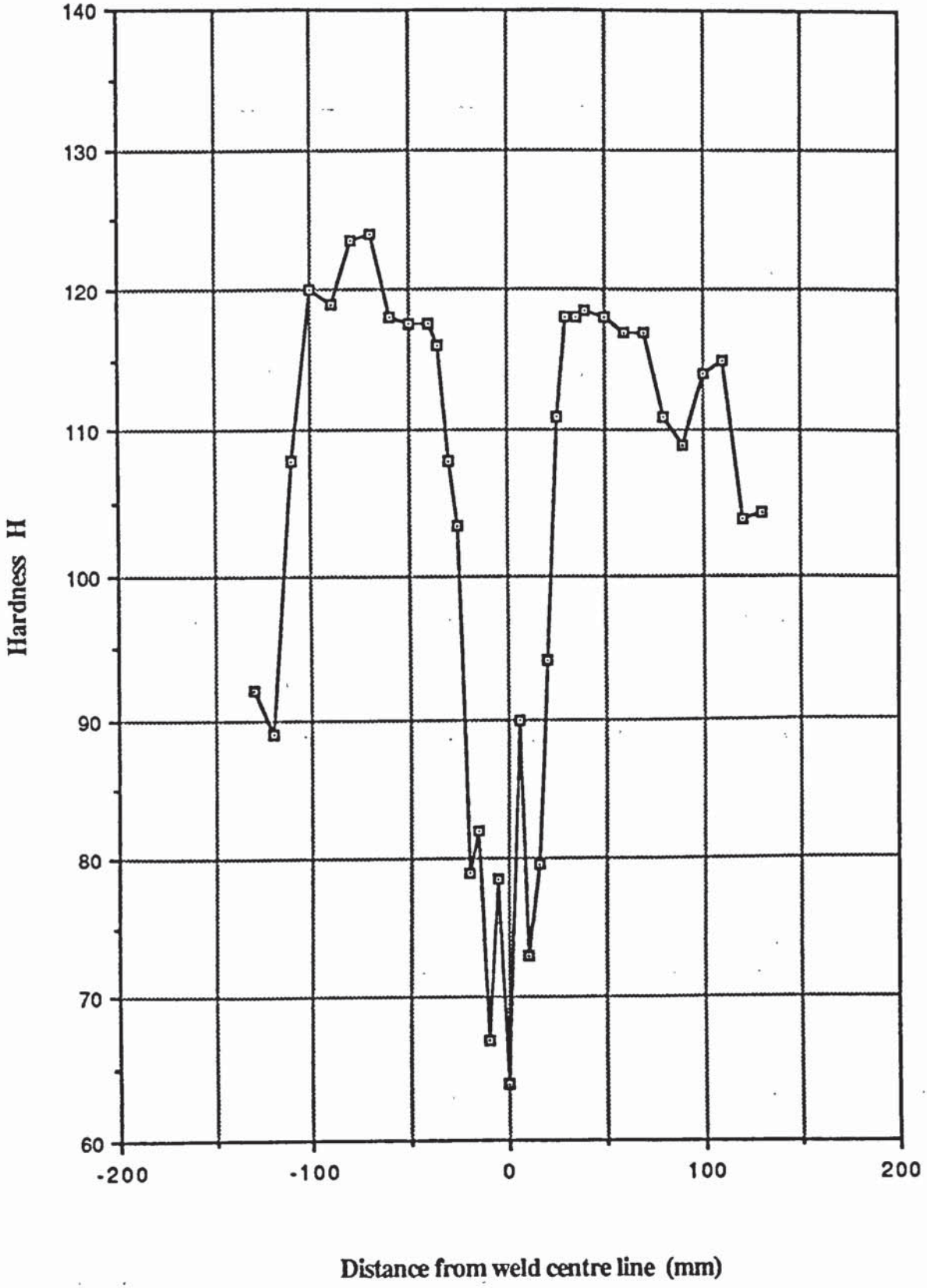

Figure 5.7 Typical hardness traverse along line 1 of butt welded specimen.

Volts (V)	Amps (A)	Gas flow l/m^3	Time of weld run (sec)	Length (mm)	Run Number	Notes
28	260	25	36.10	285	1	Full cooling allowed after each pass laid
28	260	25	66.49	285	2	

Table 5.7 Welding data for butt welded specimen.

5.2.5 Fillet welded specimen.

All test fillet welds have been machined down to achieve 8mm equal leg lengths. This was carried out for the following reasons;

i) Failure is required to occur in the welds. By reducing the size of the test fillet welds, failure is assured to occur in these welds only.

ii) The exact size of the test weld profile is known.

iii) A uniform weld cross section is achieved.

iv) The 8mm size of weld leg length, would allow accurate measurements to be made of the weld profile, failure plane, and weld penetration. The effect of inaccuracy in measurement of smaller leg length would be more significant and a larger leg length would require large loads.

5.2.5.1 The transverse fillet welded specimen.

These specimens were prepared from plates of 200mm in width. The plates were clamped in a jig and welded in a sequence such that any distortion would be minimised. The final transverse weld profiles were made up by three passes of welds. Full cooling to room

temperature was allowed between each pass. Strips of 25mm widths were removed from each end to allow for weld run on and run off effects. The test weld profiles were machined down to give 8mm equal leg lengths. The size of the transverse test specimen is given in figure 5.8 and the location of failure planes and weld penetration in figure 5.9. Demec spots were used to measure the shear distortion on six of the test pieces, as shown in figures 5.9 and 5.10.

For all specimen, readings were taken of the failure load, the extent of weld penetration achieved, the failure angle of the rupture plane and the test weld length. These are recorded in table 5.8.

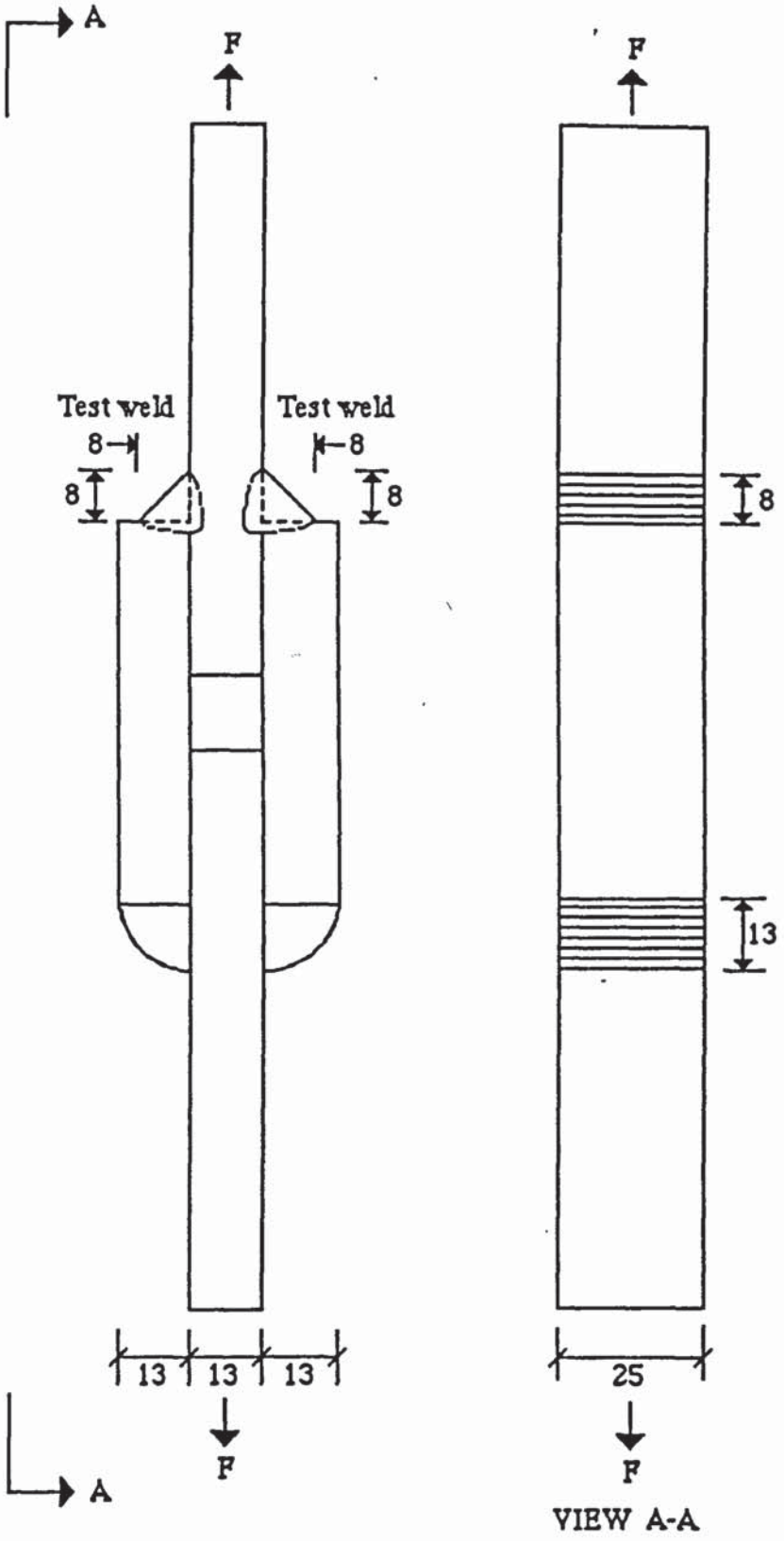

Figure 5.8 Transverse fillet welded test specimen.

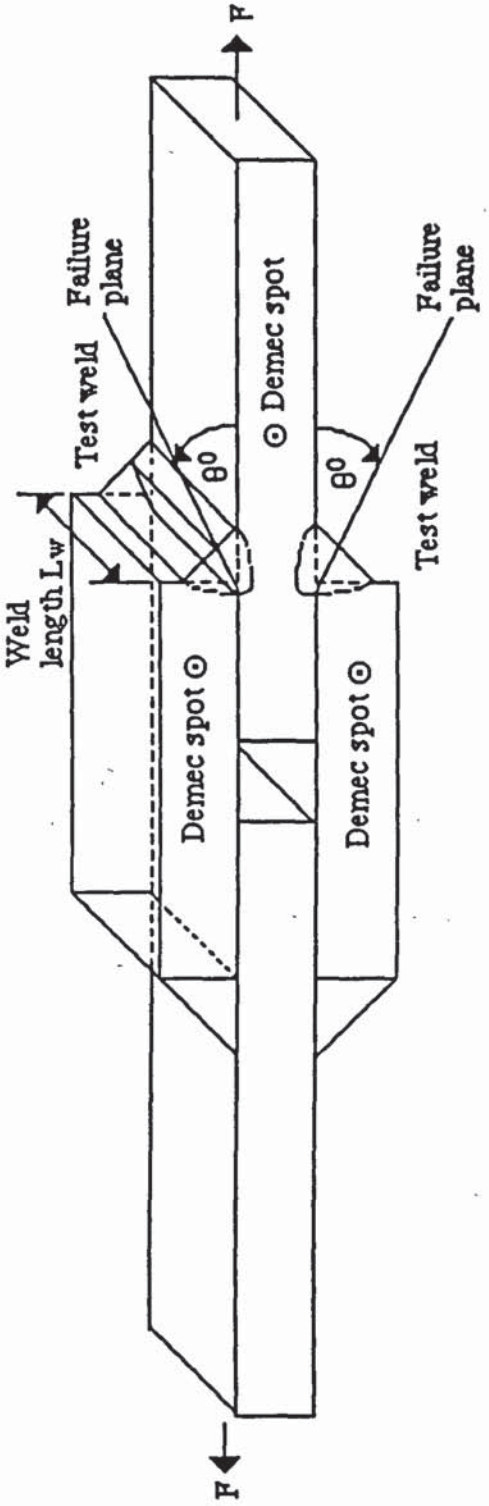

Figure 5.9 Test welds of the transverse fillet welded specimen.

Specimen number	Measured leg length ω (mm)	Measured weld length L_w (mm)	Measured horizontal penetration p (mm)	Ratio p : leg length	Experiment failure load F_{uo} (KN)	Measured failure angle θ^0
A1	8.00	25.04	1.20	0.150	58.80	15.5
A2	8.00	25.10	1.65	0.206	56.56	15.0
A3	8.01	25.10	1.95	0.243	59.38	20.5
A4	7.99	25.11	2.01	0.252	61.20	21.0
A5	8.00	25.00	1.98	0.248	59.24	16.5
A6	8.00	25.00	2.00	0.250	60.91	17.0
A7	8.01	25.01	1.90	0.237	58.22	15.5
A8	8.05	25.00	1.99	0.247	60.09	19.0
A9	8.00	25.02	2.60	0.325	62.30	21.5
A10	8.00	25.00	2.00	0.250	58.63	19.5
A11	8.00	24.98	2.10	0.263	59.25	19.0
A12	8.02	25.01	1.94	0.242	59.30	21.0
A13	7.99	25.00	1.99	0.249	59.90	20.5
				MEAN	59.52±1.44	18.58±2.37

Table 5.8 Experimental results for transverse fillet welds.

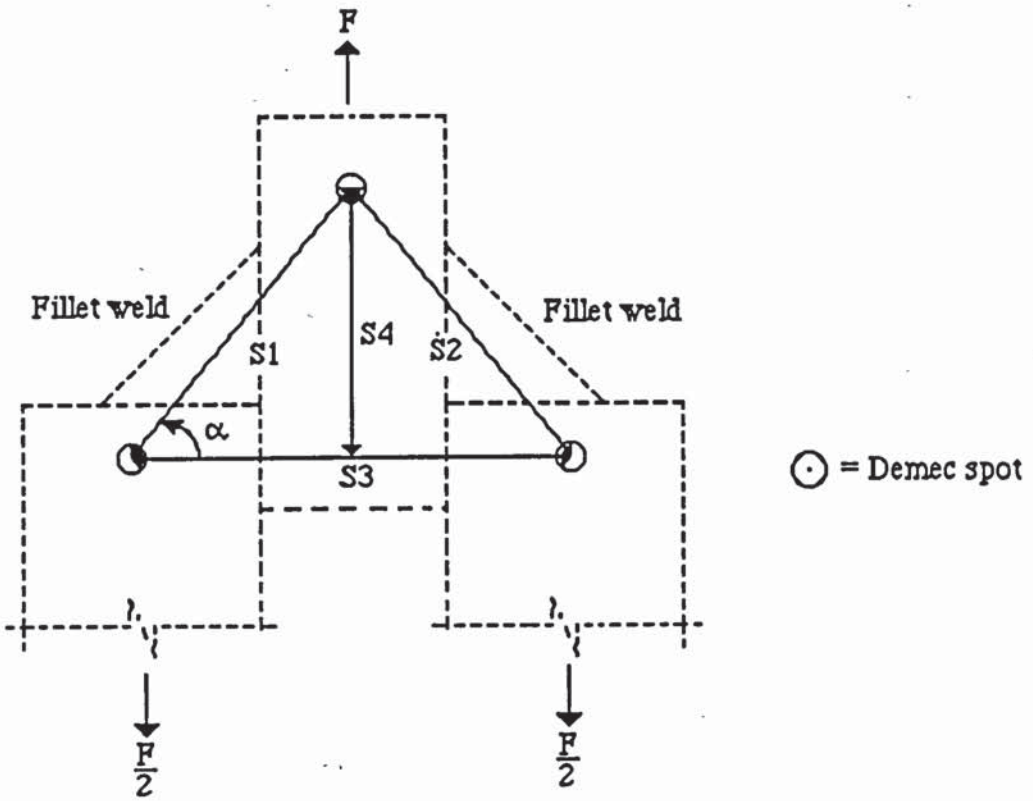

Figure 5.10 Demec gauge measurements and calculations for transverse fillet specimen.

From the above diagram;

$$\cos \alpha = \frac{S_1^2 + S_3^2 - S_2^2}{2 S_1 S_3}$$

and $$S_4 = S_1 . \sin \alpha$$

S_3 is assumed to be constant,

S_4 is the displacement of welds in the direction of applied load F.

Load (KN)	SP. A1	SP. A2	SP. A3	SP. A4	SP. A5	SP. A6
0	0	0	0	0	0	0
1.64	0	0	0.017	0.0149	-0.010	0.0153
2.5	0.0308	0.0068	0.0412	0.0244	-0.0024	0.0287
5.0	0.0354	0.0233	0.0473	0.0309	-0.0058	0.0375
7.52	0.0441	0.0398	0.0548	0.0406	0.0071	0.0516
10.02	0.0590	0.0523	0.0688	0.0531	0.0016	0.0575
12.52	0.0725	0.0842	0.0830	0.0635	0.0445	0.0895
15.04	0.0834	0.0996	0.1009	0.0744	0.0411	0.1060
17.52	0.1040	0.0879	0.1085	0.0865	0.0714	0.1210
20.02	0.1073	0.1007	0.1800	0.1105	0.0769	0.1536
22.54	0.1255	0.1262	0.1431	0.1154	0.0760	0.1693
25.00	0.1394	0.1476	0.1614	0.1305	0.0877	0.1832
27.52	0.1503	0.1698	0.1730	0.1475	0.0916	0.1853
30.02	0.1670	0.2091	0.1887	0.1671	0.1102	0.2204
32.52	0.1930	0.2546	0.2184	0.2436	0.1269	0.2450
35.24	0.2211	0.2816	0.2465	0.2211	0.1528	0.2663
37.52	0.2468	0.3197	0.2664	0.2406	0.1809	0.2982
40.06	0.2692	0.3617	0.2888	0.2730	0.2047	0.3270
42.55	0.3123	0.3996	0.3267	0.3137	0.2174	0.3557
45.06	0.3398	0.4705	0.3618	0.3616	0.2579	0.4051
47.50	0.4030	0.5330	0.4180	0.4212	0.3305	0.4558
50.06	0.4700	0.6381	0.4928	0.4994	0.3644	0.5032
52.54	0.5703	0.7685	0.5690	0.6146	0.4439	0.5750
55.12	-	1.0220	-	0.8777	0.5464	0.6759
57.60	-	-	-	-	0.7342	0.8366
Failure load (KN)	58.80	56.56	59.38	61.20	59.24	60.91

Table 5.9 Extension of transverse welds along the applied load.

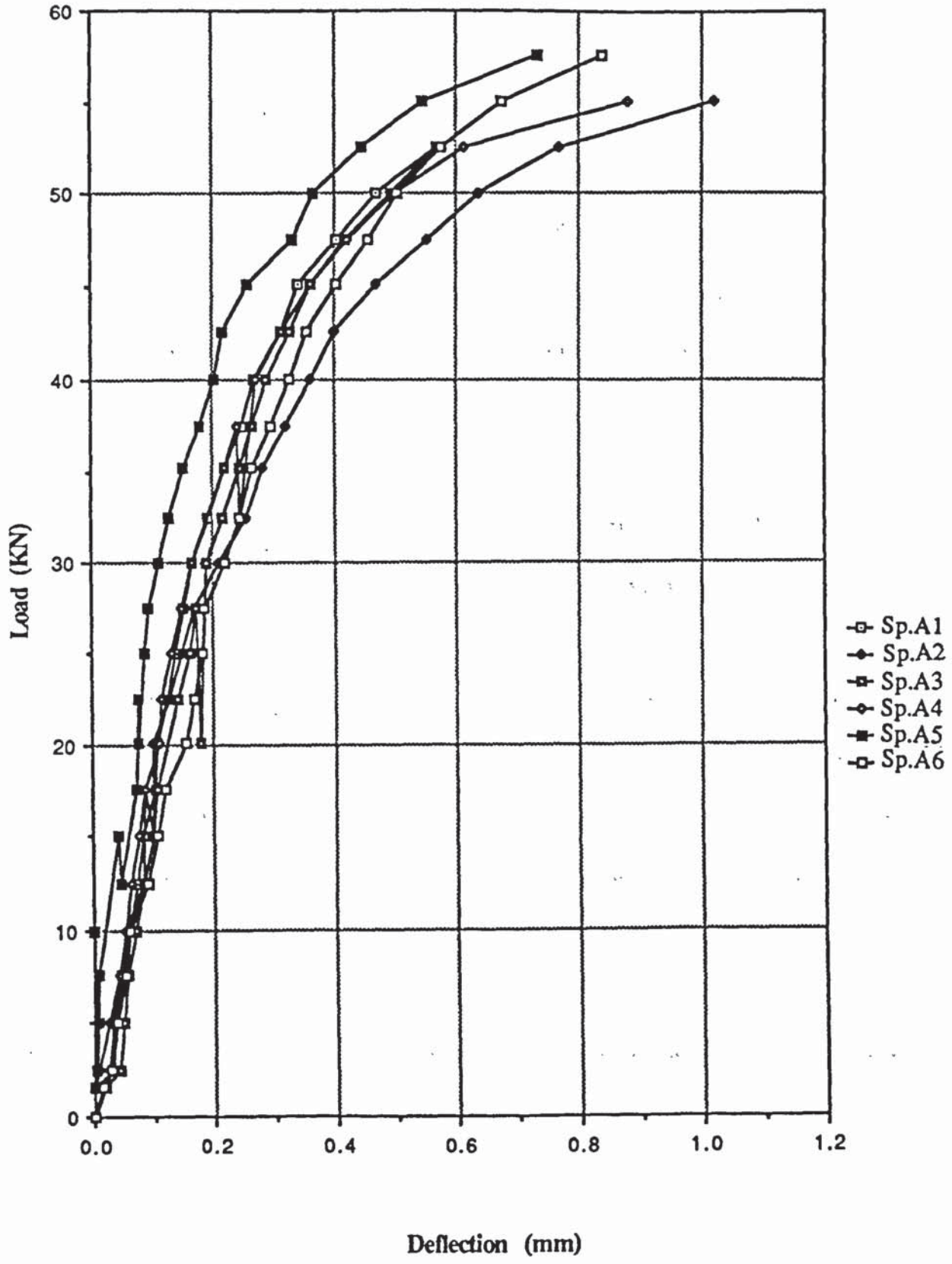

Figure 5.11 Load vs shear distortion graphs for transverse fillet welds.

5.2.5.2 The longitudinal fillet welded specimen.

These specimens, unlike the transverse fillet welded specimen were prepared individually. The size of specimen is shown in figure 5.12. The width of the load transfer plate was kept equal to the plate thickness of 13mm. The width of the loading plates A and B, figure 5.12, was kept to three times this width. This enabled welds of approximately 13mm to be layed in three passes, with full cooling allowed to room temperature after each pass. All specimen were held in a jig fixture and welds were layed in an alternate opposing sequence to minimise any distortion.

As shown in figure 5.12, test welds at one end of the specimen were machined down to achieve the required 8mm leg lengths. The reasons for this have been outlined in section 5.2.4. However, an additional case exists here for machining the test welds. The load transferring plates are small in length and cross section. The extent of the heat affected zone generated from welding, would affect the full thickness of these load transfer plates, extending beyond the length of weld laid.The strength of such plates would be expected to be close to that of the weld metal. This could affect the failure from occuring in the welds only.

To allow for run on and run off effects, the test weld lengths were machined down in length, 20mm from either ends. This resulted in a reduction of the length of the loading plate A and of the load transferring plates, at one end of the specimen, figure 5.12.

Side welds were laid on loading plate B, to ensure failure occurred in the test welds at loading plate A only.

Demec spots were used on six specimens, to measure the shear distortion occurring in the longitudinal fillet welds. These readings can be found in table 5.10.

The location of the readings of the angle of failure plane, extent of penetration and of the weld profile are shown in figure 5.13. These readings and those of the failure load are recorded in table 5.11.

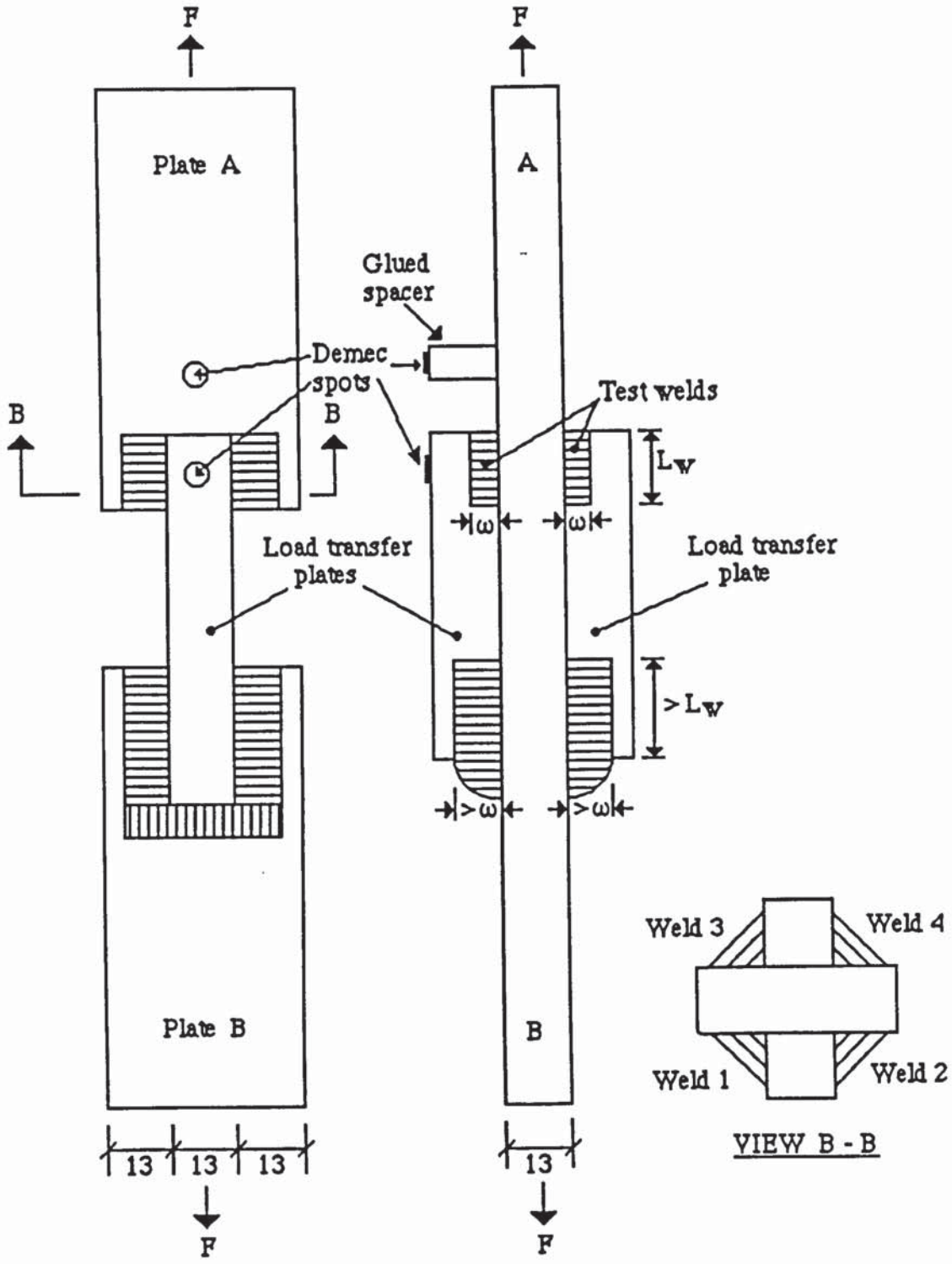

Figure 5.12 Longitudinal fillet welded test specimen.

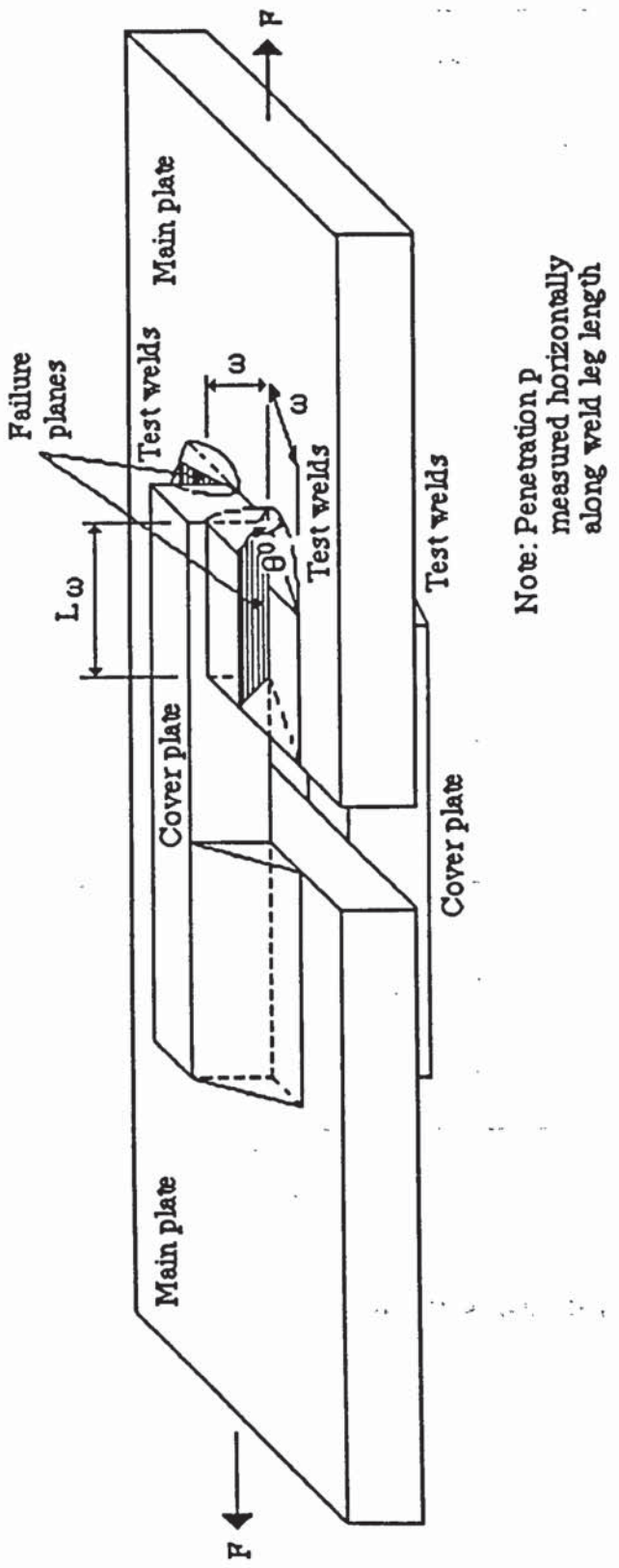

Figure 5.13 Test welds of the longitudinal fillet weld specimen.

Load (KN)	SP. S1	SP. S2	SP. S3	SP. S4	SP. S5	SP. S6
0	0	0	0	0	0	0
1.68	0.0025	0.0051	0.0051	0.0127	-0.0012	0.0026
2.52	0.0025	0.0076	0.0076	0.0152	0.0064	0.0076
5.04	0.0178	0.0127	0.0228	0.0381	0.0292	0.0178
7.56	0.0559	0.0229	0.0306	0.0533	0.0610	0.0229
10.04	0.0660	0.0356	0.0457	0.0914	0.0800	0.0356
12.56	0.0914	0.0813	0.0914	0.1333	0.0673	0.0483
15.04	0.1092	0.0762	0.0787	0.1333	0.0877	0.0823
17.50	0.1270	0.0864	0.0787	0.1244	0.1054	0.0823
20.00	0.1549	0.0915	0.0952	0.1448	0.0953	0.0940
22.54	0.1575	0.1067	0.1168	0.1730	0.1334	0.1245
25.08	0.1880	0.1194	0.1295	0.2000	0.1613	0.1448
27.52	0.2134	0.1473	0.1549	0.2387	0.1715	0.1956
30.02	0.2515	0.1575	0.1879	0.2972	0.1918	0.2007
32.52	0.3226	0.2032	0.2413	0.3429	0.2375	0.2337
35.04	0.3429	0.2667	0.2845	0.3809	0.2934	0.2845
37.52	0.3962	0.3408	0.3581	0.4165	0.3645	0.3584
40.00	0.4826	0.4268	0.4318	0.5029	0.4560	0.4623
42.50	0.6172	0.5838	0.5613	0.5562	0.5906	0.5665
45.02	-	0.7112	0.7112		0.7125	0.8154
Failure load (KN)	44.10	46.95	45.30	45.64	47.50	47.54

Table 5.10 Extension of longitudinal fillet welds in direction of applied load.

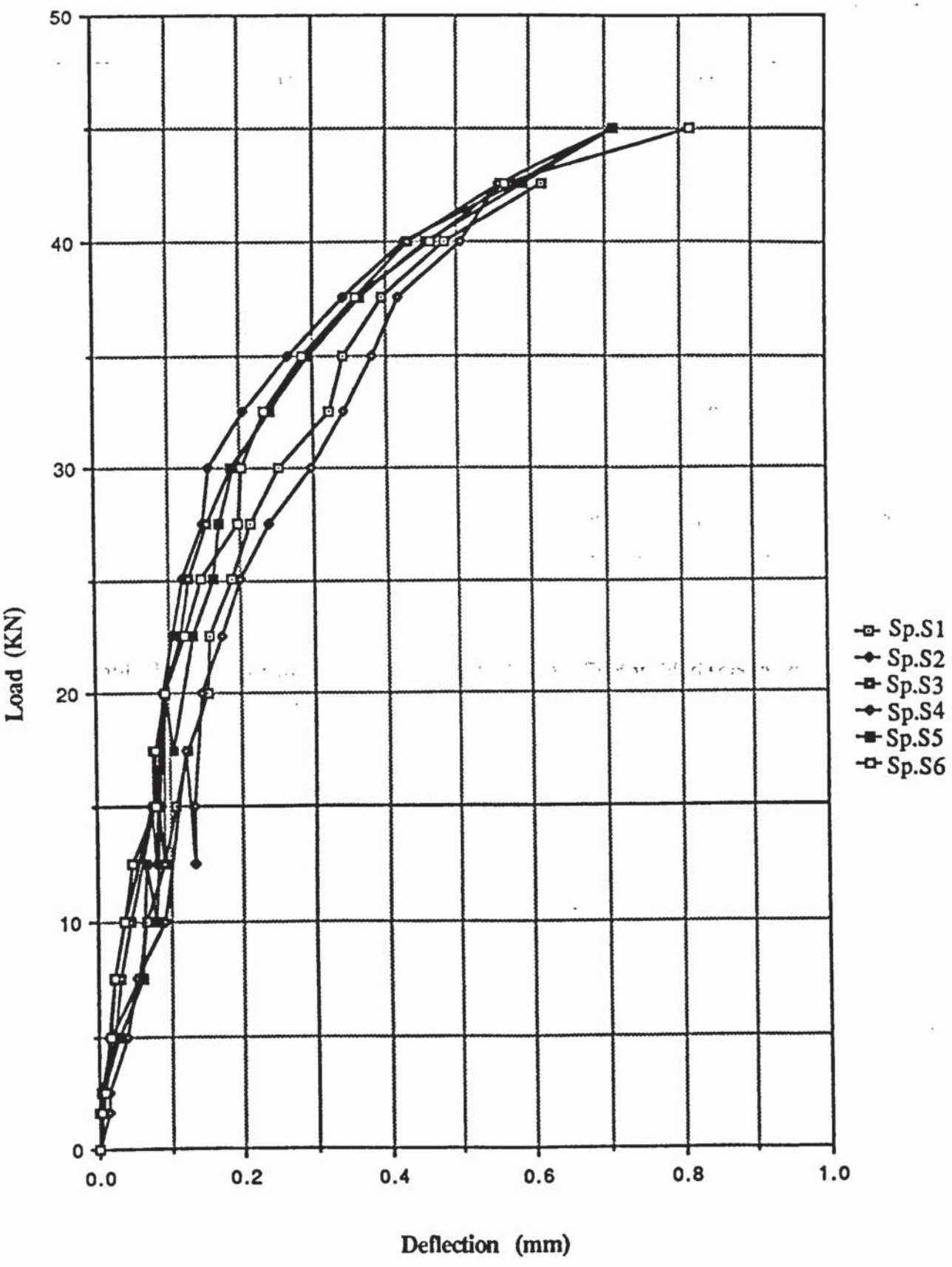

Figure 5.14 Load vs shear distortion for longitudinal fillet welds.

Specimen number	Measured leg length ω (mm)	Measured weld length L_w (mm)	Measured horizontal penetration p (mm)	Ratio p : leg length	Experiment failure load F_{u0} (KN)	Measured failure angle θ^0
S1	8.00	15.00	1.25	0.156	44.10	51.0
S2	8.01	15.00	1.31	0.164	46.95	48.0
S3	8.01	15.00	1.20	0.150	45.30	50.5
S4	8.00	15.02	1.25	0.156	45.64	51.5
S5	8.10	15.04	1.23	0.152	47.50	55.0
S6	8.00	15.04	1.35	0.169	47.54	52.5
S7	8.02	15.03	1.95	0.243	50.35	51.0
S8	8.00	15.00	1.99	0.249	47.92	58.0
S9	8.01	15.01	1.78	0.222	46.65	50.5
S10	8.00	15.00	2.01	0.251	48.64	50.5
S11	8.00	15.03	1.95	0.243	50.42	55.0
S12	8.01	15.00	1.98	0.247	48.10	53.0
S13	8.00	15.00	2.00	0.250	47.93	58.0
				MEAN	47.45±1.82	50.78 ± 1.98

Table 5.11 Experimental results for longitudinal fillet welded specimens.

5.2.5.3 The cruciform shaped specimen.

Fifteen cruciform shaped specimen were single pass welded using cruciform shaped spacers. These were clamped together in a jig and full cooling allowed after each weld pass laid. Each individual specimen was obtained by saw cutting and machining away the cruciform spacers. The weld profile was then machined to equal leg lengths of 8mm. The weld length and the plate was machined down from 13mm to the dimensions shown in table 5.12.The dimensions of a typical test piece are shown in figure 5.15.

Each specimen was tested to failure by applying an equal biaxial load. Readings were taken of the failure load, angle of weld failure plane and the extent of penetration , for each specimen. These results are tabulated in table 5.12.

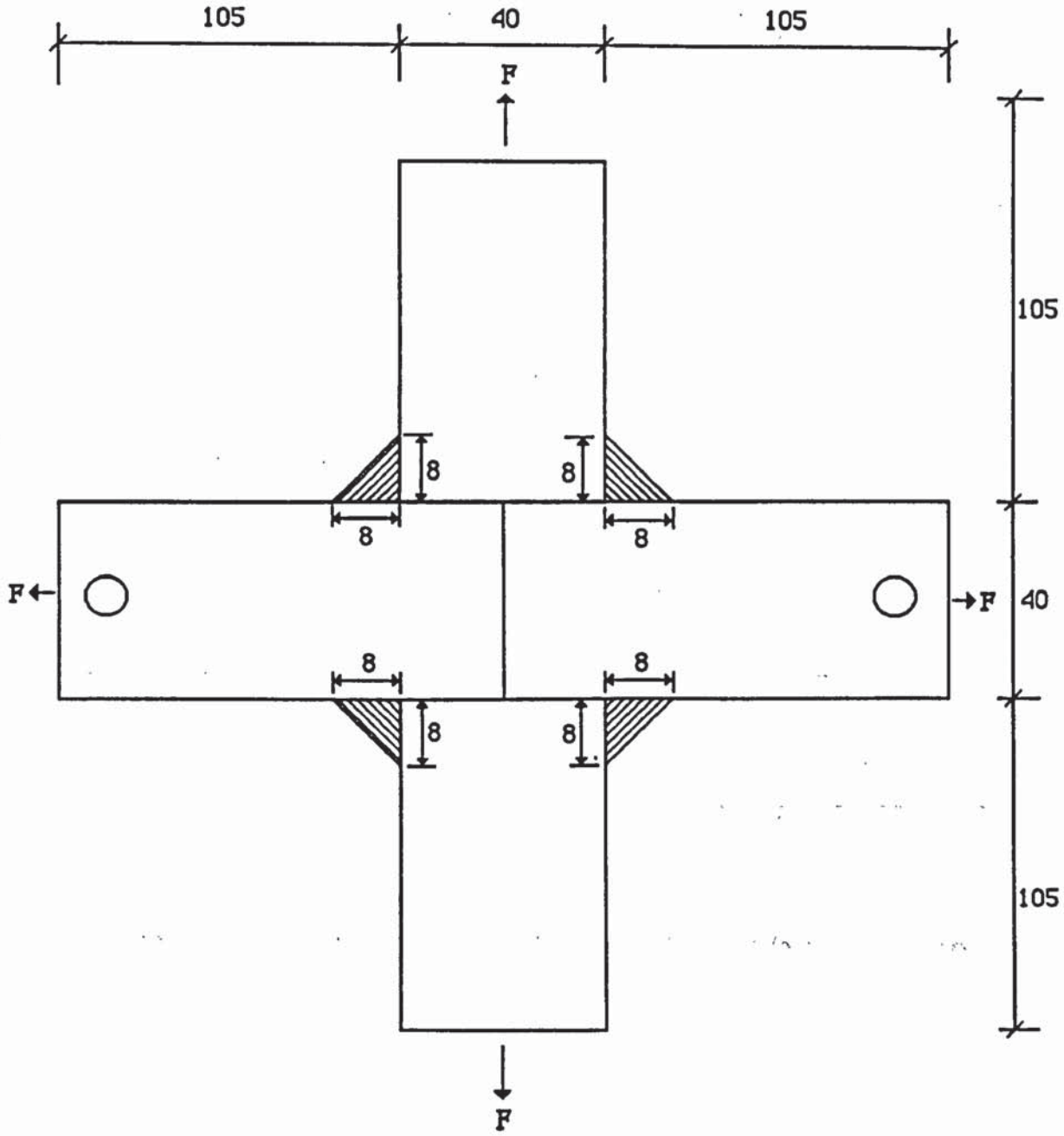

Figure 5.15 Equal, biaxially loaded cruciform test specimen.

Specimen number	Measured leg length ω (mm)	Measured weld length L_w (mm)	Measured horizontal penetration p (mm)	Ratio p : leg length	Experiment failure load F_{u0} (KN)	Measured failure angle θ^0
C1	8.00	10.04	2.31	0.289	23.48	18.0
C2	8.00	10.43	2.02	0.253	25.76	21.5
C3	8.01	10.72	2.20	0.275	27.56	15.5
C4	8.00	10.12	1.93	0.241	24.31	13.0
C5	8.00	10.10	2.01	0.251	25.51	19.0
C6	8.03	10.44	2.11	0.263	25.25	21.0
C7	8.01	10.00	2.25	0.281	27.92	20.0
C8	8.00	10.00	1.96	0.245	22.15	15.0
C9	8.00	10.00	2.02	0.253	23.11	15.5
C10	8.00	10.01	1.99	0.249	25.70	16.0
C11	8.00	10.50	2.05	0.256	26.25	22.0
C12	8.00	10.30	2.00	0.250	25.91	19.0
C13	8.00	10.40	2.29	0.286	27.35	19.5
C14	8.00	10.20	1.90	0.238	22.31	17.5
C15	8.00	10.00	1.93	0.241	23.50	20.5
				MEAN	25.071±1.86	18.2±2.70

Table 5.12 Experimental results for cruciform shaped biaxial, (equal) loaded specimen.

5.2.5.4 The temporary space frame end plate connection.

The typical type of space frame where the temporary end plate connection is used, is shown in figure 5.16.

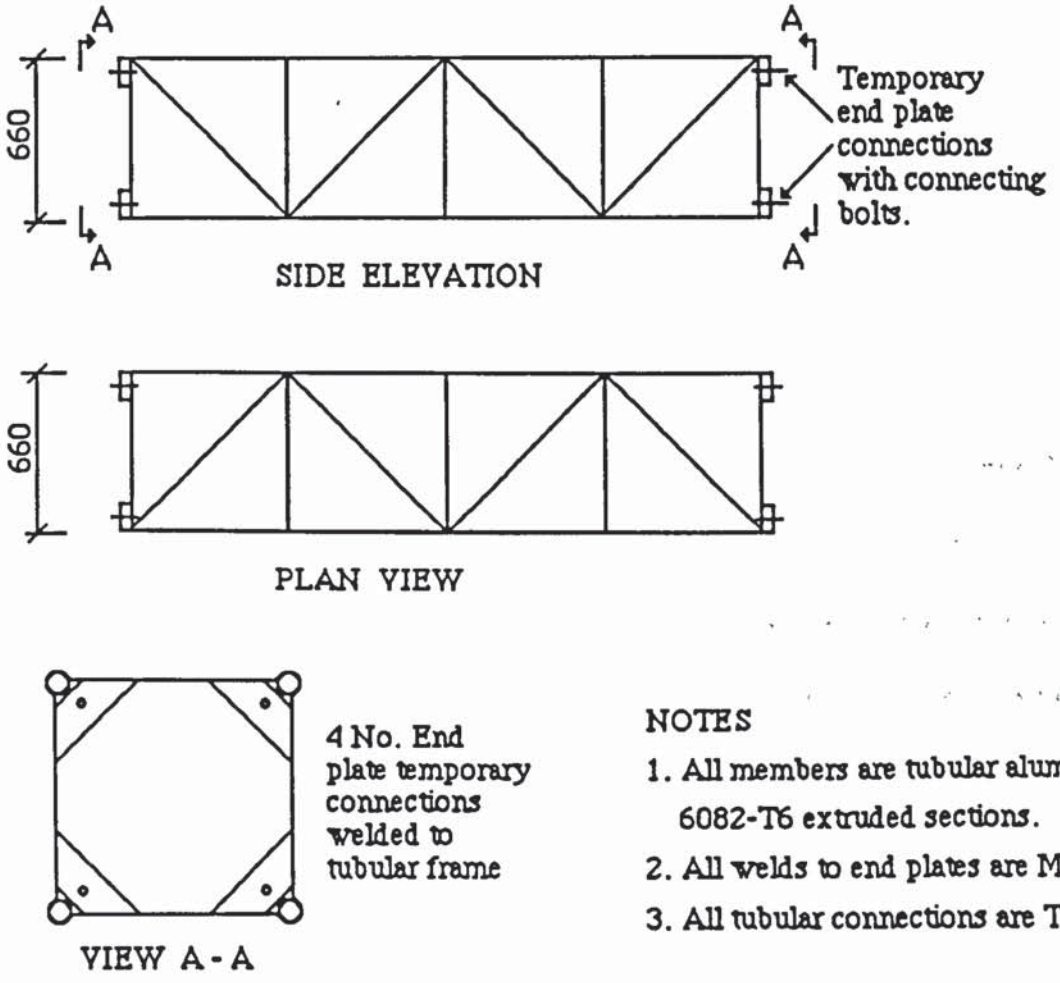

Figure 5.16 General arrangement of a space frame with temporary end plate connections.

To experimentally test the end plate connection, a symmetrical shaped test specimen of the type shown in figure 5.17, was developed and designed. The shape and loading arrangement applied on this test piece ensures that it simulates the actual end plate connection in the space frame, as closely as is practically possible. This overcomes the need to use large size frames and loading arrangements.

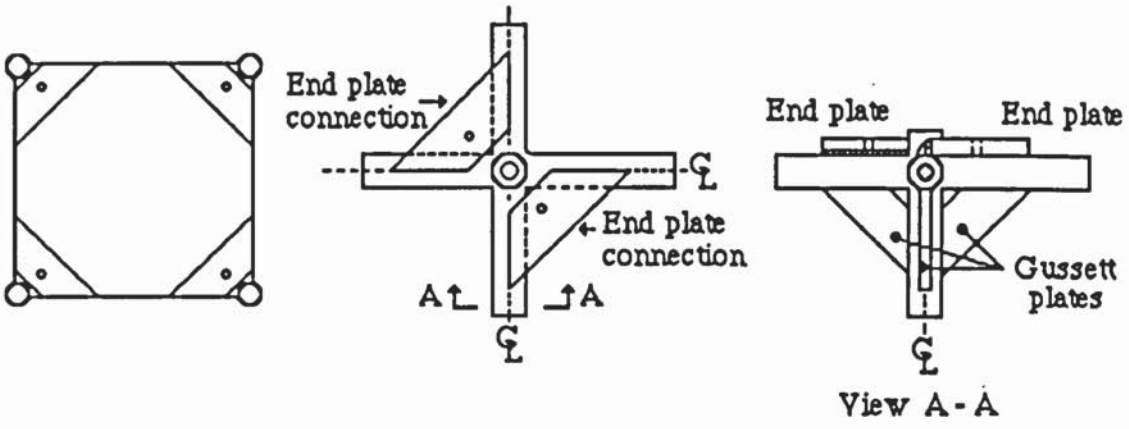

Figure 5.17 A symmetrical shaped experimental end plate connection simulating the actual temporary end plate in a space frame.

The test specimen, shown in figure 5.17, incorporates a pair of identical end plate connections. This enables the two end plates to be simultaneously tested, on the one specimen. Both end plates are of the same size as would be used in the space frames. They are symmetrically located and welded on to horizontal tubular arms. Their position on these tubes is also identical as would be on a space frame, i.e. they are welded into the corners of two tubular arms.

The horizontal tubes are close welded around a vertical tubular length. Gusstee plates are welded from this member to the tubular arms, figure 5.17.

Both end plates have been designed to be loaded equally in a tensile manner, by a pair of HSFG bolts. This loading arrangement is discussed in section 5.2.5.4.2.

Failure of the end plate connection is expected to occur in the welds only, at all times. For

this condition, the end plates have been designed using the yield line method of analysis. From this analysis it is found that for the plates to fail, their thickness must be 1.3mm. The plate thickness used for the test specimen is 13mm. This is more than adequate to ensure failure does not occur in the plate. However other factors prevailed in the choice of this thick a plate. These are ;

i). A sufficient size of weld may be deposited, as discussed earlier in section 5.2.5.

ii). The extent and severity of the HAZ is reduced significantly, as recommended by Robertson and Dwight[3,4].

The tubular sections used for the specimen were of 13mm thickness and 50mm diameter.This choice was governed by the following factors;

i) To ensure collapse of the tubular walls does not occur during welding.

ii) The extent and severity of the HAZ be minimised.

iii) No displacement or torsion occurs along any of the tubular arm lengths.

iv) Failure does not occur in the tubular welded joints or the tubes themselves.

v) Welds laid between the end plates and tubes are of a sufficient size. More importantly the size of leg lengths achieved must be equal. It is known that the slightest variation in the size of tensile weld leg lengths, greatly effects the failure load[11].

For the test specimen the diameter of tube chosen will affect the size of the horizontal weld leg length. A plate welded onto a small diameter tube will result in a radial horizontal leg length. To achieve a straight leg length, a larger diameter tube is required, as shown in figure 5.18.

A check at the design stage on the effect of loading on the tubes, revealed over stressing in them. This indicated failure would occur in the welds connecting the tubes and not in the welds between the end plates and tubes.Gusset plates were designed to overcome this overstressing in the tubes.They were welded between the vertical and horizontal tubular lengths, as shown in figure 5.17.

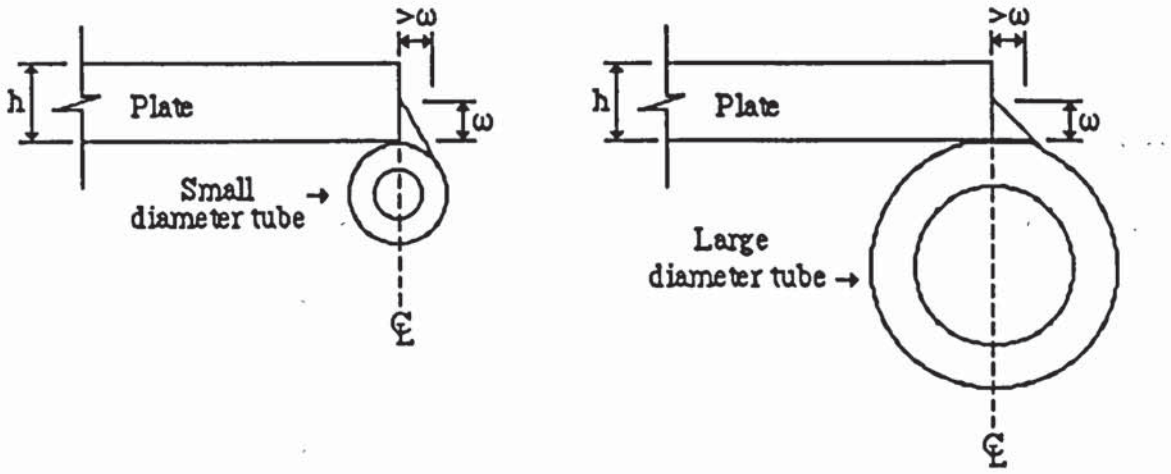

Figure 5.18 Effect of tube size on weld leg length.

5.2.5.4.1 Preperation of the test specimen.

The preperation of these specimens was divided into three stages;

i) Welding of tubular sections,

ii) Welding of gusset plates,

iii) Welding of end plates.

i) Welding of tubular sections.

The ends of four tubular lengths were prepared to close fit perpendicularly around a main vertical tube. Each tube was individually cleaned and tacked on to the vertical member.

Each tubular arm of the final tacked stage was clamped in a specially adapted jig. Welds were layed by the TIG process around each tube's circumference. Cooling of welds to room temperature was allowed after each tube had been welded on. Full clamping was in operation throughout the welding and cooling processes, to minimise any distortion.

ii) Welding of gusset plates.

Gusset plates were first tacked and then single pass MIG welded, between the horizontal and vertical tubular members. Full cooling of welds to room temperature was only allowed once a set of opposite welds had been laid.

iii) Welding of end plates.

The end plates were finally welded on to the tubular arms. Welds were laid by the manual MIG welding process. Special care and attention was taken to achieve symmetry of these plates, when welded on. Any unsymmetrical positioning of the plates would result in uneven loading conditions to occur. For all specimens, the distance between the centres of the holes in the end plates was kept constant.

To minimise the extent and severity of heat affected zones, tacking was restricted to the extreme edge tips of the plate lengths. These were both small and narrow in size.

Three weld passes made up the final weld profile on each side of the plates, as shown in figure 5.19.

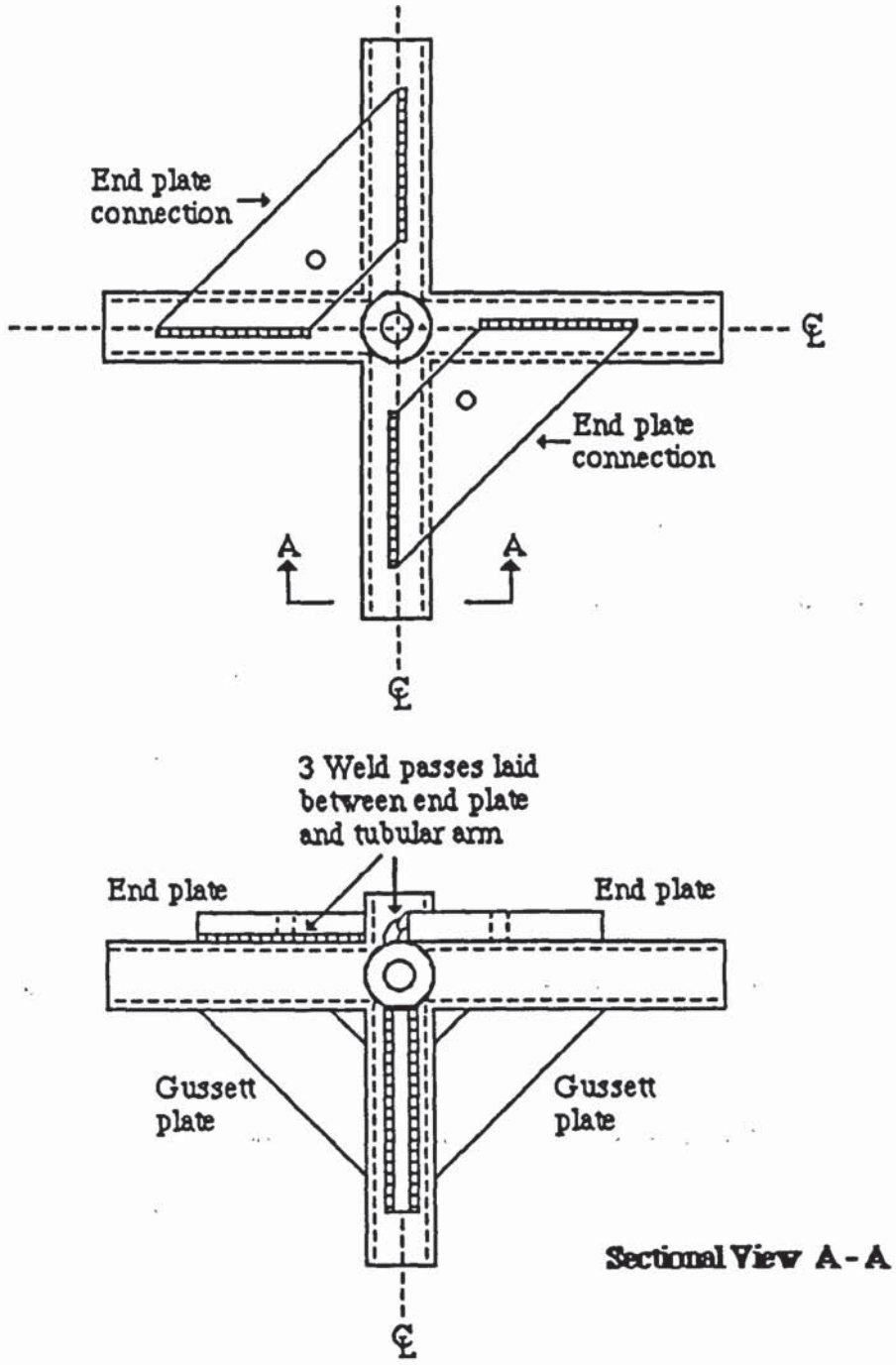

Figure 5.19 View of end plate connections and gusset plates welded onto tubular arms.

The final size of the weld leg lengths laid were equal to the end plate thickness. Full cooling of the welds was allowed after each pass laid. The welding sequence was that welds were laid on opposite sides, to minimise distortion in the plates. Any distortion occuring in the tubes, at this stage would restricted by the gussetts in place. The only significant distortion

that could take place, was that in the 'springing up' of the end plate edges. This was overcome by the weld tacks in place.

No run on and run off plates were used, because of the geometry of the specimen.
To ensure failure occurred in the welds only, the weld profiles were machined down to 8mm equal leg lengths. The reasons for this are given in section 5.2.5.

Rectangular rossette strain gauges were attached to the end connection plates (A and B) of six test specimens F1 to F6, as to the manufacturers specifications. The arrangement is shown in figure 5.20. Due to the symmetrical nature of the test specimen, rosettes were not located at all points on end plate B as on plate A.

A further four strain gauges were attached on the gusset plate below end plate A. These gauges are used to monitor any torsion or bending effects occuring along the tubular arms.

Dimensions of each final prepared test specimen were taken as to those shown in figure 5.21 and are given in tables 5.13 and 5.14.

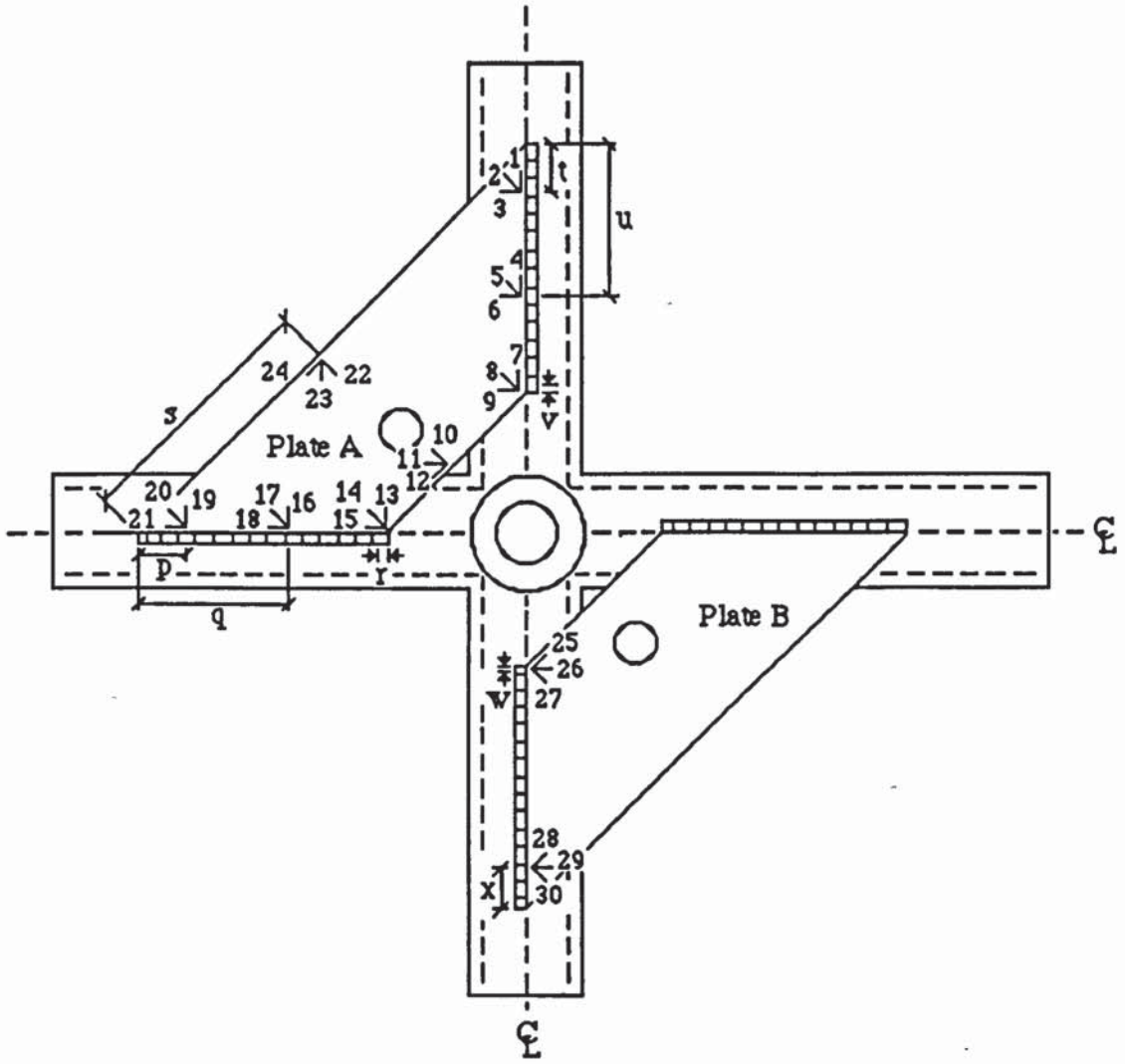

Figure 5.20 Rossette strain gauge layout for specimen type F

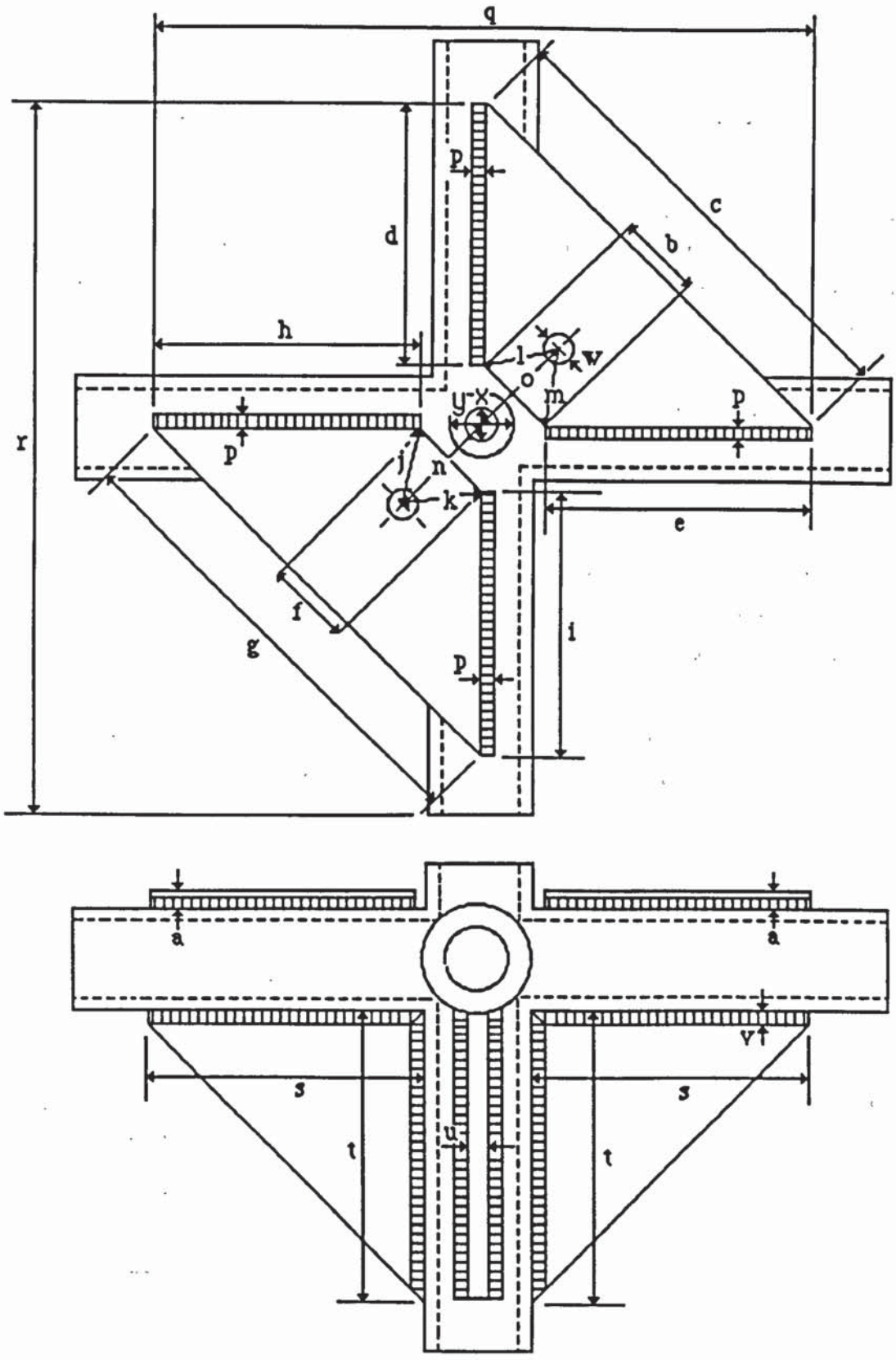

Figure 5.21 Experimental test specimen type F

Dim. (mm)	F1	F2	F3	F4	F5	F6	F7	F8	F9	F10
a	13.01	13.00	13.01	13.00	13.00	13.02	13.00	13.01	13.00	13.01
b	62.00	62.00	62.00	62.01	62.00	63.01	62.00	62.00	62.01	62.00
c	289.00	288.00	289.10	290.30	289.10	289.00	290.01	290.00	289.10	289.00
d	160.00	160.01	160.00	160.00	160.01	160.00	160.00	160.01	160.00	160.05
e	160.00	160.00	160.00	160.00	160.00	160.00	160.00	160.00	160.00	160.00
f	62.01	62.00	62.00	62.00	62.00	62.00	62.01	62.03	62.00	62.00
g	289.02	289.00	289.00	290.01	289.00	289.00	289.00	289.00	289.00	289.00
h	160.00	160.00	160.00	160.10	160.00	160.00	160.00	160.00	160.00	159.50
i	160.00	160.00	160.00	160.00	160.00	160.00	160.00	160.00	160.00	160.00
j	60.00	60.00	60.00	60.00	60.00	60.00	60.00	60.00	60.00	60.00
k	60.00	60.00	60.00	60.00	60.00	60.00	60.00	60.00	60.00	60.00
l	60.00	60.00	60.00	60.00	60.00	60.00	60.00	60.00	60.00	60.00
m	60.00	60.00	60.00	60.00	60.00	60.00	60.00	60.00	60.00	60.00
n	85.00	86.00	85.00	85.00	86.50	85.00	85.50	85.50	88.00	85.00
o	85.00	85.00	85.50	85.00	86.00	85.00	85.00	86.00	87.00	85.00
p	8.00	8.00	8.00	8.00	8.00	8.00	8.00	8.00	8.00	8.00
q	410.00	411.00	410.00	412.00	411.00	411.00	410.00	410.00	410.00	412.00
r	411.00	411.00	410.00	410.00	410.00	410.00	411.00	410.00	410.00	413.00
s	180.00	180.00	180.00	180.00	180.00	180.00	180.00	180.00	180.00	180.00
t	180.00	180.00	180.00	180.00	180.00	180.00	180.00	180.00	180.00	180.00
u	13.01	13.00	13.03	13.01	13.00	13.01	13.02	13.01	13.00	13.00
v	8 - 10	8 - 10	8 - 10	8 - 10	8 - 10	8 - 10	8 - 10	8 - 10	8 - 10	8 - 10
w	22.00	22.00	22.00	22.00	22.00	22.00	22.00	22.00	22.00	22.00
x	24.00	24.00	24.01	24.00	24.00	24.00	24.00	24.00	24.00	24.00
y	50.50	50.51	50.50	50.49	50.50	50.45	50.50	50.51	50.48	50.50

Table 5.13 Dimension measurements for test specimens F1 to F10.

Dim. (mm)	F11	F12	F13	F14	F15
a	13.00	13.00	13.00	13.00	13.00
b	62.00	62.00	62.00	62.01	62.01
c	290.50	289.00	289.00	289.00	289.00
d	160.00	160.00	160.00	160.00	160.00
e	160.00	160.00	160.00	160.00	160.00
f	62.10	62.00	62.00	62.00	62.00
g	289.00	298.10	290.10	289.00	290.00
h	160.00	159.60	159.6	160.00	160.00
i	160.00	160.00	160.00	160.00	160.00
j	60.00	60.00	60.00	60.00	60.00
k	60.00	60.00	60.00	60.00	60.00
l	60.00	60.00	60.00	60.00	60.00
m	60.00	60.00	60.00	60.00	60.00
n	85.00	86.00	85.00	85.00	85.00
o	85.50	86.00	85.00	85.00	85.00
p	8.00	8.00	8.00	8.00	8.00
q	410.00	410.00	411.00	410.00	410.00
r	410.00	411.00	410.00	410.00	411.00
s	180.00	180.00	180.00	180.00	180.00
t	180.00	180.00	180.00	180.00	180.00
u	13.01	13.01	13.02	13.01	13.00
v	8 - 10	8 - 10	8 - 10	8 - 10	8 - 10
w	22.00	22.00	22.00	22.00	22.00
x	24.00	24.00	24.00	24.00	24.00
y	50.50	50.50	50.49	50.50	50.50

Table 5.14 Dimension measurements for test specimens F11 to F15.

5.2.5.4.2 Testing procedure for the end plate test connection.

These end plate test specimen were tested to failure on an Avery Dennison testing machine. The loading arrangement is shown in plates 5.1 and 5.2. Two 22mm diameter HSFG bolts are inserted through the end plates and bolted onto a mild steel loading beam. The loading beam - designed using the simple elastic theory - was connected into the stationary jaws of the testing machine. Application of loads on the plates was achieved by inserting a solid mild steel rod through the test specimen's vartical tube. This rod was gripped by the jaws of the moving head, of the Dennison machine. Using this loading arrangement it is expected that a symmetrical vertical loading of the plates is achieved.

The deflections of each end plate were measured using dial gauges for the six specimens F1 to F6. The arrangement and location of these gauges are shown in figure 5.22 and table 5.16. Dials 11 and 12 were positioned on the bolt which passes through plate A, and on the vertical loading rod respectively.These readings were necessary to record any extensions occurring in either the bolt and, or the rod. These could then be accounted for in the end plate deflections. All dial readings were taken at each load increament until failure of the specimen occurred. In most cases the readings recorded were at or very slightly below the failure load. The deflections recorded for specimen F1 are given in table 5.15 and those for specimens F2 to F6 in appendix C.

Strains from the rossette gauges were recorded using an automatic digital, thirty channel recorder. Strain gauges on the gusset plate were recorded on a manual strain recorder. All readings were taken at each load increament, until failure of the specimen occurred.

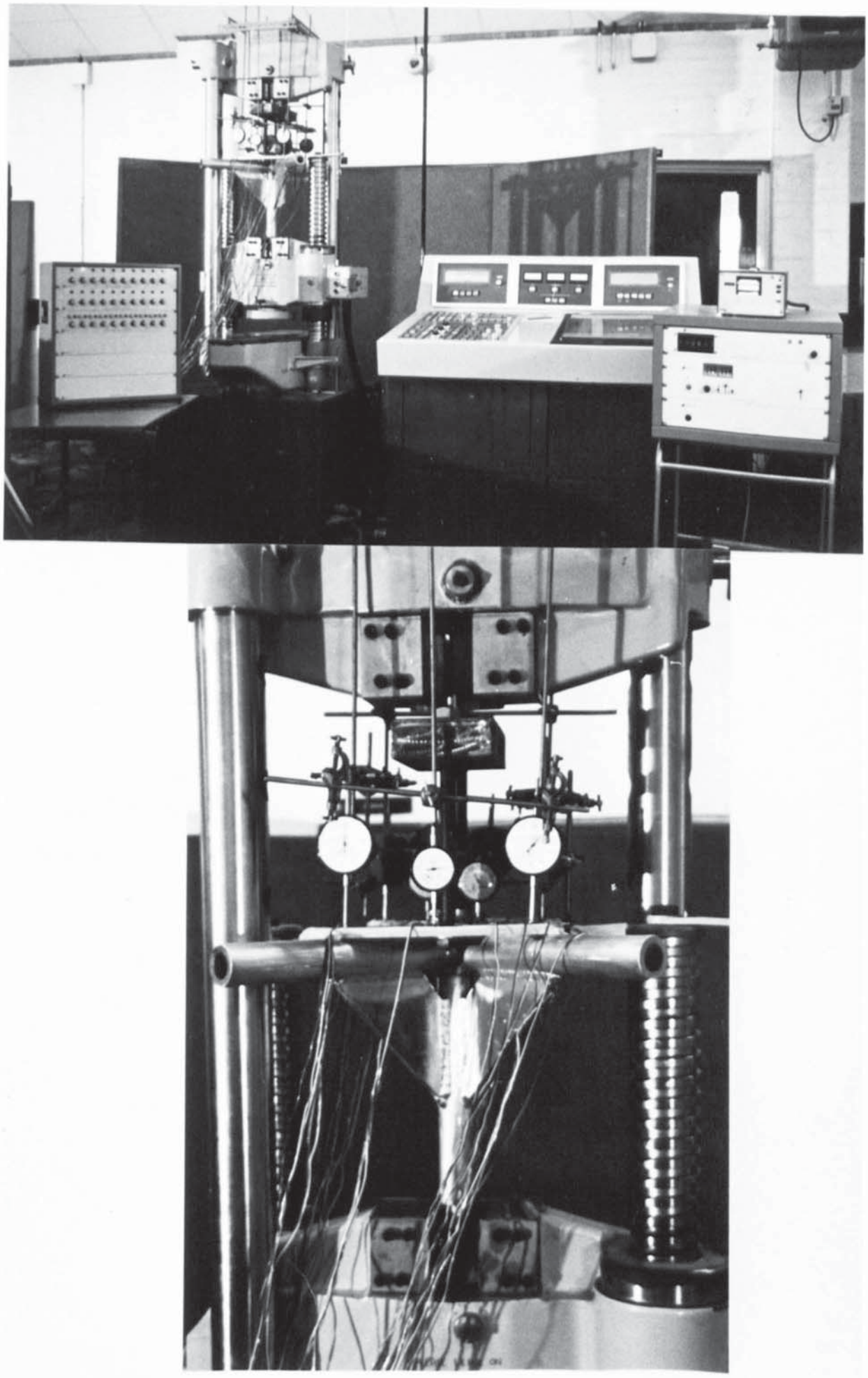

Plate 5.1 Testing arrangement of end plate test specimen type F.

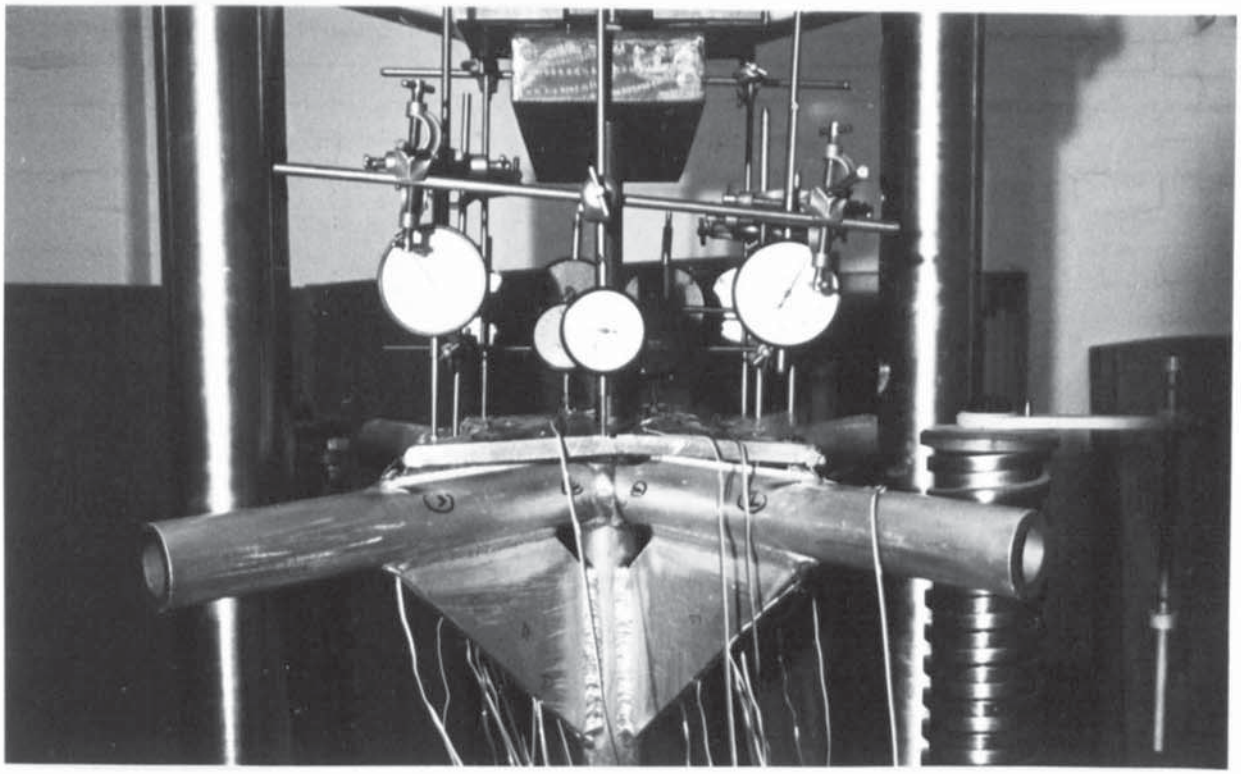

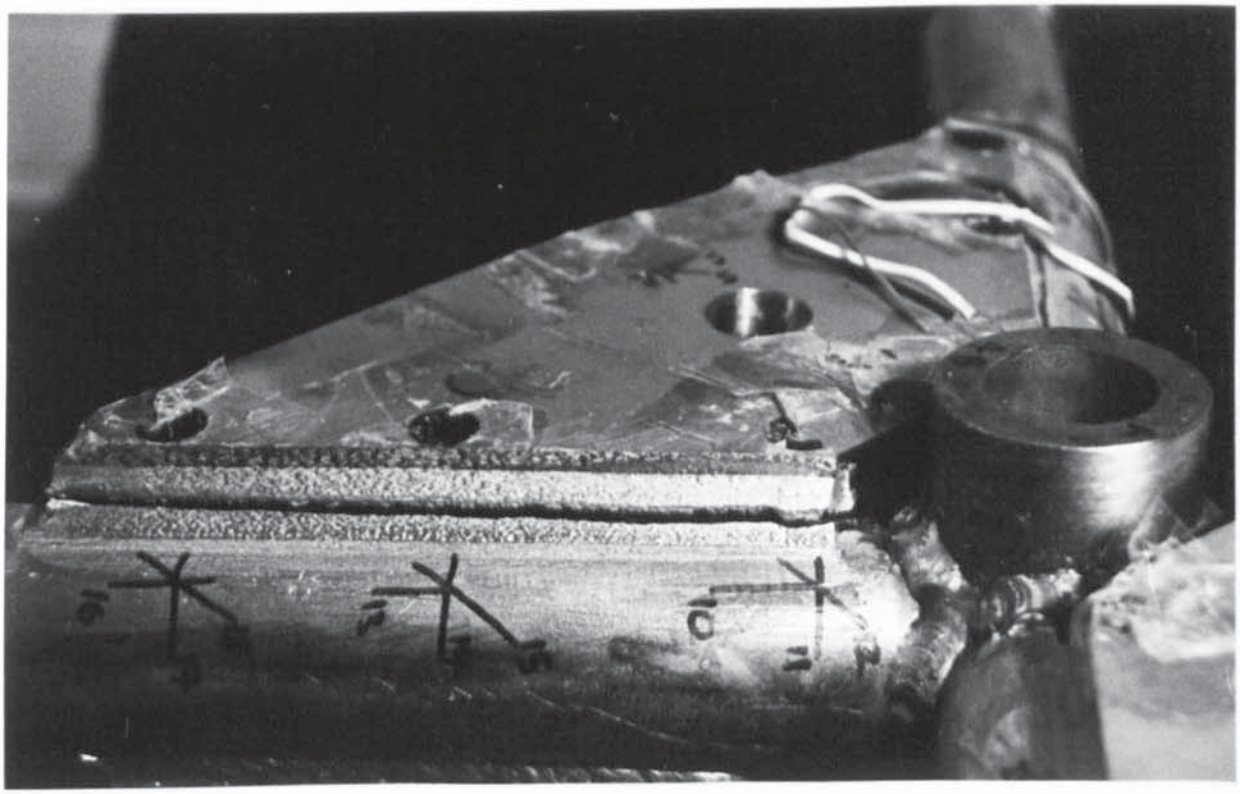

Plate 5.2 Failure of end plate test specimen type F.

However, where stresses were high, strain gauges failed before the specimen. Due to the vast amount of data obtained, only a typical set of readings, - those for specimen F1 are given - in appendix C.

Load (KN)	DG 1	DG 2	DG 3	DG 4	DG 5	DG 6	DG 7	DG 8	DG 9	DG 10	DG 11	DG 12
1.0	0	0	0	0	0	0	0	0	0	0	0	0
2.6	-0.53	-0.42	-0.15	-0.21	-0.22	0.12	0.11	-0.01	-0.09	-0.03	-0.21	-0.09
5.0	-1.06	-0.87	-0.10	-0.50	-0.55	0.24	0.15	-0.06	-0.28	-0.21	-0.50	-0.38
7.6	-1.45	-1.25	-0.49	-0.78	-0.84	0.20	0.15	-0.08	-0.46	-0.49	-0.76	-0.65
10.0	-1.76	-1.51	-0.86	-1.01	-1.06	0.11	0.16	-0.10	-0.60	-0.65	-0.97	-0.84
12.6	-1.99	-1.70	-1.15	-1.23	-1.25	0	0.15	-0.13	-0.74	-0.80	-1.15	-0.99
17.6	-2.34	-1.90	-1.60	-1.75	-1.65	-0.30	0.06	-0.31	-1.02	-1.10	-1.47	-1.21
22.6	-2.64	-2.40	-1.88	-1.86	-1.84	-0.51	0.02	-0.51	-1.28	-1.36	-1.77	-1.39
27.6	-2.93	-2.15	-2.17	-2.13	-2.11	-0.72	-0.02	-0.72	-1.51	-1.60	-2.06	-1.55
30.0	-3.07	-2.19	-2.32	-2.26	-2.23	-0.82	-0.04	-0.83	-1.64	-1.71	-2.20	-1.63
35.0	-3.38	-2.27	-2.60	-2.53	-2.51	-1.04	-0.06	-1.06	-1.90	-1.97	-2.49	-1.79
40.0	-3.69	-2.30	-2.86	-2.77	-2.75	-1.26	-0.08	-1.28	-2.16	-2.22	-2.77	-1.94
45.0	-4.00	-2.31	-3.13	-3.05	-3.04	-1.45	-0.08	-1.54	-2.44	-2.47	-3.07	-2.09
50.0	-4.35	-2.33	-3.43	-3.35	-3.33	-1.69	-0.08	-1.82	-2.75	-2.76	-3.42	-2.25
55.0	-4.69	-2.50	-3.71	-3.64	-3.62	-1.91	-0.05	-2.08	-3.02	-3.02	-3.73	-2.40
60.0	-5.04	-2.50	-4.01	-3.94	-3.93	-2.15	0	-2.35	-3.33	-3.29	-4.07	-2.54
65.0	-5.41	-2.47	-4.34	-4.26	-4.25	-2.43	0.06	-2.65	-3.67	-3.61	-4.44	-2.66
70.0	-5.81	-2.42	-4.69	-4.63	-4.60	-2.74	0.15	-3.00	-4.02	-3.95	-4.86	-2.78
72.6	-6.04	-2.35	-4.90	-4.85	-4.80	-2.91	0.21	-3.20	-4.22	-4.14	-5.11	-2.84
75.0	-6.30	-2.25	-5.12	-5.07	-5.01	-3.11	0.30	-3.39	-4.45	-4.35	-5.35	-2.89
77.6	-6.62	-2.05	-5.29	-5.34	-5.28	-3.38	0.40	-3.65	-4.72	-4.60	-5.67	-2.92
80.0	-6.99	-1.78	-5.72	-5.67	-5.58	-3.64	0.54	-3.93	-5.05	-4.93	-6.10	-2.98
82.6	-7.50	-1.35	-6.14	-6.09	-5.95	-4.06	0.76	-5.34	-5.48	-5.36	-6.57	-3.00
85.0	-8.08	-0.67	-6.67	-6.63	-6.45	-4.50	1.03	-5.81	-6.00	-5.86	-7.24	-3.01
87.6	-9.00	0.23	-7.50	-7.43	-7.18	-5.33	1.59	-6.55	-6.81	-6.67	-8.26	-3.01
90.0	-9.90	0.96	-8.34	-8.27	-7.95	-6.05	2.18	-7.21	-8.55	-7.46	-8.27	-3.04

Table 5.15 Dial gauge readings for test specimen F1

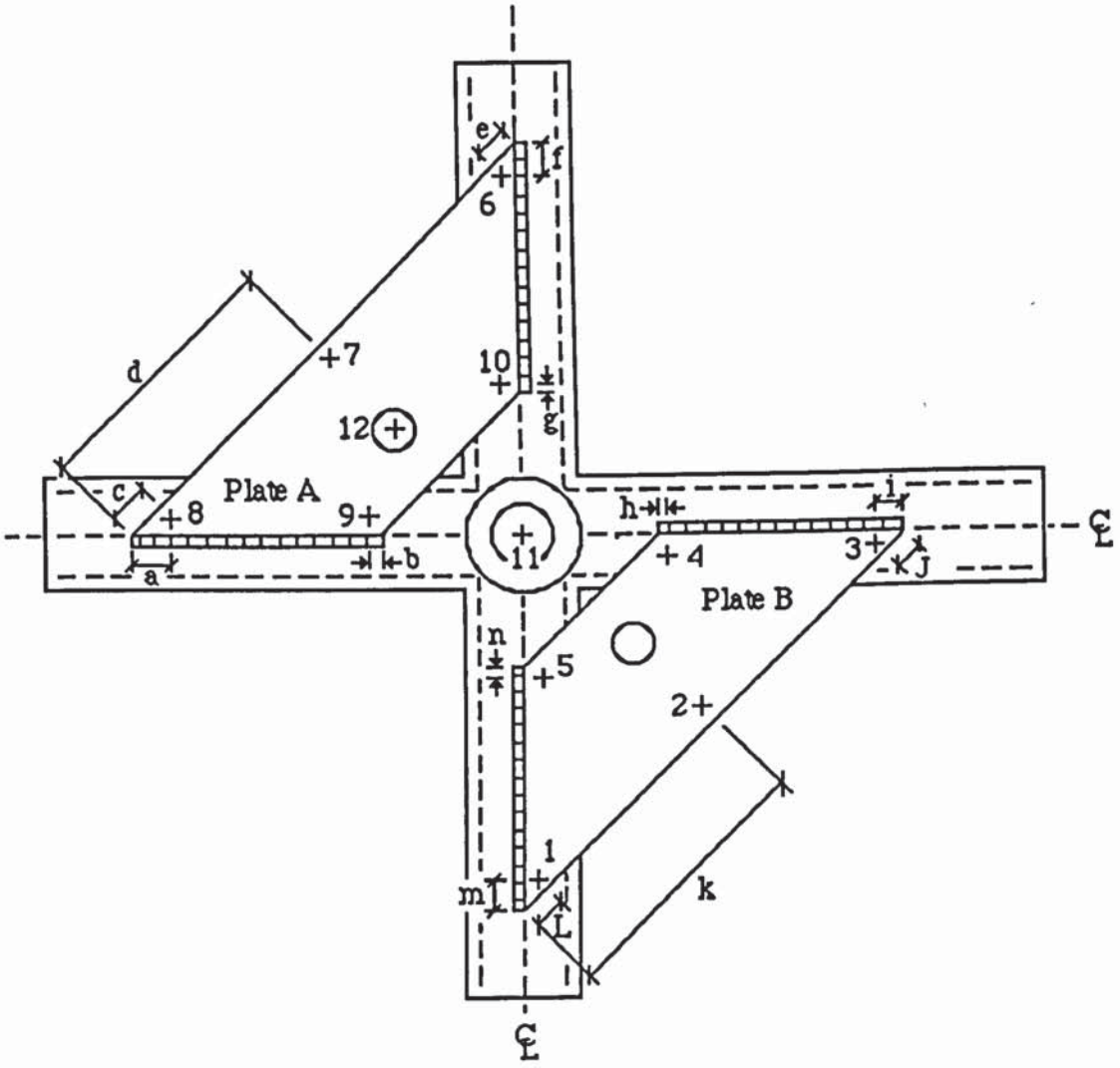

Figure 5.22 Location of dial gauges on test specimens type F

Spec. / Dim. (mm)	F1	F2	F3	F4	F5	F6
a	5	6	15	8	10	3
b	4	4	10	12	10	5
c	5	5	9	12	3	11
d	145	140	150	147	150	145
e	5	8	12	8	7	8
f	7	6	10	11	10	8
g	5	3	10	3	5	7
h	3	5	5	6	6	13
i	8	10	12	12	5	5
J	8	7	10	3	7	8
k	145	145	148	150	150	150
L	5	5	12	3	8	9
m	6	5	8	8	6	7
n	3	3	8	5	10	5
p	10	7	10	10	9	10
q	80	80	85	80	80	80
r	5	5	5	5	5	5
s	145	145	145	145	145	145
t	8	9	10	10	9	10
u	80	83	80	80	80	80
v	5	5	5	5	5	5
w	5	5	5	5	5	5
x	10	10	10	10	9	10

Table 5.16 Measured readings of location of dial gauges and strain gauges for specimens type F.

5.3 Measurement of weld failure planes.

All weld failure planes were measured on a shadow graph recorder. This gives the peak values at various points along the weld length. All other variations of the failure plane along the weld length get covered by this method of measurement. The recorded weld failure plane is thus the apparent failure plane which is greater than that which would occur at a specific point. The shadow graph results thus represent the failure envelope along the weld length. It was observed from seperate measurements using a universal measuring machine that the extent of horizontal weld penetration varied by up to 1.5mm along the weld lengths. Therefore it would be expected that the failure angle readings recorded are only the apparent failure planes and slightly greater than the actual failure condition.

CHAPTER 6 FINITE ELEMENT ANALYSIS OF END PLATE.

6.1 Introduction.

In this chapter a finite element (F.E.) numerical analysis is carried out on the trapezium shaped plate connection Type F. This type of analysis was chosen after having exhausted the various literature published on plate deflection equations. It was found that no general deflection equation existed which could be applied to the trapezium plate. This is attributed to the fact that complex boundary conditions exist for the trapezium plate - two opposite edges fixed while the other two are free edges, figure 4.1.

It is acknowledged by Timoshenko(53) and Lowe(54), that although at first it might appear free edges in plates are relatively simple to deal with, they are in fact the most difficult boundary condition to be confronted. Two reasons are given, the first being the inadequacy of the plate theory to satisfy all the three force variables - a bending moment, twisting moment and shear force - at the free edge, which would be zero. The second reason is the complexity of the manulipulation of imposed boundary conditions which are to be expressed as the second and third derivatives of the displacement function.

It was therefore proposed to analyse the plate numerically by the Finite Element Method (F.E.M), which was available as a computer package - PAFEC Finite Element - on the VAX-B Cluster main frame system. Interactive graphic analysis was achieved by an accompanying software called PIGS - Pafec Interactive Graphics System.

The aim of analysing the trapezium plate numerically is to establish the validity of the

assumption of a fixed end condition existing along the welded edges of the trapezium plate. Also it is expected the results would help confirm that correct experimental testing procedure were adopted.

6.2 The finite element method.

The finite element method (FEM) is a powerful computer based technique which can be used to accurately analyse the behaviour of a continuum structure, subjected to any complex loads and boundary conditions. This method is basically an extension of the matrix methods of solution for skeletal structures. As designers and analysts from various disciplines have gained easier access to computers and computer software, the FEM has gained wide spread recognition and become an indespensable tool.

The FEM proceeds to analyse the behaviour of a continuum by artificially dividing it into a finite number of elements, generally known as a mesh. Individual elements are connected together at nodal points as shown in figure 6.1. An assumed approximate function, usually of polynomial form, is chosen to represent the displacement of an element. Contunity of each element is satisfied at the nodal points only, but in most cases the chosen function is such that it is also satisfied along the common boundaries. The matrix method of analysis is then formulated (usually by the stiffness displacement method) to analyse each element and in turn the whole continuum. The repetative nature of the FEM makes it particularly suited for computer implementation. Thus, complex or multi-storey framed buildings can be readily analysed, which would otherwise have not been possible or too intensive to attempt.

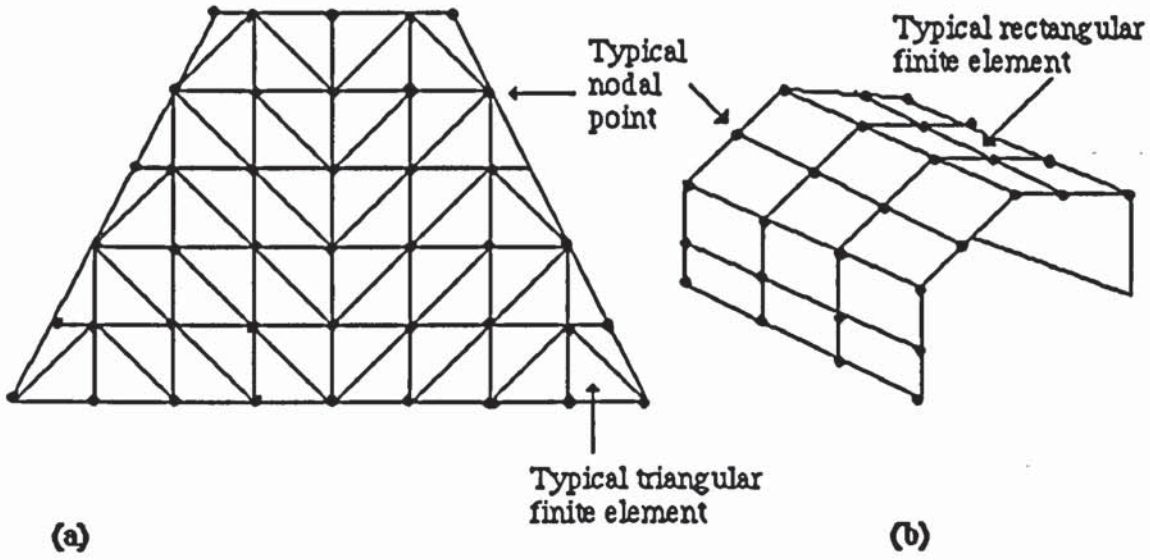

Figure 6.1 Typical finite element idealisations of continua.

(a) Dam wall, (b) Folded plate[55].

To achieve good results from the FEM, the user should grasp some knowledge and experience on the element types available and have an approximate view of the likely stress distributions expected.

6.3 Finite elements.

Different shapes and families of elements exist - from the simple line, one dimensional elements to more complex and sophisticated twenty noded isoparametric three dimensional elements. However the choice is normally restricted to a few types, depending upon the nature of analysis (plane elasticity, plate flexure or shell problems), degree of accuracy required and the computer working capacity. The most common types of elements used are the rectangular and triangular shaped ones, figure 6.2.

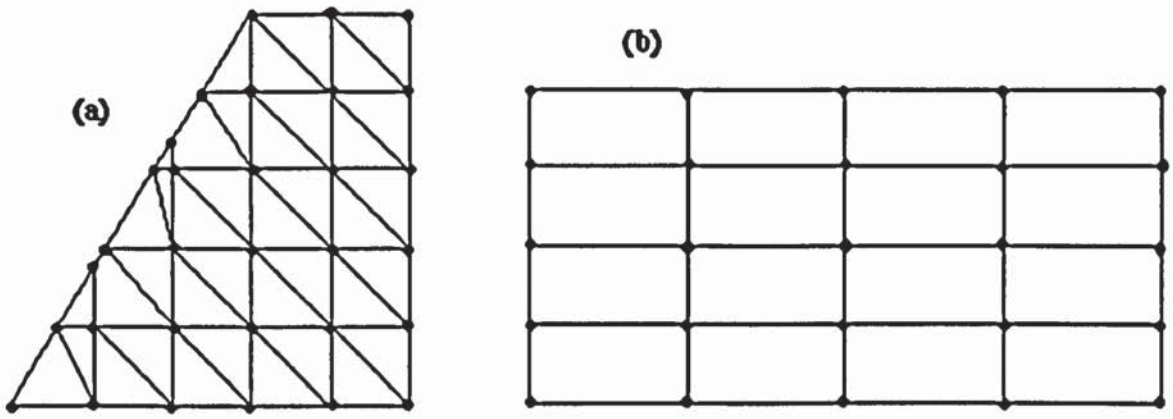

Figure 6.2 Typical finite element idealisations (a) triangular elements (b) rectangular elements[55].

Each shape of element is described by an individual displacement function and each family by a general function. It is found by numerous authors [55,56,57] that certain shapes of elements achieve better results than others. This is principally due to the accuracy of the assumed displacement function chosen. It is because of this that rectangular shaped elements are preferred to triangular elements. Nevertheless, good results can be achieved by increasing the number of elements in the zone of interest. Also, due to the approximate nature of the displacement functions used, a sufficient number of elements are needed to achieve an acceptable representation of the overall continuum. The term 'sufficient' varies to the particular problem under consideration. The accuracy of results increases with the number of elements taken, but this requires increased computer capacities and processing times which lead to greater financial outlay reqirements. As a general rule, meshes are recommended by Rocky[55], Pafec[56] and Zienkiewicz[57] to be more finely graded where sharp changes of stresses are expected

i.e. near openings or points of loading as shown by figure 6.3.

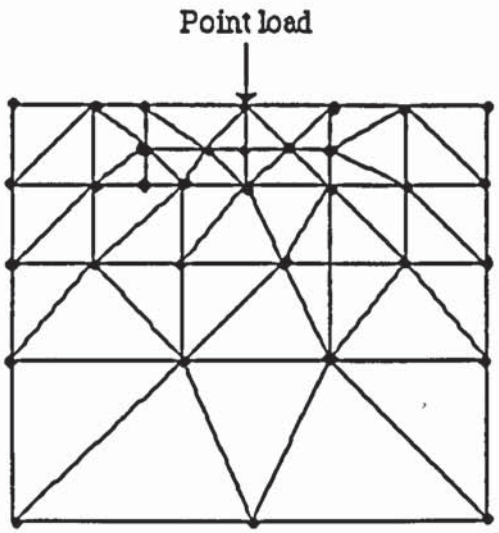

Figure 6.3 Typical example of a graded mesh[55].

6.4 Finite element computer software.

6.4.1 Program for automatic finite element calculations - PAFEC.

Although designers may resort to write their own finite element (FE) computer programmes, it is easier, faster and more accurate to use the comprehensive FE computer packages available today. One such FE package used extensively in industry is PAFEC. PAFEC is the acronym for Program for Automatic Finite Element Calculations. It is a large scale, general purpose 2D or 3D, linear and non-linear, FE analysis system. A comprehensive element library and systems capabilities exist. Typical examples of element types available are shown in figure 6.4.

The procedures required to operate PAFEC are quite straight forward. The user inputs

data via a data file in a prescribed modular form. The file is then run to process the displacements, stresses or other chosen analysis. All decisions in the formulation of the FE analysis are left to the user. Thus, it is important the user has some knowledge of the finite elements available and the results he wishes to obtain.

6.4.2 Pafec Interactive Graphics System - PIGS.

All results and data from the PAFEC runs can be interactivated on the Pafec Interactive Graphics System, known as PIGS. This is an extremely powerful aid for the user of finite elements. It enables him to produce graphical representations of the input or output data interactively. Thus, any wrong data or choice of analysis can be ironed out without having to supply new data and re-run the program.

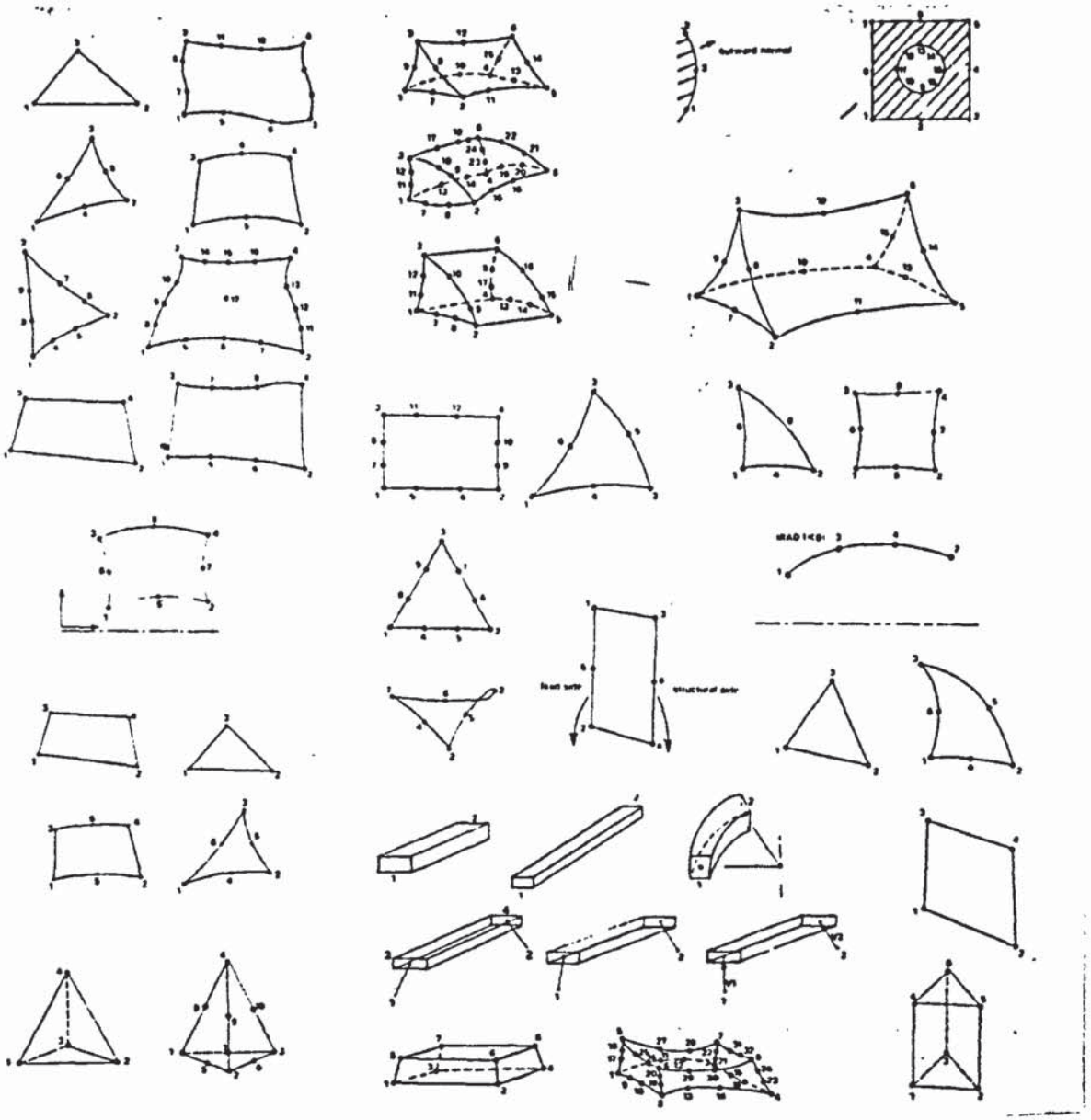

Figure 6.4 Typical types of finite elements available in PAFEC library[56].

The primary facilities on the PIGS software can be itemised as follows;

i) Finite element model generation,

ii) Mesh modification,

iii) Interactive loads and restraint placement,

iv) PAFEC file editing,

v) Full colour and shading,

vi) Stress vector and contour display,

vii) Automatic generation of high quality hard copy,

viii) Automatic PAFEC data file generation,

ix) Graph production.

Typical examples of the type of outputs which can be achieved from PIGS can be seen in figures 6.7 to 6.15.

6.5 Finite element analysis of the trapezium shaped end plate.

A PAFEC input data file is created to submit for FE analysis of the trapezium shaped plate. A typical data file is seen in figure 6.5. Nine system modules are chosen to fully analyse the plate for stresses and displacements. These modules can be itemised as follows;

i) Control,

ii) Nodes,

iii) Pafblocks,

```
TITLE TRAPEZIUM PLATE PROBLEM
CONTROL
PIGS STRESS FILE
CONTROL.END
NODES
NODE.NUMBER,X,Y
1,0.045,0
2,0,0.045
3,0.205,0
4,0,0.205
5,0.0598,0.0598
PAFBLOCKS
TYPE=1
ELEMENT.TYPE=44210
BLOCK.NUMBER,N1,N2,TOPOLOGY
1,1,2,1 3 2 4
MESH
REFERENCE,SPACING.LIST
1,60
2,60
PLATES.AND.SHELLS
PLATE.NUMBER,MATERIAL.NUMBER,THICKNESS,RAD1
1,5,0.013,0
LOADS
CASE.OF.LOAD,NODE.NUMBER,DIRECTION.OF.LOAD,VALUE.OF.LOAD
1,5,3,-25000
RESTRAINTS
NODE.NUMBER,PLANE,DIRECTION
2,1,0
1,2,0
STRESS.ELEMENT
START,FINISH
1,5000
END.OF.DATA
```

Figure 6.5 Typical PAFEC data input file

iv) Mesh,

v) Plates and shells,

vi) Loads,

v) Restraints,

vi) Stress.

The CONTROL module is used as an aid to guide the process through the various paths within the PAFEC system.

The NODES module is where co-ordinate values of nodes are inserted, to define the problem.

Automatic generation of the mesh is achieved by the use of PAFBLOCKS and MESH modules. The pafblock facility is used to reduce the magnitude of data preperation required to create a mesh. A sufficient number of nodes are required to define the layout and shape of each pafblock. These are then divided into a number of elements by referring to the mesh module. The advantage tc be gained from the use of these two modules is when re-analysis of a problem is required, with different mesh densities.

The PLATES and SHELLS module relates to the properties and thickness of the material. The properties are pre-programmed into the PAFEC software, for different materials but may be overwritten by the user. However all thicknesses of plate have to be given. The ratio of plate thickness, h , to length of plate L, is shown by pafes in figure 6.6. Ratios of h:L below 0.4 are classed as thin elements, between 0.15 and 0.6

as thick elements and finally those between 0.25 and 0.8 as 3D elements.

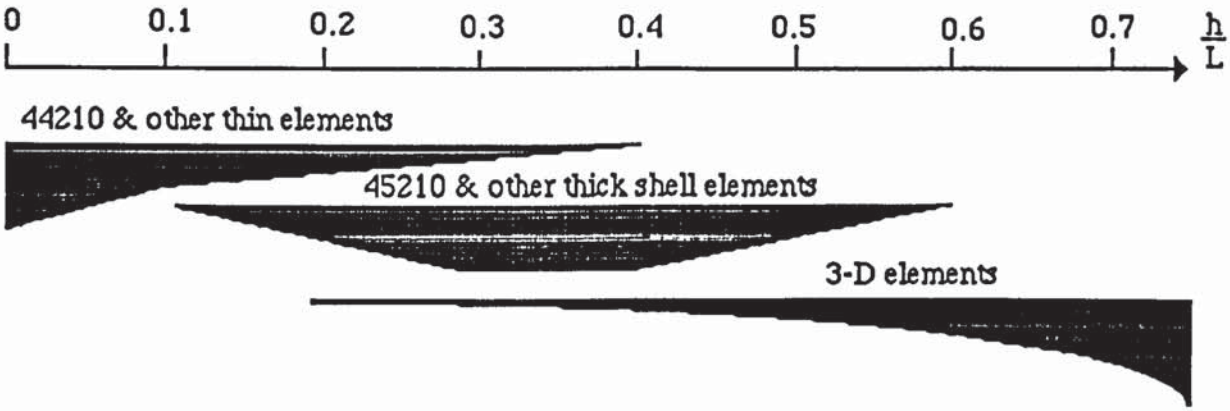

Figure 6.6 Ratios of plate thickness, h to length of plate L.

For the LOADS module, the case, location, direction and value of loads are given in a prescribed manner.

Any restraints to be applied are selected in the RESTRAINT module. These can be applied at individual nodes or alternatively as planes of restraint. The normal six degrees of freedom may be applied in any combinations.

The STRESS ELEMENTS module stresses the chosen number of elements to be stressed.

For the analysis carried out, a single two dimensional pafblock (TYPE 1 to Pafec specifications) is used to define the whole plate. The mesh density is initially chosen to be of 400 finite elements i.e a 20 x 20 mesh configuration, as seen in figure 6.7. This is varied to a mesh 35 x 35 dense and then to a 40 x 40 dense mesh, figures 6.8 and 6.9.

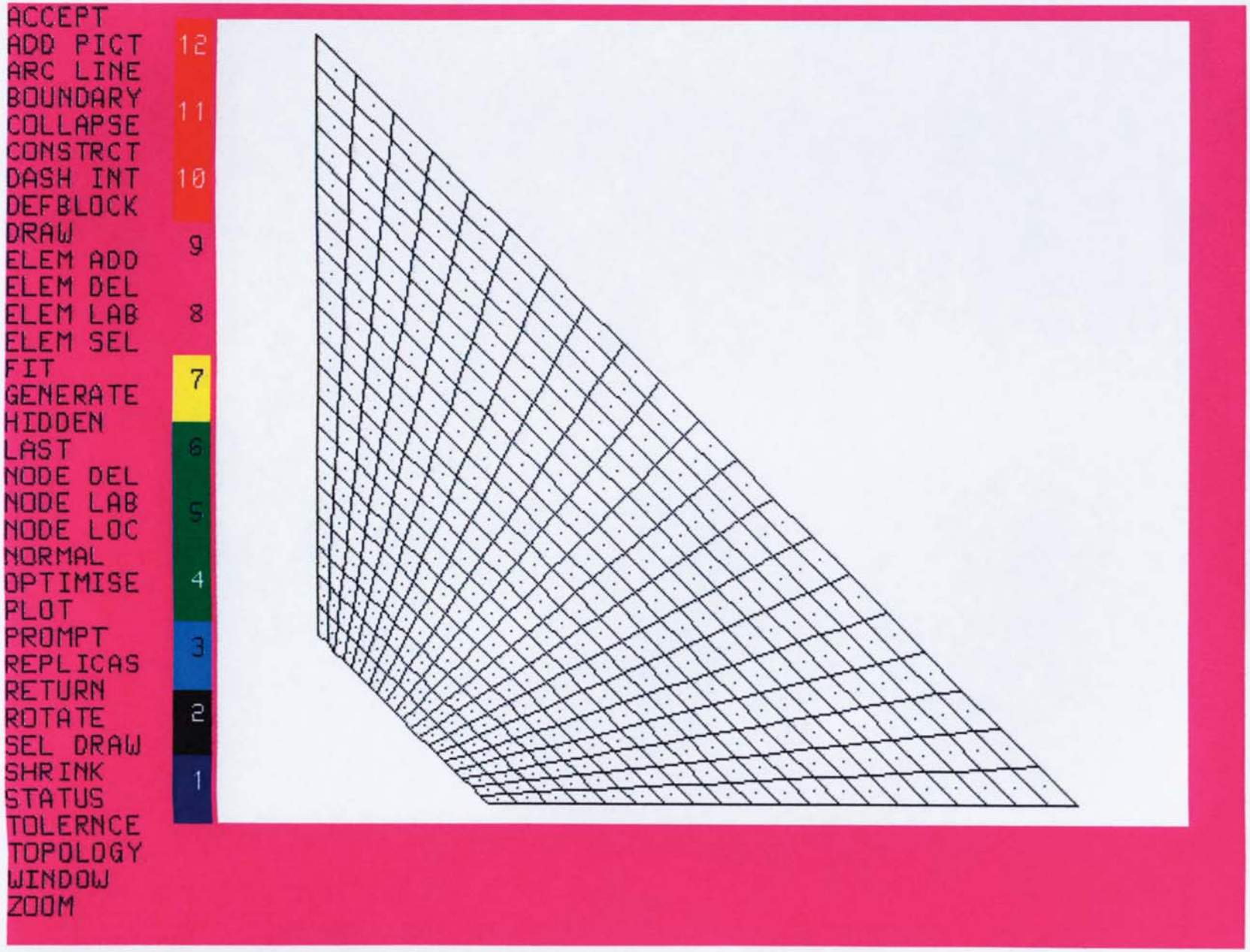

FIGURE 6.7 A 20 x 20 DENSE FINITE ELEMENT MESH OF END PLATE CONNECTION

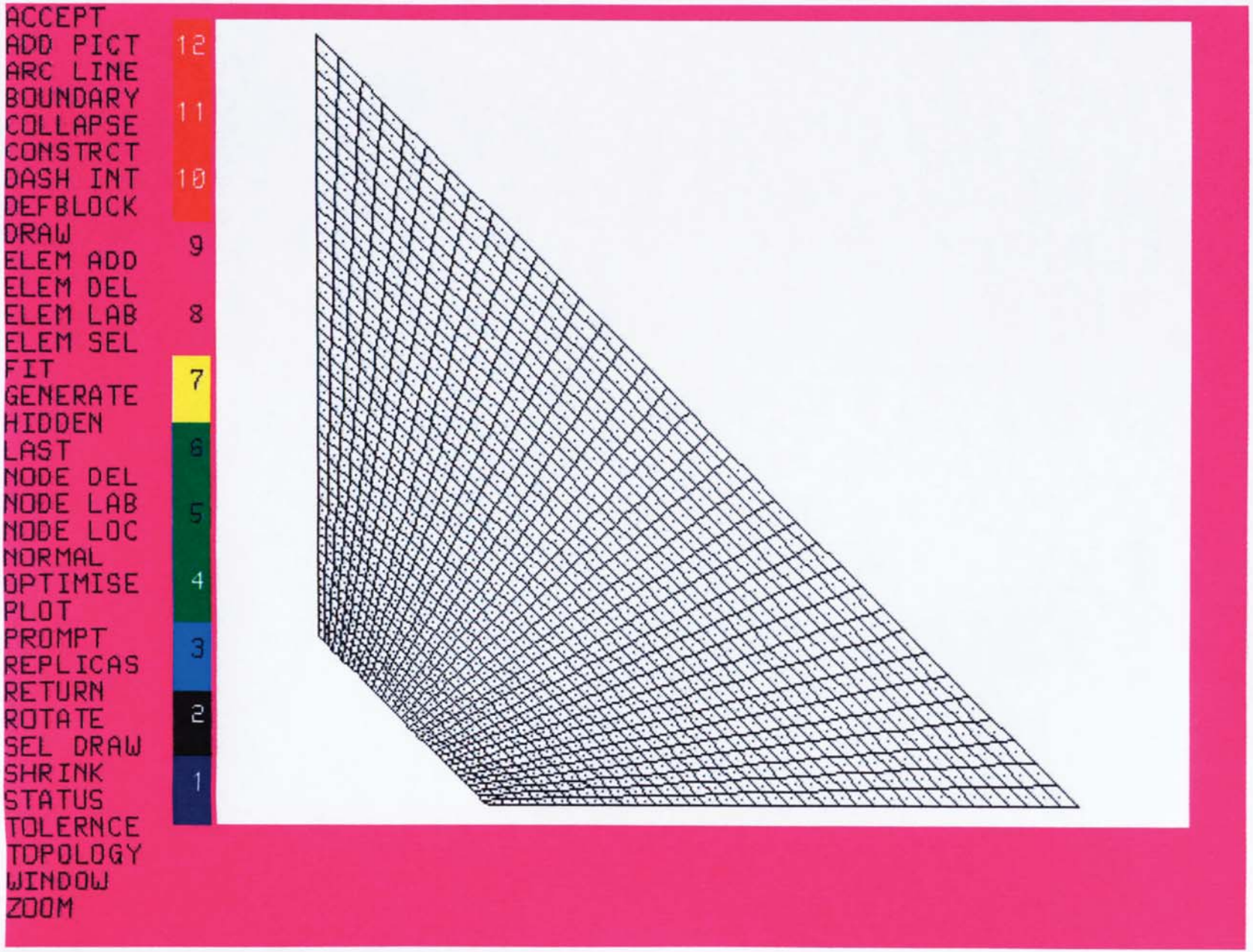

FIGURE 6.8 A 35 x 35 DENSE FINITE ELEMENT MESH OF THE END PLATE CONNECTION

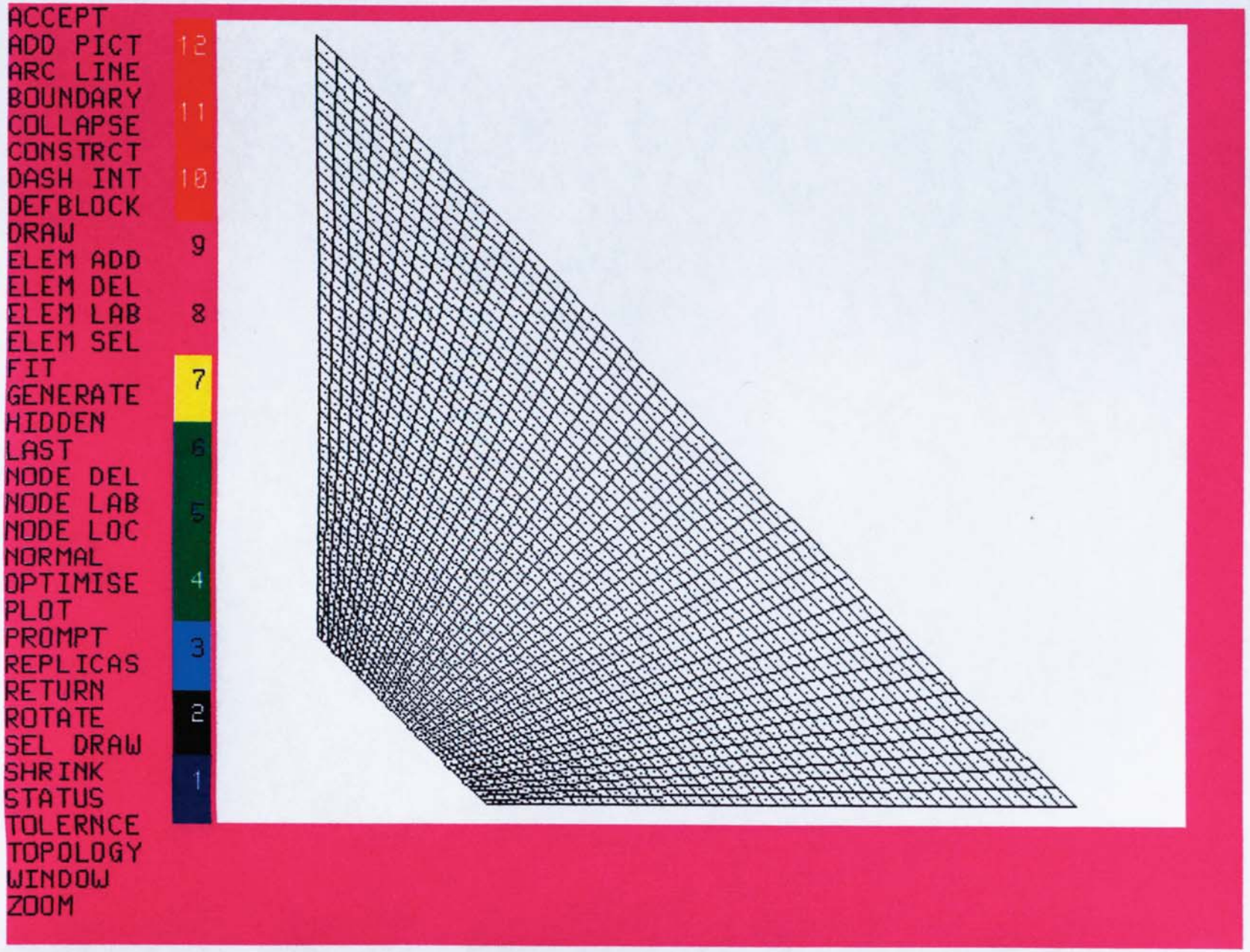

FIGURE 6.9 A 40 x 40 DENSE FINITE ELEMENT MESH OF THE END PLATE CONNECTION

The increase in mesh densities is required in order that convergence of stresses and displacements to actual values may occur. The FE analysis method is based upon an approximate deflection equation, which would generally give results closer to the actual deflections than to actual stresses. This can be explained by two factors; first because stress is a derivative function of the deflection, and deflection itself being approximated by a polynomial, the convergence of stress to exact values would require more dense meshes. Secondly, any slight variation of the deflected shape in experiments, would change the stresses from the expected values. It is because of this that re-runs with varying mesh densities have been carried out. This can be seen in the trapezium plate problem analysed. For a fixed load of 25KN as mesh densities increase - figures 6.10 to 6.12, the convergence of stresses to experimental stress is observed. Full convergence is not exactly obtained which is explained by the second mentioned fact earlier above. However, deflected values rapidly converge to the exact values, for a lowly dense mesh, figures 6.13 to 6.15.

The loading actually applied in practice to the trapezium plate is replaced by an equivalent point load, for this analysis. This is to help simplify the FE mesh generation of the plate. Also, because the main interest of the analysis lies in the results along the welded edges of the plate and not at the point of load application. It is expected that stress distribution along or near to these welded edges would not be affected by this simplification.

The element type used from the PAFEC library is the 44210 element, which is an eight noded facet shell element, figure 6.16. This element type is expected to behave as a flat thin shell which can carry bending and membrane loads. Reasonable distortions are permitted from the basic square shape, provided flatness is preserved. Each node of the

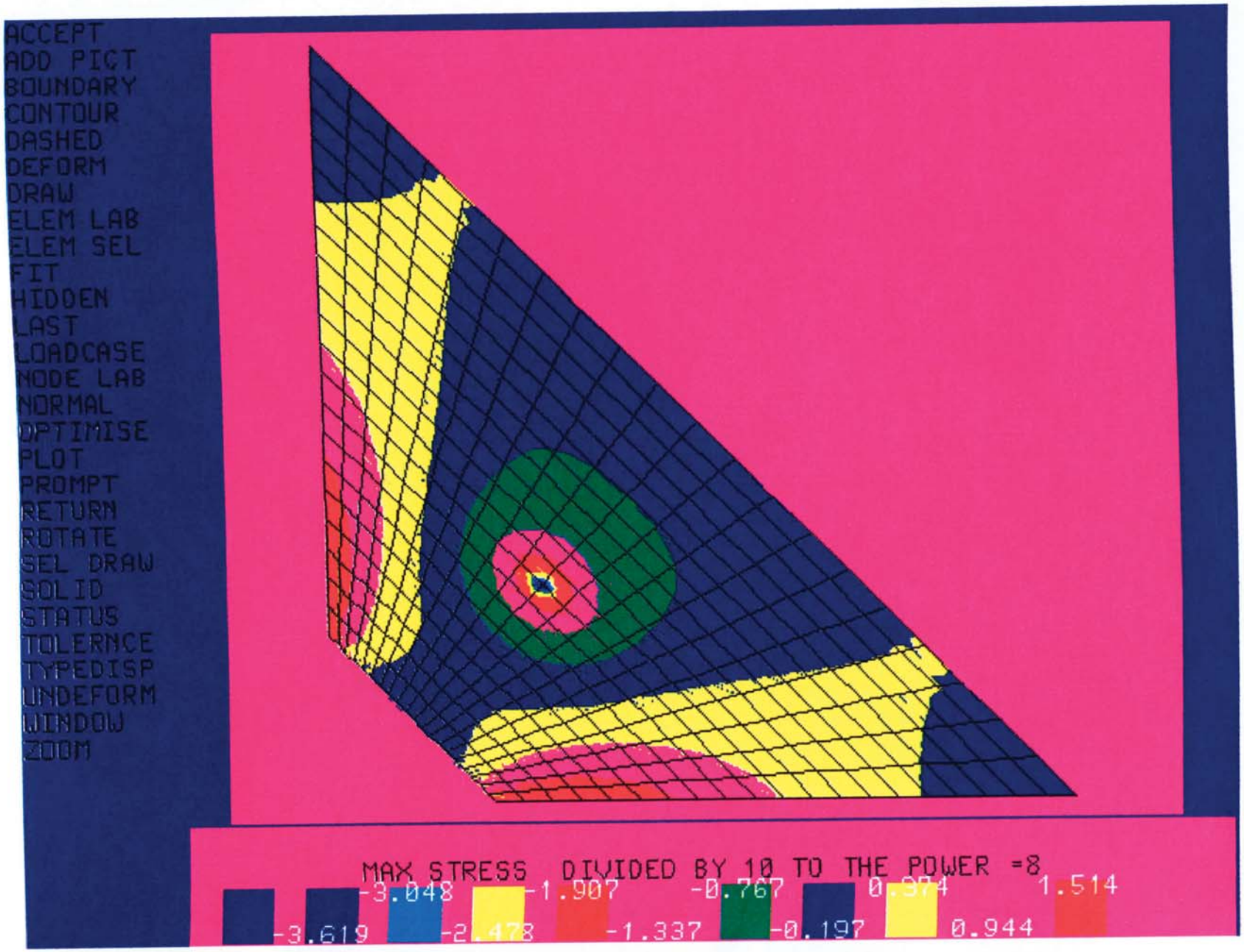

FIGURE 6.10 MAXIMUM STRESSES OF THE END PLATE CONNECTION USING A 20 x 20 DENSE FE MESH

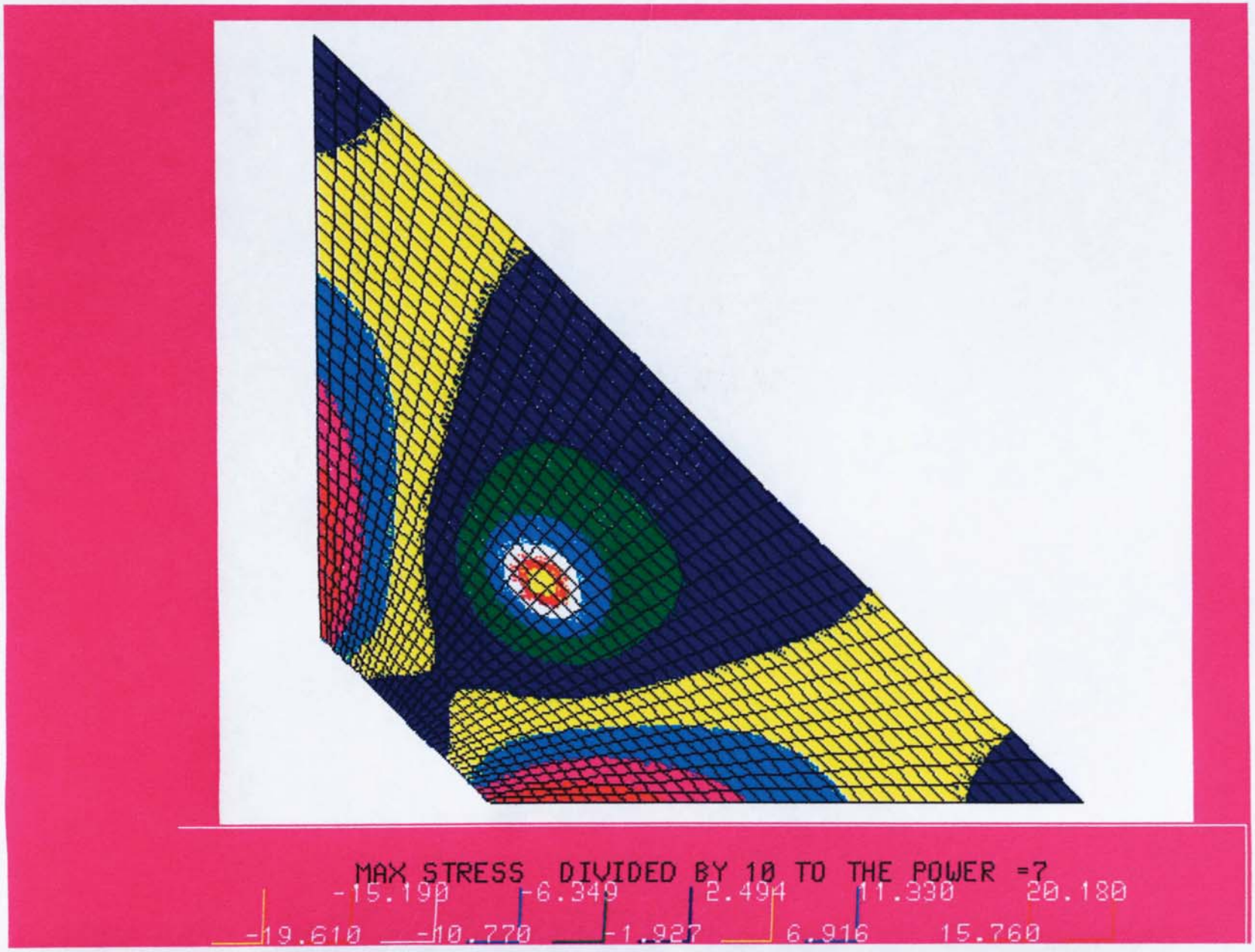

FIGURE 6.11 MAXIMUM STRESSES OF THE END PLATE CONNECTION USING A 35 x 35 DENSE FE MESH

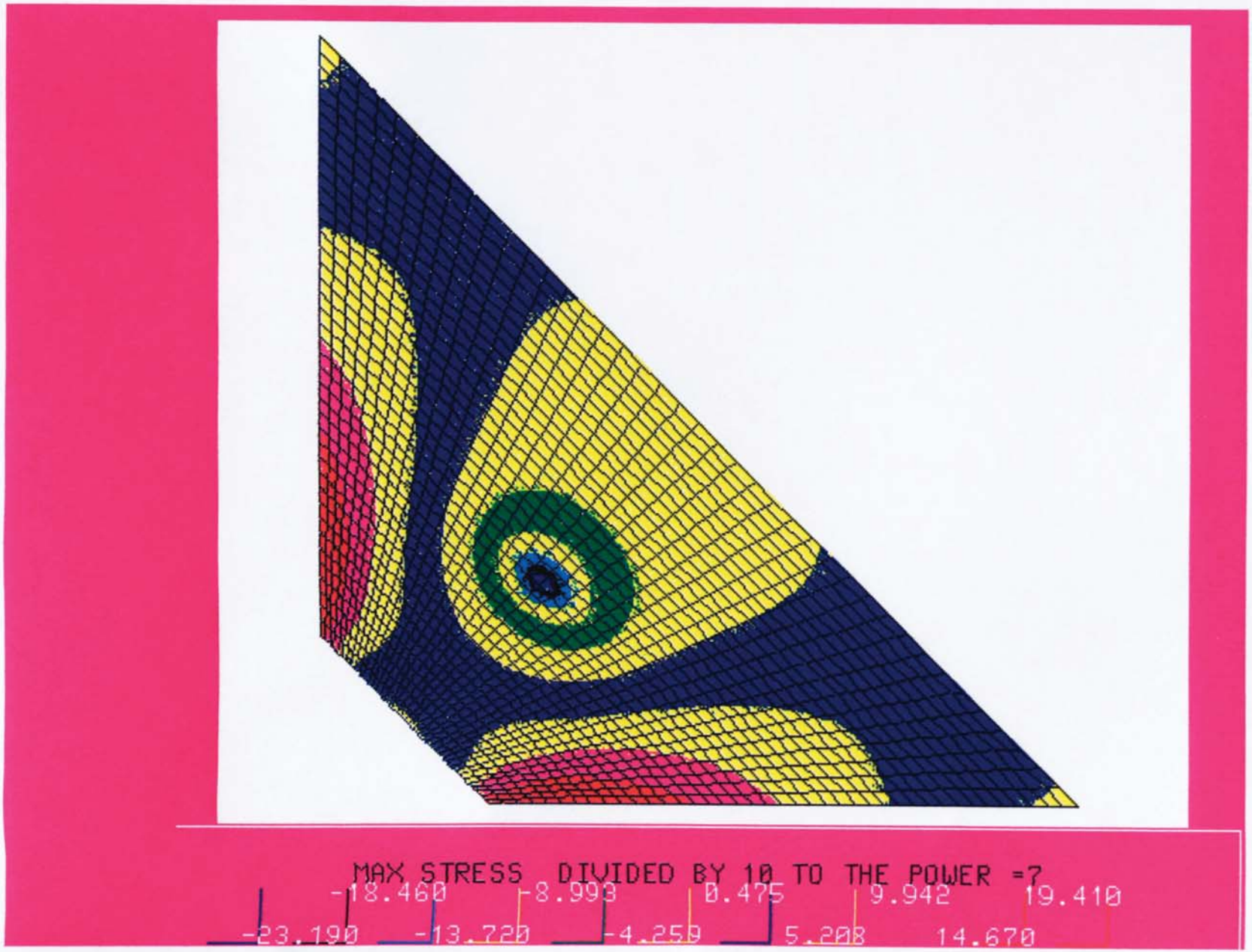

FIGURE 6.12 MAXIMUM STRESSES OF THE END PLATE CONNECTION USING A 40 x 40 DENSE FE MESH

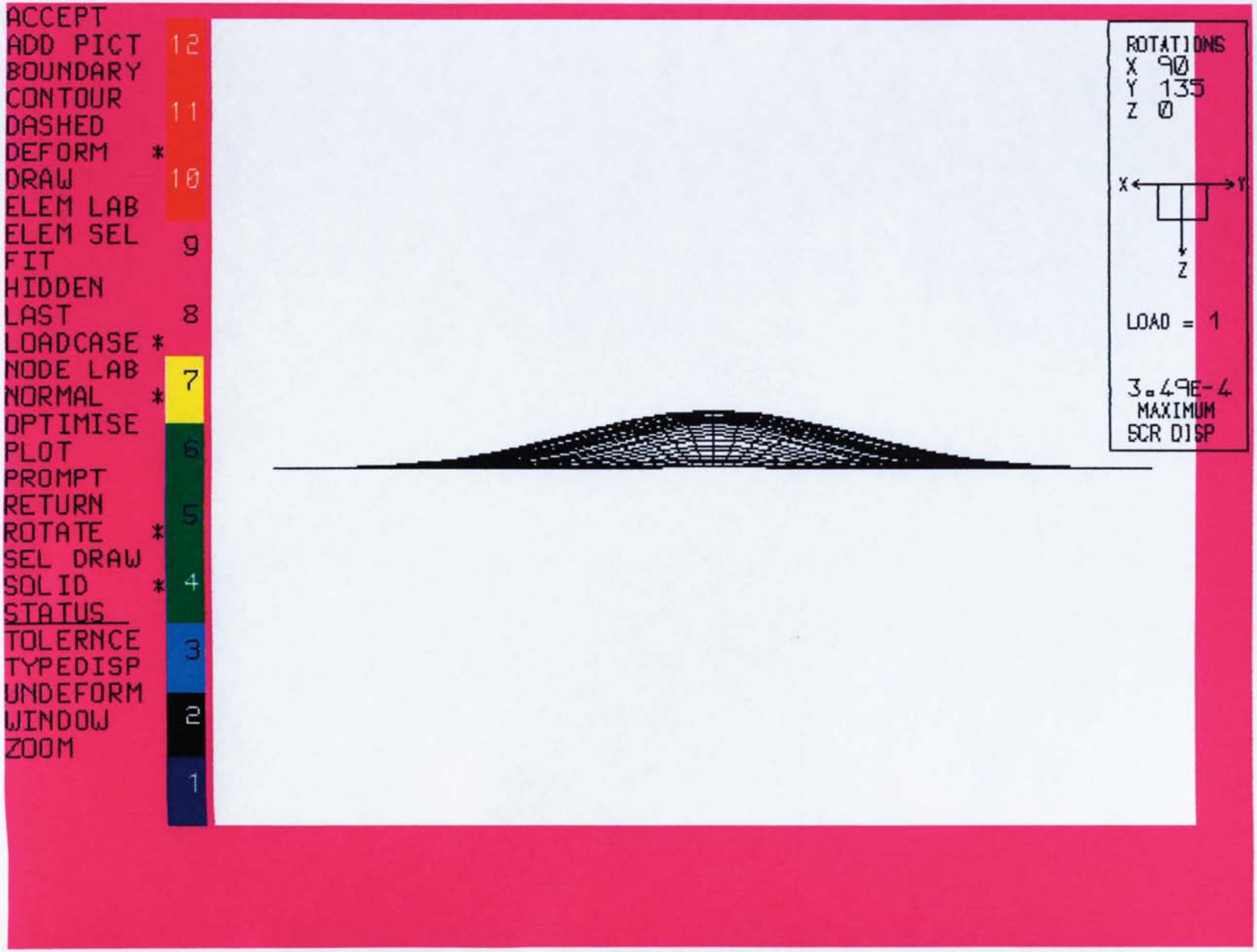

FIGURE 6.13 MAXIMUM DEFLECTION OF THE END PLATE CONNECTION USING A 20 x 20 DENSE FE MESH

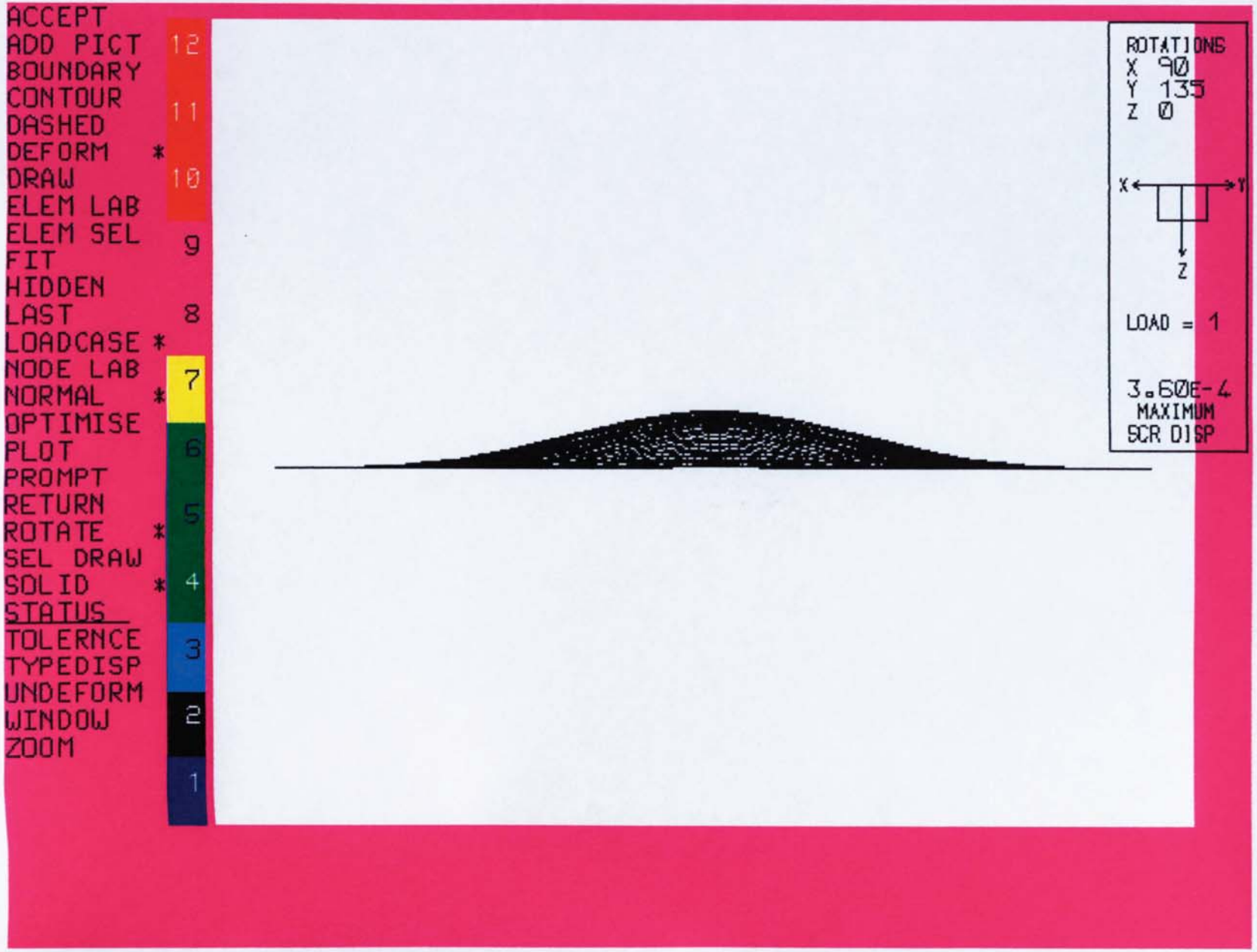

FIGURE 6.14 MAXIMUM DEFLECTION OF THE END PLATE CONNECTION USING A 35 x 35 DENSE FE MESH

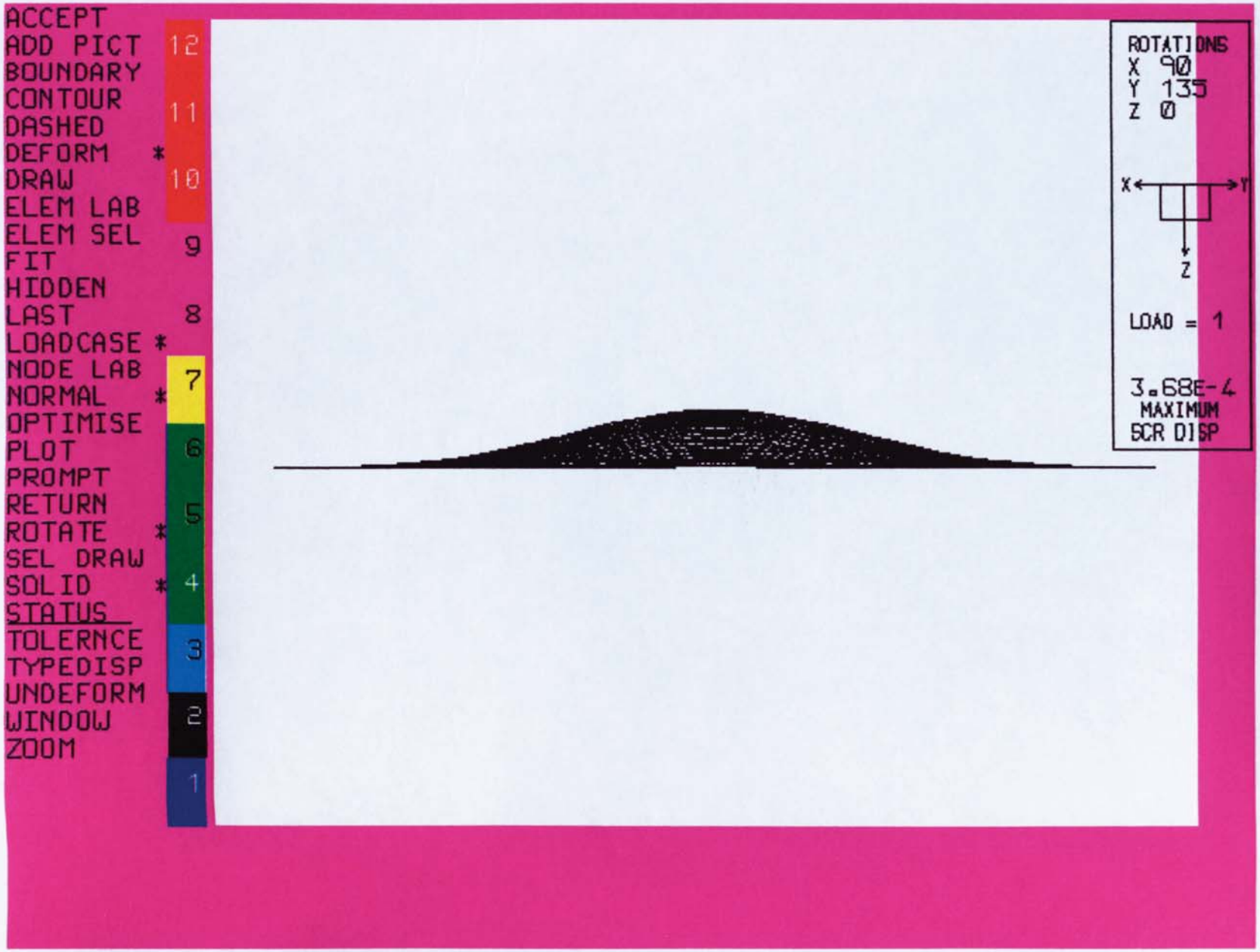

FIGURE 6.15 MAXIMUM DEFLECTION OF THE END PLATE CONNECTION USING A 40 x 40 DENSE FE MESH

element has five degrees of freedom (U_x,U_y,U_z,ϕ_x,ϕ_y) when used as a plate element. The stressing output gives values at each node and at the centre of each element.

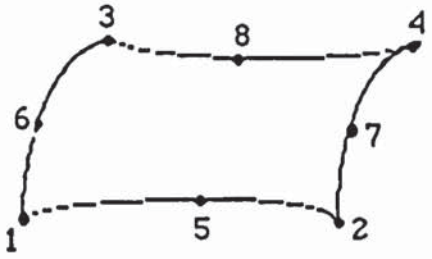

Figure 6.16 Element type 44210 used for finite element analysis.

All degrees of freedom have been restrained by planes acting along the welded edges of the trapezium plate. It is expected this is a true representation of the experimental case.

6.6 Results from finite element analysis.

Results obtained from PAFEC are only true within the elastic limit zone, because PAFEC is a linear elastic based FE analysis package. The comparisons to be made later in chapter 7 of this thesis, between the experimental results and those obtained from PAFEC are thus confined to the elastic zone. From this FE analysis it is only expected to verify the assumption that a fixed end type of condition prevails along the end plate connection's welded edges. Further, the results would also confirm that correct experimental testing procedures were adopted.

Due to the vast amount of data output from the PAFEC analysis, only typical deflections and stress output results are given in Appendix C, for the first one hundred nodes.

The maximum deflections as load increases, obtained from PAFEC are given in table 6.1 and plotted in figure 6.17. The comparison between stresses from the PAFEC output and the experimental values is to be restricted to the one load case only. This restriction is necessary because of the limitation of the analysis to the elastic zone only. Comparisons at higher loads are not possible due to non - linear effects prevailing. At lower loads effects due to the initial application of load disproportionately distorts comparisons made between PAFEC and experimental readings. The comparison is therefore proposed to be made for the 50KN experimental load value. This load case lies in the elastic limit and is chosen from the load deflection readings of the end plates.

The PIGS stress outputs at the 50KN experimental load case are given in figures 6.10 to 6.12, for the varying mesh densities of 20 x 20, 35 x 35 and 40 x 40 respectively. The maximum deflection, PIGS outputs obtained are also shown for the same mesh densities, in figures 6.13 to 6.15

Load (KN)	Maximum deflection (mm)
0	0
10	0.075
20	0.150
30	0.225
40	0.300
50	0.375
60	0.450
70	0.525
80	0.600
90	0.672

Table 6.1 PAFEC results for maximum deflection of end plate as load increases.

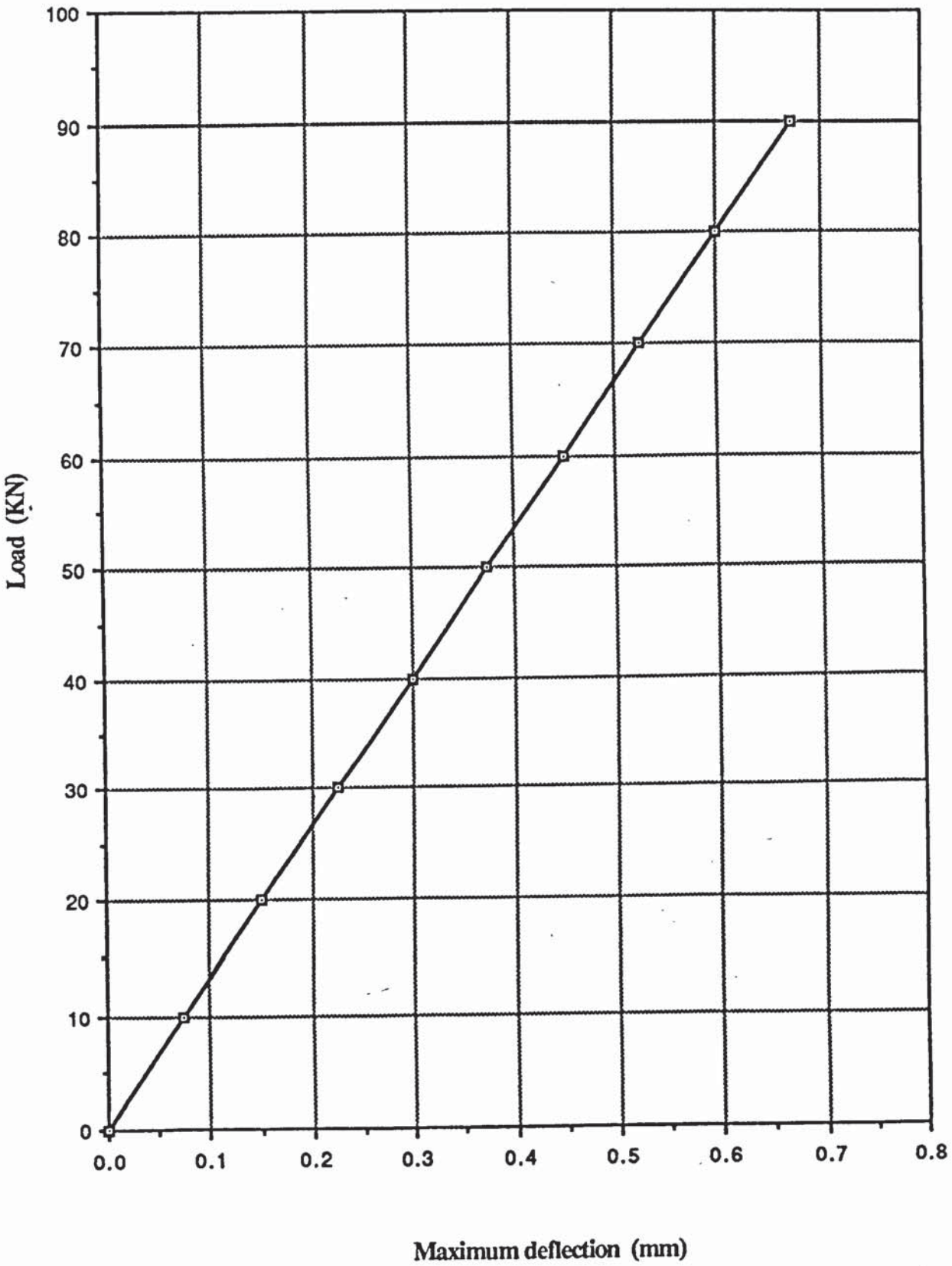

Figure 6.17 PAFEC results of load vs deflection

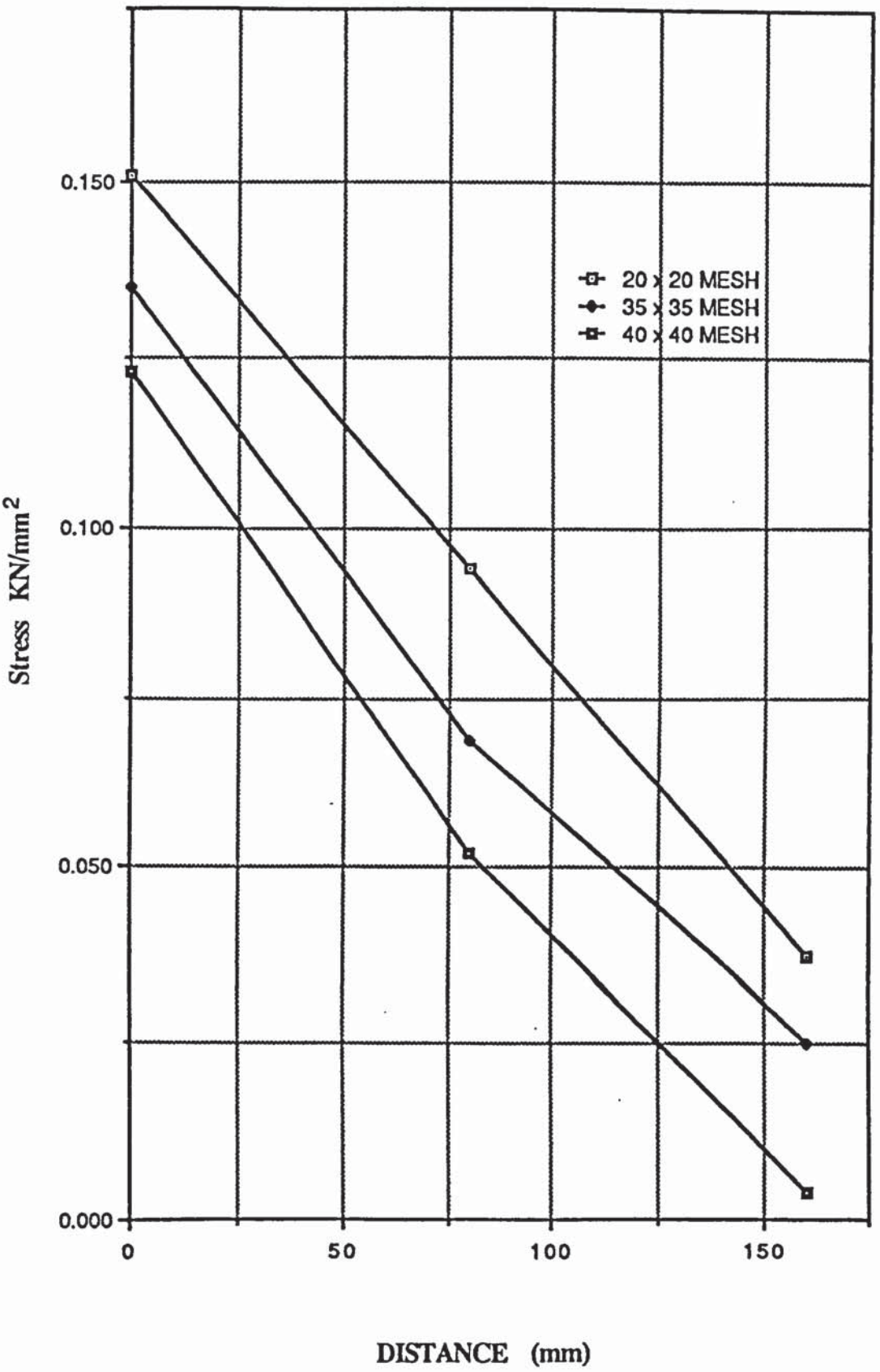

Figure 6.18 PAFEC output of stresses at points A, B and C on fixed edges of end plate, with mesh densities increasing.

6.7 Replacement of point load by an equivalent line load.

The assumption made in the extend weld failure theory in Chapter 4, that a point load can be replaced by an equivalent uniform line load is also justified using the finite element method.It was assumed that the end plate be segmented into six beam elements and the applied point load also be replaced by a uniform equivalent line load. An experimental equivalent uniform distributed load of 50KN is applied at six nodal points along the width ab of the end plate, (as seen in figure 4.4) in the finite element analysis. The analysis is varied for mesh densities of 20 x 20, 35 x 35 and 40 x 40. PIGS stress output results for these varying mesh densities are shown in figures 6.19 to 6.21.

In this section of the finite element analysis only the state of the stress distribution along the welded (fixed) edges of the end plate is being investigated into. It is expected that by replacing the point load with the equivalent uniformly distributed line load, the stresses should not alter by any significant value along the assumed fixed plate edges.

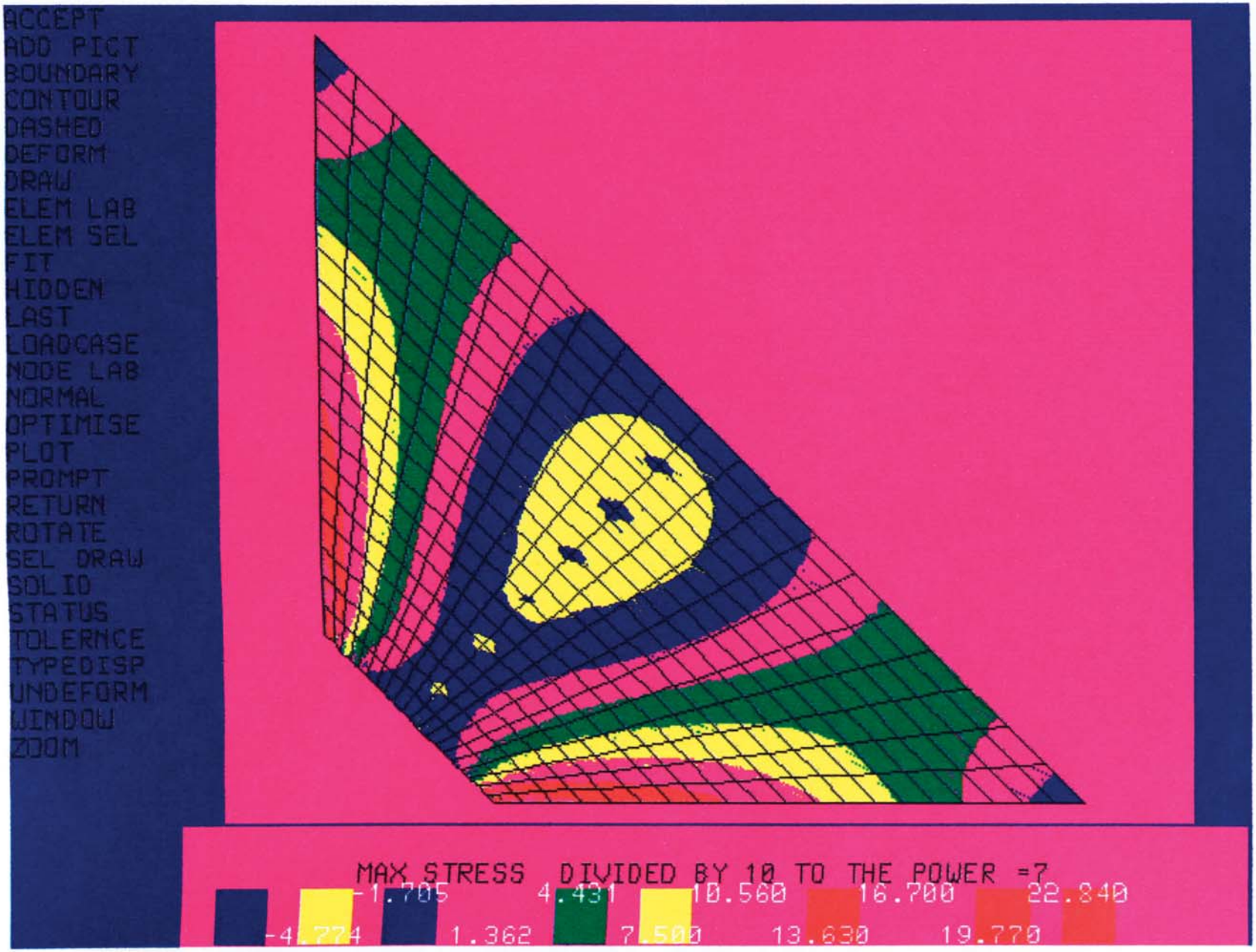

FIGURE 6.19 MAXIMUM STRESSES OF THE END PLATE CONNECTION FOR A UNIFORM LINE LOAD USING A 20 x 20 DENSE FE MESH

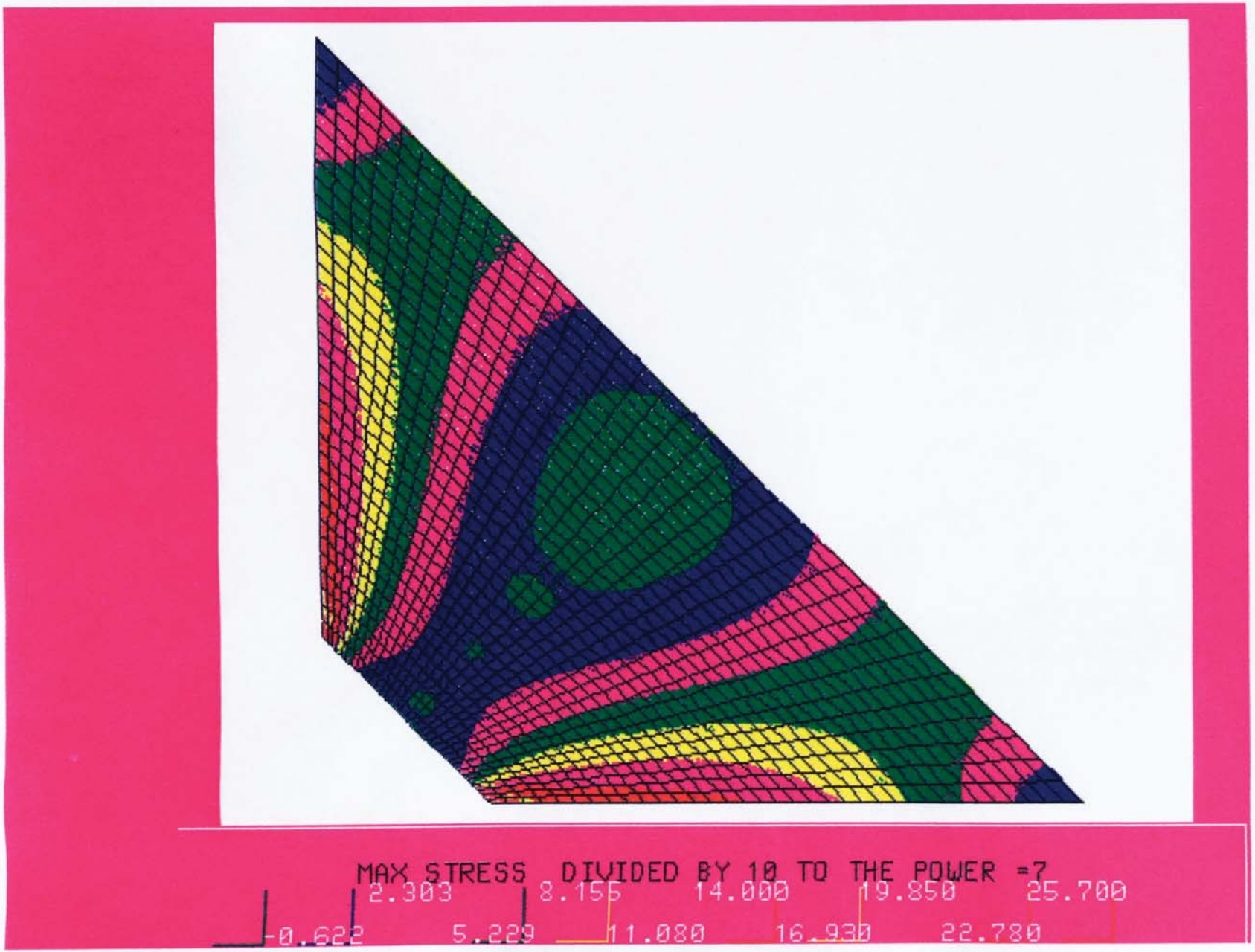

FIGURE 6.20 MAXIMUM STRESSES OF THE END PLATE CONNECTION FOR A UNIFORM LINE LOAD USING A 35 x 35 DENSE FE MESH

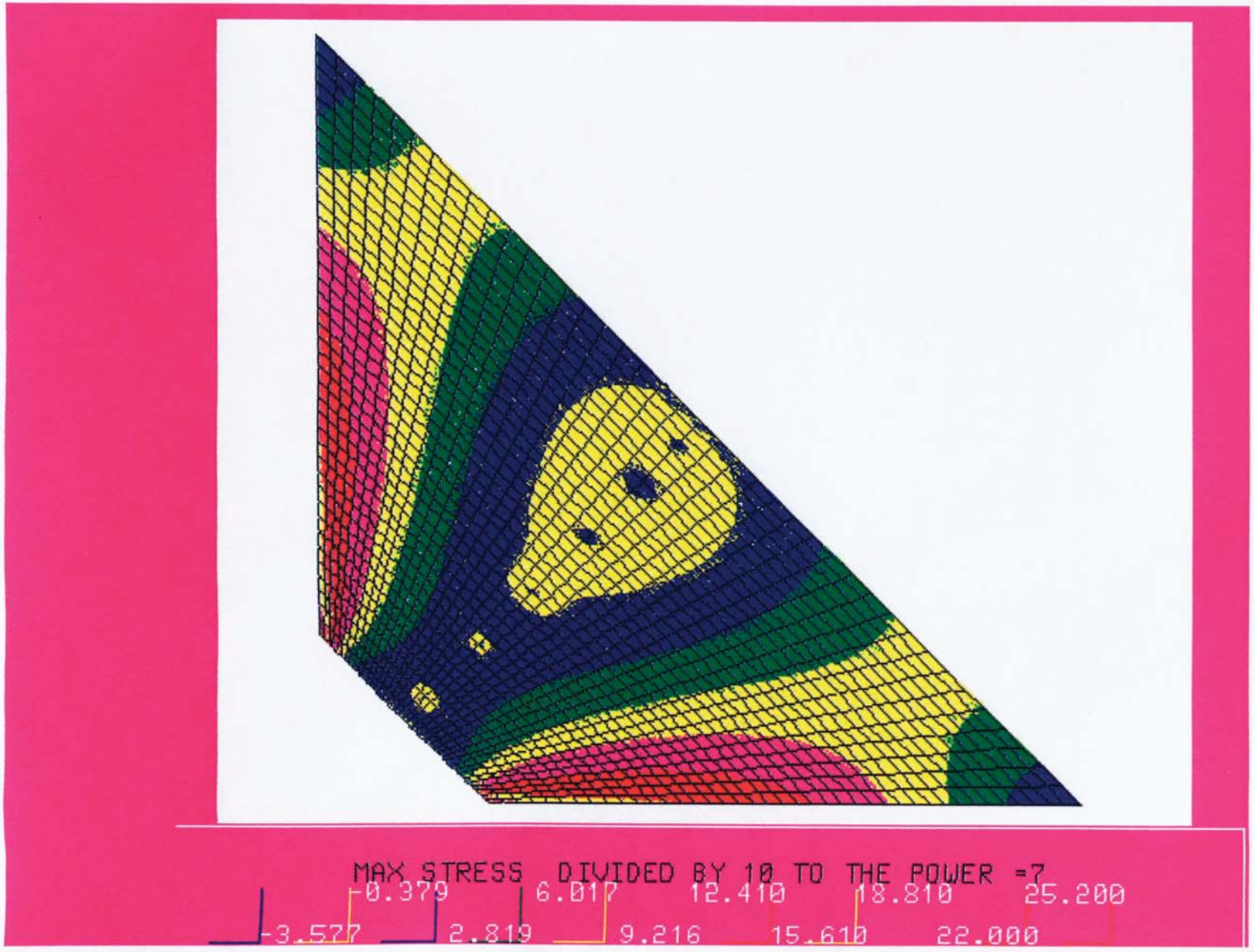

FIGURE 6.21 MAXIMUM STRESSES OF THE END PLATE CONNECTION FOR A UNIFORM LINE LOAD USING A 40 x 40 DENSE FE MESH

CHAPTER 7 DISCUSSION OF RESULTS.

7.1 Tensile coupons.

The results from the tensile coupons Tables 5.2 to 5.4 are used to obtain figure 7.1 which shows that the ratio of the ultimate tensile strength of HAZ to parent metal (6082-T6) is 0.57, and for the proof stress a ratio of 0.52. These compare favourably with data published by Soetens [6], and that of Pirner [3], and Mazzolani [47], whose ratios for the ultimate tensile strengths are 0.63, 0.60 and 0.66 respectively and the proof stress in the region of 0.50.

The ratio of the ultimate tensile strength of the weld metal 4043A (NG21) to the parent metal 6082-T6 is found to be 0.56 which is in the region to that obtained for the HAZ to parent metal. However, the ratio of weld metal to parent metal proof stress is 0.37, which is lower than that for the HAZ to parent metal ratio of 0.52. These values also compare favourably with those obtained by Soetens [6] - a ratio of 0.60 for the UTS of weld to parent metal and 0.35 for the proof stress of weld to parent metal.

The ultimate tensile strength of the HAZ and weld metal are of a comparable value - the ratio of UTS of HAZ to weld metal found to be 1.02 - implying failure should occur in the weld material for a uniform cross section. The weld metal is also found to have a significantly lower proof stress than the HAZ - a ratio of the weld to HAZ of 1.41, which from a serviceability limit or permissible stresses design point would mean failure occuring in the weld metal.

An important finding by Soetens [5,6] and also later confirmed by Robertson and

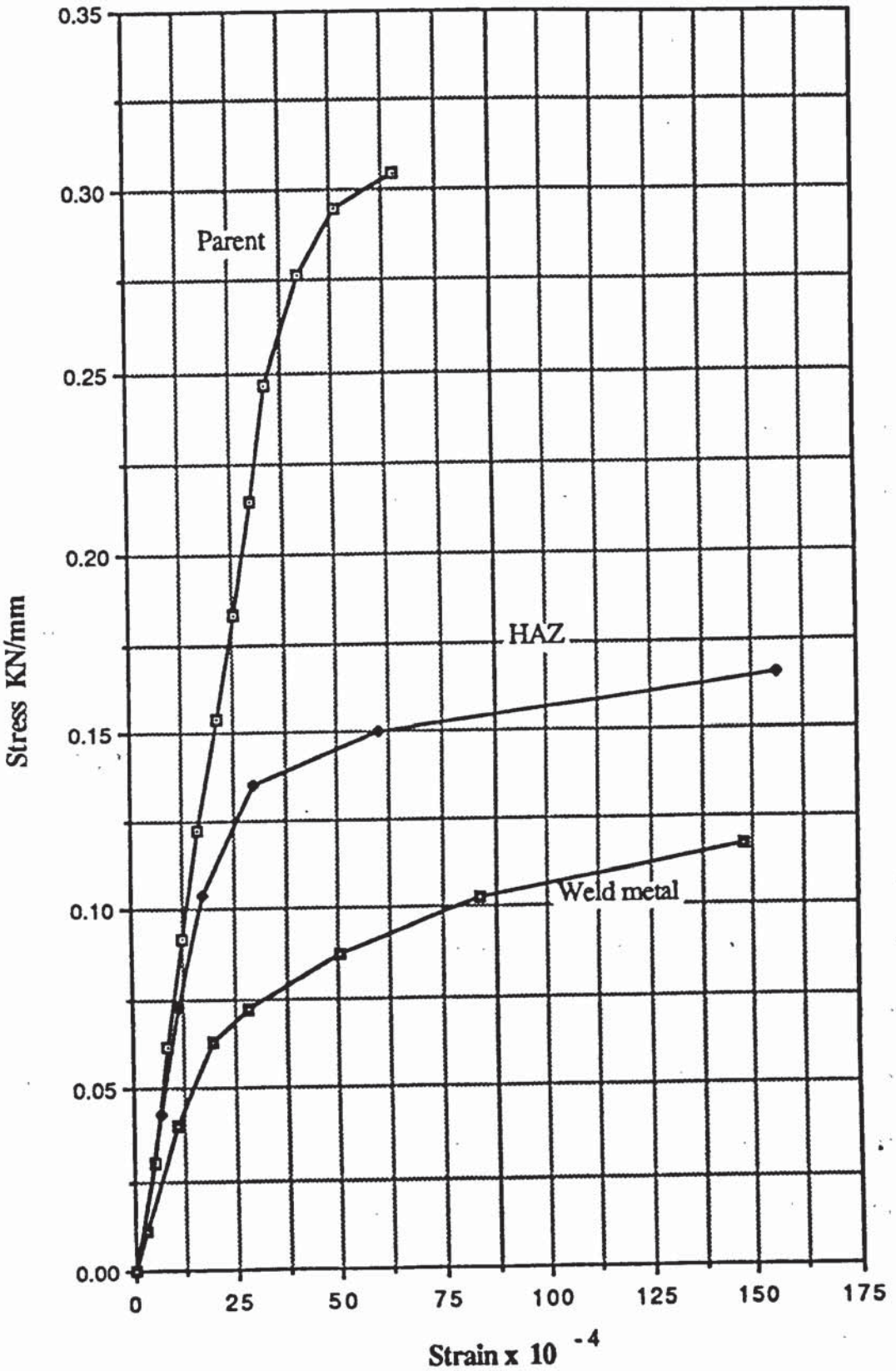

Figure 7.1 Typical stress - strain curves for coupons from 6082-T6 aluminium alloy

Dwight [3,4] is that the UTS for HAZ's is dependant upon plate thickness. The relationships found and discussed above are based solely upon tests from plate of 13mm thickness. However the weld and parent metal UTS values are independent of the plate thickness.

The proof and ultimate stresses published in CP118 Table 1, and BS 8118 Table 2.2 (Part 1), for plate section aluminium alloy 6082 - T6 are; $\sigma_{0.2}$ = 240 N/mm^2 and σ_u = 295 N/mm^2. Both these values are lower than those obtained by the author, Robertson and Dwight and Soetens. No ultimate or proof stress values are given in CP118 or BS 8118 for the HAZ or weld metals. Only permissible and design stresses are given by them respectively.

7.2 Hardness traverse.

With regards to the code of practice CP118, extensive classification and guidance is not given for HAZ's in aluminium. The code only requires aluminium other than in the annealed condition to be designed on the assumption that a reduced strength zone (RSZ) extends over a distance of 25mm (1") in all directions from the centre line of a butt weld and from the root of a fillet weld. However, the work conducted by Robertson and Dwight on HAZ's in aluminium alloys has been recognised by the Committe for the Draft British Standard BS 8118 - Code of Practice for the Design of Aluminium Structures - and have fully incorporated it into the Draft Code of Practice. The work conducted by the author is compared with the findings and suggestions made by Robertson and Dwight.

7.2.1 Extent of the HAZ.

From the hardness traverses carried out by the author, it is observed that a distinct softened zone exists immediately adjacent to the weld metal.This is the Heat Affected Zone (HAZ), as discussed in chapter 2. The start of this HAZ, referred to by Robertson and Dwight [3,4] as the distance X_A, is found in these tests to average approximately 15mm either side of the weld centre line. The extent of the HAZ, X_B is also found from these tests to average approximately 30mm on either side of the weld centre line, seen in figure 5.7 and Appendix A.

These results compare favourably with Robertson and Dwights own experimental findings for X_A and X_B, to average 25 and 12mm respectively, for a similar butt welded specimen of 6082-T6 type alloy. The slightly smaller values for X_A and X_B obtained by Robertson and Dwight can be attributed to the fact that their welded specimens were prepared by the mechanical MIG process, whereas the authors were by the manual MIG process.

7.2.2 Severity of the HAZ.

It was also observed from the hardness traverse tests that the softest part is generally the weld metal, although softer spots were observed at random points in the HAZ, figure 5.7 and Appendix A. This is mainly due to the random nature of dwelling of the flame torch, during the manual MIG welding process.

A relationship between the UTS and hardness values is derived from the readings

plotted in figure 7.2. Defining the material zones as Robertson and Dwight have - soft material existing at a distance less than X_A and non-soft material existing at a distance greater than X_A, where X_A is the distance shown in figure 2.5, Chapter 2. The following relationships are found to exist;

for non-soft material $\sigma_u = 2.90 . H$ Equation (7.1)

for soft material $\sigma_u = 2.65 . H$ Equation (7.2)

However a better fit line is observed to exist for both the soft and non-soft materials, seen in figure 7.1, and given by equation--;

$\sigma_u = 2.80 . H$ Equation (7.3)

Compared to Robertson and Dwight's derived relationships, given by equations 7.4 and 7.5 below, a close agreement for the non-soft material is observed, but not the soft material.

non-soft material $\sigma_u = 2.84 . H$ Equation (7.4)

soft material $\sigma_u = 3.17 . H$ Equation (7.5)

This difference can be partly explained by the fact that Robertson and Dwight's specimens were welded using combined filler metals 5556 (NG61) and 5356 , whereas the author has used filler metal 4043A (NG21) throughout. The findings by Soetens [5,6] on the UTS of filler metals 5356 and 4043A indicate filler metal to be approximately 12 percent stronger than filler metal 4043A, when used with alloy 6082-T6. The other factor is that Robertson and Dwight's derived equations are based upon data for both the alloys 6082 and 7019. It is known from their own findings and from Soetens, that UTS values differ for parent, HAZ and weld metals between the two alloys and therefore so do their hardness values. Thus a better relationship would be obtained between UTS and hardness values, if based upon individual alloy and filler metal combinations, than on a mixture of alloys and filler metals. The author's derived

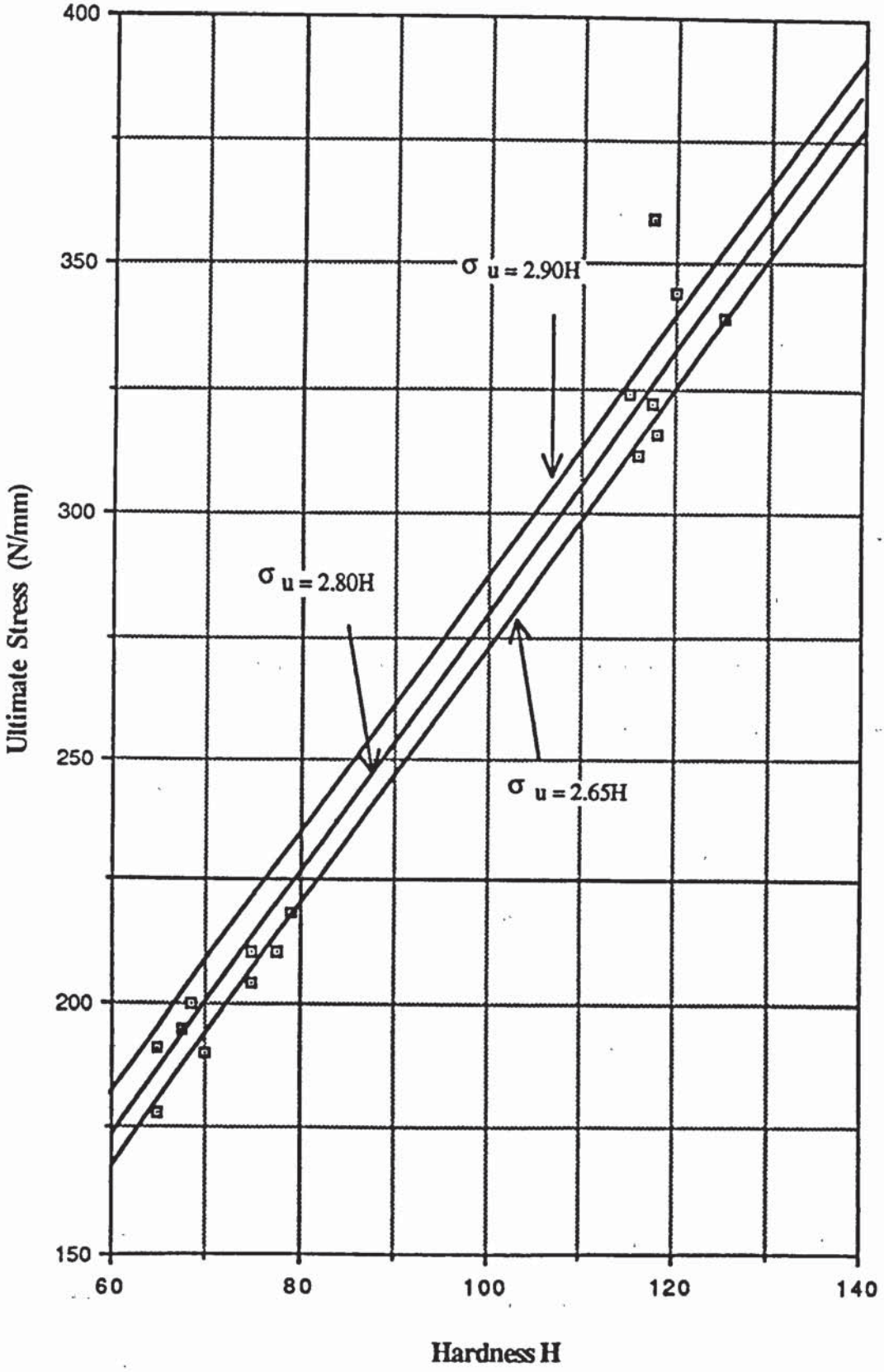

Figure 7.2 Relationship between ultimate strength and hardness for 6082-T6

relationship for UTS to hardness values are based upon a single alloy / filler metal combination.

7.3 Tensile fillet welds.

For tensile fillet welds, the theoretical relationships derived between weld penetration p , and failure load F are shown in table 3.1, chapter 3. These are plotted in graphical form in figures 7.3 to 7.6. In figure 7.3 it is seen that as penetration values increase the weld failure load also increases. The relationship is linear for all values of weld penetration.

The code of practice BS 4870, stipulates that the maximum extent of horizontal weld penetration p, for fillet welds be limited to $p \leq 3mm$, regardless the size of weld laid. Generally this requirement is readily complied with as indicated by Smith and Newman (24,25). They found that under normal standard welding conditions, the average horizontal weld penetration achieved is equal to 0.3 times the weld leg length value. If one considers the average maximum weld size laid by a single pass to be 10mm, then the limit of $p \leq 3mm$ is not violated. Therefore the linear relationship shown in figure 7.3, between load and penetration up to 0.3 times the weld leg length penetration value, suggests a zone up till where acceptable penetration values are achieved. Beyond this value, excessive penetration effects begin to dominate the failure load and penetration relationship.

The graph in figure 7.3 can be used to read off the expected failure load for any tensile fillet weld with a known penetration value or vice versa. Alternatively the general failure equations presented in chapter 3 can be used.

The other important relationship arrived at in chapter 3, for tensile fillet welds is that for the failure plane. It is shown that by achieving weld penetration the weld model is

effectively an unequal leg length weld. The weld failure plane is shown to be dependant upon the extent of penetration achieved. If the extent of penetration is known then the location of the failure plane can be predicted or vice versa, using the equation derived in chapter 3. The relationship is shown graphically in figure 7.4.

The effect of penetration upon the length of the weld failure plane is also shown in figure 7.5. As penetration values increase, then the length of the failure plane also increases. This is as would be expected, since it is found that the weld failure load also increases as discussed earlier. The relationship between the length of failure plane and failure load is shown in figure 7.6.

7.3.1 Comparison of tensile weld failure theories.

Comparisons are made between the author's proposed tensile weld failure theory and those of Kamtekar's [11], Kato and Morita's [12] and the β-formula[14]. For aluminium fillet welded specimens comparisons are also made with the predictions obtained using BS 8118.

The first comparison is made using experimental results obtained by the author on tensile aluminium welded specimens. The experimental results for these tests are given in chapter 5, table 5.6. The predicted results are tabulated in tables 7.1 and the comparisons in table 7.2, of this chapter.

The predicted results using the authors proposed theory and that of Kato and Morita's, give results closest to the experimental results. These are to within ten and four percent respectively, of the experimental values. Kamtekar's theory predicts the failure load to within 34 percent, the β-formula to within 69 percent and BS 8118 to 24 percent.

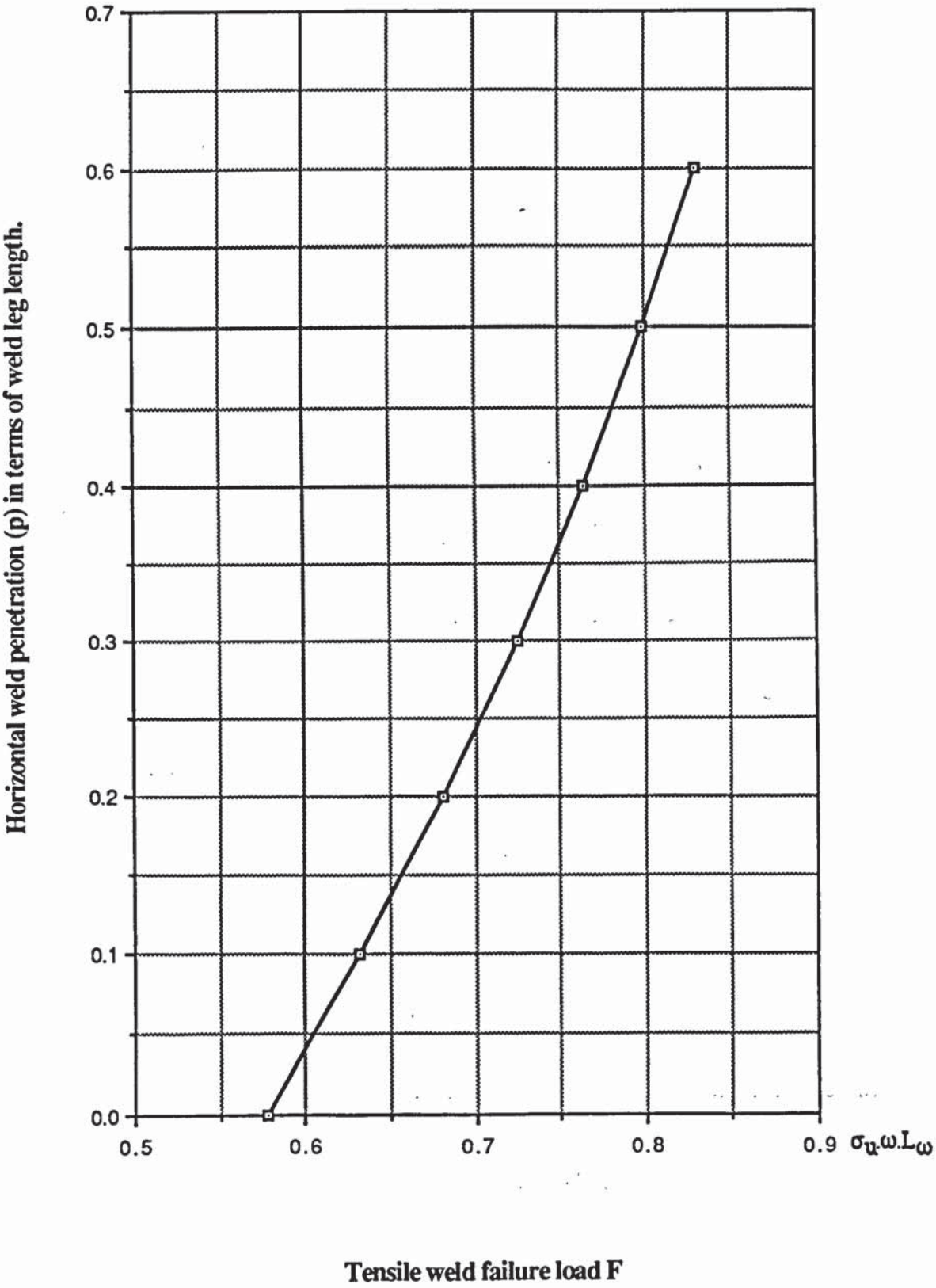

Figure 7.3 Graph of penetration (p) vs tensile fillet weld failure load.

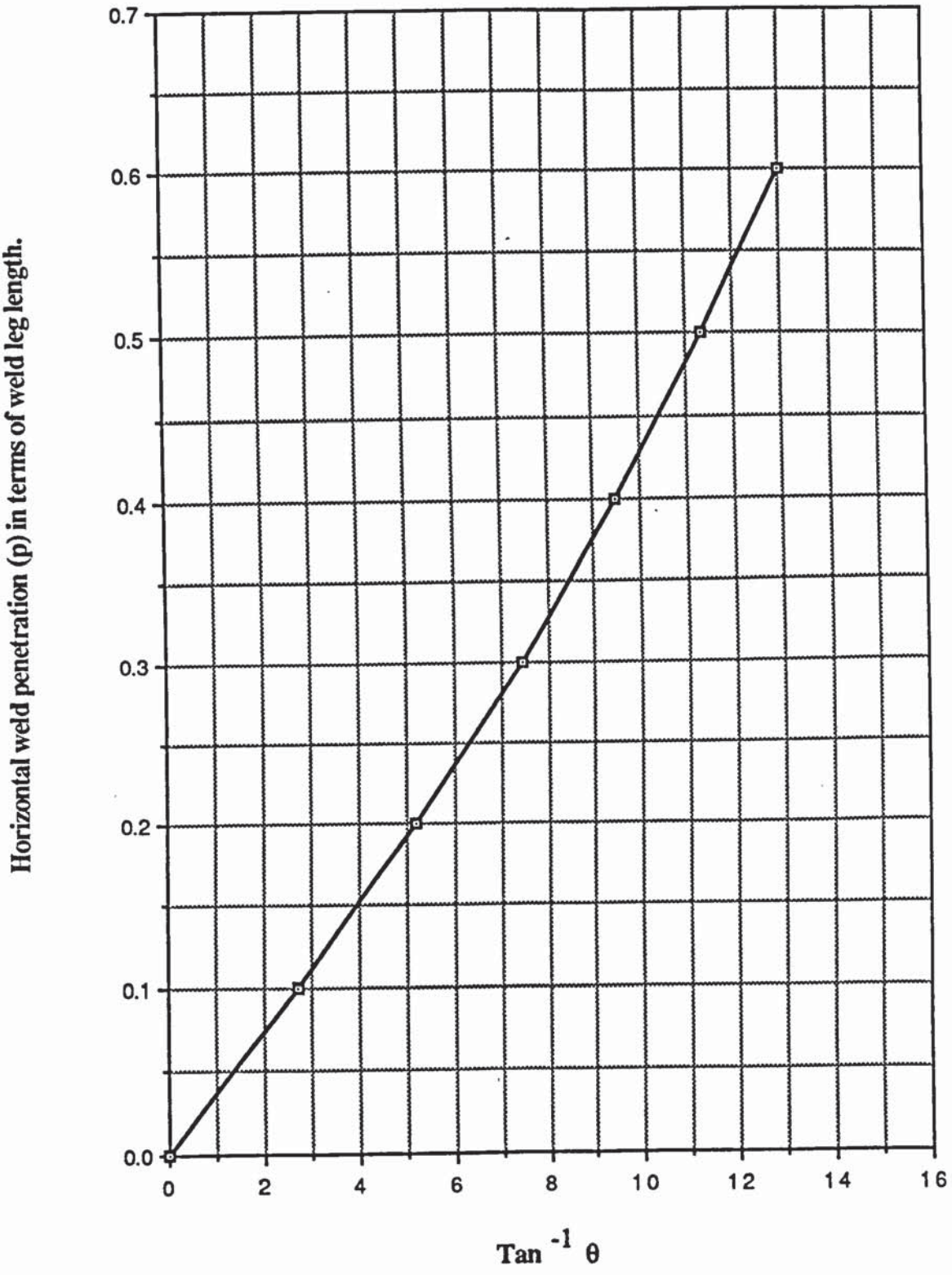

Figure 7.4 Graph of penetration (p) vs Tan $^{-1}$ θ for tensile fillet welds.

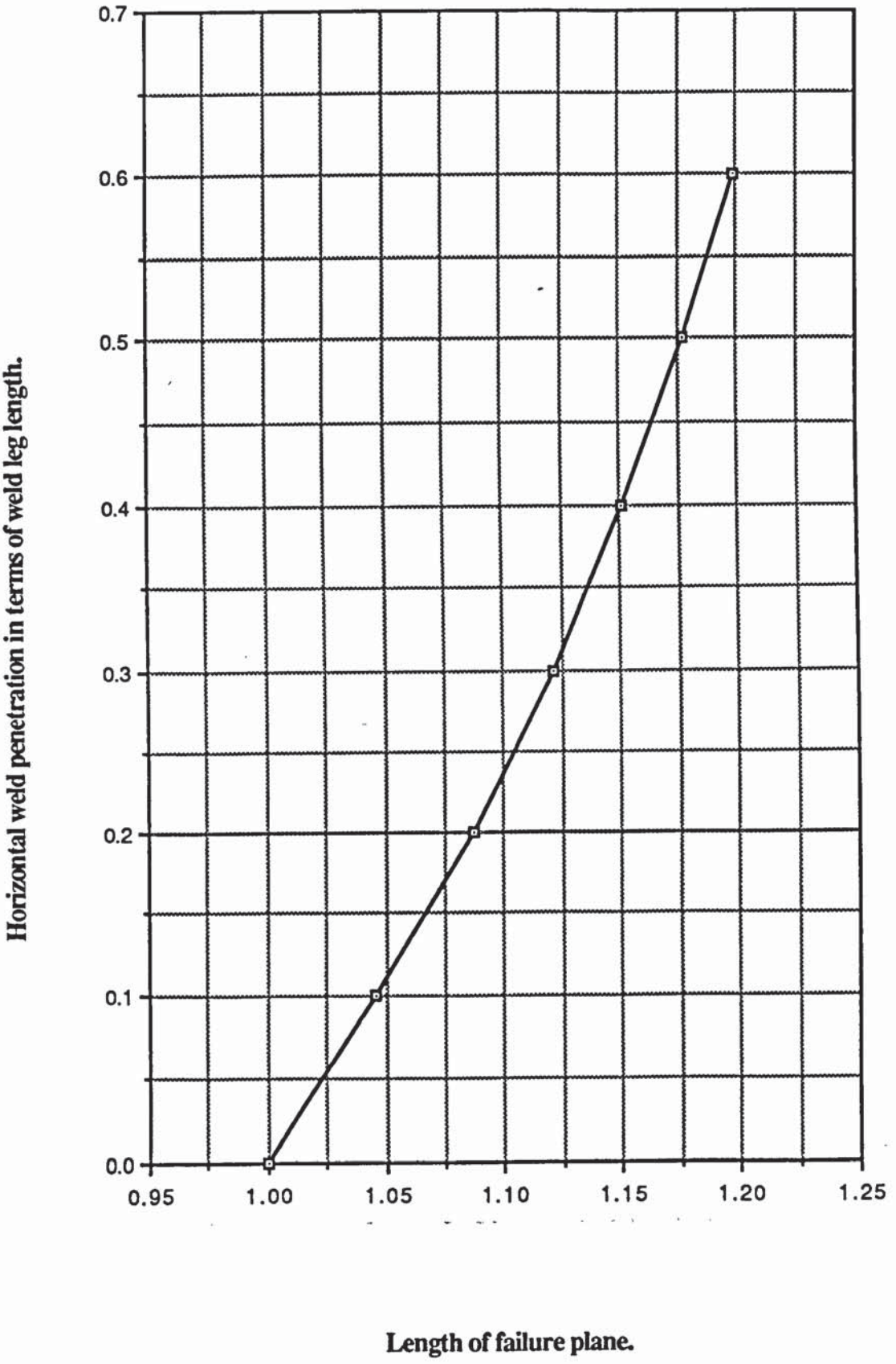

Figure 7.5 Graph of penetration (p) vs length of failure plane for tensile fillet welds.

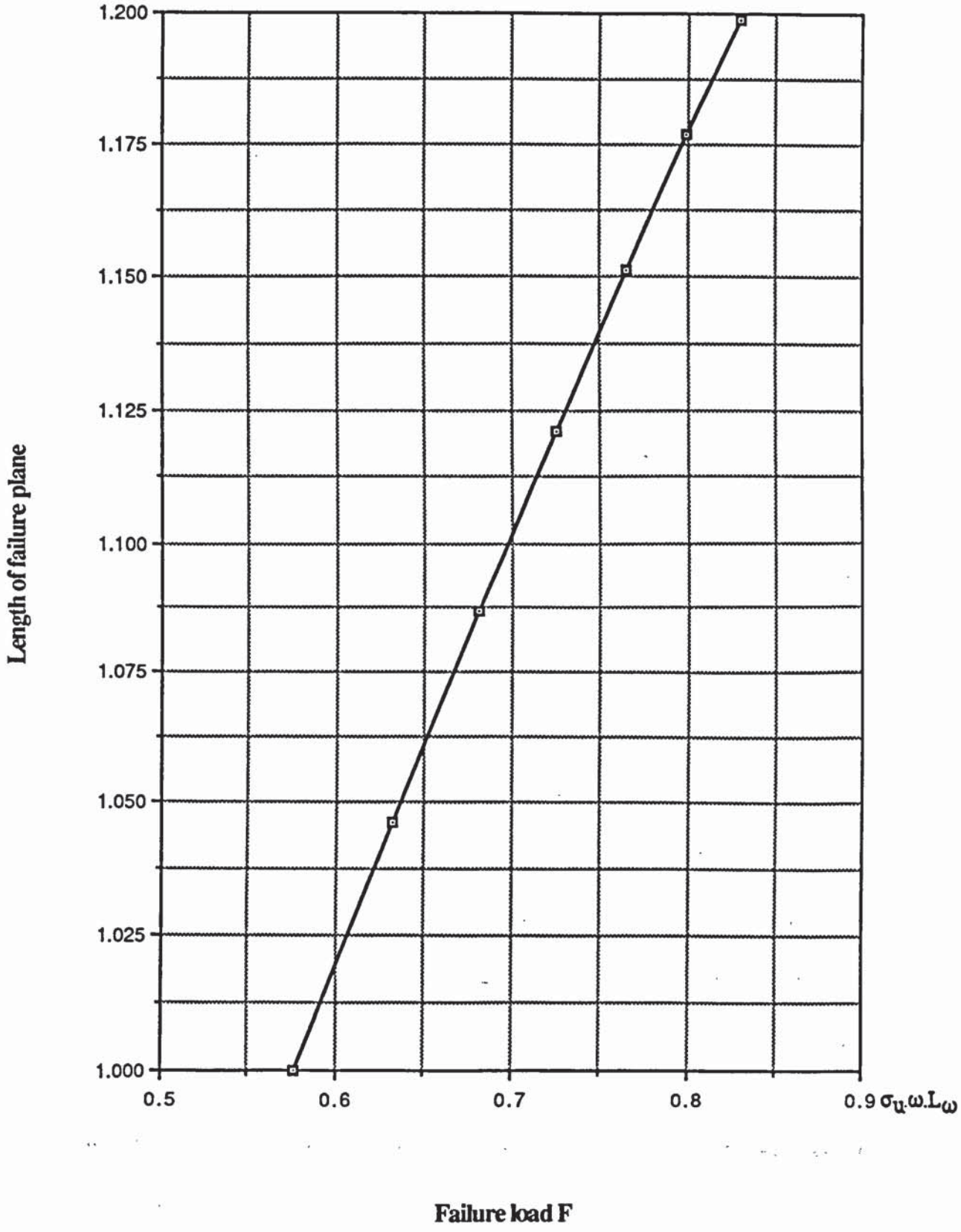

Figure 7.6 Graph of length of failure plane vs tensile failure load.

The other predictions compared are those concerning the weld failure plane angles. From the experimental results on tensile welds - tables 5.8 and 5.12, it is seen that the failure plane angles do change as penetration values alter. With regards to this point, only the author's theory predicts that the location of weld failure planes should change for any changes in weld penetration, as shown in table 7.1 and figures 7.4 and 7.5. Kamtekar's theory predicts two locations of the failure plane - either the vertical (90^0) or the horizontal (0^0) weld leg length.This is only true when there is zero penetration. But it is accepted that fusion must occur beyond the prepared end faces, for all structural welds and therefore penetration must exist at all times. Kato and Morita's theory also predicts a constant failure plane. In this case it is predicted to lie at 22.5^0, measured up from the weld horizontal leg length lying in the direction of applied load. With regards to the β-formula, this does not predict a failure plane but is based upon the assumption that the throat of the weld is always the failure plane in a weld.

In table 7.2, the author's, Kamtekar's, Kato and Morita's predicted and the β-formula and BS 8118 assumed failure planes are compared. It is seen that the author's theory under predicts the location of the failure plane. All the other theories compared, over predict the location of the failure plane. In Kamtekar's only a comparison with the vertical predicted failure plane is conducted.This is because the other failure plane is predicted at 0^0, and division by zero is infinite. When the vertical predicted failure plane is compared, it is found to be an overprediction of the experimental value by 84 percent. Kato and Morita's theory overpredicts by 34 percent and both the β-formula and BS 8118 by 66 percent

Sp. No	Expt. failure load F_u (KN)	Ratio p: ω	Expt. failure angle ϕ_0^0	Author's predicted failure load F_{u1} (KN)	Author's predicted failure angle ϕ_1^0	Kamtekar's predicted failure load F_{u2} (KN)	Kamtekar's predicted failure angle ϕ_2^0	Kato et al predicted failure load F_{u3} (KN)	Kato et al predicted failure angle ϕ_3^0	β Formula predicted failure load F_{u4} (KN)	BS 8118 predicted failure load F_{u5}	Failure angles $\phi_4^0 = \phi_5^0$ *
A1	58.80	0.150	14.05	50.855	3.99	44.654	0 or 90	53.208	22.5	35.156	46.109	45
A2	56.56	0.206	13.01	53.049	5.35	44.761	0 or 90	55.947	22.5	35.241	48.480	45
A3	59.38	0.243	14.20	54.415	6.18	44.817	0 or 90	57.745	22.5	35.284	50.037	45
A4	61.20	0.252	18.38	54.608	6.39	44.723	0 or 90	58.000	22.5	35.211	50.258	45
A5	59.24	0.248	11.87	54.302	6.30	44.583	0 or 90	57.630	22.5	35.101	49.938	45
A6	60.91	0.250	14.60	54.370	6.34	44.583	0 or 90	57.746	22.5	35.101	50.038	45
A7	58.22	0.237	13.32	54.014	6.05	44.657	0 or 90	57.249	22.5	35.158	49.608	45
A8	60.09	0.247	16.51	54.607	6.27	44.862	0 or 90	57.977	22.5	35.319	50.238	45
A9	62.30	0.325	16.31	56.854	7.96	44.619	0 or 90	61.259	22.5	35.128	53.083	45
A10	58.63	0.250	16.96	54.370	6.34	44.583	0 or 90	57.746	22.5	35.101	50.038	45
A11	59.25	0.263	16.37	54.764	6.63	44.547	0 or 90	58.276	22.5	35.072	50.498	45
A12	59.30	0.242	18.47	54.254	6.16	44.712	0 or 90	57.538	22.5	35.202	49.858	45
A13	59.90	0.249	10.52	54.268	6.32	44.527	0 or 90	57.630	22.5	35.056	49.938	45

* ϕ_4^0 and ϕ_5^0 are assumed failure planes by β formula and BS 8118.

Table 7.1 Comparison of author's experimental results on tensile fillet welded aluminium specimen.

Spec. No.	$\frac{F_u}{F_{u1}}$	$\frac{F_u}{F_{u2}}$	$\frac{F_u}{F_{u3}}$	$\frac{F_u}{F_{u4}}$	$\frac{F_u}{F_{u5}}$	$\frac{\phi_0^0}{\phi_1^0}$	$\frac{\phi_0^0}{\phi_2^0}$ *	$\frac{\phi_0^0}{\phi_3^0}$	$\frac{\phi_0^0}{\phi_4^0} = \frac{\phi_0^0}{\phi_5^0}$
A1	1.156	1.317	1.105	1.673	1.275	3.521	0.156	0.624	0.312
A2	1.066	1.264	1.011	1.605	1.667	2.431	0.145	0.578	0.289
A3	1.091	1.325	1.028	1.683	1.187	2.300	0.158	0.631	0.316
A4	1.121	1.368	1.055	1.738	1.218	2.876	0.204	0.817	0.408
A5	1.091	1.329	1.028	1.688	1.186	1.884	0.132	0.528	0.264
A6	1.120	1.366	1.055	1.735	1.217	2.303	0.162	0.649	0.324
A7	1.078	1.304	1.017	1.656	1.174	2.202	0.148	0.592	0.296
A8	1.100	1.340	1.036	1.701	1.196	2.633	0.183	0.734	0.367
A9	1.096	1.396	1.017	1.774	1.174	2.049	0.181	0.725	0.362
A10	1.078	1.315	1.015	1.670	1.172	2.675	0.188	0.754	0.377
A11	1.082	1.330	1.017	1.689	1.173	2.469	0.182	0.728	0.364
A12	1.093	1.326	1.031	1.685	1.189	2.998	0.205	0.821	0.410
A13	1.104	1.345	1.039	1.709	1.200	1.665	0.117	0.468	0.234
MEAN	1.098	1.333	1.035	1.693	1.233	2.462	0.166	0.665	0.333
σ_{n-1}	0.024	0.033	0.025	0.042	0.133	0.493	0.027	0.109	0.054

* Comparison for 90^0 predicted plane only.

Table 7.2 Comparison between predicted results and author's experimental tensile fillet weld results.

A second comparison between the author's proposed theory and Kamtekar's, Kato and Morita's theories and the β-formula, is made using the test results of Higgs [15]. These results were obtained by Higgs on tensile lap welded steel specimen and the results are shown in table 7.3. Unfortunately, Higgs has not recorded the extent of penetration achieved in these specimen, but the failure angles and failure loads were recorded. For these tests, the author has assumed a constant value of penetration p = 0.3.Leg Length (ω) to exist for all welds. This value is chosen to represent an average value achieved for standard welding conditions, as found and suggested by Smith [24,25].

Higg's specimen number	Measured leg length ω (mm)	Measured weld length L_ω (mm)	Test failure load F_u (KN)	Measured failure angle ϕ^0_0
T1	4.0	32.00	108	15.50
T3	4.0	32.50	110	14.50
T7	4.0	33.70	99	17.25
T9	4.0	33.50	106	18.50
T11	4.0	33.50	108	22.25
T13	4.0	35.00	82	31.00
T14	4.0	17.30	51	17.50
T15	4.0	14.00	47	19.00
T16	4.0	14.20	51	22.50

Table 7.3 Higgs[15] experimental transverse fillet welded specimen results.

Higgs Spec. No.	Author's predicted failure load F_{u1} (KN)	Author's predicted failure angle ϕ_1^0	Kamtekar's predicted failure load F_{u2} (KN)	Kamtekar's predicted failure angle ϕ_2^0	Kato et al predicted failure load F_{u3} (KN)	Kato et al predicted failure angle ϕ_3^0	β Formula predicted failure load F_{u4} (KN)	β Formula failure angle ϕ_4^0
T1	96.57	7.43	76.86	0 or 90	103.53	22.50	78.31	45
T3	98.08	7.43	78.06	0 or 90	105.15	22.50	79.53	45
T7	101.70	7.43	80.94	0 or 90	109.03	22.50	82.47	45
T9	101.10	7.43	80.46	0 or 90	108.38	22.50	81.98	45
T11	101.10	7.43	80.46	0 or 90	108.38	22.50	81.98	45
T13	105.62	7.43	84.06	0 or 90	113.24	22.50	85.65	45
T14	52.21	7.43	41.55	0 or 90	55.97	22.50	42.33	45
T15	42.25	7.43	33.63	0 or 90	45.29	22.50	34.26	45
T16	42.85	7.43	34.11	0 or 90	45.94	22.50	37.75	45

Notes: 1) Assumed weld penetration throughout = 0.3 . Leg Length

2) $\sigma_{u\ weld} = 520\ N/mm^2$

3) Taken $\beta = 0.85$

Table 7.4 Predicted failure loads and planes for Higg's transverse welded specimens.

Higg's Spec. No.	$\frac{F_u}{F_{u1}}$	$\frac{F_u}{F_{u2}}$	$\frac{F_u}{F_{u3}}$	$\frac{F_u}{F_{u4}}$	$\frac{\phi_0^0}{\phi_1^0}$	$\frac{\phi_0^0}{\phi_2^0}$ *	$\frac{\phi_0^0}{\phi_3^0}$	$\frac{\phi_0^0}{\phi_4^0}$
T1	1.118	1.405	1.043	1.379	2.086	0.172	0.689	0.344
T3	1.122	1.409	1.046	1.383	1.952	0.161	0.644	0.322
T7	0.973	1.223	0.908	1.200	2.322	0.192	0.767	0.383
T9	1.048	1.317	0.978	1.293	2.490	0.206	0.822	0.411
T11	1.068	1.342	0.997	1.317	2.995	0.247	0.989	0.494
T13	0.776	0.975	0.724	0.957	4.172	0.344	1.378	0.689
T14	0.977	1.227	0.911	1.205	2.355	0.194	0.778	0.389
T15	1.112	1.400	1.038	1.372	2.557	0.211	0.844	0.422
T16	1.190	1.495	1.110	1.351	3.028	0.250	1.000	0.500
MEAN	1.043	1.310	0.973	1.273	2.663	0.220	0.879	0.439
σ_{n-1}	0.122	0.154	0.114	0.138	0.673	0.055	0.222	0.111

* Comparison for 90^0 predicted plane only.

Table 7.5 Comparison between predicted results and Higg's experimental results.

The comparison shows that the nearest prediction of the failure load is obtained by Kato and Morita's theory. This is very closely followed by the author's own theoretical prediction. Kato and Morita's theory slightly over predicts the experimental failure load by three percent, while the author's slightly under predicts by four percent. However, these results must be viewed in light of the average penetration assumed for all specimens. In practise a constant penetration value is not going to exist throughout. Further, the assumed penetration value is based upon average welding conditions. No information is given by Higgs as to whether he achieved these conditions.

Also found is that Kamtekar's theory underestimates the failure load by 31 percent and the β-formula by 27 percent. The point to note here is that neither of these methods takes penetration into consideration. This would explain why such a marked difference exists between these predicted failure loads and those predicted using the author's or Kato and Morita's theories.

With regards to predicting the location of the failure plane, the results obtained using the author's proposed theory, are based upon the initial assumed extent of penetration 0.3ω. Since the actual values are not available, these results can only be taken as indicatively to those predicted by the other theories.

For the assumed constant penetration value of 0.3.Leg Length (ω), the author's theory predicts a constant failure plane, to within seven degrees of the experimental recorded values. The other theories by Kamtekar, Kato and Morita and the β-formula, overpredict the location by 88, 12 and 57 percent respectively. However, it must be noted that since Kamtekar's theory predicts two constant failure planes - the horizontal (0^0), or the vertical (90^0) weld leg length - only the vertical predicted plane can be

compared in ratio terms. This is because division by zero is infinity. Nevertheless, even if a difference between the horizontal predicted failure plane and the actual experimental value is estimated, it is seen that this then underestimates the location of the failure by an average of 20^0.

For Higg's test specimens, it might seem that Kato and Morita's constant failure plane prediction is the best, since it is the closest to the experimental measured values. However, the author's predictions also lie very close to these experimental results, but are hampered from predicting even better results due to the unknown actual penetration values achieved by Higgs.

A third comparison between the author's, Kamtekar's, Kato and Morita's theories and the β-formula is conducted. In this case the experimental results obtained by Kato and Morita on steel fillet welded tensile specimens are used. Kato and Morita have taken care to record the extent of penetration achieved in each welded specimen. Also the weld profile, length and failure load have been recorded and are reproduced in table 7.6. However, the angle of the failure plane has not been recorded. Nevertheless, a comparison is conducted using these results, concentrating on the failure loads predicted. The predictions are derived in table 7.7 and their comparisons in table 7.8.

Kato et al's specimen number	Measured leg length ω (mm)	Measured weld length L_ω (mm)	Horz. measured penetration p (mm)	Ratio p : ω	σ_u weld N/mm^2	Expt. failure load F_u (KN)
$S_1$5B	4.936	40	1.060	0.215	588	206.0
$S_1$5R	4.950	40	0.806	0.163	575	153.5
$S_1$10B	10.154	40	0.863	0.085	600	347.0
$S_1$15B	15.302	40	0.792	0.052	595	518.5
$S_1$15R	15.104	40	0.297	0.020	553	461.5
$S_1$20B	19.997	40	1.358	0.068	607	675.0
$S_1$30B	29.996	40	0.551	0.018	607	888.0
$S_1$40B	40.036	40	1.188	0.030	607	1232.0
$S_1$40R	35.228	40	0.226	0.006	557	935.0

Table 7.6 Kato and Morita's experimental transverse fillet welded specimen results.

Kato et al's Spec. No.	Author's predicted failure load F_{u1} (KN)	Author's predicted failure angle ϕ_1^0	Kamtekar's predicted failure load F_{u2} (KN)	Kamtekar's predicted failure angle ϕ_2^0	Kato et al predicted failure load F_{u3} (KN)	Kato et al predicted failure angle ϕ_3^0	β Formula predicted failure load F_{u4} (KN)	β Formula failure angle ϕ_4^0
$S_1$5B	159.84	5.54	134.06	0 or 90	160.00	22.5	136.58	45
$S_1$5R	151.16	4.31	131.46	0 or 90	151.90	22.5	133.94	45
$S_1$10B	304.30	2.33	281.40	0 or 90	309.10	22.5	286.70	45
$S_1$15B	441.83	1.45	420.53	0 or 90	451.69	22.5	428.46	45
$S_1$15R	393.42	0.57	385.79	0 or 90	392.11	22.5	393.06	45
$S_1$20B	597.47	1.88	560.64	0 or 90	608.82	22.5	571.21	45
$S_1$30B	855.97	0.51	840.97	0 or 90	882.72	22.5	856.83	45
$S_1$40B	1155.62	0.85	1122.45	0 or 90	1187.48	22.5	1143.62	45
$S_1$40R	911.72	0.17	906.30	0 or 90	943.36	22.5	923.39	45

Table 7.7 Comparison of Kato and Morita's transverse welded specimen results.

Kato et al's specimen number	$\frac{F_u}{F_{u1}}$	$\frac{F_u}{F_{u2}}$	$\frac{F_u}{F_{u3}}$	$\frac{F_u}{F_{u4}}$
$S_1$5B	1.129	1.537	1.288	1.508
$S_1$5R	1.015	1.168	1.011	1.146
$S_1$10B	1.140	1.233	1.126	1.210
$S_1$15B	1.174	1.233	1.148	1.210
$S_1$15R	1.173	1.196	1.177	1.174
$S_1$20B	1.130	1.204	1.109	1.182
$S_1$30B	1.037	1.056	1.006	1.036
$S_1$40B	1.066	1.098	1.038	1.077
$S_1$40R	1.026	1.032	0.991	1.013
MEAN	1.098	1.195	1.099	1.173
σ_{n-1}	0.063	0.140	0.098	0.146

Table 7.8 Comparison between predicted weld failure loads for Kato and Morita's transverse weld specimens.

Examining the predicted failure loads, reveals that the author's, Kamtekar's and Kato and Morita's theories and the β-formula predict the failure load to within approximately ten, twenty, ten, and eighteen percent, respectively. Generally it is seen that where the extent of penetration achieved is very small, the predicted results by all theories being compared are fairly close. However, where penetration values are significant then the author's and Kato and Morita's theories predict the best failure load results.

Also, the only significant variation to be expected when weld penetration is significant is the prediction of the failure plane. Unfortunately, since Kato and Morita have failed to record the experimental failure plane, a comparison cannot be made with any observed values. Theoretically, the author's theory predicts a varying failure plane as the penetration values change. These predictions generally lie close to the horizontal weld leg length, between 0.17^0 and 5.54^0, table 7.7. This prediction would also confirm and explain the observations made by other authors and especially Higgins and Preece[28]. They observed that for tensile fillet welds of equal leg lengths, the failure plane lies close to the weld leg length lying in the direction of the applied load. With this in mind, it would be expected Kamtekar's prediction of 0^0 i.e. the horizontal leg length, would be the comparable predicted failure plane. Kato and Morita's theory predicts the failure plane to be constantly at 22.5^0 from the horizontal weld leg length, while the β-formula assumes the weld throat as the failure plane at all times.

A final and fourth comparison is conducted using the experimental results obtained by Soetens[6,14] on aluminium fillet welded tensile specimens. His results are shown in table 7.9.

Sp. No.	Filler metal	Alloy	Average penet. p (mm)	Horz. penet. p.Cos45 (mm)	Average throat t (mm)	Average leg length ω (mm)	Ratio p.Cos45 : ω	σ_u weld N/mm^2	Average weld length L_w (mm)	Expt. failure load F_u (KN)	Expt. failure angle ϕ^0
1	4043	6082	1.6	1.31	5.5	7.778	0.168	212	50.62	108.20	27.5
2	4043	6063	2.1	1.485	5.5	7.778	0.191	175	50.84	98.44	25.0
3	4043	7020	4.0	2.828	5.8	8.202	0.345	235	50.62	132.00	37.5
4	5356	5083	2.0	1.414	5.9	8.344	0.170	264	50.64	146.16	30.0
5	5356	6063	2.3	1.626	5.5	7.778	0.209	196	50.20	109.74	30.0
6	5356	6082	2.6	1.839	5.5	7.778	0.236	233	50.76	109.44	25.0
7	5356	7020	2.3	1.626	6.5	9.192	0.177	276	50.30	142.22	27.5
Additional tests											
8	4043	6082	4.6	3.253	5.6	7.920	0.411	212	51.00	130.14	32.5
9	5356	5083	2.4	1.697	5.5	7.778	0.218	264	50.76	154.38	27.5
10	5356	6082	2.1	1.485	5.5	7.778	0.191	233	50.44	111.54	27.5
11	5356	7020	2.5	1.768	6.3	8.910	0.198	276	49.89	153.82	29.0

Table 7.9 Soeten's average experimental results for aluminium transverse fillet welded specimens.

Soetens Spec. No.	Author's predicted failure load F_{u1} (KN)	Author's predicted failure angle ϕ_1^0	Kamtekar's predicted failure load F_{u2} (KN)	Kamtekar's predicted failure angle ϕ_2^0	Kato et al predicted failure load F_{u3} (KN)	Kato et al predicted failure angle ϕ_3^0	β Formula predicted failure load F_{u4} (KN)	BS 8118 predicted failure load F_{u5} (KN)	Failure angles $\phi_4^0 = \phi_5^0$
1	111.23	4.43	96.38	0 or 90	116.69	22.5	97.96	100.32	45
2	93.73	4.98	79.91	0 or 90	98.61	22.5	95.63	76.97	45
3	145.11	8.37	112.66	0 or 90	157.00	22.5	157.02	166.68	45
4	148.87	4.48	128.81	0 or 90	156.09	22.5	142.25	122.90	45
5	104.94	5.41	88.37	0 or 90	110.71	22.5	103.37	93.04	45
6	128.40	6.03	106.22	0 or 90	136.09	22.5	117.81	104.60	45
7	171.16	4.65	147.35	0 or 90	179.70	22.5	157.07	180.60	45
8	131.64	9.67	98.88	0 or 90	144.53	22.5	141.78	134.84	45
9	143.79	5.61	120.36	0 or 90	151.92	22.5	142.59	123.19	45
10	123.82	4.98	105.55	0 or 90	130.26	22.5	109.84	97.52	45
11	166.99	5.15	141.67	0 or 90	175.92	22.5	155.79	179.13	45

Table 7.10 An indicative prediction for Soeten's transverse fillet welded aluminium specimens.

Soetens Spec. No.	$\frac{F_u}{F_{u1}}$	$\frac{F_u}{F_{u2}}$	$\frac{F_u}{F_{u3}}$	$\frac{F_u}{F_{u4}}$	$\frac{F_u}{F_{u5}}$	$\frac{\phi_0^0}{\phi_1^0}$	$\frac{\phi_0^0}{\phi_2^0}$ *	$\frac{\phi_0^0}{\phi_3^0}$	$\frac{\phi_0^0}{\phi_4^0} = \frac{\phi_0^0}{\phi_5^0}$ **
1	0.973	1.123	0.927	1.562	1.079	6.208	0.306	1.222	0.611
2	1.050	1.232	0.998	1.456	1.279	5.020	0.277	1.111	0.556
3	0.910	1.172	0.841	1.189	0.792	4.480	0.417	1.667	0.833
4	0.982	1.135	0.936	1.453	1.189	6.696	0.333	1.333	0.666
5	1.046	1.242	0.991	1.501	1.180	5.545	0.333	1.333	0.666
6	0.852	1.030	0.804	1.314	1.046	4.146	0.278	1.111	0.556
7	0.831	0.965	0.791	1.281	0.788	5.914	0.306	1.222	0.611
8	0.989	1.316	0.900	1.298	0.965	3.361	0.361	1.444	0.722
9	1.074	1.283	1.016	1.531	1.253	4.902	0.306	1.222	0.611
10	0.900	1.057	0.856	1.436	1.144	5.522	0.306	1.222	0.611
11	0.921	1.086	0.874	1.396	0.859	5.631	0.322	1.289	0.644
MEAN	0.957	1.149	0.903	1.402	1.052	5.220	0.322	1.289	0.644
σ_{n-1}	0.081	0.111	0.078	0.117	0.178	0.964	0.040	0.159	0.079

* Comparison for 90^0 predicted plane only.
** Same assumed failure plane by β Formula and BS 8118

Table 7.11 Comparison of predicted failure results using Soeten's experimental data.

In this case, although Soetens has measured the weld penetration and failure angles for his test specimens, only averaged values are given for each chosen filler metal, alloy combination specimen. No readings are given for individual test specimens. Further, no readings are given of the size of weld leg lengths achieved - only averaged throat values are recorded. Also, no indications are given as to whether the weld profiles were machined down or not. The weld leg lengths given in table 7.9, have been calculated by the author based upon the average throat values. It would therefore be expected that using these average values in the failure theories being compared, will lead to approximate predictions. Thus the results and comparisons made in tables 7.10 and 7.11 are only to be taken as a general indication of the accuracy achievable by each theory.

Bearing the above mentioned in mind, it is seen that all the failure theories predict comparable failure loads.However, it should be noted that although the β-formula and BS 8118 predict safe failure loads, they are nevertheless excessively conservative.

Comparing the predicted failure plane angles to Soetens measured values , shown in tables 7.10 and 7.11, the authors proposed theory underpredicts these measured failure angles. The same is true of Kato and Morita's constant predicted failure plane angle of 22.5^0, but to a lesser extent. The inaccuracy of the author's theoretical predictions can be attributed to the fact that only average values of weld penetration were available, to predict the failure angles. Also, the failure angles measured by Soetens might require re-adjustment, if they were not measured from the tip of the horizontal penetration. No indications are given by Soetens as to from which point he measured the reported failure angle values.

Kamtekar'e theory predicts the vertical and horizontal weld leg lengths as the failure planes. Comparing these to Soetens measured failure angle values, shows the former to be an over prediction while the latter an under prediction. Basically, neither the vertical or the horizontal leg lengths coincide with the failure planes measured.

The β-formula and BS 8118's assumed failure plane of the weld throat is also seen to be an over cautious assumption, when compared to Soetens experimental results.

From the overall comparisons made between the different tensile weld failure theories, it is found that the author's proposed theory predicts results very close to experimental findings. This theory not only accurately predicts the failure loads of the welds but also closely predicts the location of the failure plane. These results are achieved only by using the author's theory because weld penetration is directly accounted for in the weld model and failure analysis.

Only Kato and Morita's theory, which indirectly accounts for weld penetration by modifying the weld throat, predicts failure loads close to the authors. However, due to its over simplified approach the corresponding weld failure plane prediction remains crude i.e. failure is expected to always occur along a fixed plane at 22.5^0 from the horizontal weld leg length.

Using Kamtekar's theory generally under predicts weld failure loads quite significantly - at times by up to 33 percent, seen in table 7.2. Further, this theory always predicts two weld failure planes - the vertical and horizontal leg lengths. Kamtekar acknowledges this ambiguity by suggesting that the horizontal weld leg length must be taken as the correct

failure plane since Higgins and Preece's [28] findings and others show the failure plane to lie close to this leg length.

In Kamtekar's published paper [11] on his theory, he compares his theoretical predictions to Kato and Morita's experimental test results using their experimental data, which are shown in table 7.6. For the failure load predictions he uses Kato and Morita's modified weld leg length values which indirectly account for the extent of weld penetration achieved.This is seen to be incorrect by the author since Kamtekar's theory totally ignores weld penetrations at all times. Consequently the predicted results he compares suggest a closer prediction to experimental values than would be achieved when using his theory. The author has shown in table 7.7 what Kamtekar's theory predicts when using the unmodified leg length values in Kato and Morita's experimental tests. The results indicate under prediction of the weld failure loads by approximately 20 percent.

7.4 Shear fillet welds.

From the author's proposed theory on shear fillet welds, derived in chapter 3, it was shown that increases in weld penetration, increased the failure loads. This was also shown in table 3.3 and the derived relationship is given below;

$$F = \frac{(1 + p)\,\sigma_u L_\omega \omega}{\sqrt{6}} \qquad \text{Equation 7.6}$$

where p = ratio of horizontal penetration to weld leg length.

This equation is plotted in figure 7.7. It is observed that unlike for tensile welds, the shear failure load is linearly dependant upon the extent of penetration.

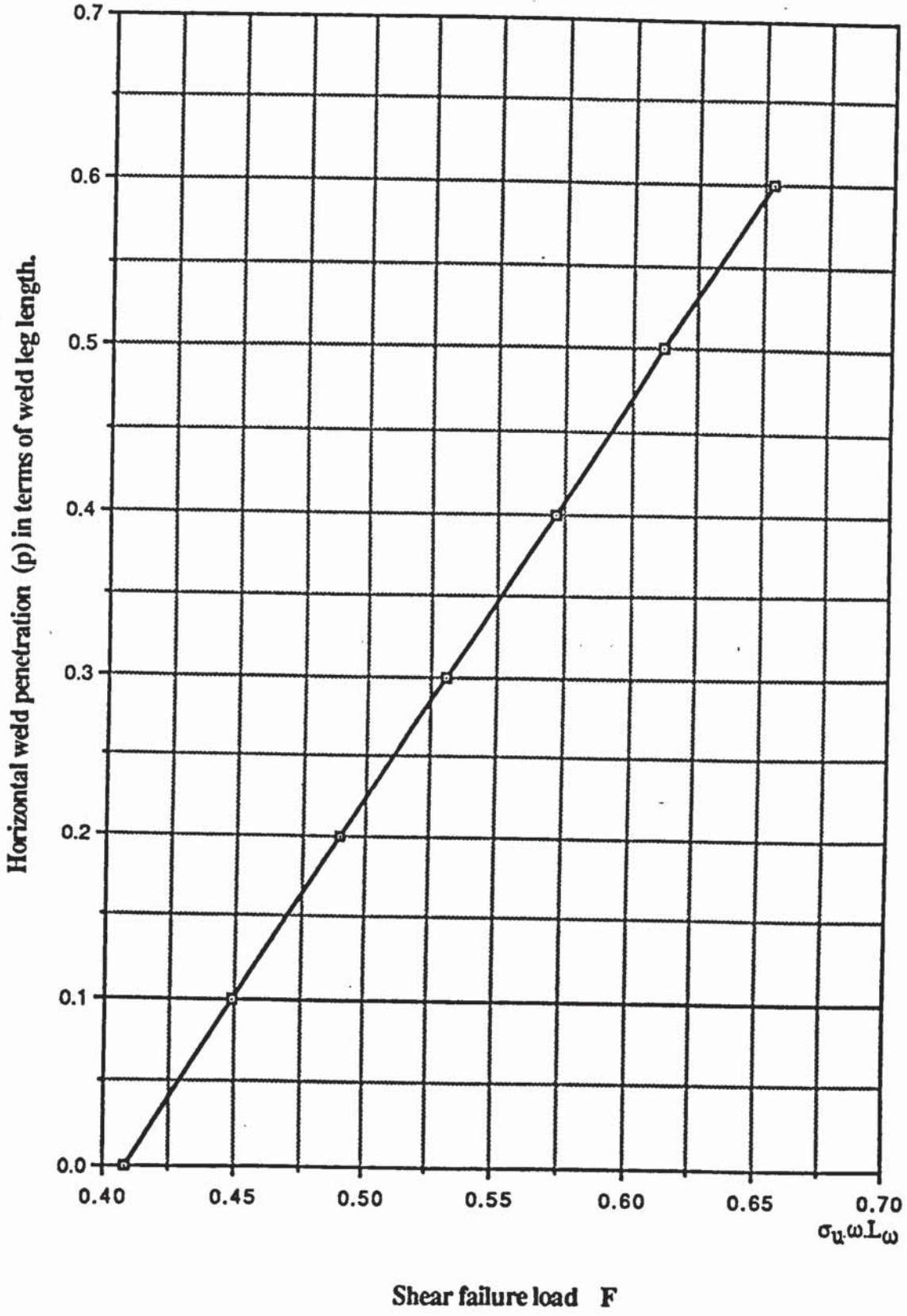

Figure 7.7 Graph of penetration (p) vs shear weld failure load.

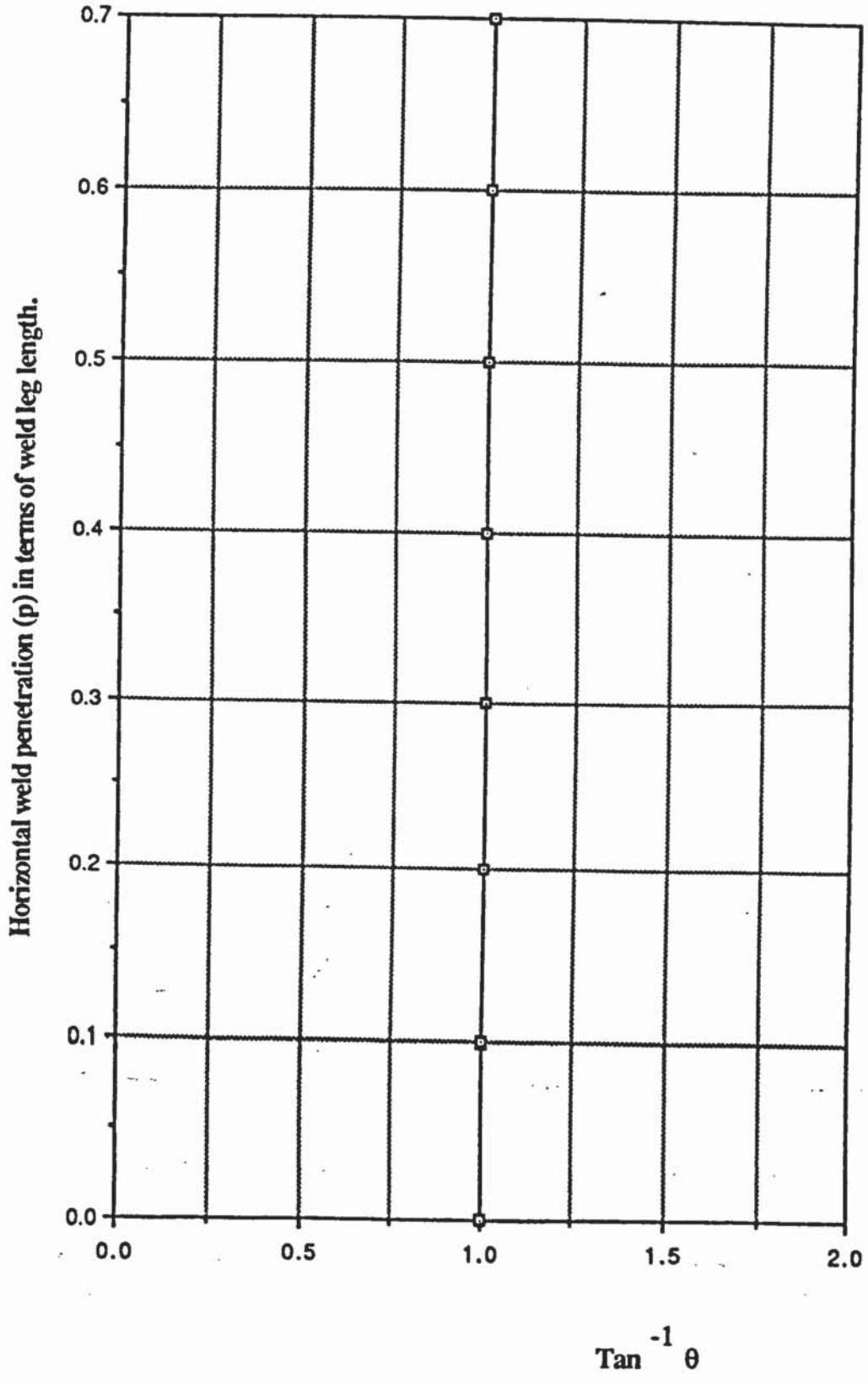

Figure 7.8 Graph of horizontal weld penetration (p) vs Tan^{-1} θ for shear fillet welds.

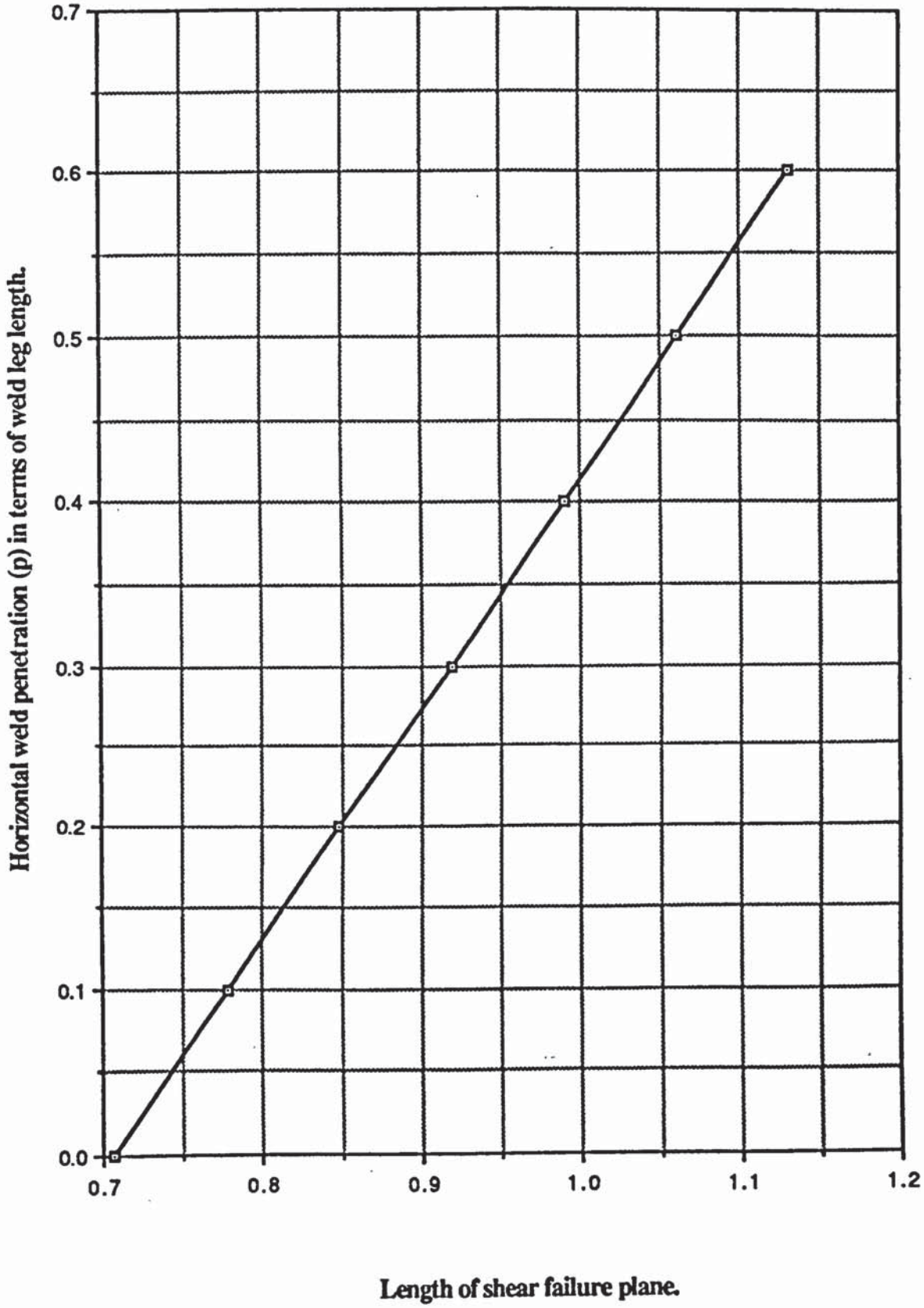

Figure 7.9 Graph of penetration (p) vs length of shear failure plane.

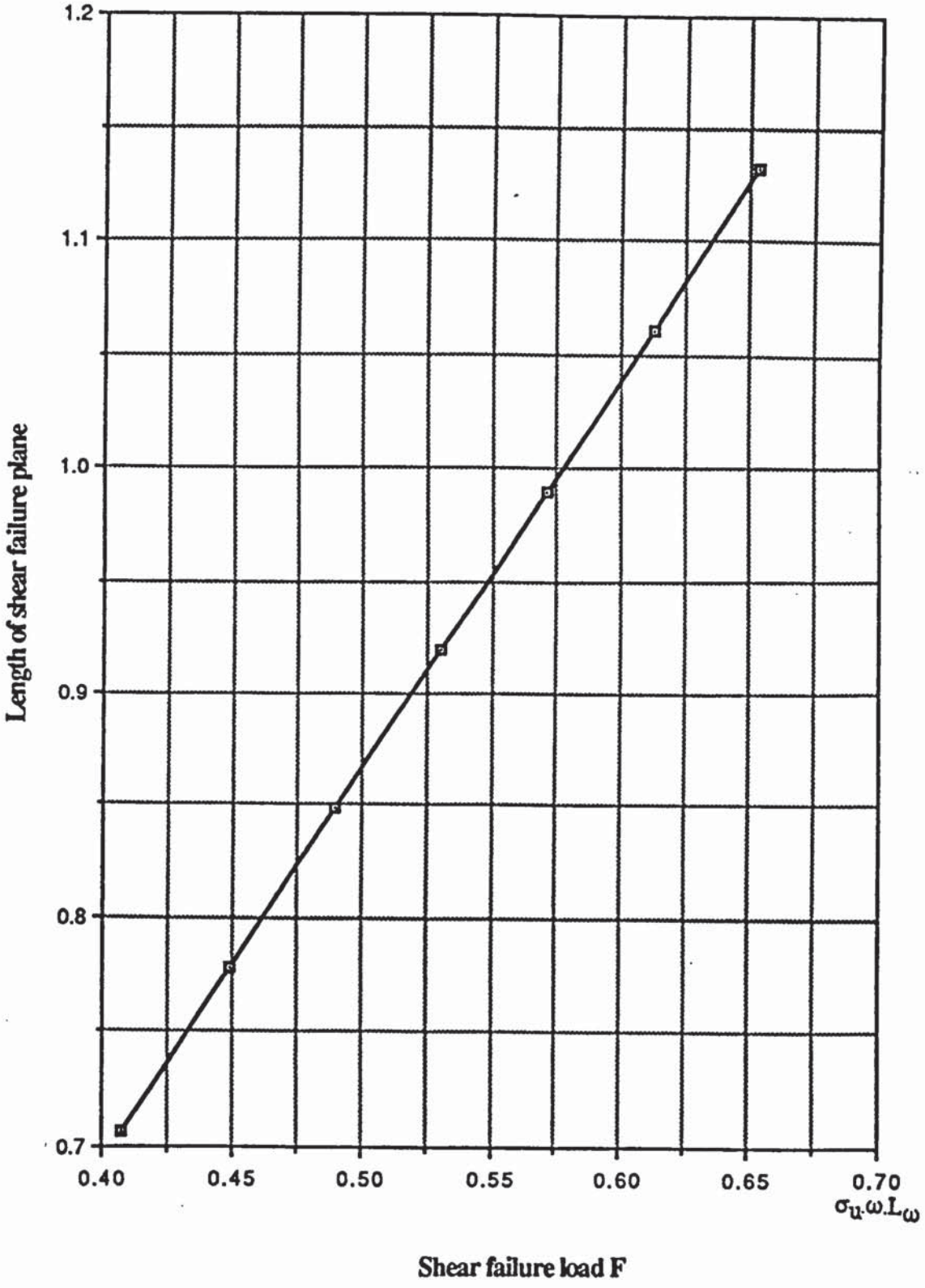

Figure7.10Graph of length of shear failure plane vs failure load

In the same table 3.3, the location of the failure plane in shear fillet welds, is seen to always be at 45^0 from the horizontal leg length, even though penetration values increase. This relationship is also shown graphically in figure 7.8. This result indicates that the failure plane assumptions made by the β-formula and BS 8118 are more realistic for shear fillet welds than for tensile fillet welds.

These theoretical findings also indicate that shear fillet welds are not as sensitive to changes in penetration values, as are tensile fillet welds. This result also verifies Kamtekar's finding, that any small changes in the weld cross sectional area effects tensile fillet welds more acutely than shear fillet welds. Also from figure 7.7 it is seen that unlike for tensile fillet welds, excessive weld penetration has no effects upon the weld failure load. This finding would suggest that excessive weld penetration is a problem related only to welds in tension.

7.4.1 Comparison of shear weld failure theories.

Theoretical predictions made by the author's, Kamtekar's, Kato and Morita's theories the β-formula and BS 8118, for the failure of shear fillet welds, are compared. For this, the experimental results from the author's, Kato and Morita's (12) and Soetens (6,14,) test programmes are used. No comparisons were possible from Higg's experimental programme, since no tests were done by him on shear fillet welds.

The first comparison made uses the experimental results obtained by the author. These results are for aluminium welded shear connections, and are given in table 5.11, chapter 5. The predictions of weld failure loads and planes are given in tables 7.12 and their comparisons in table 7.13.

Sp. No	Expt. failure load F_u (KN)	Ratio p: ω	Expt. failure angle ϕ_0^0	Author's predicted failure formula	Author's predicted failure load F_{u1} (KN)	Kamtekar's predicted failure load F_{u2} (KN)	Kato et al predicted failure load F_{u3} (KN)	β formula predicted failure load F_{u4} (KN)	BS 8118 predicted failure load F_{u5} (KN)	Failure angles * $\phi_1^0, \phi_2^0, \phi_3^0, \phi_4^0, \phi_5^0$
S1	44.10	0.156	42.52	1.88 UTL	43.74	37.82	43.74	34.391	35.706	45
S2	46.95	0.164	39.76	1.90 UTL	44.07	37.87	44.07	34.434	35.975	45
S3	45.30	0.150	42.39	1.87 UTL	43.55	37.87	43.55	34.434	35.551	45
S4	45.64	0.156	42.94	1.88 UTL	43.80	37.87	43.80	34.437	35.755	45
S5	47.50	0.152	46.23	1.88 UTL	44.24	38.40	44.24	34.914	36.111	45
S6	47.54	0.169	43.21	1.90 UTL	44.33	37.92	44.33	34.483	36.187	45
S7	50.35	0.243	42.80	2.03 UTL	47.24	37.99	47.24	34.546	38.563	45
S8	47.92	0.249	44.19	2.03 UTL	47.24	37.82	47.24	34.391	38.563	45
S9	46.65	0.222	46.73	1.99 UTL	46.33	37.89	46.33	34.457	37.817	45
S10	48.64	0.251	38.28	2.04 UTL	47.34	37.82	47.34	34.391	38.640	45
S11	50.42	0.243	41.97	2.03 UTL	47.15	37.90	47.15	34.460	38.485	45
S12	48.10	0.247	40.29	2.03 UTL	47.24	37.87	47.24	34.434	38.563	45
S13	47.93	0.250	44.13	2.04 UTL	47.29	37.82	47.29	34.391	38.601	45

UTL = Ultimate Tensile Load = $\sigma_u \omega L_\omega$

* Failure angles $\phi_1^0, \phi_2^0, \phi_3^0, \phi_4^0, \phi_5^0$, predicted by Author, Kamtekar, Kato and Morita, the β formula and BS 8118 respectively.

Table 7.12 Prediction of shear failure loads and angles using the author's longitudinal test specimen results.

Authors Spec. No.	$\frac{F_u}{F_{u1}}$	$\frac{F_u}{F_{u2}}$	$\frac{F_u}{F_{u3}}$	$\frac{F_u}{F_{u4}}$	$\frac{F_u}{F_{u5}}$	***
S1	1.008	1.166	1.008	1.282	1.235	0.945
S2	1.065	1.240	1.065	1.363	1.305	0.884
S3	1.040	1.196	1.040	1.316	1.274	0.942
S4	1.042	1.205	1.042	1.325	1.277	0.954
S5	1.074	1.237	1.074	1.361	1.315	1.027
S6	1.072	1.254	1.072	1.379	1.314	0.960
S7	1.066	1.325	1.066	1.458	1.306	0.951
S8	1.014	1.267	1.014	1.393	1.243	0.982
S9	1.007	1.231	1.007	1.354	1.234	1.038
S10	1.028	1.286	1.028	1.414	1.259	0.851
S11	1.069	1.331	1.069	1.463	1.310	0.933
S12	1.018	1.270	1.018	1.397	1.247	0.895
S13	1.014	1.267	1.014	1.394	1.242	0.981
MEAN	1.040	1.252	1.040	1.377	1.274	0.950
σ_{n-1}	0.027	0.048	0.027	0.052	0.032	0.053

*** $\frac{\phi_0^0}{\phi_1^0} = \frac{\phi_0^0}{\phi_2^0} = \frac{\phi_0^0}{\phi_3^0} = \frac{\phi_0^0}{\phi_4^0} = \frac{\phi_0^0}{\phi_5^0}$

Table 7.13 Comparison of predicted results for author's experimental longitudinal fillet weld specimens.

In table 7.13, it is seen that the best prediction of the experimental failure load is that made by the author's and Kato and Morita's theories. In fact both these theories predict identical failure load values, which are to within 4 percent of the experimental value. Kamtekar's theory under predicts the failure load to approximately 25 percent, while the β-formula and BS 8118 by a massive 38 and 27 percent respectively.

All the three theories predict the weld throat as the failure plane. The β-formula and BS 8118 assumes this to be the failure plane. This result is seen to be a slight over prediction - by 5 percent, to the experimental findings from the author's tests.

Using the experimental results, reproduced in table 7.14, obtained by Kato and Morita from shear fillet welded steel specimens, the three theories and the β-formula are further compared. The predicted results are given in table 7.15, and their comparisons in table 7.16.

Kato et al's shear specimen number	Measured leg length ω (mm)	Measured weld length L_ω (mm)	Horz. measured penetration p (mm)	Ratio p : ω	σ_u weld N/mm^2	Expt. failure load F_u (KN)
$S_2$5B	5.035	15	0.622	0.124	598	107.80
$S_2$5R	4.794	15	0.099	0.021	548	79.80
$S_2$7B	7.170	21	1.428	0.199	599	188.50
$S_2$10B	9.914	30	1.584	0.160	600	351.50
$S_2$10R	10.253	30	0.622	0.061	543	318.50
$S_2$12B	11.483	36	1.217	0.106	595	483.00
$S_2$15B	15.146	45	0.608	0.040	585	841.00
$S_2$20B	20.082	60	1.343	0.067	600	1445.00
$S_2$20R	17.423	60	0.976	0.056	560	1026.00
$S_2$15R	15.160	45	1.047	0.069	548	751.00
$S_2$22B	20.450	66	1.272	0.062	600	1584.00

Table 7.14 Kato and Morita's experimental longitudinal fillet welded specimen results[12].

Kato et al's shear specimen number	Author's predicted failure formula	Author's predicted failure load F_{u1} (KN)	Kamtekar's predicted failure load F_{u2} (KN)	Kato et al predicted failure load F_{u3} (KN)	β Formula predicted failure load F_{u4} (KN)	Failure angles ** ϕ_1^0, ϕ_2^0, ϕ_3^0, ϕ_4^0,
$S_2$5B	1.83 UTL	82.86	73.75	82.86	86.77	45
$S_2$5R	1.66 UTL	65.68	64.35	65.68	75.71	45
$S_2$7B	1.95 UTL	176.62	147.28	176.62	173.27	45
$S_2$10B	1.84 UTL	337.97	291.41	337.97	342.84	45
$S_2$10R	1.73 UTL	289.29	272.75	289.29	320.88	45
$S_2$12B	1.80 UTL	444.23	401.66	444.23	472.54	45
$S_2$15B	1.69 UTL	677.24	651.11	677.24	766.01	45
$S_2$20B	1.74 UTL	1259.53	1180.58	1259.53	1388.91	45
$S_2$20R	1.72 UTL	1009.53	955.98	1009.53	1124.68	45
$S_2$15R	1.74 UTL	652.65	610.49	652.65	718.22	45
$S_2$22B	1.73 UTL	1404.69	1322.43	1404.69	1555.80	45

UTL = Ultimate Tensile Load = $\sigma_u \omega L_\omega$

** Failure angles ϕ_1^0, ϕ_2^0, ϕ_3^0, ϕ_4^0, predicted by Author, Kamtekar, Kato and Morita and the β formula, respectively.

Table 7.15 Prediction of failure loads and angles for Kato and Moritas longitudinal test specimens.

Kato et al's shear specimen number	$\frac{F_u}{F_{u1}}$	$\frac{F_u}{F_{u2}}$	$\frac{F_u}{F_{u3}}$	$\frac{F_u}{F_{u4}}$
$S_2$5B	1.301	1.462	1.301	1.242
$S_2$5R	1.215	1.240	1.215	1.054
$S_2$7B	1.067	1.280	1.067	1.088
$S_2$10B	1.040	1.206	1.040	1.025
$S_2$10R	1.101	1.168	1,101	0.993
$S_2$12B	1.087	1.203	1.087	1.022
$S_2$15B	1.242	1.292	1.242	1.098
$S_2$20B	1.147	1.224	1.147	1.040
$S_2$20R	1.016	1.073	1.016	0.912
$S_2$15R	1.151	1.230	1.151	1.046
$S_2$22B	1.128	1.200	1.128	1.018
MEAN	1.136	1.234	1.136	1.049
σ_{n-1}	0.088	0.095	0.088	0.081

Table 7.16 Comparison between predicted failure results for Kato and Morita's longitudinal fillet welded specimen .

It is found in table 7.15, that again the author's and Kato and Morita's theories, predict identical failure load values. These predictions are the closest to actual experimental values, to within 14 percent. The next best prediction of the failure load, is that obtained using the β-formula to within 5 percent.

Since Kato and Morita failed to record the weld failure angles, a comparison is not possible between predicted and measured values. However, the point to note is that all the theories predict the same plane along which failure should occur. This plane is located at 45^0 measured up from the horizontal weld leg length. Although the predicted angle is the same by all the three theories and the β-formula, the location of the plane varies according to the author's weld model i.e the author's predicted angle is to be measured from the tip of the extent of horizontal penetration. This point of measurement is also followed by Soetens in his experimental measurements and indirectly by Kato and Morita, although they both fail to emphasis this point. In Kamtekar's case the angle is measured from the point of intersection of the vertical and horizontal leg lengths.

The final set of experimental data available for comparing predicted failure loads and failure planes, is that published by Soetens [6,14]. His experimental results have been obtained from shear fillet welded, aluminium test specimens. Unfortunately, as mentioned in the earlier section on tensile fillet welds, that although Soetens has measured the failure plane angles and weld penetration values, he only publishes average values for a given filler metal / alloy combination test specimen. This restricts the theories from predicting values close to experimental results for individual specimens. Therefore, in order to make a fair comparison all the other readings have also been averaged, for each given filler metal / alloy combination. These results are

given in table 7.17.

Sp. No.	Filler metal	Alloy	Average penet. p (mm)	Horz. penet. p.Cos45 (mm)	Average throat t (mm)	Average leg length ω (mm)	Ratio p.Cos45 : ω	σ_u weld N/mm^2	Average weld length L_w (mm)	Expt. failure load F_u (KN)	Expt. failure angle ϕ^0
1	5356	5083	3.30	2.333	5.80	8.202	0.284	264	50.80	243.96	35
2	5356	6082	3.20	2.263	6.00	8.485	0.267	233	51.00	190.22	32
3	5356	7020	2.20	1.556	5.90	8.344	0.187	276	51.00	241.80	33
4	4043	6082	3.80	2.687	5.30	7.495	0.359	212	51.82	178.60	37
5	4043	7020	3.80	2.687	5.20	7.354	0.365	235	50.84	196.70	41

Table 7.17 Soeten's average experimental results for longitudinal fillet welded test specimens.

Soeten's shear specimen number	Author's predicted failure formula	Author's predicted failure load F_{u1} (KN)	Kamtekar's predicted failure load F_{u2} (KN)	Kato et al predicted failure load F_{u3} (KN)	β Formula predicted failure load F_{u4} (KN)	BS 8118 predicted failure load F_{u5} (KN)	Failure angles ** $\phi_1^0, \phi_2^0, \phi_3^0, \phi_4^0, \phi_5^0$
1	2.09UTL	230.72	179.64	230.72	171.07	196.63	45
2	2.06UTL	208.56	164.66	208.56	143.17	165.27	45
3	1.93UTL	227.56	191.79	227.56	174.36	233.37	45
4	2.21UTL	182.66	134.47	182.66	122.24	169.24	45
5	2.23UTL	195.90	143.48	195.90	136.65	212.87	45

UTL = Ultimate Tensile Load = $\sigma_u \omega L_\omega$

** Failure angles $\phi_1^0, \phi_2^0, \phi_3^0, \phi_4^0, \phi_5^0$ predicted by Author, Kamtekar, Kato and Morita, the β formula and BS 8118 respectively.

Table 7.18 Prediction of failure loads and planes for Soeten's longitudinal test specimens.

Soetens Spec. No.	$\frac{F_u}{F_{u1}}$	$\frac{F_u}{F_{u2}}$	$\frac{F_u}{F_{u3}}$	$\frac{F_u}{F_{u4}}$	$\frac{F_u}{F_{u5}}$	$\frac{\phi_0^0}{\phi_1^0} = \frac{\phi_0^0}{\phi_2^0} = \frac{\phi_0^0}{\phi_3^0} = \frac{\phi_0^0}{\phi_4^0} = \frac{\phi_0^0}{\phi_5^0}$
1	1.057	1.358	1.057	1.942	1.241	0.778
2	0.912	1.155	0.912	1.652	1.151	0.711
3	1.063	1.261	1.063	1.803	1.036	0.733
4	0.978	1.328	0.978	1.900	1.055	0.822
5	1.004	1.371	1.004	1.961	0.924	0.911
MEAN	1.003	1.295	1.003	1.409	1.081	0.791
σ_{n-1}	0.062	0.089	0.062	0.052	0.120	0.800

Table 7.19 Comparison between predicted results for Soeten's longitudinal welded specimens.

The theoretical predictions of failure are given in table 7.18, and their comparisons in table 7.19. It is found, yet again that the author's and Kato and Morita's theories predict identical failure load values. Further, these predicted values are the closest to the experimental results, in this case to within 3 percent, as seen in table 7.19. The second best failure load prediction is that obtained using BS 8118. This predicts the failure load to within approximately 8 percent. Kamtekar's theory under predicts the experimental failure load value by 30 percent. Finally, the β-formula is found to grossly under predict the failure value by 41 percent.

No differences or variations exist between the predicted failure plane values. This is because all the three theories predict and the β-formula and BS 8118 assumes, the

failure plane to be at 45^0 measured from the horizontal weld leg length. However, comparing the predicted failure plane value to the experimentally measured values by Soeten's in table 7.19, it is seen that the prediction is an over estimation by approximately 20 percent. This can be explained by the fact that Soetens measured failure angle values are averaged values and also the measured values might require re-adjustment, to account for penetration as discussed in section 5.3.1, chapter 5.

From the overall comparisons between the shear weld failure theories, it is found that the author's theory predicts identical weld failure loads and failure planes to those predicted by Kato and Morita's theory. This result is interesting since both theories analyse the shear weld using different weld models and method of analysis. The author's theory (derived in chapter 3) directly accounts for penetration in its weld model and failure analysis, whereas Kato and Morita's theory merely adds on the extent of penetration to the failure plane length. Using these theories - the author's and Kato and Morita's, the predicted failure load and plane values are remarkably close to those obtained experimentally.

Kamtekar's theory, the β-formula and BS 8118 consistently under predict the experimental failure load, - at times by up to 30, 41 and 27 percent, respectively. Only the location of the failure plane, which is predicted by Kamtekar's theory and assumed by the β-formula as being at 45^0 measured up from the horizontal leg length, is the same as the author's and Kato and Morita's predictions. This is also in good agreement with the experimentally recorded values.

Generally by using the author's and Kato and Morita's shear weld failure theories, better

and closer predictions to the experimental values are obtained, than by using the other theories compared.

As mentioned earlier in the tensile fillet weld analysis section 7.3.1, Kamtekar has used effective weld leg length values from Kato and Morita's experimental results, to compare his theoretical predictions to the experimental values, whereas his theory does not take penetration into consideration. Consequently, the comparisons published in his paper[11], predict closer failure load values to the experimental results. The results using Kamtekar's theory with the normal leg length values are shown in table 7.15. These have been compared to the other theoretical predictions in table 7.16. The discussion of these predictions have already been made above.

7.5 Cruciform shaped test specimens.

For the cruciform shaped specimens the welds are constantly in tension. The experimental recorded results were given in chapter 5, table 5.12. The predicted failure loads and failure planes are given in table 7.20, using the author's, Kato and Morita's, and Kamtekar's tensile theories, and also those predicted by the β-formula and BS 8118. The comparison of all these predictions are given in table 7.21.It is found the predictions for failure are of the same nature as seen and discussed for the tensile lap welded specimens in section 7.3.1. Briefly it is that the author's, failure theory predicts very close failure loads and planes to the experimental values. The next best failure predictions made are those by Kato and Morita's theory. Kamtekar's theory, the β-formula and BS 8118 are found to substantially under predict the failure load by 38 and 75 and 27 percent respectively, shown in table 7.21.

Sp. No	Expt. failure load F_u (KN)	Ratio p: ω	Expt. failure angle ϕ_0^0	Author's predicted failure load F_{u1} (KN)	Author's predicted failure angle ϕ_1^0	Kamtekar's predicted failure load F_{u2} (KN)	Kamtekar's predicted failure angle ϕ_2^0	Kato et al predicted failure load F_{u3} (KN)	Kato et al predicted failure angle ϕ_3^0	β Formula predicted failure load F_{u4} (KN)	BS 8118 predicted failure load F_{u5} (KN)	Failure angle $\phi_4^0 = \phi_5^0$ *
C1	23.48	0.289	15.61	22.36	7.30	17.91	0 or 90	23.91	22.5	14.096	20.718	45
C2	25.76	0.253	18.61	22.73	6.41	18.60	0 or 90	24.14	22.5	14.644	20.918	45
C3	27.56	0.275	13.94	23.67	6.89	19.14	0 or 90	25.28	22.5	15.070	21.906	45
C4	24.31	0.241	12.34	21.89	6.14	18.05	0 or 90	23.21	22.5	14.209	20.113	45
C5	25.51	0.251	16.83	21.98	6.36	18.01	0 or 90	23.35	22.5	14.180	20.236	45
C6	25.25	0.263	18.10	22.91	6.63	18.69	0 or 90	24.45	22.5	14.713	21.188	45
C7	27.92	0.281	17.14	22.19	7.02	17.86	0 or 90	23.70	22.5	14.058	20.536	45
C8	22.15	0.245	13.89	21.68	6.23	17.83	0 or 90	23.01	22.5	14.040	19.936	45
C9	23.11	0.253	14.19	21.79	6.41	17.83	0 or 90	23.14	22.5	14.040	20.055	45
C10	25.70	0.249	14.62	21.76	6.32	17.85	0 or 90	23.10	22.5	14.054	20.015	45
C11	26.25	0.256	18.90	22.92	6.47	18.73	0 or 90	24.37	22.5	14.742	21.120	45
C12	25.91	0.250	16.85	22.40	6.34	18.37	0 or 90	23.79	22.5	14.461	20.616	45
C13	27.35	0.286	16.71	23.12	7.13	18.55	0 or 90	24.72	22.5	14.602	21.420	45
C14	22.31	0.238	15.90	22.02	6.07	18.19	0 or 90	23.33	22.5	14.321	20.211	45
C15	23.50	0.241	18.06	21.63	6.14	17.83	0 or 90	22.94	22.5	14.040	19.876	45

* ϕ_4^0 and ϕ_5^0 are the assumed failure planes by the β formula and BS 8118 respectively.

Table 7.20 Prediction of failure loads and angles for the author's cruciform shaped test specimens.

Cruc. Spec. No.	$\frac{F_u}{F_{u1}}$	$\frac{F_u}{F_{u2}}$	$\frac{F_u}{F_{u3}}$	$\frac{F_u}{F_{u4}}$	$\frac{F_u}{F_{u5}}$	$\frac{\phi_0^0}{\phi_1^0}$	$\frac{\phi_0^0}{\phi_2^0}$ *	$\frac{\phi_0^0}{\phi_3^0}$	$\frac{\phi_0^0}{\phi_4^0} = \frac{\phi_0^0}{\phi_5^0}$ **
C1	1.050	1.311	0.982	1.666	1.133	2.168	0.173	0.694	0.347
C2	1.133	1.385	1.067	1.759	1.231	2.903	0.207	0.827	0.414
C3	1.164	1.440	1.090	1.829	1.258	2.023	0.155	0.620	0.310
C4	1.111	1.347	1.047	1.711	1.209	2.010	0.137	0.548	0.274
C5	1.161	1.416	1.092	1.799	1.261	2.646	0.187	0.748	0.374
C6	1.102	1.351	1.033	1.716	1.912	2.730	0.201	0.804	0.402
C7	1.258	1.564	1.178	1.986	1.360	2.441	0.190	0.762	0.381
C8	1.022	1.242	0.963	1.578	1.111	2.230	0.154	0.617	0.309
C9	1.061	1.300	0.999	1.646	1.152	2.215	0.158	0.631	0.315
C10	1.181	1.440	1.113	1.829	1.284	2.314	0.162	0.650	0.325
C11	1.145	1.402	1.077	1.781	1.243	2.919	0.210	0.840	0.420
C12	1.157	1.411	1.089	1.792	1.257	2.658	0.187	0.749	0.374
C13	1.183	1.475	1.106	1.873	1.277	2.343	0.186	0.743	0.371
C14	1.013	1.227	0.957	1.558	1.104	2.619	0.177	0.707	0.353
C15	1.087	1.318	1.025	1.674	1.182	2.942	0.201	0.803	0.401
MEAN	1.122	1.375	1.055	1.747	1.265	2.477	0.179	0.716	0.358
σ_{n-1}	0.067	0.089	0.062	0.114	0.193	0.320	0.022	0.088	0.044

* Comparison for 90^0 predicted plane only.

** Same assumed failure plane by the β formula and B S 8118

Table 7.21 Comparison between predicted results, for author's cruciform shaped specimens.

7.6 Comparison of the variation in strength between tensile and shear fillet welds.

The author's theory also shows that variations in the extent of weld penetration, markedly effects the strength between tensile and shear fillet welds. These strength variations, for equal leg length welds, are shown in table 7.22.

Leg Length ω (mm)	Horizontal penetration p (mm)	Tensile failure load F_t $\sigma_u.\omega.L_\omega$ (KN)	Shear failure load F_s $\sigma_u.\omega.L_\omega$ (KN)	$\frac{F_t}{F_s}$	$\left[\frac{F_t - F_s}{F_s}\right].100$
ω	0	0.5774	0.4083	1.4142	41.42
ω	0.1ω	0.6322	0.4490	1.4080	40.80
ω	0.2ω	0.6815	0.4899	1.3911	39.11
ω	0.3ω	0.7254	0.5307	1.3668	36.68
ω	0.4ω	0.7646	0.5715	1.3379	33.79
ω	0.5ω	0.7994	0.6124	1.3054	30.54
ω	0.6ω	0.8304	0.6532	1.2713	27.13

Table 7.22 Variation in strength between tensile and shear fillet welds as penetration values increase.

It is seen that when no penetration is present, tensile fillet welds are 41.41 percent stronger than shear fillet welds - both welds being of a comparable size. As penetration values increase, then the strength of the tensile weld to the shear weld decreases quite significantly. At a penetration value of 0.6 times the weld leg length, tensile welds are 27 percent stronger than shear fillet welds. The relationship between the extent of penetration and the strength of tensile welds over shear welds is also shown graphically

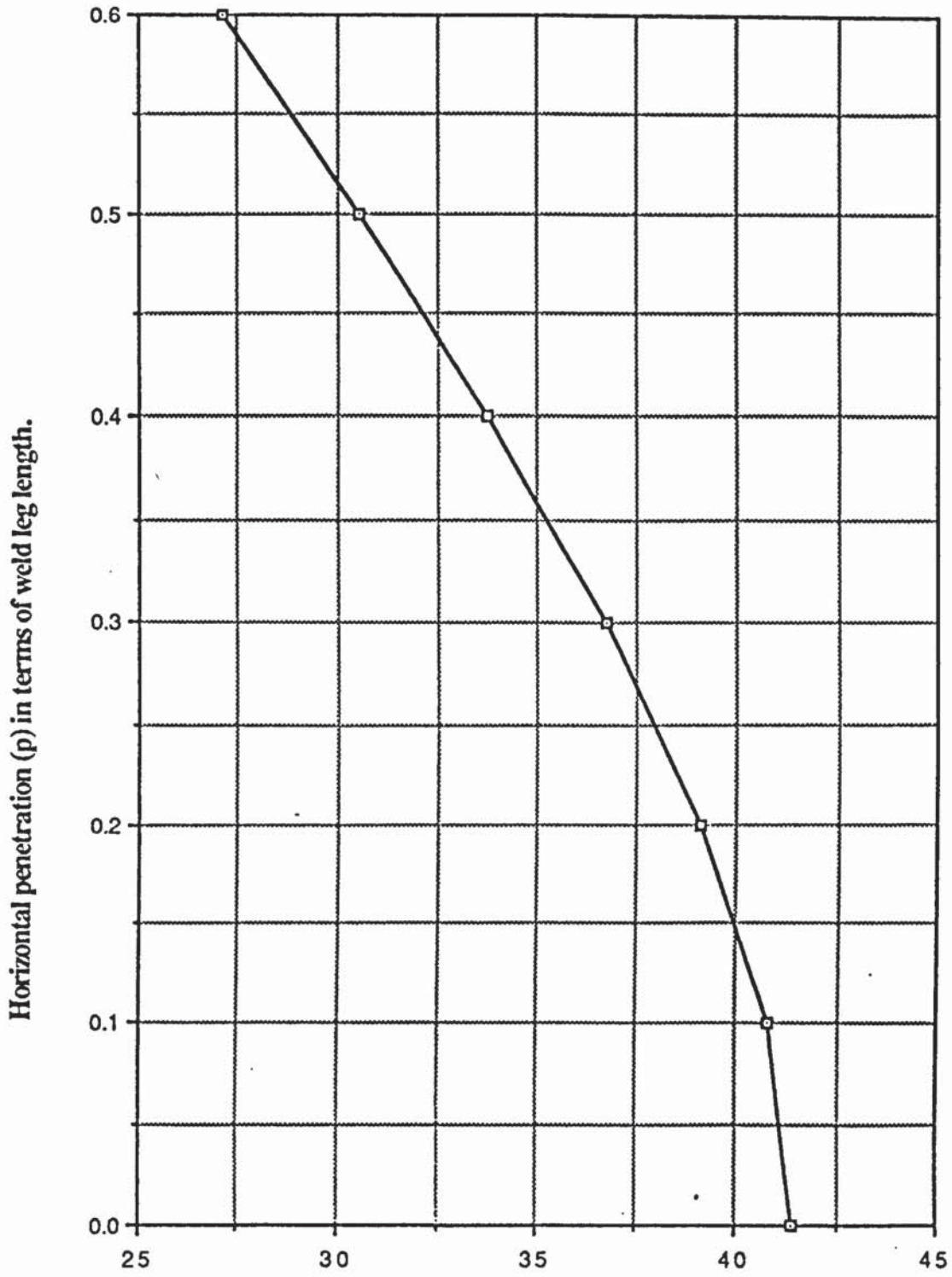

Figure 7.11 Effect of change in weld penetration on the strength between tensile and shear fillet welds.

in figure 7.11.

It is seen that for penetration values up to 0.1 times the weld leg length values, the percentage change in the strength of tensile welds with respect to the strength of shear welds is minimal. However, a marked change occurs for penetration values greater than 0.1 times the weld leg length values.

This revelation is quite unique. It would explain why in the past numerous authors have reported differing strengths to exist between tensile and shear fillet welds. All their experimental programmes and theories on fillet welds, only agree that the strength of the tensile weld is always greater than the shear weld. They all differ on the variation in the strength between tensile and shear welds. Expressed as a factor of the tensile weld strength to shear weld strength Jensen [33] reported it to be 1.272, Freeman [32] as 1.333, Schreiner [34] 1.45, Archer [41] ; 1.563, Higggs [15] ; 1.5, and Soetens [6,14] ; 1.50. While Kamtekar [11] theoretically predicted it as 1.42 and Kato and Morita [12] as 1.46.

The author would suggest that all these findings may well be correct. Since different welding equipments, techniques , and all the other parameters influencing weld penetration (discussed in chapter 2) used by the various authors, would inevitably result in varying penetrations being achieved. Then no doubt when comparing the experimental results of these authors, with no account of penetration being taken, marked variations between the results would occur. For the results obtained theoretically by some of the authors, it is suggested that the discrepancies arise from their weld profile model analysed. No account of penetration is taken into their weld models or weld analysis, as discussed in chapter 2.

7.7.1 Failure predictions of the temporary end plate connection.

The experimental weld failure loads and failure angles of the temporary end plate connections F1 to F15 are given in table 7.23. Also shown in this table are the predicted failure values obtained using the author's proposed method of failure analysis derived in chapter 4, and Kamtekar's failure equation 4.8, which is a specific case of the author's prediction when weld penetration is zero. Comparisons of these predictions to the experimental results are made in table 7.24. No predictions of weld failure loads and planes are made using Kato and Morita's theory, the β-formula or BS 8118. This is because none of these can accommodate the moments acting along the welds of the end plate connection.

In table 7.24 it is seen that the author's failure load predictions of the weld are to within approximately 10 percent, while those of Kamtekar's underpredict by a huge 52 percent. Further the weld failure planes predicted by the author's theory are to within 15 percent of the experimental values. Kamtekar's theory predicts the weld leg lengths as the failure planes. The vertical leg length (90^o) failure prediction is compared to the experimental failure values, is seen to be a gross over prediction of the actual experimental value, by 80 percent. A numerical comparison is not possible with the other, horizontal leg length predicted failure plane since division by zero is infinite. However a difference between the experimental and horizontal leg length (0^o) average is 18^o, while the difference in the averages between the author's predicted and the experimental recorded failure planes is a mere 2.26^o. The reason for these differences in the failure predicted values of the author's and Kamtekar's, is the fact that the author's theory directly accounts for the extent of weld penetration achieved, while Kamtekar's does not.

Such close agreements of the author's predicted failure results to the experimental values verify that the author's proposed failure theory (derived in chapter 4) for the welds in the end plate connection is a correct and remarkably good theory to use.

A point to note is that although the codes of practice BS 8118 and CP 118 do not permit fillet welds to carry any moments, the author's predicted results show that the end plate connection can be designed with a single weld to accommodate the applied moment. However, the load carrying capacity of the connection due to the presence of bending stresses is greatly reduced when compared to the connection where no moments are acting on the welds. If the end plate connection welds were to be designed to BS 8118 the welds would be considered as transverse welds, each having a load carrying capacity of 109KN. However due to the presence of moments their actual experimental load carrying capacity averages to approximately 23.5KN.

Spec. Number	Measured weld length L_ω (mm)	Measured leg length ω (mm)	Horz. measured penetration p (mm)	Ratio p : ω	Expt. failure load F_u (KN)	Expt. failure angle ϕ°_0	Author's predicted failure load F_{u1} (KN)	Author's predicted failure angle ϕ^0_1	Kamtekar's predicted failure load F_{u2} (KN)	Kamtekar's predicted failure angle ϕ^0_2
F1	160.0	8.0	2.89	0.361	92.60	20.0	94.593	8.69	61.363	0 or 90
F2	160.0	8.0	2.36	0.295	93.60	18.5	82.903	7.32	61.363	0 or 90
F3	160.0	8.0	2.50	0.313	95.40	21.0	88.217	7.71	61.363	0 or 90
F4	160.0	8.0	2.00	0.250	92.40	17.0	82.105	6.34	61.363	0 or 90
F5	160.0	8.0	2.19	0.274	92.96	18.5	83.433	6.87	61.363	0 or 90
F6	160.0	8.0	1.97	0.246	95.40	17.0	80.246	6.25	61.363	0 or 90
F7	160.0	8.0	2.10	0.263	92.20	18.0	82.157	6.63	61.363	0 or 90
F8	160.0	8.0	2.30	0.288	93.35	19.0	85.028	7.17	61.363	0 or 90
F9	160.0	8.0	2.08	0.260	95.34	19.0	81.839	6.56	61.363	0 or 90
F10	160.0	8.0	1.90	0.238	90.22	17.0	79.714	6.07	61.363	0 or 90
F11	160.0	8.0	2.40	0.300	92.36	17.5	86.781	7.43	61.363	0 or 90
F12	160.0	8.0	2.20	0.275	92.96	17.5	83.433	6.89	61.363	0 or 90
F13	160.0	8.0	2.57	0.321	95.72	18.0	89.279	7.87	61.363	0 or 90
F14	160.0	8.0	2.30	0.287	94.32	17.0	85.028	7.15	61.363	0 or 90
F15	160.0	8.0	2.40	0.300	92.62	17.0	86.781	7.43	61.363	0 or 90

Table 7.23 Prediction of weld failure loads and angles for the temporary end plate connections.

Specimen Number	$\frac{F_u}{F_{u1}}$	$\frac{F_u}{F_{u2}}$	$\frac{\phi_0^0}{\phi_1^0}$	$\frac{\phi_0^0}{\phi_2^0}$ *
F1	0.979	1.509	1.008	2.30
F2	1.129	1.525	1.125	2.53
F3	1.081	1.555	1.210	2.72
F4	1.125	1.506	1.211	2.68
F5	1.114	1.515	1.208	2.69
F6	1.189	1.555	1.230	2.72
F7	1.122	1.503	1.224	2.72
F8	1.098	1.521	1.185	2.65
F9	1.165	1.554	1.304	2.90
F10	1.132	1.470	1.272	2.80
F11	1.064	1.505	1.048	2.36
F12	1.114	1.515	1.138	2.54
F13	1.072	1.560	1.011	2.29
F14	1.109	1.537	1.062	2.38
F15	1.067	1.509	1.018	2.29
MEAN	1.104	1.523	1.150	2.57
σ_{n-1}	0.049	0.025	0.099	0.203

* Comparison for 90^0 predicted failure plane only.

Table 7.24 Comparison between experimental and predicted failure loads and angles for temporary end plate connections type F.

7.7.2 Experimental and FE results of point loaded end plate connection.

From the finite element (FE) method used to analyse the end plate connection, it is found that the maximum deflection occurs at all times at the mid point of the longest free edge side, for the point load under consideration. These results can be seen in Chapter 6, figures 6.13 to 6.6.15. When compared with the experimental readings recorded from the test specimens type F, it is found that the FE results are generally in very close agreement. This is shown in the typical load deflection comparison graphs for test specimen F1 between the PAFEC and experimental results in figure 7.12. Other comparison graphs obtained for the test specimens F2 to F6 are also shown in appendix B.

Furthermore, the experimental recorded stress distributions along the welded edges of the end plates also compare favourably with the FE stress distributions obtained in figures 6.10 to 6.12. A typical comparison graph between the experimental and FE stress results is shown in figure 7.13. Thus, the assumption made in chapter 4, that the welded edges of the end plate behave as though they are fully fixed is justified by these findings. The results also show that correct testing arrangements have been used to obtain the results.

Results from the FE analysis of the end plate when loaded by a uniformly distributed line load, verify the other assumption made in chapter 4, that the applied point load can be replaced by an equivalent uniform line load. For the experimental point load case of 50KN applied to the end plate connection, it is seen in figures 6.10 to 6.12, that the maximum stress distributions along the welded edges of the end plate are virtually the same as for the case when an equivalent uniform line load is applied, figures 6.19 to 6.21.

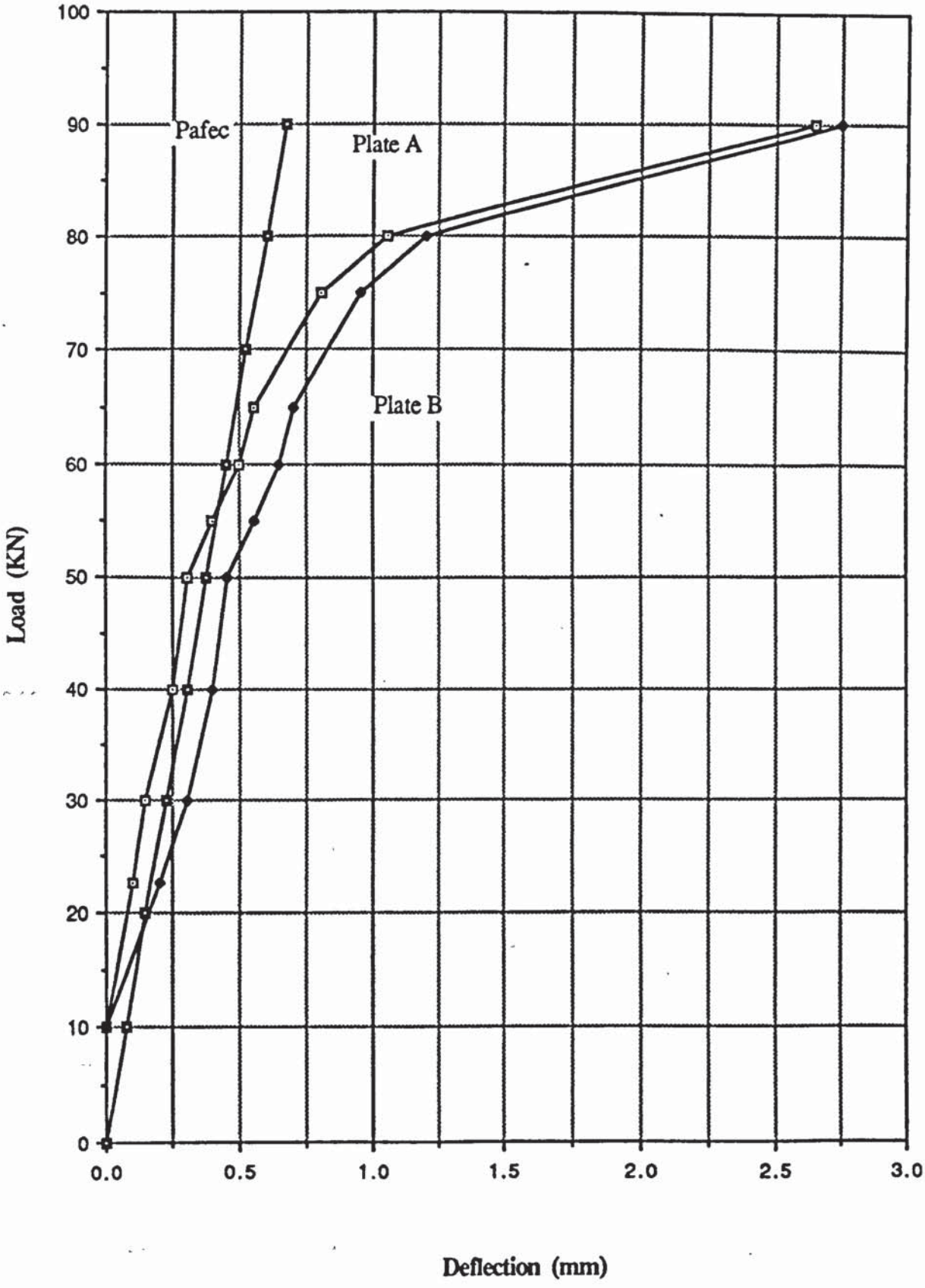

Figure7.12 Comparison of Load vs deflection for Sp F1

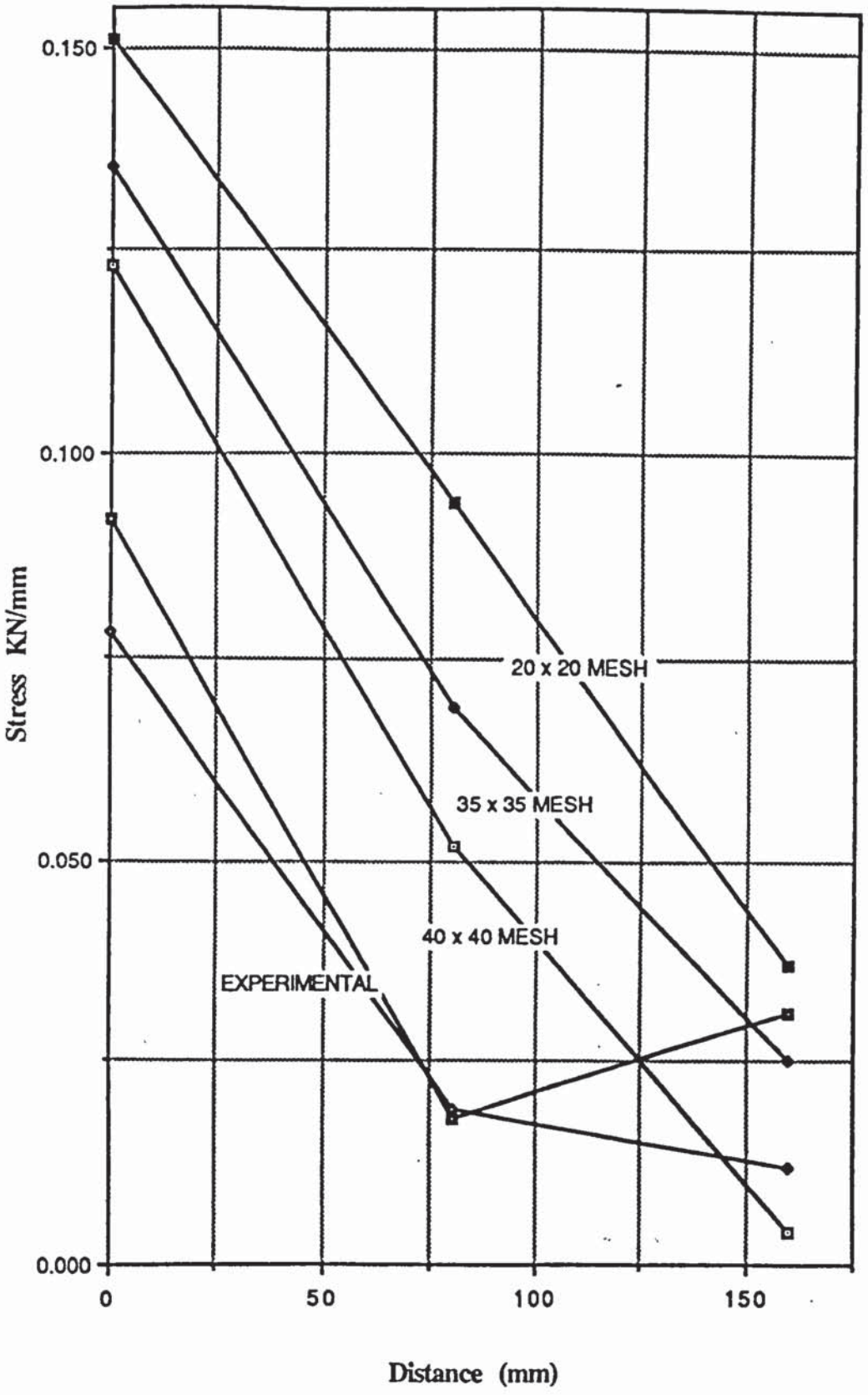

Figure 7.13 A typical comparison graph of experimental and PAFEC stresses along the fixed edge of the end plate connection.

CHAPTER 8 CONCLUSIONS.

The following conclusions are drawn from the theoretical work derived and experimental results reported in this thesis.

1. The extent of the HAZ in aluminium alloy 6082 - T6 can be well calculated using Ian and Dwight's proposed equations.

2. A better prediction of the severity of the HAZ, for aluminium alloy 6082 - T6 is obtained when the individual alloy, filler metal combination is considered, than by using Ian and Dwight's general proposed equations for severity.

3. Weld failure loads and failure planes can be predicted using the proposed weld model incroporating weld penetration - for any amount of weld pentration.

4. For tensile fillet welds, it has been shown by the author that;

   i) Weld failure loads increase as weld penetration values increase.

   ii) The location of the weld failure plane changes as weld penetration changes.

   iii) The length of the weld failure plane increases as weld penetration increases.

   iv) A unique failure plane exists for a given weld penetration value.

   v) Close predictions to experimentally recorded values of the tensile weld failure loads and planes are achieved using the author's tensile weld failure theory.

5. For shear fillet welds, the author has shown;

   i) Weld failure loads increase as weld penetration values increase.

   ii) The angle of the weld failure plane is always at 45^0 to the horizontal weld leg length, despite any increases in weld penetration.

   iii) The length of the weld failure plane increases as weld penetration increases.

   iv) Close predictions to the experimentally recorded results of shear weld failure loads and planes are achieved using the author's shear weld failure theory.

6. From the author's proposed weld failure theories, it is found that the variation in strength between tensile and shear fillet welds is dependant upon the extent of weld penetration achieved.

7. From a comparison between experimental and theoretical, tensile and shear weld failure predictions, the author's proposed theories are recommended in preference to Kamtekar's, Kato and Morita's and the β-formula.

8. For the temporary end plate connection;

   i) The author's proposed tensile weld failure theory can be extended to predict the weld failure loads and failure planes, for the side welds subjected to an out of plane force.

   ii) The assumption of the side welds to the end plate connection, achieving a fully fixed end condition is justified by the close theoretical finite element results to the

experimentally obtained values.

iii) Close weld failure load and failure angle predictions to the experimentally recorded values are achieved for the end plate connection, using the author's extended weld failure theory and method of analysis.

CHAPTER 9 RECOMMENDATIONS FOR FURTHER WORK.

1. Further tests required for different alloy / filler metal combinations, to produce seperate hardness to ultimate tensile strength relationships, for each alloy / filler metal combination.

2. Extend the author's theoretical approach to predict weld failure loads and angles for both tensile and shear fillet welds, with unequal leg lengths. Also from this establish relationship between unequal leg length tensile and shear fillet welds.

3. Conduct an experimental programme on tensile and shear fillet welds of different sizes of weld leg lengths, but at same weld penetration values, i.e. keeping weld penetration constant vary size of weld leg lengths for both types of equal and unequal leg lengths.

4. Test temporary end plate connections in a pair of space frames.

5. For the end plate test specimens type F, variations in the thickness of plates and weld sizes be investigated.

6. Further investigate into the benefits and advantages to be gained by using the new alloy 7019 instead of the alloy 6082, for the temporary space frame connection.

REFERENCES.

1. Buxton,P. "Recent aluminium structures". Symposium on the draft code of practice for the design of aluminium structures, October 1985.

2. Light and Sound International Limited.

3. Robertson, I. "Strength loss in welded aluminium structures". Ph.D. Thesis, University of Cambridge, September 1985.

4. Robertson, I. Dwight, J.B "Heat affected zone softening in welded aluminium". Third international conference on aluminium weldments, Munich, April 1985.

5. Soetens, F. "Welded connections in aluminium alloy structures". Second international conference on aluminium weldments, Munich, F.R.G., May 1982.

6. Soetens, F. "Welded connections in aluminium alloy structures".

Report of IBBC - TNO No. BI - 81 - 27, June 1981.

7. B.S.8118 "Draft British Standard", Code of practise for the design of aluminium structures.

8. C.P 118 "The structural use of aluminium", British Standard Code of Practice, 1969.

9. B.S.5950, Part 1. "Structural use of steelwork in building". 1985.

10. Bibber, L.C. "The theory of stress in welds". The Welding Journal, Vol. 9, No. 4, 1930.

11. Kamtekar, A.G. "A new analysis of the strength of some simple fillet welded connections". The Journal of Constructional Steel Research, Vol. 2, No. 2, June 1982.

12. Kato, B.
Morita, K. "Strength of transverse fillet welded joints". Welding Research Supplement, February 1974, 59s - 64s.

13. Aluminium Welding Seminar. "Selection of aluminium alloys and fillers for welding"
Technical papers 3.0 - 3.28.

14. Soetens, F. "Welded connections in aluminium alloy structures - progress report on fillet welds". Institute TNO, Report No. BI - 83 - 72 / 63.4.3181, October 1983.

15. Higgs, J.D. "A failure criterion for fillet welds". Ph.D. Thesis, The university of Aston in Birmingham, January 1981.

16. Aluminium Welding Seminar. "MIG welding of aluminium".
Technical papers 6.0 - 6.32.

17. Kemp, C.J. "Basic principles of inert gas metal arc welding".

18. American Welding Society. "Welding processes-arc". Vol. 2, Welding handbook, Seventh edition, 1978.

19. Kortliks "Aluminium welding process, a comparison - MIG and TIG".

20. Pascoe, K.J. "The properties of engineering materials". Third edition, 1978.

21. Aluminium Welding Seminar. "Influence of design on welded fabrication". Technical papers 8.0 - 8.25.

22. Rosenthal, D. "The theory of moving sources of heat and its application to metal treatments". Transactions of the ASME., 68, p849, 1946.

23. Kelsey, R.A. "Effect of heat input on welds in aluminium alloy 7039". Welding Journal Research Supplement, 1971.

24. Smith, A.A. "CO_2 welding of steel". The Welding Institute, Abington, Cambridge.

25. Smith, A.A.
Newman, R.P "Penetration in fillet welds made with automatic CO_2 welding". IIW Doc. XII - 237 - 64.

26. B.S.4870, Part 1. "Approval testing of welding procedures - fusion welding of steel". 1981.

27. B.S.4870, Part 2. "Approval testing of welding procedures - TIG or MIG welding of aluminium and its alloys". 1981.

28. Higgins, T.R.
Preece, F.R. "Proposed working stresses for fillet welds in building construction". The Welding Journal Research Supplement, October 1968.

29. Kato, B.
Morita, K. "The strength of fillet welded joints". International Institute of Welding, Doc. No. XV - 267 - 69 1969.

30. Soetens, F. "Welded connections in aluminium alloy structures - progress report". Paper presented at Annual Meeting of IIW, Trondheim, June 1983.

31. Schuster, L.W. "Welded pressure vessels". The Welding Journal, Vol. 9, No.5, May 1930.

32. Freeman, F.R. "The strength of welded joints". The Welding Journal, June 1932.

33. Jensen, C.D.

"Combined stresses in fillet welds".
The Welding Journal, No.2, February 1934.

34. Schreiner, N.G.

"The behaviour of fillet welds when subjected to bending stresses".
The Welding Journal, pp.1 - 16, September 1935.

35. Jennings, C.H.

"Welding design".
The Welding Journal, October 1936.

36. Jensen, C.D.
Crispen, R.E.

"Stress distribution in welds subjected to bending".
The Welding Journal Research Supplement, October 1938.

37. Shedd, T.C.

"Structural design in steel".
John Wiley and Sons Inc.,(Publishers).

38. Norris, C.H.

"Photoelastic investigation of stress distribution in transverse fillet welds".
The Welding Journal, Vol. 24, 1945.

39. Koenigsberger, F. "Design stresses in fillet weld connections". Proceedings of the Institute of Mechanical Engineers, 165, 1951.

40. Vreedenburgh, C.G.J. "New principles for the calculation of welded joints". The Welding Journal, Vol. 33, No.8, August 1954.

41. Archer, F.E.
Fischer, H.K. "Fillet welds subjected to bending and shear". Civil Engineer and Public Works Review, Vol. 54, Kitchen, E.M. No.634, April 1959.

42. Commission XV of IIW "Calculation formulae for welded connections subject to static loads". Welding in the World, Vol. 2, 4, 1964.

43. Clark, P.J. "Basis of design for fillet welded joints under static loading". Conference Proc., Vol. 1, 1971, Welding Institute Improving Welding Product Design, paper 10.

44. Van Douwen, A.A.
Witteveen, J.
"Proposed modification of the I.S.O. formulae for the calculation of welded joints".
Lastechniek, 32, (6), 1966.

45. Gatto, F.
Mazzolani, F.M.
Mori, D
"Experimental study of residual stresses and mechanical properties of welded sections in Al - Si - Mg alloy 6082".
ECCS - Committee 16, Doc. 16 - 77 - 5, 1977.

46. Vinokurov, V.
Sagalevitch, V
"Strains and stresses in welded aluminium structures".
Paper presented at the colloquium on aluminium and its alloys in welded construction. Porto, Sept. 1981.

47. Mazzolani, F.M.
"The bases of the European recommendations for the design of aluminium alloys structures".
Allumino, Feb. 1980 (2).

48. Kamtekar, A.G.
"The strength of planar fillet weld groups subjected to a shearing force applied outside their planes".
Civil Engineering Department, University of Birmingham, England.

49. Mendleson, A. "Plasticity : theory and application". Macmillan and Company, New York, 1968.

50. Southwell, R.V. "An introduction to the theory of elasticity for engineers and physicists". Second edition, Oxford University Press, 1941.

51. Aluminium Welding Seminar "Quality control in aluminium welding". Technical papers 7.0 - 7.19.

52. Gray
Spencer

53. Timoshenko, S.
Woinowsky-Krieger, S. "Theory of plates and shells".Second edition, International student edition, McGraw - Hill - Kogakusha Publishers Limited.

54. Lowe, P.G. "Basic principles of plate theory", Surrey University Press, 1982.

55. Rockey, K.C.,
Evans, H.R.,
Griffiths, D.W., "The finite element method, a basic introduction for engineers". Granada Publishing, London, England.

Nethercot, D.A.

56. Henshell, R.D. "PAFEC theory, results".
PAFEC Limited, Strelley Hall, Nottingham, England.

57. Zienkiewicz, O.C. "The finite element method in engineering science".
McGraw - Hill Publishing Co. Ltd., 1971.

APPENDIX A

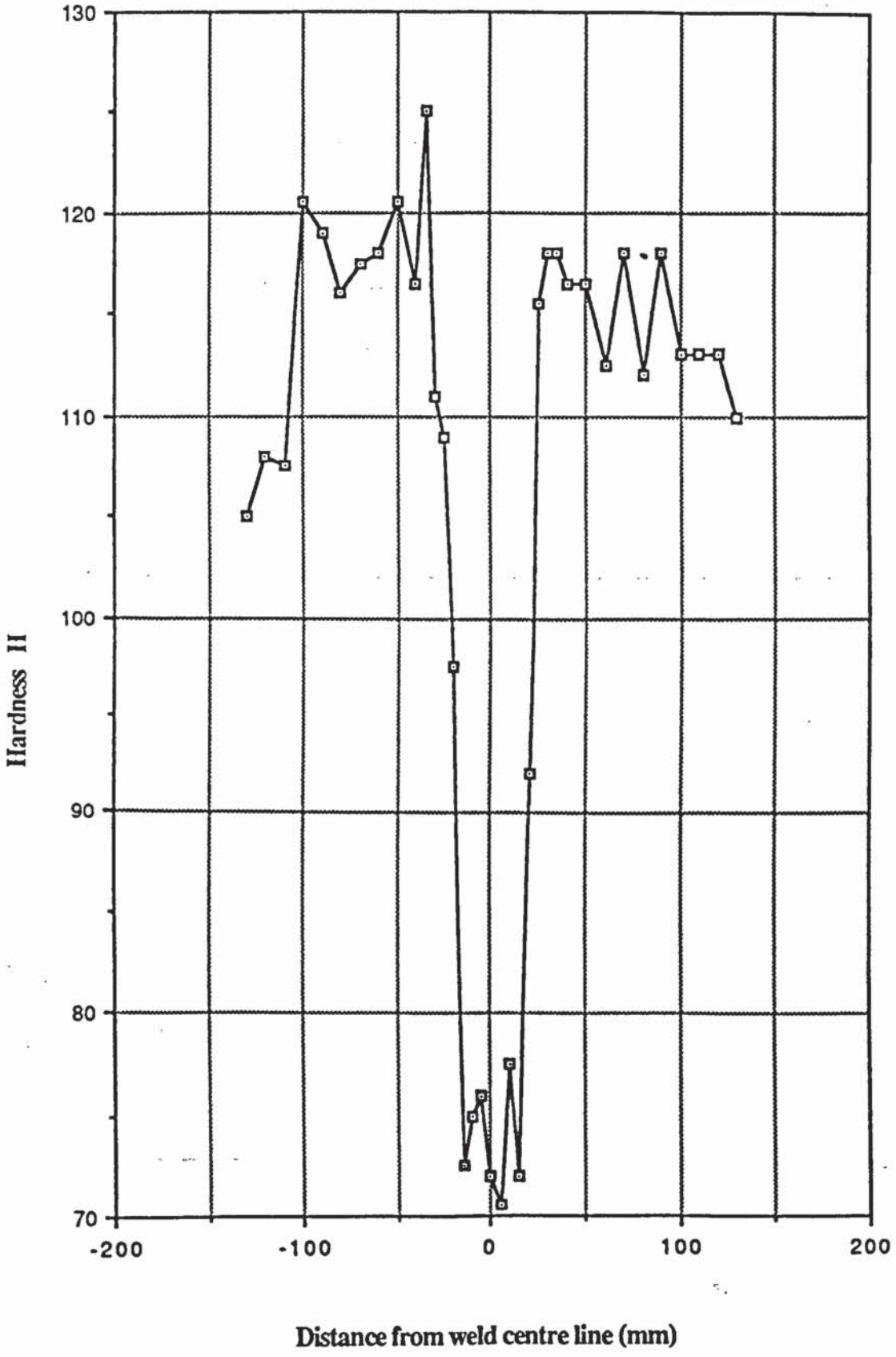

Figure A1 Hardness traverse for line 2 along butt welded specimen.

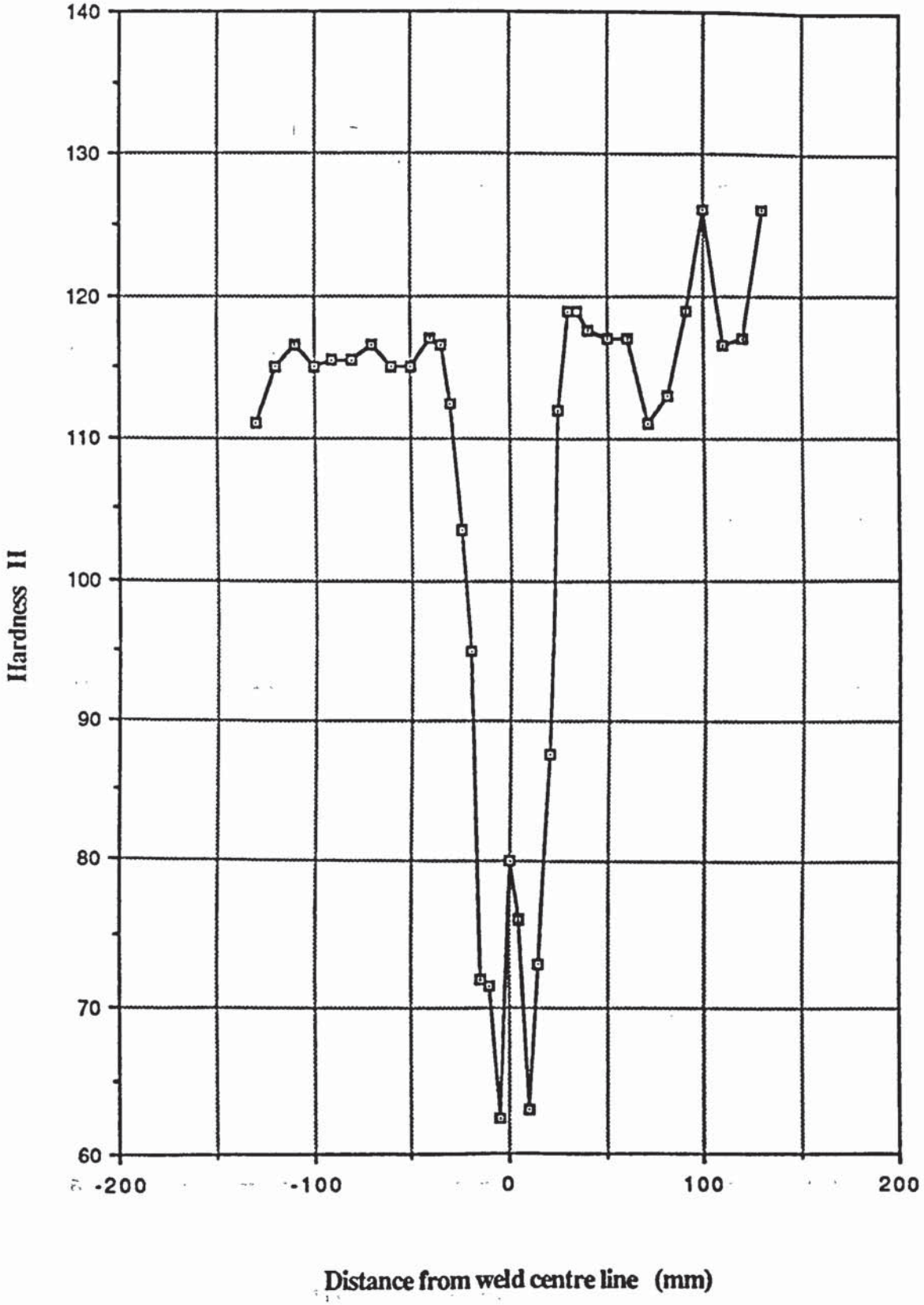

Figure A2 Hardness traverse for line 3 along butt welded specimen.

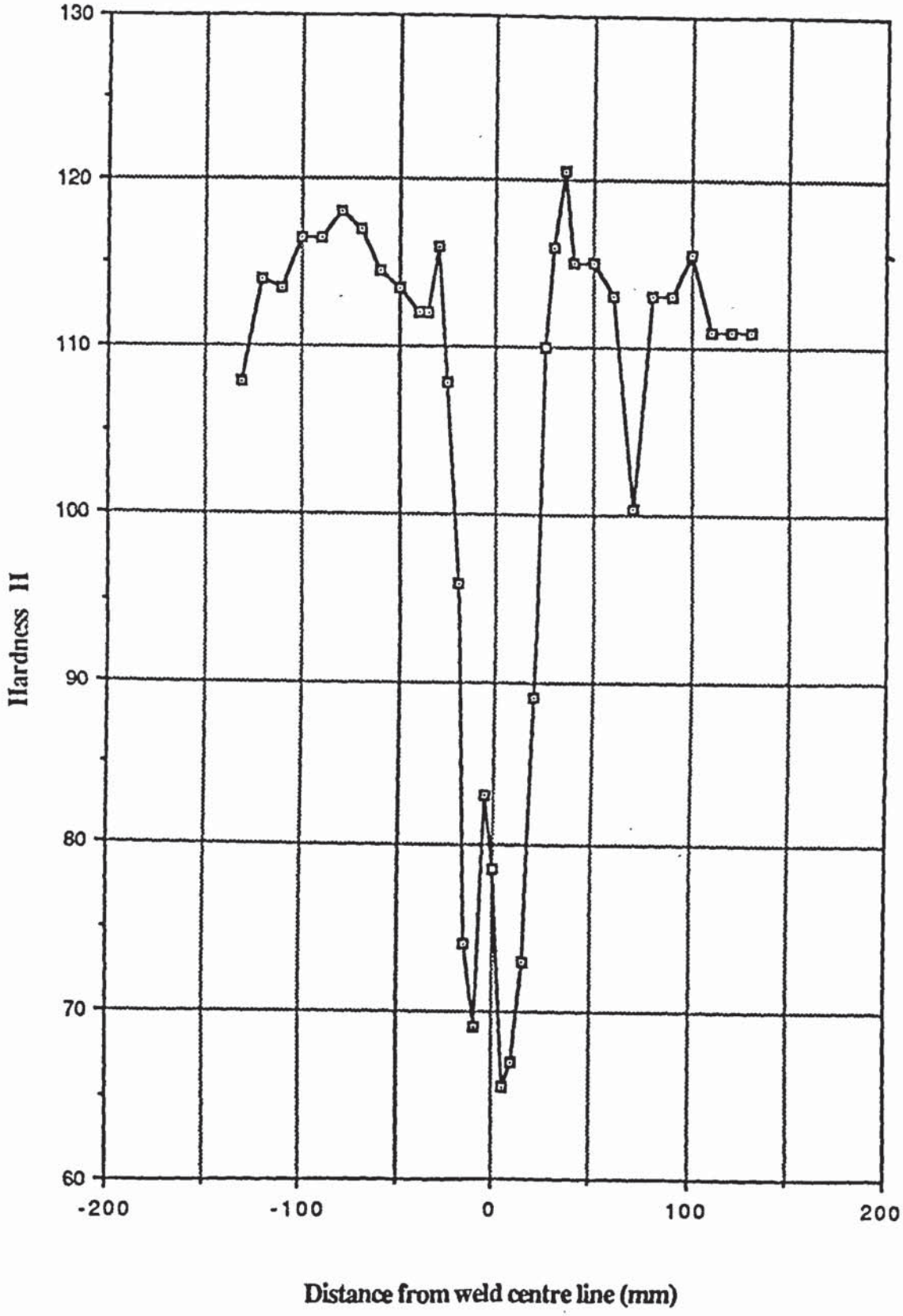

Figure A3 Hardness traverse for line 4 along butt welded specimen.

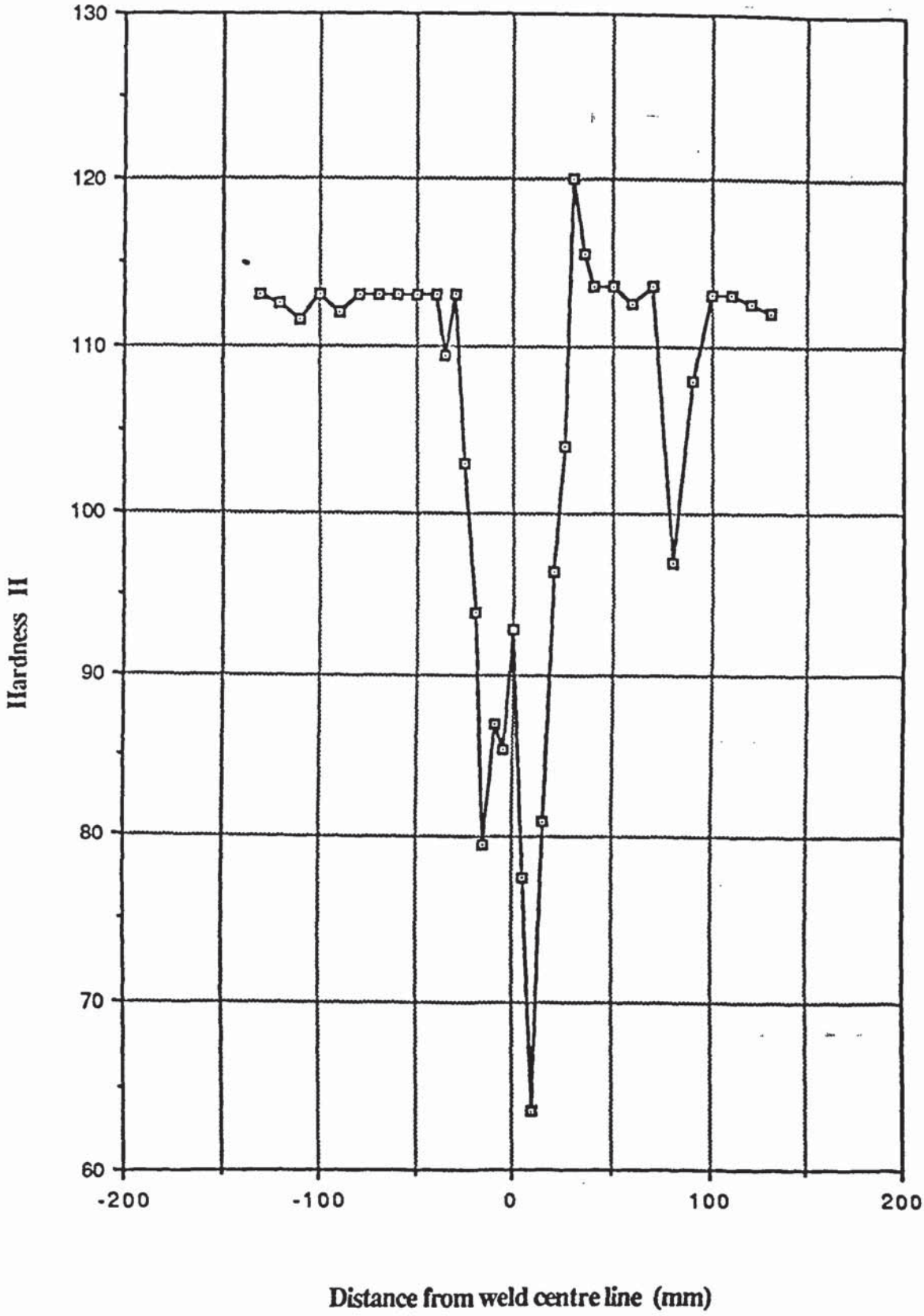

Figure A4 Hardness traverse for line 5 along butt welded specimen.

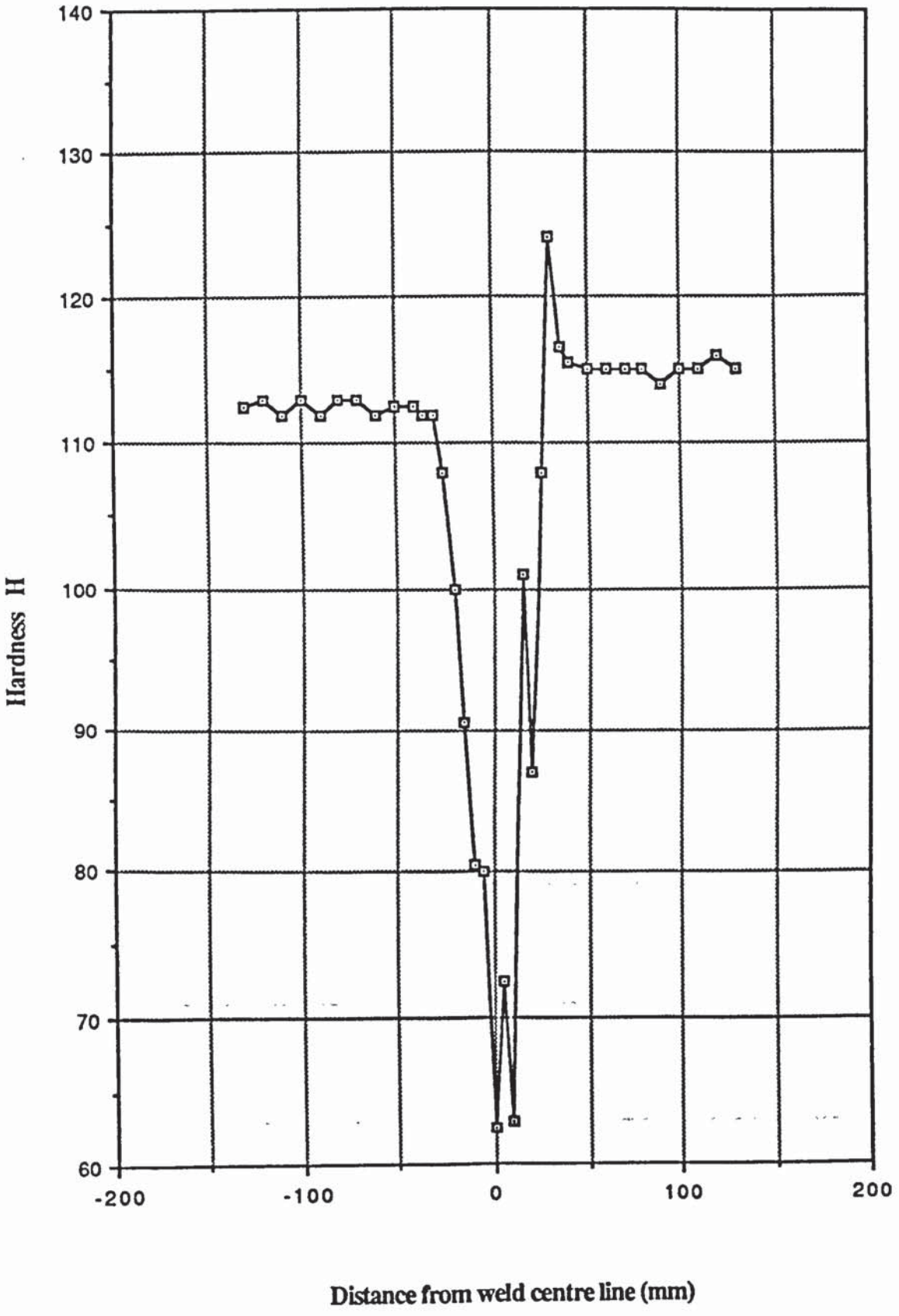

Figure A5 Hardness traverse for line 6 along butt welded specimen.

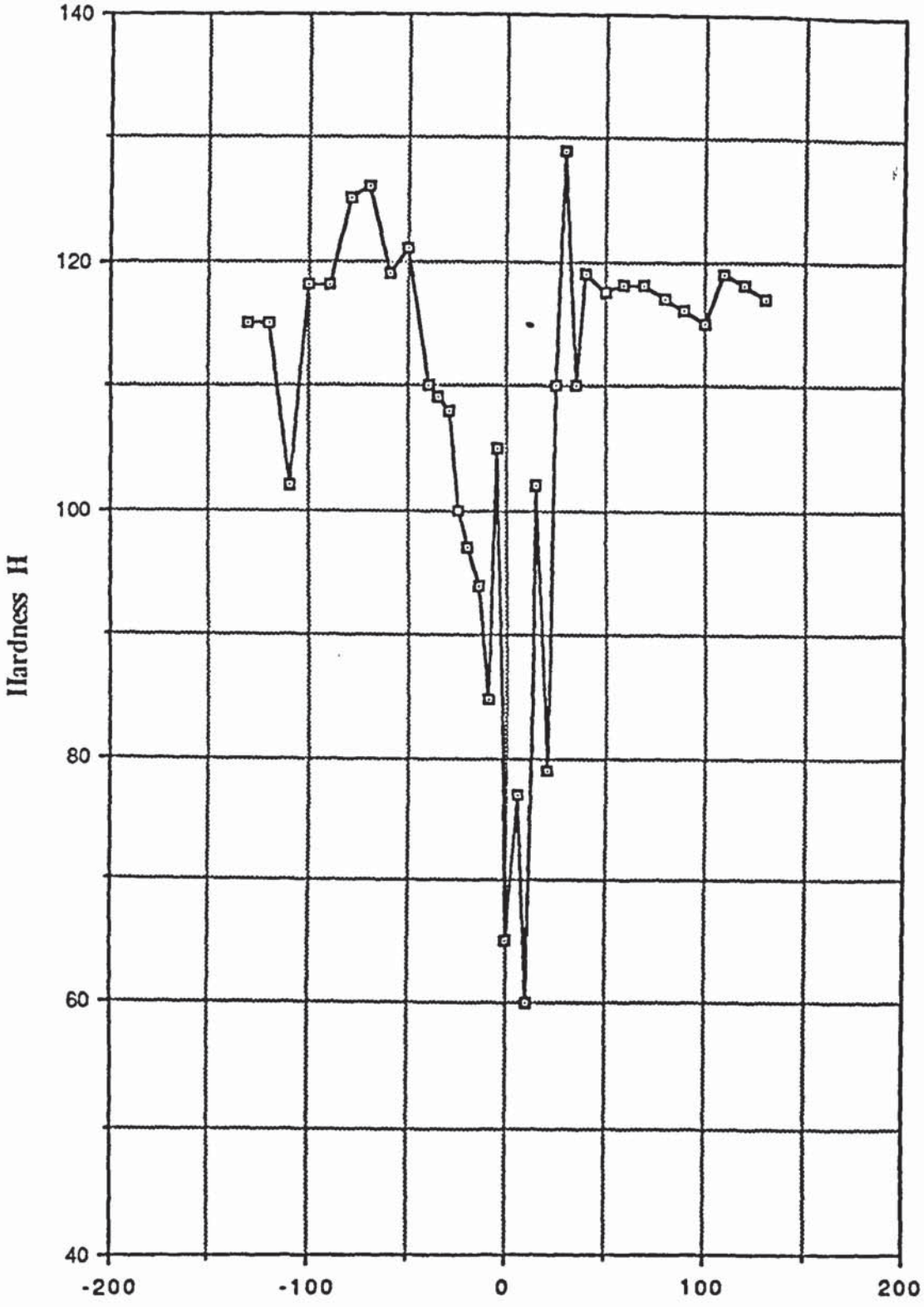

Figure A6 Hardness traverse for line 7 along butt welded specimen.

APPENDIX B

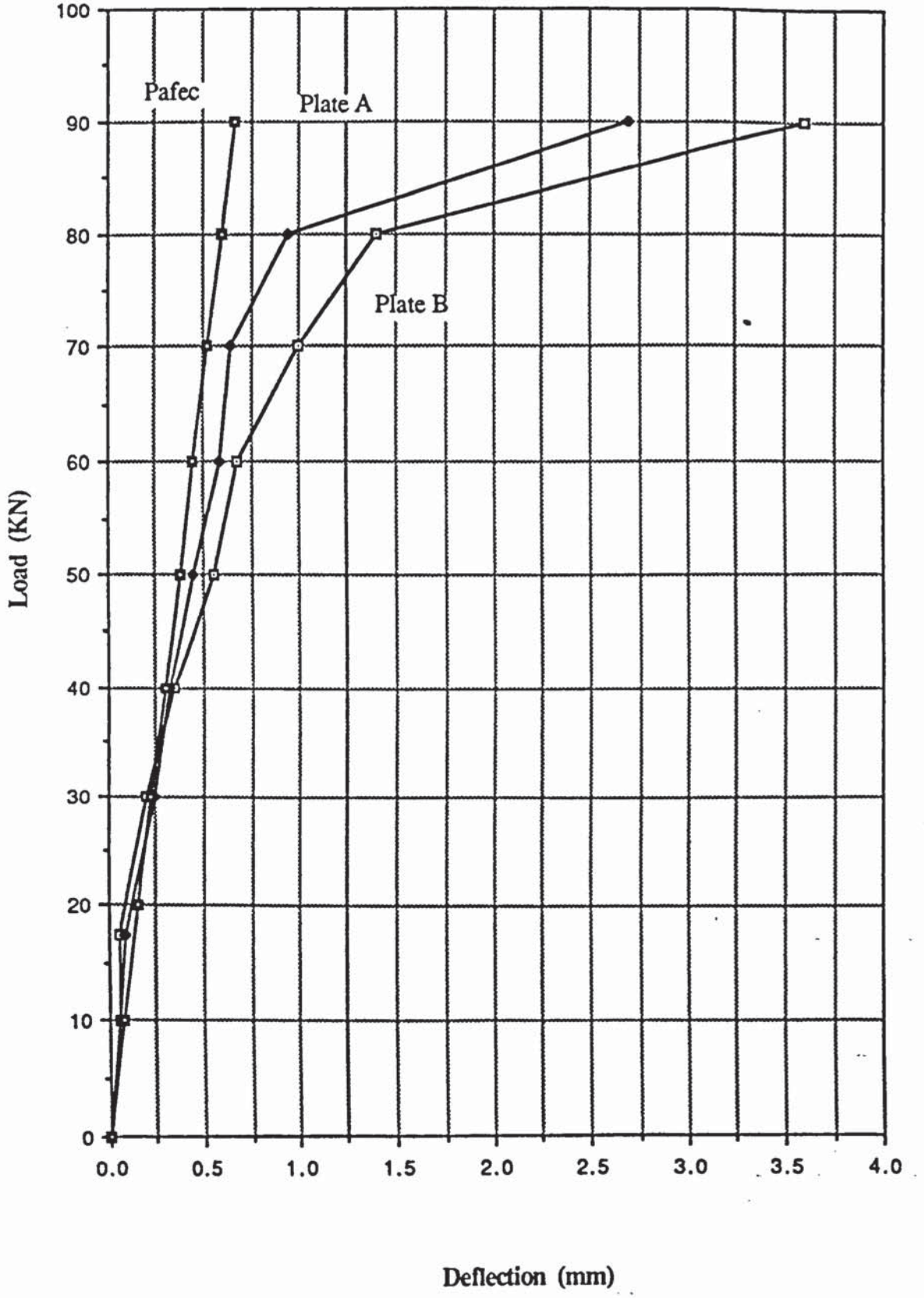

Figure B1 Comparison of Load vs deflection for specimen F2

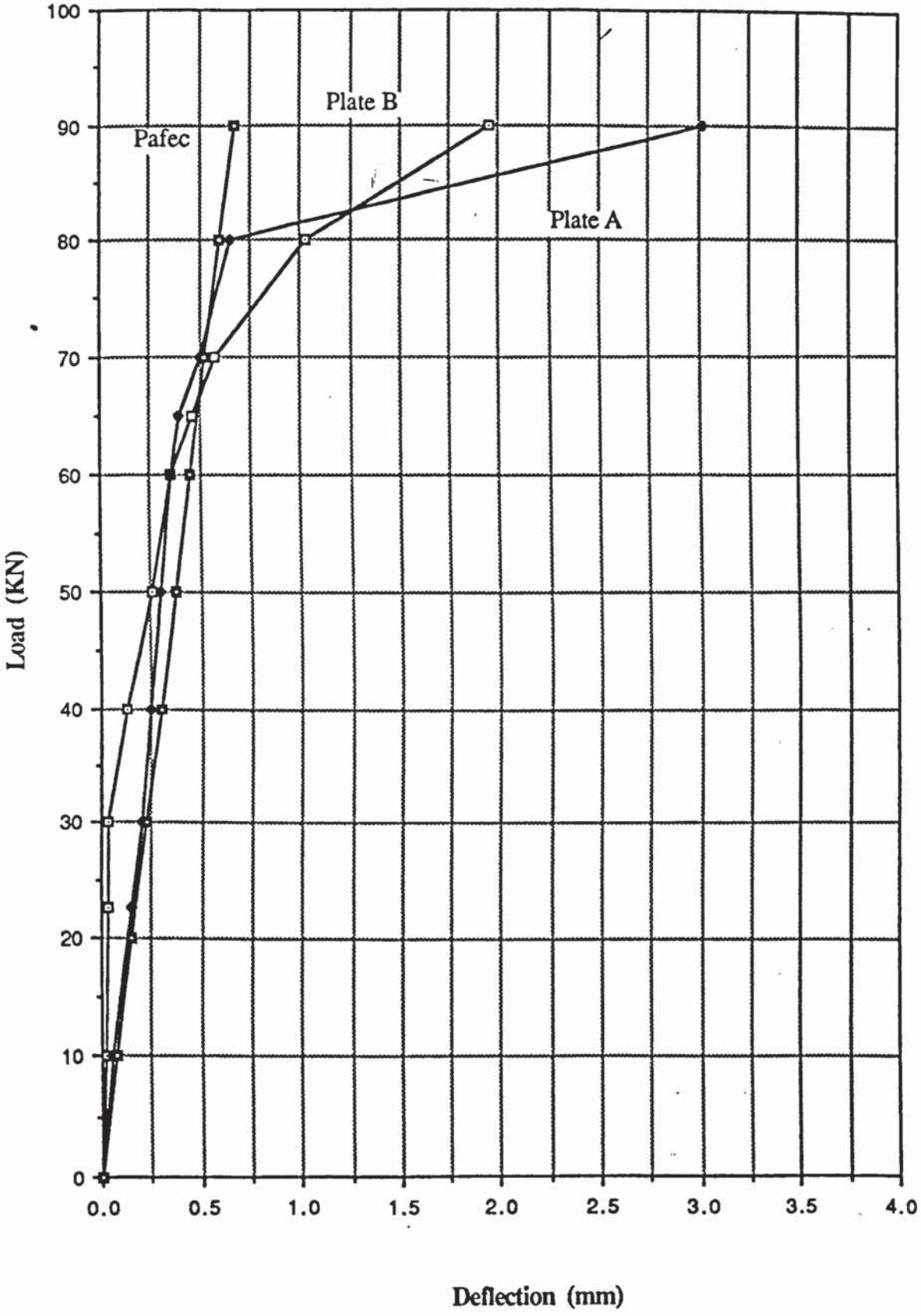

Figure B2 Comparison of Load vs Deflection for specimen F3

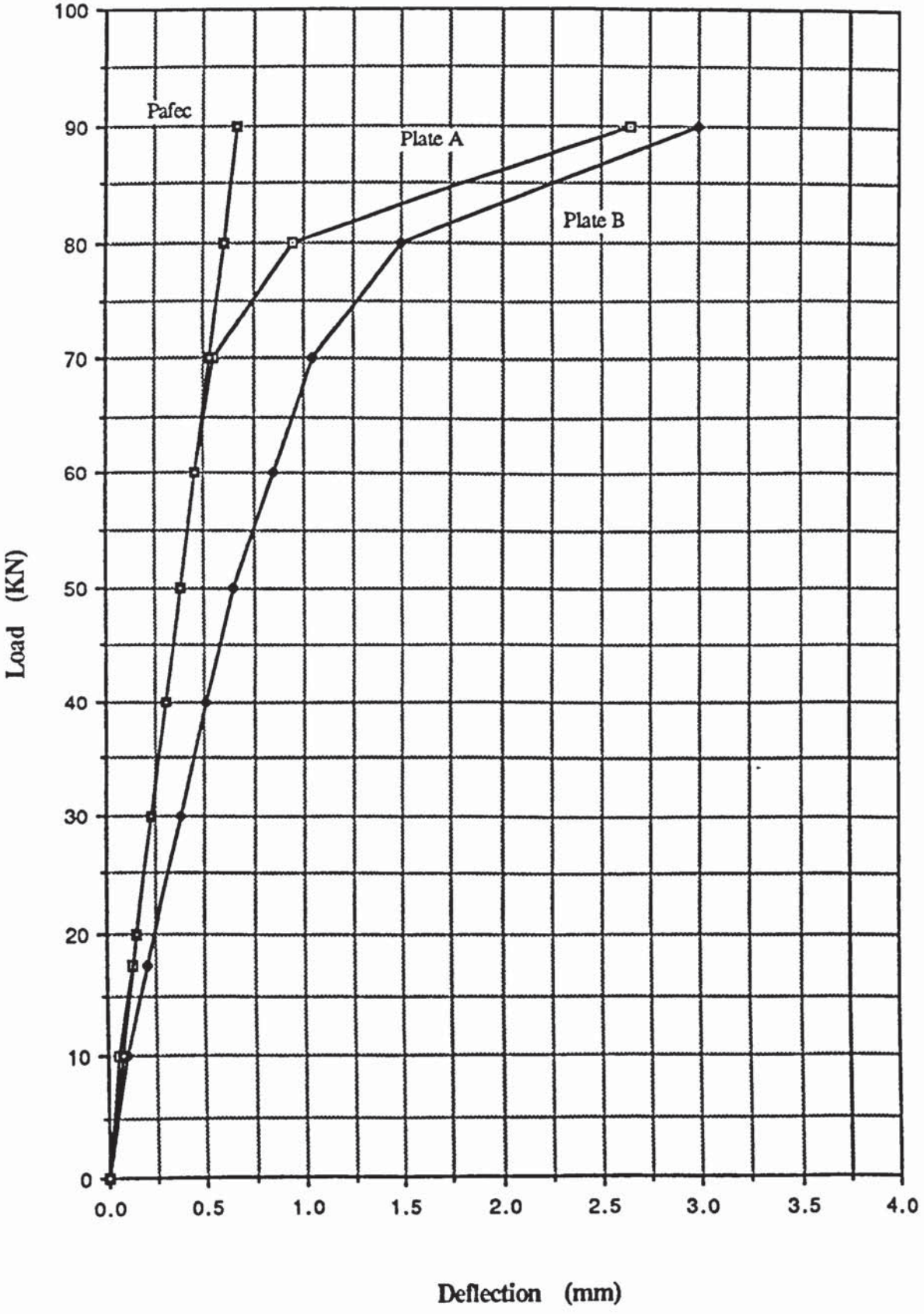

Figure B3 Comparison of Load vs Deflection for specimen F4.

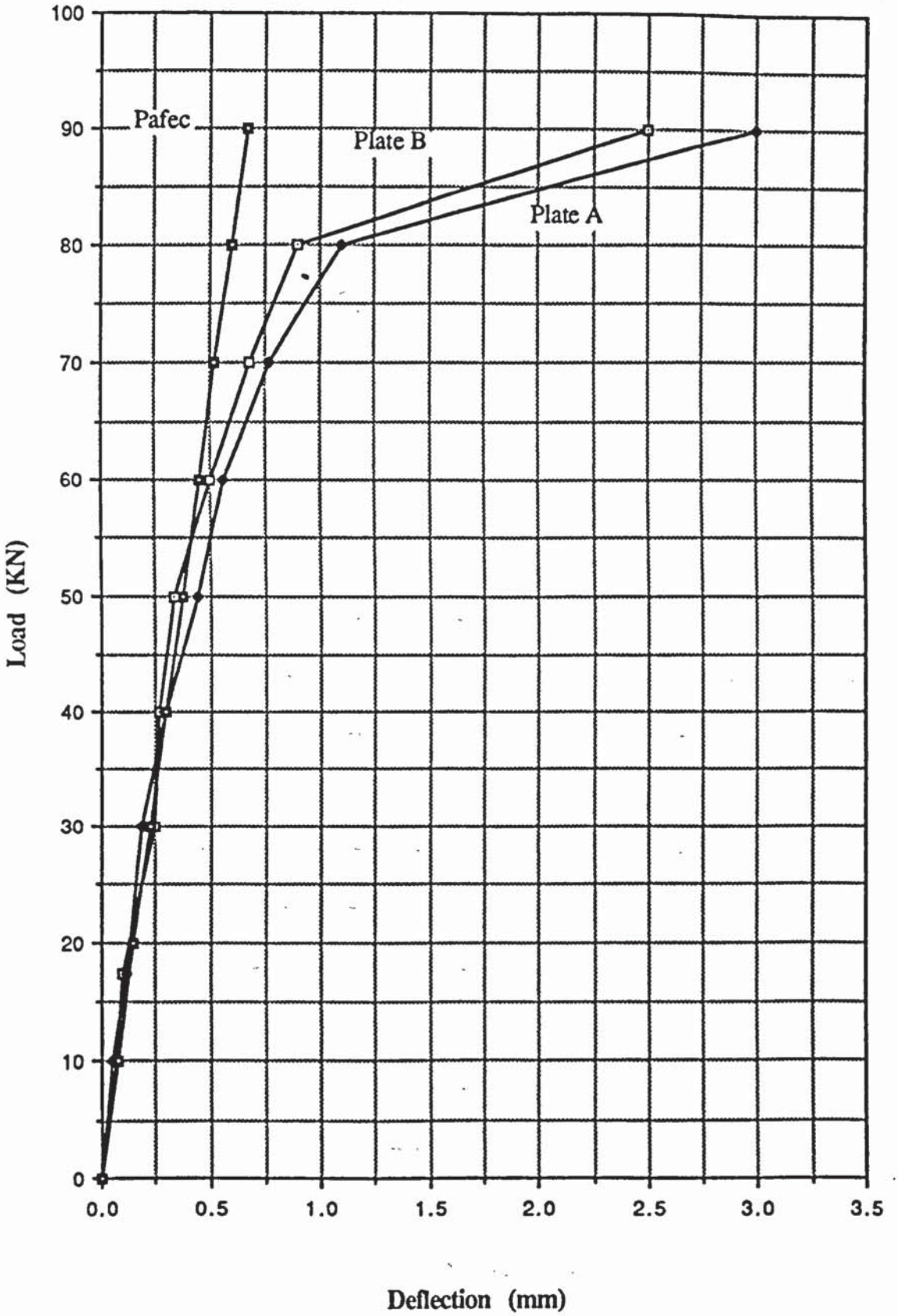

Figure B4 Comparison of Load vs Deflection for specimen F5.

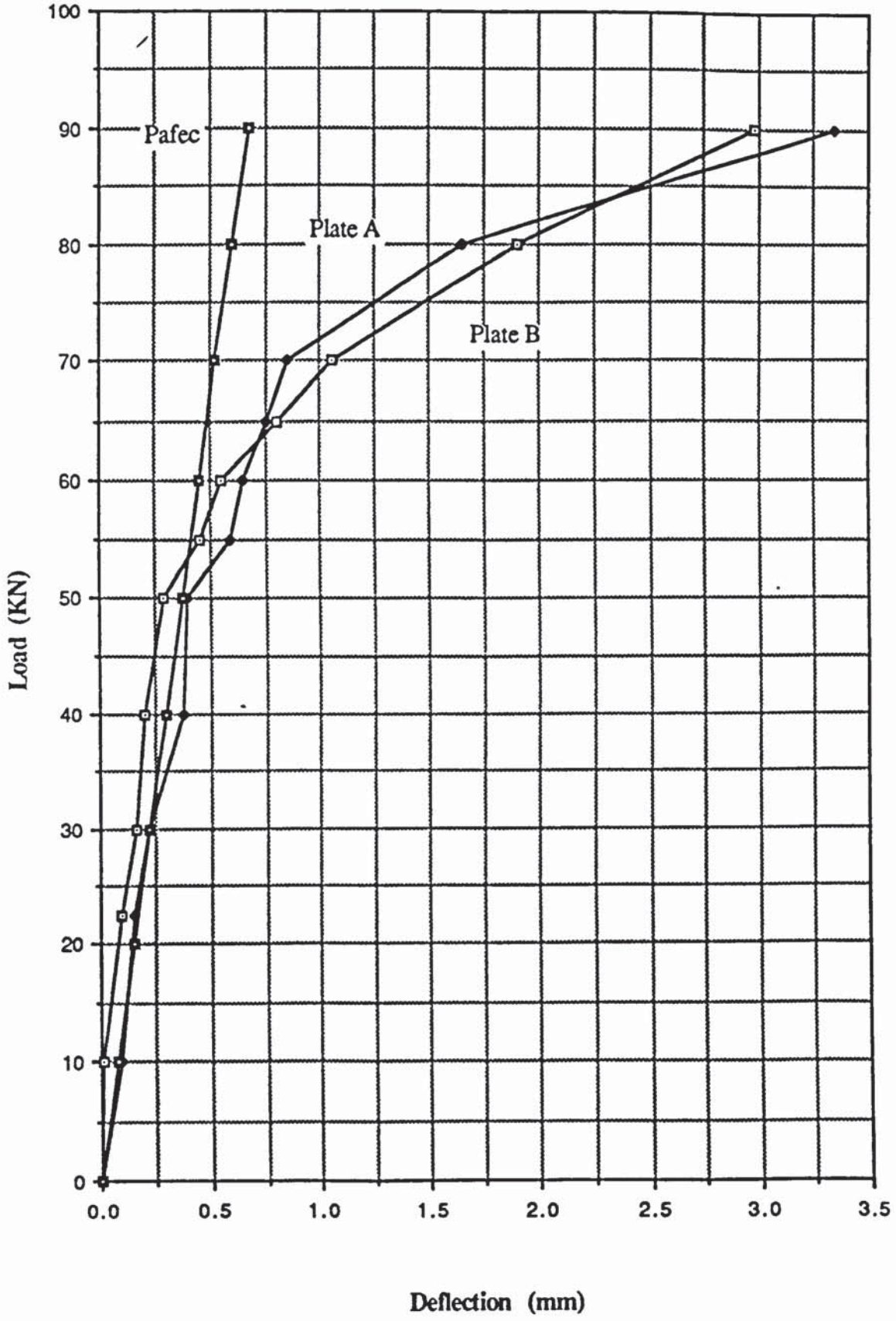

Figure B5 Comparison of Load vs Deflection for specimen F6.

APPENDIX C

ELEMENT TYPE 44210 8-NODE QUADRILATERAL

PRINCIPAL STRESSES - SIGMA 1 IS THE MAXIMUM VALUE OF STRESS IN THE PLANE OF THE ELEMENT
SIGMA 2 IS THE MINIMUM VALUE OF STRESS IN THE PLANE OF THE ELEMENT

ANGLES OF SIGMA-1 ANGLE IS MEASURED POSITIVE FROM THE ELEMENT X-AXIS IN A POSITIVE SENSE ABOUT THE ELEMENT Z AXIS

ELEM NO	LOAD CASE	NODE NO	TOP SURFACE SIGMA-1	TOP SURFACE SIGMA-2	TOP SURFACE ANGLE	MIDDLE SURFACE SIGMA-1	MIDDLE SURFACE SIGMA-2	MIDDLE SURFACE ANGLE	BOTTOM SURFACE SIGMA-1	BOTTOM SURFACE SIGMA 2	BOTTOM SURFACE ANGLE
1	1	1	1.76E+08	-2.69E+07	55.9	0.00E+00	0.00E+00	0.0	2.69E+07	-1.76E+08	-34.1
1	1	35	2.30E+08	-2.82E+07	86.5	0.00E+00	0.00E+00	0.0	2.82E+07	-2.30E+08	-3.5
1	1	51	-1.20E+07	-1.42E+08	52.2	0.00E+00	0.00E+00	0.0	1.42E+08	1.20E+07	37.8
1	1	6	2.79E+08	8.71E+07	82.0	0.00E+00	0.00E+00	0.0	-8.71E+07	-2.79E+08	8.0
1	1	-1	1.44E+08	3.63E+07	85.2	0.00E+00	0.00E+00	0.0	-3.63E+07	-1.44E+08	-4.8
1	1	52	1.94E+08	2.90E+07	84.1	0.00E+00	0.00E+00	0.0	-2.90E+07	1.94E+08	-5.9
1	1	7	2.07E+08	6.21E+07	79.7	0.00E+00	0.00E+00	0.0	-6.21E+07	-2.07E+08	-10.3
1	1	36	2.03E+08	7.30E+07	80.6	0.00E+00	0.00E+00	0.0	-7.30E+07	-2.03E+08	1.4
1	1	53	1.47E+08	6.04E+07	75.6	0.00E+00	0.00E+00	0.0	-6.04E+07	-1.47E+08	-14.4
2	1	7	1.15E+08	3.75E+07	87.1	0.00E+00	0.00E+00	0.0	-3.75E+07	1.15E+08	2.9
2	1	36	2.08E+08	7.18E+07	89.1	0.00E+00	0.00E+00	0.0	-7.18E+07	-2.08E+08	0.9
2	1	53	1.45E+08	4.02E+07	81.5	0.00E+00	0.00E+00	0.0	-4.02E+07	-1.45E+08	-8.5
2	1	8	1.81E+08	5.95E+07	88.9	0.00E+00	0.00E+00	0.0	-5.95E+07	-1.81E+08	-1.1
2	1	-2	1.88E+08	6.40E+07	89.7	0.00E+00	0.00E+00	0.0	6.40E+07	-1.88E+08	0.3
2	1	54	1.67E+08	5.88E+07	-88.3	0.00E+00	0.00E+00	0.0	-5.88E+07	-1.67E+08	1.7
2	1	9	2.01E+08	6.60E+07	-87.4	0.00E+00	0.00E+00	0.0	-6.60E+07	-2.01E+08	2.6
2	1	37	1.79E+08	5.33E+07	89.8	0.00E+00	0.00E+00	0.0	-5.33E+07	-1.79E+08	0.2
2	1	55	1.51E+08	5.05E+07	88.7	0.00E+00	0.00E+00	0.0	-5.05E+07	1.51E+08	-1.3
3	1	9	2.19E+08	7.21E+07	-89.9	0.00E+00	0.00E+00	0.0	-7.21E+07	-2.19E+08	0.1
3	1	37	1.79E+08	5.88E+07	89.7	0.00E+00	0.00E+00	0.0	-5.88E+07	1.79E+08	-0.3
3	1	55	1.61E+08	4.70E+07	88.0	0.00E+00	0.00E+00	0.0	-4.70E+07	-1.61E+08	-2.0
3	1	10	2.03E+08	6.71E+07	-90.0	0.00E+00	0.00E+00	0.0	-6.71E+07	-2.03E+08	0.0
3	1	-3	1.78E+08	5.86E+07	-89.6	0.00E+00	0.00E+00	0.0	-5.86E+07	-1.78E+08	-0.4
3	1	56	1.63E+08	5.27E+07	-89.5	0.00E+00	0.00E+00	0.0	-5.27E+07	-1.63E+08	0.5
3	1	11	1.86E+08	6.13E+07	89.9	0.00E+00	0.00E+00	0.0	-6.13E+07	-1.86E+08	-0.1
3	1	38	1.79E+08	5.91E+07	-89.6	0.00E+00	0.00E+00	0.0	-5.91E+07	-1.79E+08	0.4
3	1	57	1.49E+08	4.83E+07	-88.1	0.00E+00	0.00E+00	0.0	-4.83E+07	-1.49E+08	1.9
4	1	11	1.86E+08	6.15E+07	89.9	0.00E+00	0.00E+00	0.0	-6.15E+07	-1.86E+08	-0.1
4	1	38	1.74E+08	5.69E+07	-88.8	0.00E+00	0.00E+00	0.0	-5.69E+07	-1.74E+08	1.2
4	1	57	1.59E+08	5.09E+07	-90.0	0.00E+00	0.00E+00	0.0	-5.09E+07	-1.59E+08	0.0
4	1	12	1.82E+08	5.99E+07	-90.0	0.00E+00	0.00E+00	0.0	-5.99E+07	-1.82E+08	0.0
4	1	-4	1.68E+08	5.54E+07	-88.7	0.00E+00	0.00E+00	0.0	-5.54E+07	-1.68E+08	1.3
4	1	58	1.57E+08	5.07E+07	-87.8	0.00E+00	0.00E+00	0.0	-5.07E+07	-1.57E+08	2.2
4	1	13	1.72E+08	5.67E+07	-90.0	0.00E+00	0.00E+00	0.0	-5.67E+07	-1.72E+08	0.0
4	1	39	1.63E+08	5.35E+07	-88.6	0.00E+00	0.00E+00	0.0	-5.35E+07	-1.63E+08	1.4
4	1	59	1.36E+08	4.43E+07	-86.2	0.00E+00	0.00E+00	0.0	-4.43E+07	-1.36E+08	3.8
5	1	13	1.73E+08	5.70E+07	89.9	0.00E+00	0.00E+00	0.0	-5.70E+07	-1.73E+08	-0.1
5	1	39	1.60E+08	5.23E+07	-88.0	0.00E+00	0.00E+00	0.0	-5.23E+07	-1.60E+08	2.0
5	1	59	1.45E+08	4.64E+07	-88.1	0.00E+00	0.00E+00	0.0	-4.64E+07	-1.45E+08	1.9
5	1	14	1.63E+08	5.36E+07	-90.0	0.00E+00	0.00E+00	0.0	-5.36E+07	-1.63E+08	0.0
5	1	-5	1.52E+08	4.98E+07	-87.9	0.00E+00	0.00E+00	0.0	-4.98E+07	-1.52E+08	2.1
5	1	60	1.42E+08	4.56E+07	-86.1	0.00E+00	0.00E+00	0.0	-4.56E+07	-1.42E+08	3.9

ELEM NO	LOAD CASE	NODE NO	TOP SURFACE SIGMA 1	TOP SURFACE SIGMA 2	TOP SURFACE ANGLE	MIDDLE SURFACE SIGMA 1	MIDDLE SURFACE SIGMA 2	MIDDLE SURFACE ANGLE	BOTTOM SURFACE SIGMA 1	BOTTOM SURFACE SIGMA 2	BOTTOM SURFACE ANGLE
5	1	15	1.49E+08	4.93E+07	90.0	0.00E+00	0.00E+00	0.0	-4.93E+07	-1.49E+08	0.0
5	1	40	1.45E+08	4.75E+07	87.8	0.00E+00	0.00E+00	0.0	-4.75E+07	1.45E+08	2.2
5	1	61	1.24E+08	4.01E+07	84.4	0.00E+00	0.00E+00	0.0	4.01E+07	-1.24E+08	5.6
6	1	15	1.50E+08	4.94E+07	89.9	0.00E+00	0.00E+00	0.0	4.94E+07	-1.50E+08	-0.1
6	1	40	1.42E+08	4.62E+07	87.2	0.00E+00	0.00E+00	0.0	4.62E+07	1.42E+08	2.8
6	1	61	1.32E+08	4.22E+07	86.3	0.00E+00	0.00E+00	0.0	-4.22E+07	-1.32E+08	3.7
6	1	16	1.40E+08	4.61E+07	90.0	0.00E+00	0.00E+00	0.0	-4.61E+07	-1.40E+08	0.0
6	1	-6	1.33E+08	4.35E+07	87.1	0.00E+00	0.00E+00	0.0	4.35E+07	-1.33E+08	2.9
6	1	62	1.26E+08	4.03E+07	-84.5	0.00E+00	0.00E+00	0.0	-4.03E+07	-1.26E+08	5.5
6	1	17	1.28E+08	4.22E+07	89.9	0.00E+00	0.00E+00	0.0	4.22E+07	-1.28E+08	-0.1
6	1	41	1.25E+08	4.12E+07	87.2	0.00E+00	0.00E+00	0.0	4.12E+07	-1.25E+08	2.8
6	1	63	1.09E+08	3.51E+07	-82.9	0.00E+00	0.00E+00	0.0	-3.51E+07	-1.09E+08	7.1
7	1	17	1.28E+08	4.23E+07	89.9	0.00E+00	0.00E+00	0.0	4.23E+07	1.28E+08	-0.1
7	1	41	1.23E+08	4.00E+07	86.5	0.00E+00	0.00E+00	0.0	-4.00E+07	1.23E+08	3.5
7	1	63	1.16E+08	3.71E+07	84.8	0.00E+00	0.00E+00	0.0	-3.71E+07	1.16E+08	5.2
7	1	18	1.10E+08	3.90E+07	90.0	0.00E+00	0.00E+00	0.0	-3.90E+07	1.10E+08	0.0
7	1	-7	1.14E+08	3.74E+07	86.5	0.00E+00	0.00E+00	0.0	3.74E+07	-1.14E+08	3.5
7	1	64	1.09E+08	3.48E+07	83.2	0.00E+00	0.00E+00	0.0	-3.48E+07	-1.09E+08	6.8
7	1	19	1.00E+08	3.55E+07	90.0	0.00E+00	0.00E+00	0.0	-3.55E+07	-1.00E+08	0.0
7	1	42	1.07E+08	3.51E+07	86.6	0.00E+00	0.00E+00	0.0	3.51E+07	-1.07E+08	3.4
7	1	65	9.56E+07	3.06E+07	81.7	0.00E+00	0.00E+00	0.0	-3.06E+07	-9.56E+07	8.3
8	1	19	1.00E+08	3.56E+07	89.9	0.00E+00	0.00E+00	0.0	3.56E+07	-1.00E+08	-0.1
8	1	42	1.05E+08	3.40E+07	85.9	0.00E+00	0.00E+00	0.0	-3.40E+07	1.05E+08	4.1
8	1	65	1.00E+08	3.22E+07	83.5	0.00E+00	0.00E+00	0.0	-3.22E+07	1.00E+08	6.5
8	1	20	9.87E+07	3.26E+07	90.0	0.00E+00	0.00E+00	0.0	-3.26E+07	-9.87E+07	0.0
8	1	8	9.60E+07	3.16E+07	85.9	0.00E+00	0.00E+00	0.0	-3.16E+07	-9.60E+07	4.1
8	1	66	9.41E+07	2.97E+07	-82.1	0.00E+00	0.00E+00	0.0	-2.97E+07	-9.41E+07	7.9
8	1	21	8.93E+07	2.95E+07	89.9	0.00E+00	0.00E+00	0.0	-2.95E+07	-8.93E+07	-0.1
8	1	43	9.00E+07	2.95E+07	-85.9	0.00E+00	0.00E+00	0.0	-2.95E+07	-9.00E+07	4.1
8	1	67	8.26E+07	2.61E+07	-80.5	0.00E+00	0.00E+00	0.0	-2.61E+07	-8.26E+07	9.5
9	1	21	8.95E+07	2.95E+07	89.9	0.00E+00	0.00E+00	0.0	-2.95E+07	-8.95E+07	-0.1
9	1	43	8.85E+07	2.87E+07	-85.3	0.00E+00	0.00E+00	0.0	-2.87E+07	-8.85E+07	4.7
9	1	67	8.63E+07	2.74E+07	-82.2	0.00E+00	0.00E+00	0.0	-2.74E+07	-8.63E+07	7.8
9	1	22	8.11E+07	2.67E+07	89.9	0.00E+00	0.00E+00	0.0	-2.67E+07	-8.11E+07	0.1
9	1	-9	8.11E+07	2.63E+07	-85.1	0.00E+00	0.00E+00	0.0	-2.63E+07	-8.11E+07	4.9
9	1	68	8.04E+07	2.50E+07	-80.8	0.00E+00	0.00E+00	0.0	-2.50E+07	8.04E+07	9.2
9	1	23	7.27E+07	2.40E+07	89.9	0.00E+00	0.00E+00	0.0	2.40E+07	-7.27E+07	0.1
9	1	44	7.49E+07	2.45E+07	-85.1	0.00E+00	0.00E+00	0.0	-2.45E+07	-7.49E+07	4.9
9	1	69	7.07E+07	2.17E+07	-79.1	0.00E+00	0.00E+00	0.0	-2.17E+07	-7.07E+07	10.9
10	1	23	7.26E+07	2.40E+07	89.9	0.00E+00	0.00E+00	0.0	-2.40E+07	-7.26E+07	-0.1
10	1	44	7.37E+07	2.30E+07	84.5	0.00E+00	0.00E+00	0.0	-2.30E+07	-7.37E+07	5.5
10	1	69	7.34E+07	2.29E+07	-80.6	0.00E+00	0.00E+00	0.0	-2.29E+07	-7.34E+07	9.4
10	1	24	6.47E+07	2.13E+07	-89.9	0.00E+00	0.00E+00	0.0	-2.13E+07	-6.47E+07	0.1
10	1	-10	6.68E+07	2.14E+07	-84.0	0.00E+00	0.00E+00	0.0	-2.14E+07	-6.68E+07	6.0
10	1	70	6.81E+07	2.05E+07	-79.3	0.00E+00	0.00E+00	0.0	-2.05E+07	-6.81E+07	10.7
10	1	25	5.71E+07	1.88E+07	89.7	0.00E+00	0.00E+00	0.0	-1.88E+07	-5.71E+07	-0.3
10	1	45	6.09E+07	1.99E+07	-83.9	0.00E+00	0.00E+00	0.0	-1.99E+07	-6.09E+07	6.1
10	1	71	5.98E+07	1.72E+07	-77.1	0.00E+00	0.00E+00	0.0	-1.72E+07	-5.98E+07	12.9
11	1	25	5.67E+07	1.87E+07	89.9	0.00E+00	0.00E+00	0.0	-1.87E+07	-5.67E+07	-0.1
11	1	45	6.01E+07	1.92E+07	-83.3	0.00E+00	0.00E+00	0.0	-1.92E+07	6.01E+07	6.7
11	1	71	6.17E+07	1.86E+07	-78.4	0.00E+00	0.00E+00	0.0	-1.86E+07	-6.17E+07	11.6

ELEM NO	LOAD CASE	NODE NO	TOP SURFACE SIGMA 1	TOP SURFACE SIGMA 2	TOP SURFACE ANGLE	MIDDLE SURFACE SIGMA 1	MIDDLE SURFACE SIGMA 2	MIDDLE SURFACE ANGLE	BOTTOM SURFACE SIGMA 1	BOTTOM SURFACE SIGMA 2	BOTTOM SURFACE ANGLE
11	1	26	4.90E+07	1.62E+07	89.9	0.00E+00	0.00E+00	0.0	1.62E+07	-4.90E+07	0.1
11	1	11	5.34E+07	1.67E+07	82.3	0.00E+00	0.00E+00	0.0	-1.67E+07	5.34E+07	7.7
11	1	72	5.70E+07	1.63E+07	77.2	0.00E+00	0.00E+00	0.0	1.63E+07	5.70E+07	12.8
11	1	27	4.21E+07	1.39E+07	89.5	0.00E+00	0.00E+00	0.0	1.39E+07	-4.21E+07	0.5
11	1	46	4.79E+07	1.55E+07	82.8	0.00E+00	0.00E+00	0.0	1.55E+07	4.79E+07	8.8
11	1	73	4.90E+07	1.20E+07	74.3	0.00E+00	0.00E+00	0.0	-1.20E+07	-4.90E+07	15.7
12	1	27	4.14E+07	1.37E+07	89.9	0.00E+00	0.00E+00	0.0	-1.37E+07	-4.14E+07	-0.1
12	1	46	4.74E+07	1.49E+07	81.5	0.00E+00	0.00E+00	0.0	-1.49E+07	4.74E+07	8.5
12	1	73	5.10E+07	1.43E+07	75.4	0.00E+00	0.00E+00	0.0	-1.43E+07	-5.10E+07	14.6
12	1	28	3.39E+07	1.12E+07	89.8	0.00E+00	0.00E+00	0.0	-1.12E+07	-3.39E+07	0.2
12	1	-12	4.08E+07	1.21E+07	79.8	0.00E+00	0.00E+00	0.0	-1.21E+07	4.08E+07	10.2
12	1	74	4.68E+07	1.23E+07	74.4	0.00E+00	0.00E+00	0.0	1.23E+07	-4.68E+07	15.6
12	1	29	2.76E+07	9.09E+06	89.8	0.00E+00	0.00E+00	0.0	9.09E+06	-2.76E+07	-1.0
12	1	47	3.57E+07	1.14E+07	79.8	0.00E+00	0.00E+00	0.0	1.14E+07	3.57E+07	11.8
12	1	75	4.05E+07	8.45E+06	70.0	0.00E+00	0.00E+00	0.0	8.45E+06	4.05E+07	19.2
13	1	29	2.66E+07	8.77E+06	90.0	0.00E+00	0.00E+00	0.0	-8.77E+06	2.66E+07	0.0
13	1	47	3.54E+07	1.08E+07	78.7	0.00E+00	0.00E+00	0.0	-1.08E+07	-3.54E+07	11.3
13	1	75	4.11E+07	1.00E+07	71.4	0.00E+00	0.00E+00	0.0	1.00E+07	-4.11E+07	18.6
13	1	30	1.97E+07	6.49E+06	89.5	0.00E+00	0.00E+00	0.0	6.49E+06	-1.97E+07	0.5
13	1	-13	2.90E+07	7.68E+06	75.6	0.00E+00	0.00E+00	0.0	7.68E+06	-2.90E+07	14.4
13	1	76	3.73E+07	8.42E+06	70.6	0.00E+00	0.00E+00	0.0	8.42E+06	-3.73E+07	19.4
13	1	31	1.46E+07	4.78E+06	87.5	0.00E+00	0.00E+00	0.0	-4.78E+06	-1.46E+07	-2.5
13	1	48	2.44E+07	7.50E+06	74.3	0.00E+00	0.00E+00	0.0	-7.50E+06	2.44E+07	15.7
13	1	77	3.16E+07	3.91E+06	66.1	0.00E+00	0.00E+00	0.0	-3.91E+06	-3.16E+07	23.9
14	1	31	1.32E+07	4.35E+06	89.8	0.00E+00	0.00E+00	0.0	-4.35E+06	-1.32E+07	0.2
14	1	48	2.44E+07	6.97E+06	74.2	0.00E+00	0.00E+00	0.0	-6.97E+06	-2.44E+07	15.8
14	1	77	3.23E+07	5.96E+06	66.7	0.00E+00	0.00E+00	0.0	-5.96E+06	-3.23E+07	23.3
14	1	32	7.44E+06	2.45E+06	88.9	0.00E+00	0.00E+00	0.0	-2.45E+06	-7.44E+06	1.1
14	1	14	1.03E+07	3.67E+06	69.4	0.00E+00	0.00E+00	0.0	-3.67E+06	-1.03E+07	20.6
14	1	78	2.91E+07	4.96E+06	65.5	0.00E+00	0.00E+00	0.0	4.96E+06	2.91E+07	24.5
14	1	33	3.94E+06	1.21E+06	88.7	0.00E+00	0.00E+00	0.0	-1.21E+06	-3.94E+06	-9.3
14	1	49	1.44E+07	4.12E+06	66.8	0.00E+00	0.00E+00	0.0	-4.12E+06	-1.44E+07	23.2
14	1	79	2.41E+07	3.52E+05	60.3	0.00E+00	0.00E+00	0.0	-3.52E+05	2.41E+07	29.7
15	1	33	2.50E+06	8.24E+05	89.3	0.00E+00	0.00E+00	0.0	-8.24E+05	-2.50E+06	0.7
15	1	49	1.41E+07	3.00E+06	66.4	0.00E+00	0.00E+00	0.0	-3.00E+06	-1.41E+07	23.6
15	1	79	2.48E+07	3.25E+06	-60.1	0.00E+00	0.00E+00	0.0	-3.25E+06	-2.48E+07	29.9
15	1	34	-2.30E+05	-7.06E+05	-4.2	0.00E+00	0.00E+00	0.0	7.06E+05	2.30E+05	85.8
15	1	-15	9.40E+06	5.27E+05	59.8	0.00E+00	0.00E+00	0.0	5.27E+05	-9.40E+06	30.2
15	1	80	1.99E+07	0.00E+05	-56.9	0.00E+00	0.00E+00	0.0	-8.00E+05	-1.99E+07	33.1
15	1	3	8.01E+05	-2.50E+06	5.8	0.00E+00	0.00E+00	0.0	2.50E+06	8.01E+05	-84.2
15	1	50	6.37E+06	6.00E+05	-53.3	0.00E+00	0.00E+00	0.0	-6.00E+05	-6.37E+06	36.7
15	1	81	1.62E+07	4.35E+05	53.4	0.00E+00	0.00E+00	0.0	-4.35E+05	-1.62E+07	36.6
16	1	51	1.10E+08	-5.57E+07	79.5	0.00E+00	0.00E+00	0.0	5.57E+07	-1.10E+08	-10.5
16	1	82	8.91E+07	-7.51E+07	83.0	0.00E+00	0.00E+00	0.0	7.51E+07	-8.91E+07	7.0
16	1	98	1.01E+07	-5.47E+07	-51.9	0.00E+00	0.00E+00	0.0	5.47E+07	-1.01E+07	30.1
16	1	52	1.37E+08	1.65E+07	87.1	0.00E+00	0.00E+00	0.0	-1.65E+07	-1.37E+08	-2.9
16	1	-16	1.09E+08	-4.59E+06	88.8	0.00E+00	0.00E+00	0.0	4.59E+06	-1.09E+08	-9.2
16	1	99	1.05E+08	-1.58E+07	83.4	0.00E+00	0.00E+00	0.0	1.58E+07	-1.05E+08	-6.6
16	1	53	1.69E+08	7.45E+07	79.8	0.00E+00	0.00E+00	0.0	-7.45E+07	-1.69E+08	-11.8
16	1	83	1.27E+08	2.65E+07	82.8	0.00E+00	0.00E+00	0.0	-2.65E+07	-1.27E+08	-8.8
16	1	100	1.18E+08	1.26E+07	72.9	0.00E+00	0.00E+00	0.0	-1.26E+07	-1.18E+08	-17.1

ELEM NO	LOAD CASE	NODE NO	TOP SURFACE SIGMA-1	TOP SURFACE SIGMA-2	TOP SURFACE ANGLE	MIDDLE SURFACE SIGMA-1	MIDDLE SURFACE SIGMA-2	MIDDLE SURFACE ANGLE	BOTTOM SURFACE SIGMA-1	BOTTOM SURFACE SIGMA-2	BOTTOM SURFACE ANGLE
17	1	53	1.40E+08	4.70E+07	86.5	0.00E+00	0.00E+00	0.0	4.70E+07	-1.40E+08	-3.5
17	1	83	1.32E+08	3.86E+07	79.0	0.00E+00	0.00E+00	0.0	3.86E+07	-1.32E+08	-11.0
17	1	100	1.20E+08	2.00E+06	75.1	0.00E+00	0.00E+00	0.0	-2.00E+06	-1.20E+08	-14.9
17	1	54	1.54E+08	5.20E+07	83.2	0.00E+00	0.00E+00	0.0	-5.20E+07	-1.54E+08	-6.8
17	1	-17	1.41E+08	4.52E+07	82.8	0.00E+00	0.00E+00	0.0	-4.52E+07	-1.41E+08	-7.2
17	1	101	1.17E+08	3.36E+07	80.5	0.00E+00	0.00E+00	0.0	-3.36E+07	1.17E+08	-9.5
17	1	55	1.63E+08	5.58E+07	89.0	0.00E+00	0.00E+00	0.0	-5.58E+07	-1.63E+08	1.0
17	1	84	1.46E+08	4.70E+07	83.8	0.00E+00	0.00E+00	0.0	-4.70E+07	-1.46E+08	-6.2
17	1	102	1.17E+08	3.66E+07	79.9	0.00E+00	0.00E+00	0.0	-3.66E+07	1.17E+08	-10.1
18	1	55	1.86E+08	5.65E+07	87.6	0.00E+00	0.00E+00	0.0	5.65E+07	-1.86E+08	-2.4
18	1	84	1.36E+08	4.60E+07	85.4	0.00E+00	0.00E+00	0.0	4.60E+07	-1.36E+08	-4.6
18	1	102	1.30E+08	3.43E+07	79.2	0.00E+00	0.00E+00	0.0	3.43E+07	-1.30E+08	-10.8
18	1	56	1.62E+08	5.16E+07	85.2	0.00E+00	0.00E+00	0.0	-5.16E+07	-1.62E+08	4.8
18	1	18	1.44E+08	4.55E+07	85.7	0.00E+00	0.00E+00	0.0	-4.55E+07	1.44E+08	-4.3
18	1	103	1.25E+08	3.81E+07	84.4	0.00E+00	0.00E+00	0.0	-3.81E+07	1.25E+08	-5.6
18	1	57	1.54E+08	5.03E+07	89.2	0.00E+00	0.00E+00	0.0	-5.03E+07	-1.54E+08	-0.8
18	1	85	1.44E+08	4.40E+07	86.2	0.00E+00	0.00E+00	0.0	4.40E+07	1.44E+08	-3.8
18	1	104	1.16E+08	3.42E+07	85.9	0.00E+00	0.00E+00	0.0	-3.42E+07	-1.16E+08	-4.1
19	1	57	1.70E+08	5.45E+07	86.4	0.00E+00	0.00E+00	0.0	5.45E+07	-1.70E+08	-3.6
19	1	85	1.38E+08	4.34E+07	87.2	0.00E+00	0.00E+00	0.0	-4.34E+07	-1.38E+08	-2.8
19	1	104	1.26E+08	3.51E+07	84.1	0.00E+00	0.00E+00	0.0	-3.51E+07	-1.26E+08	-5.9
19	1	58	1.52E+08	4.89E+07	87.8	0.00E+00	0.00E+00	0.0	-4.89E+07	-1.52E+08	-2.2
19	1	-19	1.37E+08	4.26E+07	88.2	0.00E+00	0.00E+00	0.0	-4.26E+07	-1.37E+08	-1.8
19	1	105	1.22E+08	3.54E+07	88.0	0.00E+00	0.00E+00	0.0	-3.54E+07	-1.22E+08	-2.0
19	1	59	1.45E+08	4.72E+07	89.7	0.00E+00	0.00E+00	0.0	-4.72E+07	1.45E+08	0.3
19	1	86	1.35E+08	4.12E+07	89.2	0.00E+00	0.00E+00	0.0	-4.12E+07	-1.35E+08	-0.8
19	1	106	1.08E+08	3.19E+07	89.8	0.00E+00	0.00E+00	0.0	-3.19E+07	-1.08E+08	-0.2
20	1	59	1.55E+08	4.96E+07	88.3	0.00E+00	0.00E+00	0.0	-4.96E+07	-1.55E+08	-1.7
20	1	86	1.30E+08	4.09E+07	-89.9	0.00E+00	0.00E+00	0.0	-4.09E+07	-1.30E+08	0.1
20	1	106	1.18E+08	3.20E+07	87.9	0.00E+00	0.00E+00	0.0	-3.20E+07	-1.18E+08	-2.1
20	1	60	1.39E+08	4.45E+07	89.6	0.00E+00	0.00E+00	0.0	-4.45E+07	-1.39E+08	-0.4
20	1	-20	1.26E+08	3.88E+07	-88.9	0.00E+00	0.00E+00	0.0	3.88E+07	-1.26E+08	1.1
20	1	107	1.13E+08	3.22E+07	-88.0	0.00E+00	0.00E+00	0.0	-3.22E+07	-1.13E+08	2.0
20	1	61	1.30E+08	4.19E+07	-88.1	0.00E+00	0.00E+00	0.0	-4.19E+07	-1.30E+08	1.9
20	1	87	1.22E+08	3.73E+07	-88.2	0.00E+00	0.00E+00	0.0	-3.73E+07	-1.22E+08	1.8
20	1	108	9.86E+07	2.83E+07	85.6	0.00E+00	0.00E+00	0.0	-2.83E+07	-9.86E+07	4.4
21	1	61	1.38E+08	4.42E+07	90.0	0.00E+00	0.00E+00	0.0	-4.42E+07	-1.38E+08	0.0
21	1	87	1.18E+08	3.68E+07	-87.2	0.00E+00	0.00E+00	0.0	-3.68E+07	-1.18E+08	2.8
21	1	108	1.07E+08	2.91E+07	-88.2	0.00E+00	0.00E+00	0.0	-2.91E+07	-1.07E+08	1.8
21	1	62	1.23E+08	3.95E+07	-88.8	0.00E+00	0.00E+00	0.0	-3.95E+07	-1.23E+08	1.2
21	1	-21	1.13E+08	3.45E+07	-86.3	0.00E+00	0.00E+00	0.0	-3.45E+07	-1.13E+08	3.7
21	1	109	1.02E+08	2.87E+07	-84.3	0.00E+00	0.00E+00	0.0	-2.87E+07	-1.02E+08	5.7
21	1	63	1.14E+08	3.65E+07	-86.7	0.00E+00	0.00E+00	0.0	-3.65E+07	-1.14E+08	3.3
21	1	88	1.09E+08	3.31E+07	-85.9	0.00E+00	0.00E+00	0.0	-3.31E+07	-1.09E+08	4.1
21	1	110	8.82E+07	2.49E+07	-81.7	0.00E+00	0.00E+00	0.0	-2.49E+07	-8.82E+07	8.3
22	1	63	1.20E+08	3.87E+07	-88.7	0.00E+00	0.00E+00	0.0	-3.87E+07	-1.20E+08	1.3
22	1	88	1.05E+08	3.26E+07	-84.8	0.00E+00	0.00E+00	0.0	-3.26E+07	-1.05E+08	5.2
22	1	110	9.58E+07	2.60E+07	-84.8	0.00E+00	0.00E+00	0.0	-2.60E+07	-9.58E+07	5.2
22	1	64	1.00E+08	3.43E+07	-87.4	0.00E+00	0.00E+00	0.0	-3.43E+07	-1.00E+08	2.6
22	1	-22	9.96E+07	3.02E+07	-84.2	0.00E+00	0.00E+00	0.0	-3.02E+07	-9.96E+07	5.8
22	1	111	9.05E+07	2.52E+07	-81.2	0.00E+00	0.00E+00	0.0	-2.52E+07	-9.05E+07	8.8

ELEM NO	LOAD CASE	NODE NO	TOP SURFACE SIGMA 1	TOP SURFACE SIGMA 2	TOP SURFACE ANGLE	MIDDLE SURFACE SIGMA 1	MIDDLE SURFACE SIGMA 2	MIDDLE SURFACE ANGLE	BOTTOM SURFACE SIGMA 1	BOTTOM SURFACE SIGMA 2	BOTTOM SURFACE ANGLE
22	1	65	9.85E+07	3.15E+07	85.4	0.00E+00	0.00E+00	0.0	-3.15E+07	9.85E+07	4.6
22	1	89	9.54E+07	2.88E+07	84.0	0.00E+00	0.00E+00	0.0	-2.88E+07	9.54E+07	6.0
22	1	112	7.87E+07	2.21E+07	-78.8	0.00E+00	0.00E+00	0.0	-2.21E+07	-7.87E+07	11.2
23	1	65	1.04E+08	3.33E+07	87.5	0.00E+00	0.00E+00	0.0	3.33E+07	1.04E+08	2.5
23	1	89	9.26E+07	2.83E+07	-82.8	0.00E+00	0.00E+00	0.0	2.83E+07	9.26E+07	7.2
23	1	112	8.50E+07	2.30E+07	82.1	0.00E+00	0.00E+00	0.0	-2.30E+07	8.50E+07	7.9
23	1	66	9.28E+07	2.93E+07	-86.2	0.00E+00	0.00E+00	0.0	-2.93E+07	9.28E+07	3.8
23	1	-23	8.72E+07	2.61E+07	82.4	0.00E+00	0.00E+00	0.0	-2.61E+07	-8.72E+07	7.6
23	1	113	8.00E+07	2.10E+07	-78.7	0.00E+00	0.00E+00	0.0	-2.10E+07	-8.00E+07	11.3
23	1	67	8.45E+07	2.66E+07	84.3	0.00E+00	0.00E+00	0.0	-2.66E+07	8.45E+07	5.7
23	1	90	8.31E+07	2.46E+07	82.3	0.00E+00	0.00E+00	0.0	-2.46E+07	8.31E+07	7.7
23	1	114	7.02E+07	1.92E+07	76.5	0.00E+00	0.00E+00	0.0	1.92E+07	-7.02E+07	13.5
24	1	67	8.91E+07	2.83E+07	86.3	0.00E+00	0.00E+00	0.0	-2.83E+07	8.91E+07	3.7
24	1	90	8.08E+07	2.41E+07	81.1	0.00E+00	0.00E+00	0.0	2.41E+07	8.08E+07	8.9
24	1	114	7.52E+07	2.00E+07	79.8	0.00E+00	0.00E+00	0.0	2.00E+07	7.52E+07	10.2
24	1	68	7.94E+07	2.46E+07	84.9	0.00E+00	0.00E+00	0.0	-2.46E+07	7.94E+07	5.1
24	1	-24	7.59E+07	2.21E+07	80.7	0.00E+00	0.00E+00	0.0	-2.21E+07	7.59E+07	9.3
24	1	115	7.00E+07	1.84E+07	-76.7	0.00E+00	0.00E+00	0.0	-1.84E+07	-7.00E+07	13.3
24	1	69	7.21E+07	2.21E+07	83.0	0.00E+00	0.00E+00	0.0	-2.21E+07	-7.21E+07	7.0
24	1	91	7.22E+07	2.06E+07	80.6	0.00E+00	0.00E+00	0.0	-2.06E+07	-7.22E+07	9.4
24	1	116	6.29E+07	1.63E+07	-74.7	0.00E+00	0.00E+00	0.0	-1.63E+07	-6.29E+07	15.3
25	1	69	7.56E+07	2.37E+07	84.9	0.00E+00	0.00E+00	0.0	-2.37E+07	7.56E+07	5.1
25	1	91	7.03E+07	1.99E+07	-79.4	0.00E+00	0.00E+00	0.0	-1.99E+07	7.03E+07	10.6
25	1	116	6.65E+07	1.69E+07	-77.5	0.00E+00	0.00E+00	0.0	-1.69E+07	-6.65E+07	12.5
25	1	70	6.73E+07	2.02E+07	-83.2	0.00E+00	0.00E+00	0.0	-2.02E+07	-6.73E+07	6.8
25	1	-25	6.60E+07	1.82E+07	-78.8	0.00E+00	0.00E+00	0.0	-1.82E+07	-6.60E+07	11.2
25	1	117	6.27E+07	1.50E+07	-74.9	0.00E+00	0.00E+00	0.0	-1.50E+07	-6.27E+07	15.1
25	1	71	6.09E+07	1.76E+07	-81.4	0.00E+00	0.00E+00	0.0	-1.76E+07	-6.09E+07	8.6
25	1	92	6.24E+07	1.66E+07	-78.5	0.00E+00	0.00E+00	0.0	-1.66E+07	-6.24E+07	11.5
25	1	118	5.65E+07	1.31E+07	-72.9	0.00E+00	0.00E+00	0.0	-1.31E+07	-5.65E+07	17.1
26	1	71	6.33E+07	1.92E+07	84.0	0.00E+00	0.00E+00	0.0	1.92E+07	-6.33E+07	7.0
26	1	92	6.11E+07	1.59E+07	77.5	0.00E+00	0.00E+00	0.0	-1.59E+07	-6.11E+07	12.5
26	1	118	5.90E+07	1.39E+07	-75.2	0.00E+00	0.00E+00	0.0	-1.39E+07	5.90E+07	14.8
26	1	72	5.63E+07	1.60E+07	81.0	0.00E+00	0.00E+00	0.0	-1.60E+07	5.63E+07	9.0
26	1	-26	5.72E+07	1.43E+07	-76.6	0.00E+00	0.00E+00	0.0	-1.43E+07	-5.72E+07	13.4
26	1	119	5.59E+07	1.17E+07	73.0	0.00E+00	0.00E+00	0.0	-1.17E+07	-5.59E+07	17.0
26	1	73	5.07E+07	1.34E+07	-79.2	0.00E+00	0.00E+00	0.0	-1.34E+07	5.07E+07	10.8
26	1	93	5.39E+07	1.29E+07	75.9	0.00E+00	0.00E+00	0.0	-1.29E+07	-5.39E+07	14.1
26	1	120	5.10E+07	9.84E+06	-70.9	0.00E+00	0.00E+00	0.0	-9.84E+06	-5.10E+07	19.1
27	1	73	5.20E+07	1.49E+07	-80.4	0.00E+00	0.00E+00	0.0	-1.49E+07	-5.20E+07	9.6
27	1	93	5.30E+07	1.20E+07	-75.1	0.00E+00	0.00E+00	0.0	-1.20E+07	-5.30E+07	14.9
27	1	120	5.26E+07	1.07E+07	-72.6	0.00E+00	0.00E+00	0.0	-1.07E+07	-5.26E+07	17.4
27	1	74	4.63E+07	1.20E+07	-77.9	0.00E+00	0.00E+00	0.0	-1.20E+07	-4.63E+07	12.1
27	1	-27	4.94E+07	1.06E+07	-73.8	0.00E+00	0.00E+00	0.0	-1.06E+07	-4.94E+07	16.2
27	1	121	5.01E+07	8.37E+06	-71.0	0.00E+00	0.00E+00	0.0	-8.37E+06	-5.01E+07	19.0
27	1	75	4.12E+07	9.19E+06	-76.3	0.00E+00	0.00E+00	0.0	-9.19E+06	-4.12E+07	13.7
27	1	94	4.63E+07	9.23E+06	-72.7	0.00E+00	0.00E+00	0.0	-9.23E+06	-4.63E+07	17.3
27	1	122	4.64E+07	6.52E+06	-68.8	0.00E+00	0.00E+00	0.0	-6.52E+06	-4.64E+07	21.2
28	1	75	4.14E+07	1.05E+07	-76.4	0.00E+00	0.00E+00	0.0	-1.05E+07	-4.14E+07	13.6
28	1	94	4.57E+07	8.10E+06	-72.2	0.00E+00	0.00E+00	0.0	-8.10E+06	-4.57E+07	17.8
28	1	122	4.72E+07	7.53E+06	-69.7	0.00E+00	0.00E+00	0.0	-7.53E+06	-4.72E+07	20.3

ELEM NO	LOAD CASE	NODE NO	TOP SURFACE SIGMA 1	TOP SURFACE SIGMA 2	TOP SURFACE ANGLE	MIDDLE SURFACE SIGMA 1	MIDDLE SURFACE SIGMA 2	MIDDLE SURFACE ANGLE	BOTTOM SURFACE SIGMA 1	BOTTOM SURFACE SIGMA 2	BOTTOM SURFACE ANGLE
28	1	76	3.71E+07	8.07E+06	73.9	0.00E+00	0.00E+00	0.0	-8.07E+06	-3.71E+07	16.1
28	1	-28	4.24E+07	6.88E+06	70.5	0.00E+00	0.00E+00	0.0	6.88E+06	-4.24E+07	19.5
28	1	123	4.52E+07	5.21E+06	68.6	0.00E+00	0.00E+00	0.0	-5.21E+06	4.52E+07	21.4
28	1	77	3.28E+07	5.30E+06	72.8	0.00E+00	0.00E+00	0.0	5.30E+06	-3.28E+07	17.2
28	1	95	3.95E+07	5.00E+06	68.9	0.00E+00	0.00E+00	0.0	-5.00E+06	3.95E+07	21.1
28	1	124	4.21E+07	3.86E+06	66.3	0.00E+00	0.00E+00	0.0	-3.86E+06	4.21E+07	23.7
29	1	77	3.23E+07	6.28E+06	71.5	0.00E+00	0.00E+00	0.0	6.28E+06	-3.23E+07	18.5
29	1	95	3.92E+07	4.62E+06	68.8	0.00E+00	0.00E+00	0.0	4.62E+06	3.92E+07	21.2
29	1	124	4.20E+07	4.65E+06	66.9	0.00E+00	0.00E+00	0.0	4.65E+06	4.20E+07	23.1
29	1	78	2.80E+07	4.43E+06	68.6	0.00E+00	0.00E+00	0.0	-4.43E+06	-2.80E+07	21.4
29	1	-29	3.60E+07	3.51E+06	66.7	0.00E+00	0.00E+00	0.0	3.51E+06	3.60E+07	23.3
29	1	125	4.15E+07	2.42E+06	-65.9	0.00E+00	0.00E+00	0.0	-2.42E+06	4.15E+07	24.1
29	1	79	2.47E+07	1.79E+06	67.0	0.00E+00	0.00E+00	0.0	-1.79E+06	-2.47E+07	23.0
29	1	96	3.33E+07	2.51E+06	64.6	0.00E+00	0.00E+00	0.0	-2.51E+06	-3.33E+07	25.4
29	1	126	3.94E+07	9.09E+05	-63.8	0.00E+00	0.00E+00	0.0	9.09E+05	-3.94E+07	26.2
30	1	79	2.47E+07	3.85E+06	65.4	0.00E+00	0.00E+00	0.0	-3.85E+06	-2.47E+07	24.6
30	1	96	3.28E+07	4.40E+05	-64.8	0.00E+00	0.00E+00	0.0	-4.40E+05	-3.28E+07	25.2
30	1	126	3.90E+07	3.42E+06	-63.2	0.00E+00	0.00E+00	0.0	-3.42E+06	-3.90E+07	26.0
30	1	80	2.06E+07	1.07E+06	-61.4	0.00E+00	0.00E+00	0.0	-1.07E+06	-2.06E+07	28.6
30	1	30	3.08E+07	8.80E+05	62.4	0.00E+00	0.00E+00	0.0	-8.80E+05	-3.08E+07	27.6
30	1	127	3.61E+07	-1.57E+06	-61.9	0.00E+00	0.00E+00	0.0	1.57E+06	-3.61E+07	28.1
30	1	81	1.48E+07	-5.81E+05	-55.4	0.00E+00	0.00E+00	0.0	5.81E+05	-1.48E+07	34.6
30	1	97	2.84E+07	-1.69E+06	-59.4	0.00E+00	0.00E+00	0.0	1.69E+06	-2.84E+07	30.6
30	1	128	3.58E+07	2.77E+06	62.1	0.00E+00	0.00E+00	0.0	-2.77E+06	-3.58E+07	27.9
31	1	98	1.02E+08	-1.44E+07	71.2	0.00E+00	0.00E+00	0.0	1.44E+07	1.02E+08	-10.8
31	1	129	7.26E+07	-2.76E+07	86.6	0.00E+00	0.00E+00	0.0	2.76E+07	-7.26E+07	-3.4
31	1	145	-2.21E+06	-3.27E+07	88.1	0.00E+00	0.00E+00	0.0	3.27E+07	2.21E+06	1.9
31	1	99	9.16E+07	-1.75E+07	81.1	0.00E+00	0.00E+00	0.0	1.75E+07	-9.16E+07	-8.9
31	1	-31	7.37E+07	-2.38E+07	76.9	0.00E+00	0.00E+00	0.0	2.38E+07	-7.37E+07	-13.1
31	1	146	7.20E+07	-2.14E+07	78.0	0.00E+00	0.00E+00	0.0	2.14E+07	-7.20E+07	-12.0
31	1	100	1.07E+08	2.02E+07	74.9	0.00E+00	0.00E+00	0.0	-2.02E+07	-1.07E+08	-15.1
31	1	130	8.82E+07	-5.14E+06	73.1	0.00E+00	0.00E+00	0.0	5.14E+06	-8.82E+07	-16.9
31	1	147	8.66E+07	-8.37E+06	65.3	0.00E+00	0.00E+00	0.0	8.37E+06	8.66E+07	-24.7
32	1	100	1.04E+08	7.91E+06	77.8	0.00E+00	0.00E+00	0.0	-7.91E+06	-1.04E+08	-12.2
32	1	130	8.50E+07	-1.48E+06	72.4	0.00E+00	0.00E+00	0.0	1.48E+06	8.50E+07	-17.6
32	1	147	8.59E+07	-1.97E+07	68.9	0.00E+00	0.00E+00	0.0	1.97E+07	8.59E+07	-21.1
32	1	101	1.14E+08	2.79E+07	71.6	0.00E+00	0.00E+00	0.0	-2.79E+07	-1.14E+08	-18.4
32	1	-32	1.03E+08	1.78E+07	70.8	0.00E+00	0.00E+00	0.0	-1.78E+07	-1.03E+08	-19.2
32	1	148	8.06E+07	2.97E+06	68.3	0.00E+00	0.00E+00	0.0	-2.97E+06	-8.06E+07	-21.7
32	1	102	1.21E+08	4.25E+07	81.1	0.00E+00	0.00E+00	0.0	-4.25E+07	-1.21E+08	-8.9
32	1	131	1.05E+08	2.26E+07	72.7	0.00E+00	0.00E+00	0.0	-2.26E+07	1.05E+08	-17.3
32	1	149	8.83E+07	1.03E+07	66.6	0.00E+00	0.00E+00	0.0	-1.03E+07	-8.83E+07	-23.4
33	1	102	1.39E+08	4.13E+07	78.7	0.00E+00	0.00E+00	0.0	-4.13E+07	-1.39E+08	-11.3
33	1	131	1.00E+08	2.49E+07	72.4	0.00E+00	0.00E+00	0.0	-2.49E+07	-1.00E+08	-17.6
33	1	149	9.42E+07	6.47E+06	67.9	0.00E+00	0.00E+00	0.0	-6.47E+06	-9.42E+07	-22.1
33	1	103	1.25E+08	3.71E+07	78.5	0.00E+00	0.00E+00	0.0	-3.71E+07	-1.25E+08	-11.5
33	1	-33	1.06E+08	2.73E+07	75.6	0.00E+00	0.00E+00	0.0	-2.73E+07	-1.06E+08	-14.4
33	1	150	8.96E+07	1.67E+07	71.9	0.00E+00	0.00E+00	0.0	-1.67E+07	-8.96E+07	-18.1
33	1	104	1.20E+08	3.65E+07	83.3	0.00E+00	0.00E+00	0.0	-3.65E+07	-1.20E+08	-6.7
33	1	132	1.07E+08	2.67E+07	78.2	0.00E+00	0.00E+00	0.0	-2.67E+07	-1.07E+08	-11.8
33	1	151	8.10E+07	1.47E+07	73.4	0.00E+00	0.00E+00	0.0	-1.47E+07	-8.10E+07	-16.6

ELEM NO	LOAD CASE	NODE NO	TOP SURFACE SIGMA 1	TOP SURFACE SIGMA 2	TOP SURFACE ANGLE	MIDDLE SURFACE SIGMA-1	MIDDLE SURFACE SIGMA-2	MIDDLE SURFACE ANGLE	BOTTOM SURFACE SIGMA-1	BOTTOM SURFACE SIGMA 2	BOTTOM SURFACE ANGLE
34	1	104	1.32E+08	3.00E+07	00.9	0.00E+00	0.00E+00	0.0	3.00E+07	-1.32E+00	-9.1
34	1	132	1.02E+08	2.69E+07	79.0	0.00E+00	0.00E+00	0.0	-2.69E+07	1.02E+08	-11.0
34	1	151	9.11E+07	1.33E+07	73.0	0.00E+00	0.00E+00	0.0	-1.33E+07	9.11E+07	-17.0
34	1	105	1.10E+08	3.37E+07	02.5	0.00E+00	0.00E+00	0.0	3.37E+07	-1.10E+08	-7.5
34	1	34	1.03E+08	2.61E+07	81.2	0.00E+00	0.00E+00	0.0	-2.61E+07	-1.03E+08	-8.8
34	1	152	8.60E+07	1.64E+07	70.7	0.00E+00	0.00E+00	0.0	1.64E+07	8.60E+07	-11.3
34	1	106	1.14E+08	3.43E+07	06.9	0.00E+00	0.00E+00	0.0	-3.43E+07	1.14E+08	-3.1
34	1	133	1.01E+08	2.40E+07	03.6	0.00E+00	0.00E+00	0.0	2.40E+07	-1.01E+08	-6.4
34	1	153	7.50E+07	1.36E+07	01.1	0.00E+00	0.00E+00	0.0	-1.36E+07	-7.50E+07	-8.9
35	1	106	1.24E+08	3.47E+07	04.6	0.00E+00	0.00E+00	0.0	-3.47E+07	-1.24E+08	-5.4
35	1	133	9.62E+07	2.42E+07	04.6	0.00E+00	0.00E+00	0.0	-2.42E+07	-9.62E+07	-5.4
35	1	153	8.38E+07	1.22E+07	79.6	0.00E+00	0.00E+00	0.0	-1.22E+07	-8.38E+07	-10.4
35	1	107	1.10E+08	3.11E+07	06.7	0.00E+00	0.00E+00	0.0	3.11E+07	1.10E+08	-3.3
35	1	-35	9.48E+07	2.31E+07	06.7	0.00E+00	0.00E+00	0.0	-2.31E+07	-9.48E+07	-3.3
35	1	154	7.84E+07	1.36E+07	05.9	0.00E+00	0.00E+00	0.0	-1.36E+07	-7.84E+07	-4.1
35	1	108	1.04E+08	3.00E+07	09.1	0.00E+00	0.00E+00	0.0	-3.00E+07	-1.04E+08	0.9
35	1	134	9.22E+07	2.16E+07	08.9	0.00E+00	0.00E+00	0.0	-2.16E+07	9.22E+07	-1.1
35	1	155	6.69E+07	1.12E+07	09.4	0.00E+00	0.00E+00	0.0	-1.12E+07	-6.69E+07	-0.6
36	1	108	1.12E+08	3.09E+07	08.4	0.00E+00	0.00E+00	0.0	-3.09E+07	-1.12E+08	-1.6
36	1	134	8.81E+07	2.15E+07	09.7	0.00E+00	0.00E+00	0.0	-2.15E+07	-8.81E+07	0.3
36	1	155	7.53E+07	1.05E+07	06.5	0.00E+00	0.00E+00	0.0	-1.05E+07	-7.53E+07	-3.5
36	1	109	9.93E+07	2.79E+07	-89.5	0.00E+00	0.00E+00	0.0	-2.79E+07	-9.93E+07	0.5
36	1	-36	8.55E+07	2.03E+07	-88.0	0.00E+00	0.00E+00	0.0	-2.03E+07	-8.55E+07	2.0
36	1	156	7.04E+07	1.14E+07	-87.0	0.00E+00	0.00E+00	0.0	-1.14E+07	-7.04E+07	3.0
36	1	110	9.27E+07	2.62E+07	-85.5	0.00E+00	0.00E+00	0.0	-2.62E+07	-9.27E+07	4.5
36	1	135	8.31E+07	1.93E+07	-86.5	0.00E+00	0.00E+00	0.0	-1.93E+07	-8.31E+07	3.5
36	1	157	5.90E+07	9.19E+06	83.0	0.00E+00	0.00E+00	0.0	-9.19E+06	-5.90E+07	7.0
37	1	110	9.95E+07	2.72E+07	-88.3	0.00E+00	0.00E+00	0.0	-2.72E+07	-9.95E+07	1.7
37	1	135	7.95E+07	1.90E+07	-84.7	0.00E+00	0.00E+00	0.0	-1.90E+07	-7.95E+07	5.3
37	1	157	6.67E+07	9.08E+06	-87.4	0.00E+00	0.00E+00	0.0	-9.08E+06	-6.67E+07	2.6
37	1	111	8.86E+07	2.47E+07	-86.4	0.00E+00	0.00E+00	0.0	-2.47E+07	-8.86E+07	3.6
37	1	-37	7.65E+07	1.79E+07	83.5	0.00E+00	0.00E+00	0.0	-1.79E+07	-7.65E+07	6.5
37	1	158	6.29E+07	9.72E+06	80.8	0.00E+00	0.00E+00	0.0	-9.72E+06	-6.29E+07	9.2
37	1	112	8.21E+07	2.28E+07	82.4	0.00E+00	0.00E+00	0.0	-2.28E+07	-8.21E+07	7.6
37	1	136	7.43E+07	1.70E+07	-82.8	0.00E+00	0.00E+00	0.0	-1.70E+07	-7.43E+07	7.2
37	1	159	5.31E+07	8.17E+06	77.0	0.00E+00	0.00E+00	0.0	-8.17E+06	-5.31E+07	13.0
38	1	112	8.81E+07	2.38E+07	-85.6	0.00E+00	0.00E+00	0.0	-2.38E+07	-8.81E+07	4.4
38	1	136	7.12E+07	1.67E+07	-80.7	0.00E+00	0.00E+00	0.0	-1.67E+07	-7.12E+07	9.3
38	1	159	5.94E+07	8.20E+06	-82.4	0.00E+00	0.00E+00	0.0	-8.20E+06	-5.94E+07	7.6
38	1	113	7.86E+07	2.15E+07	-83.9	0.00E+00	0.00E+00	0.0	-2.15E+07	-7.86E+07	6.1
38	1	-38	6.85E+07	1.56E+07	-00.1	0.00E+00	0.00E+00	0.0	-1.56E+07	-6.85E+07	9.9
38	1	160	5.65E+07	8.44E+06	-76.2	0.00E+00	0.00E+00	0.0	-8.44E+06	-5.65E+07	13.8
38	1	114	7.26E+07	1.95E+07	-80.0	0.00E+00	0.00E+00	0.0	-1.95E+07	-7.26E+07	10.0
38	1	137	6.65E+07	1.48E+07	-79.9	0.00E+00	0.00E+00	0.0	-1.48E+07	-6.65E+07	10.1
38	1	161	4.85E+07	7.59E+06	-72.8	0.00E+00	0.00E+00	0.0	-7.59E+06	-4.85E+07	17.2
39	1	114	7.79E+07	2.06E+07	-83.5	0.00E+00	0.00E+00	0.0	-2.06E+07	-7.79E+07	6.5
39	1	137	6.39E+07	1.45E+07	-77.0	0.00E+00	0.00E+00	0.0	-1.45E+07	-6.39E+07	12.2
39	1	161	5.35E+07	7.58E+06	-78.6	0.00E+00	0.00E+00	0.0	-7.58E+06	-5.35E+07	11.4
39	1	115	6.97E+07	1.82E+07	-81.8	0.00E+00	0.00E+00	0.0	-1.82E+07	-6.97E+07	8.2
39	1	-39	6.15E+07	1.34E+07	-77.6	0.00E+00	0.00E+00	0.0	-1.34E+07	-6.15E+07	12.4
39	1	162	5.12E+07	7.25E+06	73.1	0.00E+00	0.00E+00	0.0	-7.25E+06	-5.12E+07	16.9

ELEM NO	LOAD CASE	NODE NO	TOP SURFACE SIGMA 1	TOP SURFACE SIGMA 2	TOP SURFACE ANGLE	MIDDLE SURFACE SIGMA-1	MIDDLE SURFACE SIGMA 2	MIDDLE SURFACE ANGLE	BOTTOM SURFACE SIGMA 1	BOTTOM SURFACE SIGMA-2	BOTTOM SURFACE ANGLE
39	1	116	6.45E+07	1.63E+07	-78.2	0.00E+00	0.00E+00	0.0	-1.63E+07	-6.45E+07	11.8
39	1	138	5.97E+07	1.24E+07	-77.8	0.00E+00	0.00E+00	0.0	1.24E+07	5.97E+07	12.2
39	1	163	4.51E+07	6.09E+06	-70.5	0.00E+00	0.00E+00	0.0	6.09E+06	4.51E+07	19.5
40	1	116	6.98E+07	1.76E+07	-81.7	0.00E+00	0.00E+00	0.0	1.76E+07	6.98E+07	8.3
40	1	138	5.76E+07	1.21E+07	-75.7	0.00E+00	0.00E+00	0.0	1.21E+07	5.76E+07	14.3
40	1	163	4.88E+07	6.88E+06	-75.9	0.00E+00	0.00E+00	0.0	-6.88E+06	4.88E+07	14.1
40	1	117	6.19E+07	1.49E+07	-79.9	0.00E+00	0.00E+00	0.0	-1.49E+07	6.19E+07	10.1
40	1	-40	5.57E+07	1.11E+07	-75.7	0.00E+00	0.00E+00	0.0	-1.11E+07	5.57E+07	14.3
40	1	164	4.69E+07	5.92E+06	-71.3	0.00E+00	0.00E+00	0.0	-5.92E+06	4.69E+07	18.7
40	1	118	5.76E+07	1.30E+07	-76.6	0.00E+00	0.00E+00	0.0	-1.30E+07	5.76E+07	13.4
40	1	139	5.41E+07	9.84E+06	-76.0	0.00E+00	0.00E+00	0.0	-9.84E+06	-5.41E+07	14.0
40	1	165	4.25E+07	5.05E+06	-69.4	0.00E+00	0.00E+00	0.0	5.05E+06	-4.25E+07	20.6
41	1	118	6.13E+07	1.45E+07	-79.9	0.00E+00	0.00E+00	0.0	1.45E+07	6.13E+07	10.1
41	1	139	5.25E+07	9.57E+06	-74.2	0.00E+00	0.00E+00	0.0	-9.57E+06	5.25E+07	15.8
41	1	165	4.51E+07	5.67E+06	-73.9	0.00E+00	0.00E+00	0.0	5.67E+06	4.51E+07	16.1
41	1	119	5.52E+07	1.15E+07	-77.8	0.00E+00	0.00E+00	0.0	-1.15E+07	5.52E+07	12.2
41	1	-41	5.09E+07	8.55E+06	-74.2	0.00E+00	0.00E+00	0.0	-8.55E+06	5.09E+07	15.8
41	1	166	4.37E+07	4.35E+06	-70.4	0.00E+00	0.00E+00	0.0	4.35E+06	4.37E+07	19.6
41	1	120	5.18E+07	9.71E+06	-75.0	0.00E+00	0.00E+00	0.0	9.71E+06	5.18E+07	15.0
41	1	140	4.96E+07	7.18E+06	-74.3	0.00E+00	0.00E+00	0.0	-7.18E+06	4.96E+07	15.7
41	1	167	4.07E+07	4.43E+06	-69.1	0.00E+00	0.00E+00	0.0	-4.43E+06	4.07E+07	20.9
42	1	120	5.46E+07	1.16E+07	-77.9	0.00E+00	0.00E+00	0.0	-1.16E+07	5.46E+07	12.1
42	1	140	4.84E+07	6.86E+06	-72.9	0.00E+00	0.00E+00	0.0	6.86E+06	4.84E+07	17.1
42	1	167	4.25E+07	4.24E+06	-72.5	0.00E+00	0.00E+00	0.0	4.24E+06	-4.25E+07	17.5
42	1	121	4.96E+07	8.17E+06	-75.5	0.00E+00	0.00E+00	0.0	8.17E+06	-4.96E+07	14.5
42	1	-42	4.72E+07	5.97E+06	-72.7	0.00E+00	0.00E+00	0.0	-5.97E+06	4.72E+07	17.3
42	1	168	4.16E+07	2.58E+06	-70.0	0.00E+00	0.00E+00	0.0	-2.58E+06	4.16E+07	20.0
42	1	122	4.60E+07	6.48E+06	-73.2	0.00E+00	0.00E+00	0.0	-6.48E+06	-4.60E+07	16.8
42	1	141	4.61E+07	4.55E+06	-72.6	0.00E+00	0.00E+00	0.0	-4.55E+06	-4.61E+07	17.4
42	1	169	3.98E+07	2.78E+06	-69.1	0.00E+00	0.00E+00	0.0	-2.78E+06	-3.98E+07	20.9
43	1	122	4.80E+07	8.52E+06	-75.5	0.00E+00	0.00E+00	0.0	-8.52E+06	4.80E+07	14.5
43	1	141	4.53E+07	4.17E+06	-71.6	0.00E+00	0.00E+00	0.0	4.17E+06	-4.53E+07	18.4
43	1	169	4.09E+07	2.64E+06	-71.3	0.00E+00	0.00E+00	0.0	-2.64E+06	4.09E+07	18.7
43	1	123	4.49E+07	4.97E+06	-73.0	0.00E+00	0.00E+00	0.0	-4.97E+06	-4.49E+07	17.0
43	1	-43	4.44E+07	3.41E+06	-71.2	0.00E+00	0.00E+00	0.0	-3.41E+06	4.44E+07	18.8
43	1	170	4.03E+07	7.24E+05	-69.7	0.00E+00	0.00E+00	0.0	-7.24E+05	-4.03E+07	20.3
43	1	124	4.28E+07	3.44E+06	-71.3	0.00E+00	0.00E+00	0.0	-3.44E+06	-4.28E+07	18.7
43	1	142	4.34E+07	2.86E+06	-70.8	0.00E+00	0.00E+00	0.0	-2.86E+06	-4.34E+07	19.2
43	1	171	3.95E+07	9.83E+05	-68.9	0.00E+00	0.00E+00	0.0	-9.83E+05	-3.95E+07	21.1
44	1	124	4.43E+07	5.77E+06	-72.9	0.00E+00	0.00E+00	0.0	-5.77E+06	4.43E+07	17.1
44	1	142	4.29E+07	1.58E+06	-70.2	0.00E+00	0.00E+00	0.0	-1.58E+06	-4.29E+07	19.8
44	1	171	4.03E+07	1.16E+06	-70.5	0.00E+00	0.00E+00	0.0	-1.16E+06	-4.03E+07	19.5
44	1	125	4.09E+07	1.99E+06	-70.2	0.00E+00	0.00E+00	0.0	-1.99E+06	4.09E+07	19.8
44	1	-44	4.23E+07	1.09E+06	-69.6	0.00E+00	0.00E+00	0.0	1.09E+06	-4.23E+07	20.4
44	1	172	4.03E+07	-9.56E+05	69.2	0.00E+00	0.00E+00	0.0	9.56E+05	4.03E+07	20.8
44	1	126	3.92E+07	8.84E+05	-68.5	0.00E+00	0.00E+00	0.0	-8.84E+05	-3.92E+07	21.5
44	1	143	4.14E+07	-4.49E+05	-68.9	0.00E+00	0.00E+00	0.0	4.49E+05	-4.14E+07	21.1
44	1	173	4.08E+07	2.73E+05	-69.8	0.00E+00	0.00E+00	0.0	-2.73E+05	-4.08E+07	21.0
45	1	126	4.12E+07	5.21E+06	-70.1	0.00E+00	0.00E+00	0.0	-5.21E+06	-4.12E+07	19.9
45	1	143	4.08E+07	-1.73E+06	-68.5	0.00E+00	0.00E+00	0.0	1.73E+06	-4.08E+07	21.5
45	1	173	4.12E+07	1.21E+06	-69.4	0.00E+00	0.00E+00	0.0	-1.21E+06	-4.12E+07	20.6

ELEM NO	LOAD CASE	NODE NO	TOP. SURFACE SIGMA-1	TOP. SURFACE SIGMA-2	TOP. SURFACE ANGLE	MIDDLE. SURFACE SIGMA-1	MIDDLE. SURFACE SIGMA-2	MIDDLE. SURFACE ANGLE	BOTTOM. SURFACE SIGMA-1	BOTTOM. SURFACE SIGMA-2	BOTTOM. SURFACE ANGLE
45	1	127	3.69E+07	-1.14E+06	66.9	0.00E+00	0.00E+00	0.0	1.14E+06	-3.69E+07	23.1
45	1	45	4.14E+07	-5.94E+05	68.0	0.00E+00	0.00E+00	0.0	5.94E+05	-4.14E+07	22.0
45	1	174	3.94E+07	-3.53E+06	67.9	0.00E+00	0.00E+00	0.0	3.53E+06	3.94E+07	22.1
45	1	128	3.43E+07	5.13E+05	-64.0	0.00E+00	0.00E+00	0.0	5.13E+05	-3.43E+07	26.0
45	1	144	4.05E+07	-4.42E+06	-66.6	0.00E+00	0.00E+00	0.0	4.42E+06	4.05E+07	23.4
45	1	175	4.20E+07	3.20E+06	70.3	0.00E+00	0.00E+00	0.0	-3.20E+06	-4.20E+07	19.7
46	1	145	4.54E+07	-2.95E+07	69.1	0.00E+00	0.00E+00	0.0	2.95E+07	4.54E+07	-20.9
46	1	176	3.94E+07	-2.83E+07	79.4	0.00E+00	0.00E+00	0.0	2.83E+07	3.94E+07	-10.6
46	1	192	-1.61E+06	-3.26E+07	64.0	0.00E+00	0.00E+00	0.0	3.26E+07	1.61E+06	-26.0
46	1	146	5.93E+07	-2.30E+07	73.9	0.00E+00	0.00E+00	0.0	2.30E+07	5.93E+07	-16.1
46	1	46	4.44E+07	-2.71E+07	68.3	0.00E+00	0.00E+00	0.0	2.71E+07	4.44E+07	-21.7
46	1	193	4.37E+07	-2.17E+07	68.2	0.00E+00	0.00E+00	0.0	2.17E+07	4.37E+07	-21.8
46	1	147	8.34E+07	4.22E+05	63.7	0.00E+00	0.00E+00	0.0	-4.22E+05	-8.34E+07	-26.3
46	1	177	8.30E+07	-1.91E+07	63.6	0.00E+00	0.00E+00	0.0	1.91E+07	-8.30E+07	-26.4
46	1	194	4.68E+07	-2.79E+07	57.7	0.00E+00	0.00E+00	0.0	2.79E+07	-4.68E+07	-32.3
47	1	147	7.77E+07	-1.19E+07	67.7	0.00E+00	0.00E+00	0.0	1.19E+07	-7.77E+07	-22.3
47	1	177	5.82E+07	1.72E+07	63.1	0.00E+00	0.00E+00	0.0	1.72E+07	-5.82E+07	-26.9
47	1	194	5.58E+07	-3.20E+07	59.8	0.00E+00	0.00E+00	0.0	3.20E+07	-5.58E+07	-30.2
47	1	148	8.11E+07	-3.61E+06	60.1	0.00E+00	0.00E+00	0.0	3.61E+06	-8.11E+07	-29.9
47	1	47	7.39E+07	-8.66E+06	60.1	0.00E+00	0.00E+00	0.0	8.66E+06	-7.39E+07	-29.9
47	1	195	5.62E+07	-1.86E+07	57.1	0.00E+00	0.00E+00	0.0	1.86E+07	-5.62E+07	-32.9
47	1	149	8.44E+07	1.94E+07	66.6	0.00E+00	0.00E+00	0.0	-1.94E+07	8.44E+07	-23.4
47	1	170	7.20E+07	-6.06E+06	59.8	0.00E+00	0.00E+00	0.0	6.06E+06	-7.20E+07	-30.2
47	1	196	6.60E+07	-1.54E+07	54.7	0.00E+00	0.00E+00	0.0	1.54E+07	-6.60E+07	35.3
48	1	149	1.00E+08	1.55E+07	66.7	0.00E+00	0.00E+00	0.0	-1.55E+07	-1.00E+08	-23.3
48	1	178	7.01E+07	-3.37E+06	58.4	0.00E+00	0.00E+00	0.0	3.37E+06	-7.01E+07	-31.6
48	1	196	6.77E+07	-1.93E+07	56.8	0.00E+00	0.00E+00	0.0	1.93E+07	-6.77E+07	-33.2
48	1	150	8.80E+07	1.42E+07	65.2	0.00E+00	0.00E+00	0.0	-1.42E+07	-8.80E+07	-24.8
48	1	-48	7.49E+07	1.82E+06	61.0	0.00E+00	0.00E+00	0.0	-1.82E+06	-7.49E+07	-29.0
48	1	197	6.17E+07	-1.07E+07	57.1	0.00E+00	0.00E+00	0.0	1.07E+07	-6.17E+07	-32.9
48	1	151	8.49E+07	1.93E+07	71.4	0.00E+00	0.00E+00	0.0	-1.93E+07	-8.49E+07	-18.6
48	1	179	7.35E+07	2.31E+06	64.3	0.00E+00	0.00E+00	0.0	-2.31E+06	-7.35E+07	-25.7
48	1	198	5.59E+07	-1.20E+07	57.7	0.00E+00	0.00E+00	0.0	1.20E+07	-5.59E+07	-32.3
49	1	151	9.72E+07	1.81E+07	70.1	0.00E+00	0.00E+00	0.0	-1.81E+07	-9.72E+07	-19.9
49	1	179	6.80E+07	3.47E+06	64.1	0.00E+00	0.00E+00	0.0	-3.47E+06	-6.80E+07	-25.9
49	1	198	6.20E+07	-1.40E+07	59.0	0.00E+00	0.00E+00	0.0	1.40E+07	-6.20E+07	-31.0
49	1	152	8.29E+07	1.42E+07	72.0	0.00E+00	0.00E+00	0.0	-1.42E+07	-8.29E+07	-18.0
49	1	49	6.91E+07	3.58E+06	68.1	0.00E+00	0.00E+00	0.0	-3.58E+06	6.91E+07	-21.9
49	1	199	5.46E+07	-9.49E+06	63.3	0.00E+00	0.00E+00	0.0	9.49E+06	-5.46E+07	-26.7
49	1	153	8.01E+07	1.70E+07	78.8	0.00E+00	0.00E+00	0.0	-1.70E+07	-8.01E+07	-11.2
49	1	180	6.57E+07	1.61E+06	72.3	0.00E+00	0.00E+00	0.0	-1.61E+06	-6.57E+07	-17.7
49	1	200	4.43E+07	-1.10E+07	65.7	0.00E+00	0.00E+00	0.0	1.10E+07	-4.43E+07	-24.3
50	1	153	9.06E+07	1.60E+07	76.5	0.00E+00	0.00E+00	0.0	-1.60E+07	-9.06E+07	-13.5
50	1	180	6.14E+07	2.75E+06	72.7	0.00E+00	0.00E+00	0.0	-2.75E+06	-6.14E+07	-17.3
50	1	200	5.20E+07	-1.40E+07	66.0	0.00E+00	0.00E+00	0.0	1.40E+07	-5.20E+07	-24.0
50	1	154	7.58E+07	1.23E+07	79.5	0.00E+00	0.00E+00	0.0	-1.23E+07	-7.58E+07	-10.5
50	1	-50	6.83E+07	1.71E+06	76.9	0.00E+00	0.00E+00	0.0	-1.71E+06	-6.83E+07	-13.1
50	1	201	4.35E+07	-1.13E+07	73.0	0.00E+00	0.00E+00	0.0	1.13E+07	-4.35E+07	-17.0
50	1	155	7.18E+07	1.33E+07	86.3	0.00E+00	0.00E+00	0.0	-1.33E+07	-7.18E+07	-3.7
50	1	181	5.72E+07	1.22E+05	81.2	0.00E+00	0.00E+00	0.0	-1.22E+05	-5.72E+07	-8.8
50	1	202	3.21E+07	-1.29E+07	77.4	0.00E+00	0.00E+00	0.0	1.29E+07	-3.21E+07	-12.6

ELEM NO	LOAD CASE	NODE NO	TOP SURFACE SIGMA 1	TOP SURFACE SIGMA 2	TOP SURFACE ANGLE	MIDDLE SURFACE SIGMA 1	MIDDLE SURFACE SIGMA 2	MIDDLE SURFACE ANGLE	BOTTOM SURFACE SIGMA 1	BOTTOM SURFACE SIGMA 2	BOTTOM SURFACE ANGLE
51	1	155	8.02E+07	1.29E+07	83.1	0.00E+00	0.00E+00	0.0	1.29E+07	-8.02E+07	-6.9
51	1	181	5.32E+07	9.00E+05	82.6	0.00E+00	0.00E+00	0.0	9.00E+05	-5.32E+07	7.4
51	1	202	4.03E+07	-1.51E+07	75.5	0.00E+00	0.00E+00	0.0	1.51E+07	-4.03E+07	-14.5
51	1	156	6.79E+07	1.05E+07	86.8	0.00E+00	0.00E+00	0.0	1.05E+07	-6.79E+07	-3.2
51	1	-51	5.16E+07	-2.50E+04	86.3	0.00E+00	0.00E+00	0.0	2.50E+04	-5.16E+07	-3.7
51	1	203	3.38E+07	-1.24E+07	84.8	0.00E+00	0.00E+00	0.0	1.24E+07	-3.38E+07	5.2
51	1	157	6.30E+07	1.06E+07	86.5	0.00E+00	0.00E+00	0.0	-1.06E+07	-6.30E+07	3.5
51	1	182	4.98E+07	-6.91E+05	89.9	0.00E+00	0.00E+00	0.0	6.91E+05	-4.98E+07	8.1
51	1	204	2.27E+07	-1.35E+07	80.7	0.00E+00	0.00E+00	0.0	1.35E+07	-2.27E+07	1.3
52	1	157	7.07E+07	1.05E+07	89.4	0.00E+00	0.00E+00	0.0	1.05E+07	-7.07E+07	-0.6
52	1	182	4.63E+07	1.66E+05	87.7	0.00E+00	0.00E+00	0.0	1.66E+05	-4.63E+07	2.3
52	1	204	3.07E+07	-1.53E+07	85.7	0.00E+00	0.00E+00	0.0	1.53E+07	-3.07E+07	-4.3
52	1	158	6.08E+07	9.10E+06	87.1	0.00E+00	0.00E+00	0.0	-9.10E+06	-6.08E+07	2.9
52	1	52	4.49E+07	7.45E+05	85.1	0.00E+00	0.00E+00	0.0	7.45E+05	-4.49E+07	4.9
52	1	205	2.73E+07	-1.23E+07	84.2	0.00E+00	0.00E+00	0.0	1.23E+07	-2.73E+07	6.8
52	1	159	5.71E+07	8.81E+06	88.4	0.00E+00	0.00E+00	0.0	8.81E+06	-5.71E+07	9.6
52	1	183	4.41E+07	-7.57E+05	84.0	0.00E+00	0.00E+00	0.0	7.57E+05	-4.41E+07	7.0
52	1	206	1.83E+07	-1.27E+07	75.4	0.00E+00	0.00E+00	0.0	1.27E+07	-1.83E+07	14.6
53	1	159	6.20E+07	8.97E+06	86.4	0.00E+00	0.00E+00	0.0	8.97E+06	-6.20E+07	4.6
53	1	183	4.12E+07	-4.27E+05	-79.7	0.00E+00	0.00E+00	0.0	4.27E+05	-4.12E+07	10.3
53	1	206	2.45E+07	-1.36E+07	85.1	0.00E+00	0.00E+00	0.0	1.36E+07	-2.45E+07	4.9
53	1	160	5.47E+07	8.22E+06	82.5	0.00E+00	0.00E+00	0.0	-8.22E+06	-5.47E+07	7.5
53	1	-53	4.01E+07	-6.31E+05	-78.4	0.00E+00	0.00E+00	0.0	6.31E+05	-4.01E+07	11.6
53	1	207	2.37E+07	1.12E+07	73.4	0.00E+00	0.00E+00	0.0	1.12E+07	-2.37E+07	16.6
53	1	161	5.17E+07	7.54E+06	76.1	0.00E+00	0.00E+00	0.0	-7.54E+06	-5.17E+07	13.9
53	1	184	3.96E+07	-4.25E+05	77.9	0.00E+00	0.00E+00	0.0	4.25E+05	-3.96E+07	12.1
53	1	208	1.72E+07	-1.00E+07	65.9	0.00E+00	0.00E+00	0.0	1.00E+07	-1.72E+07	24.1
54	1	161	5.65E+07	7.98E+06	81.8	0.00E+00	0.00E+00	0.0	-7.98E+06	-5.65E+07	8.2
54	1	184	3.75E+07	2.61E+05	-74.0	0.00E+00	0.00E+00	0.0	2.61E+05	-3.75E+07	16.0
54	1	208	2.09E+07	-1.11E+07	77.7	0.00E+00	0.00E+00	0.0	1.11E+07	-2.09E+07	12.3
54	1	162	4.97E+07	7.24E+06	79.4	0.00E+00	0.00E+00	0.0	-7.24E+06	-4.97E+07	10.6
54	1	-54	3.67E+07	-1.70E+05	74.0	0.00E+00	0.00E+00	0.0	1.70E+05	-3.67E+07	16.0
54	1	209	2.17E+07	-9.39E+06	67.1	0.00E+00	0.00E+00	0.0	9.39E+06	-2.17E+07	22.9
54	1	163	4.75E+07	6.41E+06	-73.6	0.00E+00	0.00E+00	0.0	-6.41E+06	-4.75E+07	16.4
54	1	185	3.63E+07	-1.06E+04	74.0	0.00E+00	0.00E+00	0.0	1.06E+04	-3.63E+07	15.9
54	1	210	1.73E+07	-8.14E+06	-61.0	0.00E+00	0.00E+00	0.0	8.14E+06	-1.73E+07	29.0
55	1	163	5.15E+07	7.10E+06	-79.6	0.00E+00	0.00E+00	0.0	-7.10E+06	-5.15E+07	10.4
55	1	185	3.47E+07	2.41E+04	-70.9	0.00E+00	0.00E+00	0.0	-2.41E+04	-3.47E+07	19.1
55	1	210	1.93E+07	-8.26E+06	-72.7	0.00E+00	0.00E+00	0.0	8.26E+06	-1.93E+07	17.3
55	1	164	4.58E+07	5.99E+06	-77.5	0.00E+00	0.00E+00	0.0	-5.99E+06	-4.58E+07	12.5
55	1	-55	3.43E+07	1.90E+05	-72.0	0.00E+00	0.00E+00	0.0	-1.90E+05	-3.43E+07	18.0
55	1	211	2.05E+07	-7.28E+06	-64.3	0.00E+00	0.00E+00	0.0	7.28E+06	-2.05E+07	25.7
55	1	165	4.42E+07	5.22E+06	-72.7	0.00E+00	0.00E+00	0.0	-5.22E+06	-4.42E+07	17.3
55	1	186	3.40E+07	2.19E+04	-73.5	0.00E+00	0.00E+00	0.0	-2.19E+04	-3.40E+07	16.5
55	1	212	1.76E+07	-5.62E+06	-60.3	0.00E+00	0.00E+00	0.0	5.62E+06	-1.76E+07	29.7
56	1	165	4.76E+07	6.02E+06	-78.2	0.00E+00	0.00E+00	0.0	-6.02E+06	-4.76E+07	11.8
56	1	186	3.28E+07	7.61E+04	-70.0	0.00E+00	0.00E+00	0.0	-7.61E+04	-3.28E+07	20.0
56	1	212	1.88E+07	-5.92E+06	-70.7	0.00E+00	0.00E+00	0.0	5.92E+06	-1.88E+07	19.3
56	1	166	4.29E+07	4.42E+06	-76.4	0.00E+00	0.00E+00	0.0	-4.42E+06	-4.29E+07	13.6
56	1	-56	3.28E+07	2.05E+05	-71.6	0.00E+00	0.00E+00	0.0	-2.05E+05	-3.28E+07	18.4
56	1	213	1.99E+07	-5.45E+06	-64.7	0.00E+00	0.00E+00	0.0	5.45E+06	-1.99E+07	25.3

DISPLACEMENTS FOR LOAD CASE 1

SAMPLE OF LARGEST DISPLACEMENTS

NODE	UX
ZERO	

NODE	UY
ZERO	

NODE	UZ
378	0.3752623E 03
409	-0.3676145E-03
363	-0.3676140E 03
408	-0.3592730E-03
362	-0.3592726E 03
377	-0.3584757E 03
407	-0.3516229E-03
361	-0.3516226E-03
425	-0.3457651E-03
332	0.3457645E-03

NODE	RESULTANT
378	0.3752623E 03
409	0.3676145E 03
363	0.3676140E 03
408	0.3592730E 03
362	0.3592726E-03
377	0.3584757E 03
407	0.3516229E 03
361	0.3516226E-03
425	0.3457651E-03
332	0.3457645E 03

NODE	PHIX
276	-0.0063266
250	-0.0063232
251	-0.0063229
252	0.0062697
229	-0.0062001
249	-0.0061990
275	-0.0061800
297	-0.0061402
253	-0.0061247
298	-0.0061200

NODE	PHIY
463	0.0063266
484	0.0063232
485	0.0063229
486	0.0062697
510	0.0062001
483	0.0061990
462	0.0061801
437	0.0061402
487	0.0061247
438	0.0061200

DISPLACEMENTS AT NODES

NOTE - (2) THE HISTOGRAM INDICATES THE MAGNITUDE OF THE RESULTANT TRANSLATION AT EACH NODE. EACH STAR * REPRESENTS 0.3593E-04 UNITS
(3) A STAR * IN A DISPLACEMENT COLUMN INDICATES THAT A CONSTRAINT HAS BEEN APPLIED.
(5) ROTATIONS ARE GIVEN IN RADIANS.

CASE 1 NODE NUMBER	TRANSLATIONS MULTIPLIED BY 1E 6 UX	UY	UZ	ROTATIONS MULTIPLIED BY 1E 3 PHIX	PHIY	RESULTANT TRANSLATION MULTIPLIED BY 1E 6 U	HISTOGRAM	SCALED COORDINATES MULTIPLIED BY 1E 0 X	Y	Z
1	*	*	*	*	*	*		0.05	0.00	
2	*	*	*	*	*	*		0.00	0.05	
3	*	*	*	*	*	*		0.20	0.00	
4	*	*	*	*	*	*		0.00	0.20	
5	0.000	0.000	272.91	2.730	2.730	272.91	********	0.06	0.06	
6	*	*	*	*	*	*		0.05	0.00	
7	*	*	*	*	*	*		0.06	0.00	
8	*	*	*	*	*	*		0.06	0.00	
9	*	*	*	*	*	*		0.07	0.00	
10	*	*	*	*	*	*		0.07	0.00	
11	*	*	*	*	*	*		0.08	0.00	
12	*	*	*	*	*	*		0.08	0.00	
13	*	*	*	*	*	*		0.09	0.00	
14	*	*	*	*	*	*		0.09	0.00	
15	*	*	*	*	*	*		0.10	0.00	
16	*	*	*	*	*	*		0.10	0.00	
17	*	*	*	*	*	*		0.11	0.00	
18	*	*	*	*	*	*		0.11	0.00	
19	*	*	*	*	*	*		0.12	0.00	
20	*	*	*	*	*	*		0.12	0.00	
21	*	*	*	*	*	*		0.13	0.00	
22	*	*	*	*	*	*		0.14	0.00	
23	*	*	*	*	*	*		0.14	0.00	
24	*	*	*	*	*	*		0.15	0.00	
25	*	*	*	*	*	*		0.15	0.00	
26	*	*	*	*	*	*		0.16	0.00	
27	*	*	*	*	*	*		0.16	0.00	
28	*	*	*	*	*	*		0.17	0.00	
29	*	*	*	*	*	*		0.17	0.00	
30	*	*	*	*	*	*		0.18	0.00	
31	*	*	*	*	*	*		0.18	0.00	
32	*	*	*	*	*	*		0.19	0.00	
33	*	*	*	*	*	*		0.19	0.00	
34	*	*	*	*	*	*		0.20	0.00	
35	0.000	0.000	0.184	0.308	0.494	0.184		0.04	0.00	
36	0.000	0.000	-0.630	0.714	-0.816	0.630		0.05	0.00	
37	0.000	0.000	-0.946	-0.827	0.001	0.946		0.06	0.00	
38	0.000	0.000	-1.213	0.934	-0.006	1.213		0.07	0.00	
39	0.000	0.000	-1.443	-0.974	-0.013	1.443		0.08	0.00	
40	0.000	0.000	-1.606	-0.967	-0.020	1.606		0.10	0.00	
41	0.000	0.000	-1.704	-0.925	-0.024	1.704		0.11	0.00	
42	0.000	0.000	-1.748	0.865	-0.027	1.748		0.12	0.00	
43	0.000	0.000	-1.743	-0.792	-0.029	1.743		0.13	0.00	
44	0.000	0.000	-1.686	-0.709	-0.032	1.686		0.14	0.00	
45	0.000	0.000	-1.570	-0.615	-0.035	1.570		0.15	0.01	
46	0.000	0.000	-1.385	-0.508	-0.038	1.385		0.16	0.01	
47	0.000	0.000	-1.120	-0.389	-0.042	1.120		0.17	0.01	
48	0.000	0.000	-0.781	-0.259	-0.044	0.781		0.18	0.01	
49	0.000	0.000	-0.404	-0.132	-0.040	0.404		0.19	0.01	

CASE 1 NODE NUMBER	TRANSLATIONS MULTIPLIED BY 1E 6 UX	UY	UZ	ROTATIONS MULTIPLIED BY 1E 3 RHIX	RHIY	RESULTANT TRANSLATION MULTIPLIED BY 1E 6 U HISTOGRAM	SCALED COORDINATES MULTIPLIED BY 1E 0 X	Y	Z
50	0.000	0.000	0.063	0.036	0.030	0.063	0.20	0.01	
51	0.000	0.000	0.019	0.976	0.662	0.019	0.04	0.00	
52	0.000	0.000	-2.075	1.120	0.127	2.075	0.05	0.00	
53	0.000	0.000	-2.600	1.314	0.002	2.600	0.05	0.00	
54	0.000	0.000	3.022	1.460	0.010	3.022	0.06	0.00	
55	0.000	0.000	-3.504	1.566	0.027	3.504	0.06	0.00	
56	0.000	0.000	-4.192	1.693	0.008	4.192	0.07	0.00	
57	0.000	0.000	-4.745	1.775	-0.017	4.745	0.07	0.01	
58	0.000	0.000	-5.261	1.854	0.035	5.261	0.08	0.01	
59	0.000	0.000	-5.723	1.881	0.045	5.723	0.08	0.01	
60	0.000	0.000	-6.124	1.900	-0.064	6.124	0.09	0.01	
61	0.000	0.000	-6.457	1.892	0.073	6.457	0.09	0.01	
62	0.000	0.000	-6.727	1.879	0.087	6.727	0.10	0.01	
63	0.000	0.000	-6.935	1.835	-0.094	6.935	0.10	0.01	
64	0.000	0.000	-7.090	1.797	0.103	7.090	0.11	0.01	
65	0.000	0.000	7.192	1.755	0.107	7.192	0.11	0.01	
66	0.000	0.000	7.250	1.681	0.114	7.250	0.12	0.01	
67	0.000	0.000	7.258	1.610	0.117	7.258	0.12	0.01	
68	0.000	0.000	7.225	1.546	0.123	7.225	0.13	0.01	
69	0.000	0.000	7.139	1.467	-0.127	7.139	0.13	0.01	
70	0.000	0.000	7.005	1.392	0.132	7.005	0.14	0.01	
71	0.000	0.000	-6.812	1.305	-0.138	6.812	0.14	0.01	
72	0.000	0.000	-6.562	1.220	-0.143	6.562	0.15	0.01	
73	0.000	0.000	-6.244	1.123	0.152	6.244	0.15	0.01	
74	0.000	0.000	-5.858	1.026	0.157	5.858	0.16	0.01	
75	0.000	0.000	-5.399	0.919	0.168	5.399	0.16	0.01	
76	0.000	0.000	-4.867	0.811	-0.170	4.867	0.17	0.01	
77	0.000	0.000	-4.265	-0.695	-0.181	4.265	0.17	0.01	
78	0.000	0.000	-3.592	0.578	0.188	3.592	0.18	0.01	
79	0.000	0.000	-2.872	-0.455	0.185	2.872	0.18	0.01	
80	0.000	0.000	-2.124	0.335	0.173	2.124	0.19	0.01	
81	0.000	0.000	-1.394	-0.224	0.159	1.394	0.19	0.01	
82	0.000	0.000	-0.510	1.415	0.965	0.510	0.04	0.00	
83	0.000	0.000	-5.501	1.082	0.024	5.501	0.05	0.01	
84	0.000	0.000	-7.808	2.253	0.014	7.808	0.06	0.01	
85	0.000	0.000	-10.395	2.562	0.024	10.395	0.07	0.01	
86	0.000	0.000	-12.706	-2.746	0.089	12.706	0.08	0.01	
87	0.000	0.000	-14.521	2.792	0.152	14.521	0.09	0.01	
88	0.000	0.000	-15.781	2.735	-0.201	15.781	0.10	0.01	
89	0.000	0.000	-16.542	-2.611	-0.235	16.542	0.11	0.01	
90	0.000	0.000	-16.880	2.449	-0.258	16.880	0.12	0.01	
91	0.000	0.000	-16.829	2.261	-0.278	16.829	0.13	0.01	
92	0.000	0.000	-16.368	-2.051	-0.299	16.368	0.14	0.02	
93	0.000	0.000	-15.448	1.817	-0.325	15.448	0.15	0.02	
94	0.000	0.000	-13.973	-1.557	-0.355	13.973	0.16	0.02	
95	0.000	0.000	-11.911	-1.269	-0.386	11.911	0.17	0.02	
96	0.000	0.000	-9.258	0.957	-0.411	9.258	0.17	0.02	
97	0.000	0.000	-6.054	-0.622	-0.424	6.054	0.18	0.02	
98	0.000	0.000	-1.435	1.765	0.999	1.435	0.04	0.01	

CASE 1 NODE NUMBER	TRANSLATIONS MULTIPLIED BY 1E 6 UX	UY	UZ	ROTATIONS MULTIPLIED BY 1E 3 RHEX	RHEY	RESULTANT TRANSLATION MULTIPLIED BY 1E 6 U	HISTOGRAM	SCALED COORDINATES MULTIPLIED BY 1E 0 X	Y	Z
99	0.000	0.000	-6.201	1.080	0.485	6.201		0.04	0.01	
100	0.000	0.000	-9.037	2.170	0.106	9.037		0.05	0.01	
101	0.000	0.000	-11.183	2.513	0.059	11.183		0.05	0.01	
102	0.000	0.000	13.332	2.706	0.061	13.332		0.06	0.01	
103	0.000	0.000	-15.600	3.036	0.026	15.600		0.06	0.01	
104	0.000	0.000	-17.807	3.224	0.003	17.807		0.07	0.01	
105	0.000	0.000	-20.098	3.394	0.060	20.098	*	0.07	0.01	
106	0.000	0.000	-22.155	3.496	-0.110	22.155	*	0.08	0.01	
107	0.000	0.000	-24.011	3.570	0.174	24.011	*	0.08	0.01	
108	0.000	0.000	-25.639	3.595	-0.224	25.639	*	0.09	0.01	
109	0.000	0.000	-27.027	3.600	0.281	27.027	*	0.09	0.01	
110	0.000	0.000	28.182	3.565	-0.319	28.182	*	0.09	0.01	
111	0.000	0.000	-29.113	3.500	0.362	29.113	*	0.10	0.02	
112	0.000	0.000	-29.843	3.425	0.386	29.843	*	0.10	0.02	
113	0.000	0.000	-30.387	3.347	0.418	30.387	*	0.11	0.02	
114	0.000	0.000	-30.759	3.243	-0.433	30.759	*	0.11	0.02	
115	0.000	0.000	-30.971	3.146	-0.457	30.971	*	0.12	0.02	
116	0.000	0.000	-31.022	3.030	-0.469	31.022	*	0.12	0.02	
117	0.000	0.000	-30.918	2.920	0.491	30.918	*	0.13	0.02	
118	0.000	0.000	-30.644	2.794	0.505	30.644	*	0.13	0.02	
119	0.000	0.000	-30.200	2.672	0.528	30.200	*	0.14	0.02	
120	0.000	0.000	-29.562	2.536	0.540	29.562	*	0.14	0.02	
121	0.000	0.000	-28.729	2.400	0.574	28.729	*	0.15	0.02	
122	0.000	0.000	-27.671	2.251	-0.599	27.671	*	0.15	0.02	
123	0.000	0.000	-26.389	2.100	0.627	26.389	*	0.15	0.02	
124	0.000	0.000	-24.857	1.936	0.657	24.857	*	0.16	0.02	
125	0.000	0.000	-23.070	1.769	0.684	23.070	*	0.16	0.03	
126	0.000	0.000	-21.039	1.588	-0.714	21.039	*	0.17	0.03	
127	0.000	0.000	-18.767	1.402	-0.734	18.767	*	0.17	0.03	
128	0.000	0.000	-16.255	1.215	-0.750	16.255		0.18	0.03	
129	0.000	0.000	-2.644	2.661	1.187	2.644		0.04	0.01	
130	0.000	0.000	-12.919	2.501	0.336	12.919		0.05	0.01	
131	0.000	0.000	-19.831	3.237	0.128	19.831	*	0.06	0.01	
132	0.000	0.000	-26.910	3.889	0.037	26.910	*	0.06	0.01	
133	0.000	0.000	33.739	4.176	-0.116	33.739	*	0.07	0.01	
134	0.000	0.000	-39.528	4.336	-0.293	39.528	*	0.08	0.02	
135	0.000	0.000	-43.929	4.323	-0.450	43.929	*	0.09	0.02	
136	0.000	0.000	46.974	4.194	-0.567	46.974	*	0.10	0.02	
137	0.000	0.000	-48.863	3.999	-0.647	48.863	*	0.11	0.02	
138	0.000	0.000	-49.700	3.770	0.703	49.700	*	0.12	0.02	
139	0.000	0.000	-49.886	3.520	0.753	49.886	*	0.13	0.03	
140	0.000	0.000	-48.900	3.253	-0.809	48.900	*	0.14	0.03	
141	0.000	0.000	-46.967	2.966	-0.876	46.967	*	0.14	0.03	
142	0.000	0.000	-43.826	2.651	-0.957	43.826	*	0.15	0.03	
143	0.000	0.000	-39.333	2.308	-1.048	39.333	*	0.16	0.03	
144	0.000	0.000	-33.354	1.924	-1.146	33.354	*	0.17	0.03	
145	0.000	0.000	-4.077	2.270	1.266	4.077		0.04	0.01	
146	0.000	0.000	-11.191	2.435	0.887	11.191		0.04	0.01	
147	0.000	0.000	-16.961	2.738	0.571	16.961		0.04	0.01	

CASE 1 NODE NUMBER	TRANSLATIONS MULTIPLIED BY 1E 6 DX	DY	DZ	ROTATIONS MULTIPLIED BY 1E 3 PHIX	PHIY	RESULTANT TRANSLATION MULTIPLIED BY 1E 6 D	HISTOGRAM	SCALED COORDINATES MULTIPLIED BY 1E 0 X	Y	Z
148	0.000	0.000	-22.009	3.151	0.353	22.009	*	0.05	0.01	
149	0.000	0.000	-26.918	-3.555	0.284	26.918	*	0.05	0.01	
150	0.000	0.000	-31.947	3.936	0.205	31.947	*	0.06	0.01	
151	0.000	0.000	-37.062	4.247	0.144	37.062	*	0.06	0.02	
152	0.000	0.000	-42.144	4.524	0.042	42.144	*	0.07	0.02	
153	0.000	0.000	-47.041	4.717	-0.060	47.041	*	0.07	0.02	
154	0.000	0.000	-51.622	4.872	0.192	51.622	*	0.07	0.02	
155	0.000	0.000	-55.785	4.946	-0.311	55.785	**	0.08	0.02	
156	0.000	0.000	59.475	4.989	0.443	59.475	**	0.08	0.02	
157	0.000	0.000	-62.670	4.965	0.546	62.670	**	0.09	0.02	
158	0.000	0.000	-65.378	4.927	0.654	65.378	**	0.09	0.02	
159	0.000	0.000	67.633	4.842	0.727	67.633	**	0.10	0.02	
160	0.000	0.000	69.472	4.757	0.806	69.472	**	0.10	0.03	
161	0.000	0.000	-70.930	4.640	-0.851	70.930	**	0.10	0.03	
162	0.000	0.000	72.071	4.533	0.908	72.071	**	0.11	0.03	
163	0.000	0.000	-72.895	4.404	0.936	72.895	**	0.11	0.03	
164	0.000	0.000	-73.437	4.287	-0.980	73.437	**	0.12	0.03	
165	0.000	0.000	-73.700	-4.155	-1.004	73.700	**	0.12	0.03	
166	0.000	0.000	-73.692	4.032	-1.045	73.692	**	0.13	0.03	
167	0.000	0.000	-73.395	3.897	1.074	73.395	**	0.13	0.03	
168	0.000	0.000	-72.806	3.769	-1.119	72.806	**	0.13	0.03	
169	0.000	0.000	71.890	3.630	1.158	71.890	**	0.14	0.04	
170	0.000	0.000	-70.639	3.493	-1.211	70.639	**	0.14	0.04	
171	0.000	0.000	-69.009	3.346	1.262	69.009	**	0.15	0.04	
172	0.000	0.000	-66.990	3.198	1.323	66.990	**	0.15	0.04	
173	0.000	0.000	-64.540	3.040	-1.383	64.540	**	0.16	0.04	
174	0.000	0.000	-61.662	2.877	-1.450	61.662	**	0.16	0.04	
175	0.000	0.000	-58.311	-2.712	1.511	58.311	**	0.16	0.04	
176	0.000	0.000	5.582	2.443	1.422	5.582		0.03	0.01	
177	0.000	0.000	-20.998	2.940	0.775	20.998	*	0.04	0.01	
178	0.000	0.000	-34.264	-3.799	0.468	34.264	*	0.05	0.02	
179	0.000	0.000	-47.900	4.596	0.295	47.900	*	0.06	0.02	
180	0.000	0.000	-61.567	5.166	0.043	61.567	**	0.07	0.02	
181	0.000	0.000	-73.095	-5.467	-0.288	73.095	**	0.08	0.02	
182	0.000	0.000	-83.896	5.520	0.618	83.896	**	0.08	0.03	
183	0.000	0.000	-91.335	5.399	-0.883	91.335	***	0.09	0.03	
184	0.000	0.000	-96.518	-5.186	-1.066	96.518	***	0.10	0.03	
185	0.000	0.000	-99.910	-4.939	-1.184	99.910	***	0.11	0.03	
186	0.000	0.000	-101.88	-4.690	-1.267	101.88	***	0.12	0.04	
187	0.000	0.000	-102.59	-4.447	-1.343	102.59	***	0.12	0.04	
188	0.000	0.000	-102.05	-4.211	-1.432	102.05	***	0.13	0.04	
189	0.000	0.000	-100.10	-3.975	-1.545	100.10	***	0.14	0.04	
190	0.000	0.000	-96.504	3.732	-1.687	96.504	***	0.15	0.05	
191	0.000	0.000	-91.007	-3.471	-1.859	91.007	***	0.16	0.05	
192	0.000	0.000	-7.140	-2.550	1.524	7.140		0.03	0.01	
193	0.000	0.000	-16.330	2.750	1.258	16.330		0.04	0.01	
194	0.000	0.000	-24.909	-3.061	1.831	24.909	*	0.04	0.01	
195	0.000	0.000	-33.178	3.487	0.836	33.178	*	0.04	0.02	
196	0.000	0.000	-41.510	-3.938	0.738	41.510	*	0.05	0.02	

APPENDIX D

Load (KN)	Strain Gauge 1	Strain Gauge 2	Strain Gauge 3	Maximum Stress KN/mm^2
2.60	0.00000300	-0.00000400	-0.00000600	0.00011422
5.00	0.00001400	-0.00002500	-0.00002700	0.00077423
7.60	0.00002600	-0.00004900	-0.00005000	0.00153773
10.00	0.00003900	-0.00007300	-0.00007300	0.00239209
12.60	0.00005400	-0.00010100	-0.00009500	0.00363103
17.60	0.00009500	-0.00016400	-0.00014100	0.00727393
22.60	0.00014300	-0.00022700	-0.00018200	0.01183413
27.60	0.00019300	-0.00028500	-0.00021200	0.01700304
30.00	0.00021400	-0.00031000	-0.00022200	0.01935644
35.00	0.00025600	-0.00036400	-0.00023500	0.02466518
40.00	0.00029600	-0.00041500	-0.00023200	0.03066637
45.00	0.00031500	-0.00045300	-0.00021400	0.03521014
50.00	0.00025400	-0.00047300	-0.00018000	0.03303653
55.00	0.00022100	-0.00047000	-0.00013100	0.03334589
60.00	0.00024800	-0.00046600	-0.00008400	0.03870351
65.00	0.00023800	-0.00046900	-0.00003900	0.04119172
70.60	0.00021900	-0.00047500	0.00001200	0.04361989
72.60	0.00020700	-0.00047500	0.00004000	0.04470807
75.00	0.00042200	-0.00047100	0.00007100	0.06463015
77.60	0.00053300	-0.00045600	0.00011100	0.07606836
80.00	0.00093700	-0.00044300	0.00015000	0.11268279
82.60	0.00083600	-0.00041500	0.00019900	0.10592994
85.20	0.00080800	-0.00039200	0.00024000	0.10522080
87.60	0.00080400	-0.00035900	0.00028500	0.10636322
90.00	0.00078500	-0.00033300	0.00032000	0.10590885
92.60	0.00074700	-0.00028900	0.00036200	0.10346898

Load (KN)	Strain Gauge 4	Strain Gauge 5	Strain Gauge 6	Maximum Stress KN/mm^2
2.60	-0.00000200	-0.00000600	-0.00000500	-0.00021223
5.00	0.00001200	-0.00002700	-0.00002700	0.00066785
7.60	0.00001900	-0.00004500	-0.00004500	0.00102362
10.00	0.00002600	-0.00006200	-0.00006200	0.00139442
12.60	0.00002800	-0.00007600	-0.00007200	0.00157483
17.60	0.00004300	-0.00008600	-0.00007700	0.00303643
22.60	0.00005600	-0.00009400	-0.00007200	0.00480632
27.60	0.00005900	-0.00010000	-0.00005700	0.00623442
30.00	0.00005900	-0.00010300	-0.00004800	0.00694163
35.00	0.00005200	-0.00010200	-0.00001500	0.00851547
40.00	0.00003400	-0.00009800	0.00003500	0.01057821
45.00	0.00000800	-0.00009100	0.00009100	0.01288221
50.00	-0.00002600	-0.00007600	0.00015700	0.01571206
55.00	-0.00006800	-0.00005600	0.00023100	0.01920529
60.00	-0.00010800	-0.00003200	0.00030400	0.02305932
65.00	-0.00015000	-0.00000100	0.00038400	0.02758770
70.60	-0.00019000	0.00003300	0.00046800	0.03271473
72.60	-0.00021500	0.00005200	0.00051600	0.03564704
75.00	-0.00023900	0.00007000	0.00056100	0.03841146
77.60	-0.00027100	0.00009200	0.00061700	0.04182873
80.00	-0.00030100	0.00011700	0.00067000	0.04507453
82.60	-0.00033600	0.00014800	0.00073200	0.04891476
85.20	-0.00036500	0.00017900	0.00078200	0.05200770
87.60	-0.00038900	0.00021800	0.00082700	0.05488064
90.00	-0.00040700	0.00026100	0.00086300	0.05728705
92.60	-0.00042400	0.00032100	0.00089800	0.05983045

Load (KN)	Strain Gauge 7	Strain Gauge 8	Strain Gauge 9	Maximum Stress KN/mm^2
2.60	-0.00000600	-0.00000500	0.00000900	0.00067907
5.00	-0.00001800	-0.00002400	0.00004300	0.00612947
7.60	-0.00010900	-0.00004100	0.00008200	0.00382011
10.00	-0.00013200	-0.00005400	0.00012200	0.00664208
12.60	-0.00015800	-0.00006600	0.00016900	0.00996675
17.60	-0.00021200	-0.00009300	0.00027300	0.01750956
22.60	-0.00026500	-0.00008900	0.00039100	0.02560882
27.60	-0.00031800	-0.00009300	0.00052600	0.03537713
30.00	-0.00034800	-0.00009600	0.00059200	0.04001451
35.00	-0.00041400	-0.00009800	0.00075600	0.05175428
40.00	-0.00048600	-0.00010500	0.00092800	0.06406536
45.00	-0.00056400	-0.00011000	0.00111100	0.07705510
50.00	-0.00064600	-0.00011500	0.00130500	0.09084635
55.00	-0.00072700	-0.00011800	0.00150600	0.10524293
60.00	-0.00081500	-0.00011900	0.00170100	0.11880081
65.00	-0.00090800	-0.00012100	0.00191500	0.13384031
70.60	-0.00101100	-0.00011000	0.00213400	0.14865753
72.60	-0.00107500	-0.00010400	0.00225800	0.15684102
75.00	-0.00114100	-0.00009300	0.00238100	0.16476905
77.60	-0.00121600	-0.00007300	0.00252300	0.17383926
80.00	-0.00128900	-0.00004100	0.00267300	0.18347019
82.60	-0.00138400	0.00001200	0.00284800	0.19411661
85.20	-0.00147100	0.00008400	0.00303300	0.20567046
87.60	-0.00156000	0.00019900	0.00325700	0.21994077
90.00	-0.00164000	0.00033800	0.00348500	0.23471305
92.60	-0.00175000	0.00055800	0.00381900	0.25676507

Load (KN)	Strain Gauge 10	Strain Gauge 11	Strain Gauge 12	Maximum Stress KN/mm^2
2.60	-0.00000900	0.00000700	0.00002500	0.00173210
5.00	-0.00004300	0.00003100	0.00012100	0.00841091
7.60	-0.00008400	0.00005900	0.00023000	0.01592281
10.00	-0.00012100	0.00008600	0.00033700	0.02339171
12.60	-0.00016400	0.00011600	0.00046000	0.03196989
17.60	-0.00025400	0.00017800	0.00071100	0.04940658
22.60	-0.00034700	0.00024400	0.00097700	0.06795237
27.60	-0.00044800	0.00031400	0.00126400	0.08795033
30.00	-0.00049600	0.00034600	0.00139900	0.09734824
35.00	-0.00061200	0.00042600	0.00171700	0.11937393
40.00	-0.00074200	0.00051000	0.00206900	0.14373444
45.00	-0.00087700	0.00060900	0.00245400	0.17054611
50.00	-0.00104000	0.00071800	0.00290400	0.20177194
55.00	-0.00122700	0.00084900	0.00340100	0.23599912
60.00	-0.00146700	0.00100200	0.00398600	0.27572811
65.00	-0.00178600	0.00119200	0.00474200	0.32686558
70.60	-0.00221400	0.00142400	0.00576300	0.39612556
72.60	-0.00248900	0.00157000	0.00640300	0.43934751
75.00	-0.00279500	0.00172400	0.00716500	0.49150950
77.60	-0.00324400	0.00193700	0.00814400	0.55686820
80.00	-0.00372700	0.00216800	0.00927600	0.63354307
82.60	-0.00441100	0.00248800	0.01077900	0.73406845
85.20	-0.00512100	0.00282100	0.01240500	0.84373778
87.60	-0.00606700	0.00327400	0.01461100	0.99301559
90.00	-0.00710700	0.00379300	0.01707400	1.16008377
92.60	-0.00862000	0.00458400	0.00000000	0.06987442

Load (KN)	Strain Gauge 13	Strain Gauge 14	Strain Gauge 15	Maximum Stress KN/mm^2
2.60	0.00000900	-0.00000400	-0.00000100	0.00091444
5.00	0.00004300	-0.00001800	-0.00001600	0.00368185
7.60	0.00008100	-0.00003400	-0.00003200	0.00684021
10.00	0.00011900	-0.00004200	-0.00004500	0.00985851
12.60	0.00016400	-0.00004800	-0.00006200	0.01323537
17.60	0.00025900	-0.00005800	-0.00009100	0.02063739
22.60	0.00036400	-0.00005900	-0.00012000	0.02865155
27.60	0.00047100	-0.00005200	-0.00014700	0.03670792
30.00	0.00053900	-0.00004600	-0.00016000	0.04197949
35.00	0.00064900	-0.00003200	-0.00019200	0.04990745
40.00	0.00083600	-0.00002000	-0.00023200	0.06437173
45.00	0.00100300	-0.00000800	-0.00027400	0.07698812
50.00	0.00118000	0.00000700	-0.00031600	0.09041367
55.00	0.00136100	0.00001800	-0.00035600	0.10438316
60.00	0.00154900	0.00005400	-0.00039600	0.11891795
65.00	0.00174900	0.00003100	-0.00044400	0.13391931
70.60	0.00197000	0.00009000	-0.00050000	0.15012197
72.60	0.00209100	0.00011600	-0.00053300	0.15875673
75.00	0.00221200	0.00014800	-0.00056600	0.16726544
77.60	0.00235000	0.00019600	-0.00061000	0.17648742
80.00	0.00249500	0.00025700	-0.00065300	0.18613569
82.60	0.00266300	0.00034500	-0.00070800	0.19687784
85.20	0.00282800	0.00044900	-0.00076600	0.20713206
87.60	0.00304200	0.00060100	-0.00083100	0.22082303
90.00	0.00326800	0.00078000	-0.00089300	0.23564778
92.60	0.00358200	0.00104400	-0.00097800	0.25679570

Load (KN)	Strain Gauge 16	Strain Gauge 17	Strain Gauge 18	Maximum Stress KN/mm^2
2.60	-0.00000400	-0.00000600	0.00000300	0.00029088
5.00	-0.00002400	-0.00003100	0.00001500	0.00126150
7.60	-0.00004500	-0.00005500	0.00002900	0.00231241
10.00	-0.00006400	-0.00007100	0.00004200	0.00306423
12.60	-0.00007300	-0.00008600	0.00004900	0.00379369
17.60	-0.00007900	-0.00011300	0.00005300	0.00494792
22.60	-0.00006800	-0.00012700	0.00004500	0.00556581
27.60	-0.00003800	-0.00013100	0.00002000	0.00565967
30.00	-0.00001800	-0.00012900	0.00000600	0.00587755
35.00	0.00003800	-0.00011000	-0.00003700	0.00619380
40.00	0.00011200	-0.00007100	-0.00011200	0.00697939
45.00	0.00020900	-0.00001600	-0.00016400	0.01237351
50.00	0.00029600	0.00003600	-0.00022600	0.01739366
55.00	0.00038600	0.00008600	-0.00029700	0.02275517
60.00	0.00048100	0.00016500	-0.00036600	0.02900382
65.00	0.00057700	0.00021400	-0.00043700	0.03505307
70.60	0.00068000	0.00028900	-0.00051000	0.04198586
72.60	0.00073700	0.00032900	-0.00055100	0.04581539
75.00	0.00079100	0.00036800	-0.00058600	0.04954672
77.60	0.00085800	0.00041500	-0.00063100	0.05413361
80.00	0.00092100	0.00046200	-0.00067300	0.05851889
82.60	0.00099700	0.00051700	-0.00072300	0.06379832
85.20	0.00105400	0.00056400	-0.00075900	0.06791595
87.60	0.00110700	0.00061300	-0.00079500	0.07183044
90.00	0.00115300	0.00065800	-0.00083000	0.07523452
92.60	0.00119900	0.00070700	-0.00087500	0.07858286

Load (KN)	Strain Gauge 19	Strain Gauge 20	Strain Gauge 21	Maximum Stress KN/mm^2
2.60	-0.00000400	-0.00000500	0.00000300	0.00024781
5.00	-0.00002200	-0.00002600	0.00001700	0.00134601
7.60	-0.00004200	-0.00005100	0.00004100	0.00338799
10.00	-0.00006200	-0.00007500	0.00004700	0.00378249
12.60	-0.00008800	-0.00010700	0.00006600	0.00532785
17.60	-0.00013000	-0.00017300	0.00010000	0.00871810
22.60	-0.00015400	-0.00023500	0.00012900	0.01257206
27.60	-0.00015100	-0.00029000	0.00016500	0.01843723
30.00	-0.00014900	-0.00031200	0.00018200	0.02108361
35.00	-0.00012800	-0.00034800	0.00020300	0.02599813
40.00	-0.00007200	-0.00032600	0.00015600	0.02466454
45.00	-0.00003900	-0.00034600	0.00015300	0.02775925
50.00	-0.00000100	-0.00036100	0.00014400	0.03055091
55.00	0.00003800	-0.00037400	0.00014800	0.03446524
60.00	0.00007700	-0.00038400	0.00013700	0.03706940
65.00	0.00012100	-0.00039000	0.00012400	0.03977231
70.60	0.00016500	-0.00039400	0.00010600	0.04206835
72.60	0.00018900	-0.00039500	0.00010200	0.04374084
75.00	0.00021100	-0.00039400	0.00009000	0.04455813
77.60	0.00023700	-0.00039500	0.00008500	0.04635618
80.00	0.00026300	-0.00039200	0.00007200	0.04737326
82.60	0.00029500	-0.00038500	0.00005400	0.04835393
85.20	0.00031900	-0.00037300	0.00003200	0.04817586
87.60	0.00034400	-0.00035900	0.00001000	0.04804061
90.00	0.00036600	-0.00034300	-0.00000900	0.04781676
92.60	0.00038900	-0.00032100	-0.00003100	0.04724412

Load (KN)	Strain Gauge 22	Strain Gauge 23	Strain Gauge 24	Maximum Stress KN/mm^2
2.60	-0.00000600	0.00000800	0.00001800	0.00126716
5.00	-0.00002900	0.00003500	0.00008300	0.00579819
7.60	-0.00005200	0.00006100	0.00015900	0.01115620
10.00	-0.00007600	0.00008800	0.00022300	0.01558445
12.60	-0.00010300	0.00011900	0.00030100	0.02102684
17.60	-0.00016600	0.00018100	0.00048400	0.03375635
22.60	-0.00023300	0.00025600	0.00068300	0.04766788
27.60	-0.00031200	0.00034300	0.00090200	0.06286800
30.00	-0.00035100	0.00038600	0.00102800	0.07174116
35.00	-0.00044800	0.00049300	0.00128400	0.08942121
40.00	-0.00055600	0.00062200	0.00160700	0.11205018
45.00	-0.00066900	0.00075300	0.00193300	0.13479905
50.00	-0.00079100	0.00089000	0.00228800	0.15956934
55.00	-0.00092500	0.00103100	0.00265900	0.18529204
60.00	-0.00107400	0.00118700	0.00307100	0.21385010
65.00	-0.00125300	0.00138200	0.00356600	0.24819830
70.60	-0.00149600	0.00161700	0.00421100	0.29263234
72.60	-0.00165400	0.00177000	0.00463200	0.32164803
75.00	-0.00183300	0.00192600	0.00507900	0.35215962
77.60	-0.00209400	0.00214600	0.00574500	0.39770189
80.00	-0.00240200	0.00239500	0.00644500	0.44484574
82.60	-0.00283700	0.00271100	0.00751300	0.51734370
85.20	-0.00329200	0.00303500	0.00847100	0.58098418
87.60	-0.00390400	0.00345400	0.00989100	0.67658818
90.00	-0.00458400	0.00392100	0.01139700	0.77732652
92.60	-0.00559700	0.00461800	0.01369100	0.93128872

Load (KN)	Strain Gauge 25	Strain Gauge 26	Strain Gauge 27	Maximum Stress KN/mm^2
2.60	-0.00001200	-0.00000500	0.00001700	0.00112040
5.00	-0.00005200	-0.00002600	0.00006900	0.00455361
7.60	-0.00009000	-0.00010200	0.00012000	0.00984121
10.00	-0.00012000	-0.00012100	0.00016300	0.01281572
12.60	-0.00014800	-0.00014300	0.00021100	0.01646688
17.60	-0.00019900	-0.00018400	0.00029200	0.02258189
22.60	-0.00022200	-0.00022300	0.00037500	0.03024782
27.60	-0.00024900	-0.00025700	0.00046400	0.03806584
30.00	-0.00026000	-0.00027200	0.00050600	0.04180835
35.00	-0.00027700	-0.00030200	0.00060600	0.05099164
40.00	-0.00029400	-0.00033800	0.00071600	0.06130476
45.00	-0.00031000	-0.00037600	0.00083300	0.07238221
50.00	-0.00032600	-0.00042200	0.00095500	0.08422924
55.00	-0.00034800	-0.00047100	0.00108700	0.09676766
60.00	-0.00036800	-0.00051800	0.00123200	0.11050139
65.00	-0.00039200	-0.00057400	0.00138600	0.12518282
70.60	-0.00041800	-0.00063500	0.00156700	0.14236930
72.60	-0.00043200	-0.00067300	0.00166200	0.15161505
75.00	-0.00044300	-0.00070600	0.00175000	0.16020153
77.60	-0.00045600	-0.00074800	0.00186600	0.17154481
80.00	-0.00046500	-0.00079000	0.00197000	0.18204567
82.60	-0.00046700	-0.00084100	0.00209500	0.19519433
85.20	-0.00046300	-0.00089500	0.00221100	0.20801950
87.60	-0.00044400	-0.00097100	0.00235000	0.22470847
90.00	-0.00040600	-0.00106300	0.00248500	0.24289215
92.60	-0.00030000	-0.00120700	0.00266000	0.27110404

Load (KN)	Strain Gauge 28	Strain Gauge 29	Strain Gauge 30	Maximum Stress KN/mm^2
2.60	0.00000200	-0.00000200	-0.00002500	-0.00033267
5.00	0.00000700	-0.00003600	-0.00004400	-0.00030508
7.60	0.00001200	-0.00007400	-0.00003800	0.00211149
10.00	0.00001600	-0.00010900	-0.00009100	0.00078209
12.60	0.00002400	-0.00015800	-0.00014000	0.00074668
17.60	0.00004500	-0.00025200	-0.00014600	0.00645995
22.60	0.00007900	-0.00035800	-0.00025000	0.00781993
27.60	0.00011500	-0.00046000	-0.00031100	0.01186727
30.00	0.00013100	-0.00051000	-0.00032500	0.01469489
35.00	0.00017400	-0.00062100	-0.00038900	0.01958958
40.00	0.00022800	-0.00072300	-0.00044000	0.02585178
45.00	0.00029000	-0.00082000	-0.00049500	0.03233527
50.00	0.00035900	-0.00090500	-0.00057000	0.03764291
55.00	0.00044000	-0.00097400	-0.00061900	0.04490602
60.00	0.00052400	-0.00103100	-0.00069900	0.05003362
65.00	0.00061700	-0.00108400	-0.00070000	0.06056189
70.60	0.00071600	-0.00111900	-0.00077900	0.06616294
72.60	0.00076900	-0.00114600	-0.00081900	0.06968854
75.00	0.00082200	-0.00116800	-0.00075000	0.07943750
77.60	0.00088900	-0.00114800	-0.00076500	0.08361528
80.00	0.00095000	-0.00116200	-0.00071700	0.09249792
82.60	0.00103800	-0.00115000	-0.00061500	0.10592484
85.20	0.00111600	-0.00112300	-0.00055500	0.11527241
87.60	0.00120600	-0.00105900	0.00000000	0.15605307
90.00	0.00126100	-0.00093600	0.00000000	0.15474810
92.60	0.00131600	-0.00078600	0.00000000	0.15226482